Examining spatiotemporal changes in the phenology of Australian mangroves using satellite imagery.

Thesis submitted by:

Nicolás Younes Cárdenas

Environmental Engineer,

Master of Science in Oil and Gas Exploration and Production,

Master of Science in Natural Resource Management

December, 2020

For the Degree of Doctor of Philosophy

In the College of Science and Engineering,

Division of Tropical Environments and Societies

James Cook University

Acknowledgements

A Estefanía, por su amor y apoyo incondicional. Eres un ejemplo de valentía, coraje y perseverancia que espero poder seguir siempre. Te admiro y estoy supremamente orgulloso de ti.

A Estefanía, Mónica, German, Yohaina y Federico. Ustedes son mi fuerza, mi aliento, mi motivación y mis ganas de seguir adelante. Todo lo hago por Ustedes y mi único anhelo es que estén orgullosos de lo que hemos logrado juntos.

A Rigoberto, Manchas y Ataque.

Special thanks to Dr Karen Joyce, Dr Stefan Maier, and Dr Tobin Northfield whose support and guidance have been fundamental to the success of this project. This has been a team effort.

Thanks to Dr Yoko Ishida and the Center for Tropical Environmental and Sustainability Science (TESS) for your support, as well as the admin team in the College of Science and Engineering, and everyone at the Graduate Research School. You all do an amazing job!

I would also like to thank the following people and institutions for their support through grants, donations, data, and resources provided in support of this project:

Geoscience Australia and Dr Leo Lymburner, TropWater and Dr Damian Burrows, National Environment Science Program (NESP) Tropical Water Quality Hub (TWQ), the Wet Tropics Management Authority, and Dr Norman Duke. Special thanks to NIESGI Cia. Ltda. and Mrs Gilma Mera for her extraordinary work.

Special thanks to Michelle and Geoffrey Henderson, Manchas, Ataque y Rigoberto.

Thanks to my friends and colleagues Maria, Diana, Natalia, Katie, Cesar, Diego, Damien, and all those who have supported me through this ordeal.

All the people who develop Free and Open Source (FOSS) software packages for data analysis; I stand on the shoulders of giants: Xarray, Open Data Cube, Dask, Pandas, Numpy, QGIS.

Citations for, and contributions of other authors to, published or submitted works resulting from this thesis.

Younes Cárdenas, N., Joyce, K. E., & Maier, S. W. (2017). Monitoring mangrove forests : Are we taking full advantage of technology? International Journal of Applied Earth Observation and Geoinformation, 63(July), 1–14. doi:10.1016/j.jag.2017.07.004

Author contributions: Conceptualization, N.Y., K.J., S.M.; methods, N.Y.; data analysis, N.Y., K.J., S.M.; writing—original draft preparation, N.Y.; writing—review and editing, N.Y., K.J., S.M..

Younes, N., Joyce, K. E., Northfield, T. D., & Maier, S. W. (2019). The effects of water depth on estimating Fractional Vegetation Cover in mangrove forests. International Journal of Applied Earth Observation and Geoinformation, 83, 101924. doi:https://doi.org/10.1016/j.jag.2019.101924

Author contributions: Conceptualization, N.Y., K.J.; methods, N.Y., K.J., S.M.; field data collection, N.Y.; data analysis, N.Y.; writing—original draft preparation, N.Y.; writing—review and editing, N.Y., K.J., S.M..

Younes, N., Northfield, T. D., Joyce, K. E., Maier, S. W., Duke, N. C., & Lymburner, L. (2020). Modelling mangrove phenology from satellite images: a novel approach using Generalized Additive Models. Remote Sensing – *In press.*

Author contributions: Conceptualization, N.Y., K.J., L.L., S.M.; methods, T.N., L.L., N.Y.; field data collection, N.D.; data analysis, N.Y., T.N., N.D.; writing—original draft preparation, N.Y.; writing—review and editing, N.Y., K.J., S.M., T.N., L.L., N.D..

Younes, N., Northfield, T. D., Joyce, K. E., Maier, S. W. All models satellite-derived phenology are wrong, but some are useful. International Journal of Applied Earth Observations and Geoinformation- *In review.*

Author contributions: Conceptualization, N.Y., K.J., S.M.; methods, N.Y., K.J., S.M.; data analysis, N.Y., K.J., S.M.; writing—original draft preparation, N.Y.; writing—review and editing, N.Y., K.J., S.M..

Younes, N., Northfield, T. D., Joyce, K. E., Maier, S. W. & Lymburner, L. A continental scale assessment of mangrove phenology using all available Landsat imagery (1988-2019). *In prep*.

Abstract

Mangroves store more carbon than other tropical forests, and phenology plays an important role in regulating carbon sequestration and storage. Understanding phenology, therefore, is essential to measuring and predicting land-atmosphere interactions, the carbon and water cycles, and, ultimately, the response of vegetation to a changing climate. Mangrove phenology is often studied at the plot scale, and requires expensive and time-consuming fieldwork. Few studies have used satellites to monitor mangrove phenology, and fewer have compared field observations with satellite-derived phenology. In this thesis, I investigate the effects of water depth, spatial resolution, and site selection on satellite-derived phenology, I examine the suitability of different spectral indices to detect vegetation fraction, and I present a novel, data-driven approach to examining mangrove phenology using the Landsat archive. To validate the phenology models, I combined field observations and published data, with hundreds of satellite images from six regions in eastern and northern Australia. Here, I demonstrate that: 1) not all spectral indices perform well when detecting vegetation fraction; 2) we can use Generalized Additive Models (GAMs) on a pixel-by-pixel basis and the resulting models correlate well with field-observed phenology; 3) mangrove phenology is site dependent; 4) fully parametric methods over-simplify the phenology of mangroves; and 5) the spatial resolution, temporal coverage, site selection, and pre-processing techniques have subtle, but significant effects on the phenology models. In the future, GAMs can be combined with rainfall and temperature datasets, to determine the influence these drivers have on mangrove phenology. With increasing temperatures and erratic rainfall patterns, GAMs will become an important tool, not only to forecast changes in phenology, carbon sequestration, and vegetation growth rates, but they can also help to monitor lethal and sub-lethal conditions of vegetation stress.

Keywords:

Mangroves; Mangrove forests; Generalized Additive Models; Land Surface Phenology; Phenology; Remote Sensing; Satellite Imagery; Landsat; Sentinel 2.

Table of Contents

List of Figures

List of Tables

Abbreviations and Acronyms frequently used throughout this thesis

EVI: Enhanced Vegetation Index

FVC: Fractional Vegetation Cover

GAMs: Generalized Additive Models

PGS: Peak Growing Season

MSAVI: Modified Soil-adjusted Vegetation Index

MSAVI2: Modified Soil-adjusted Vegetation Index 2

NDVI: Normalized Difference Vegetation Index

SAVI: Soil-Adjusted Vegetation Index

SOS: Start of the growing Season

1 Introduction

1.1 The importance of mangrove forests

The terms 'mangrove forests' and 'mangroves', refer to a group of plants, shrubs, and palms that grow in estuaries of countries in tropical regions (Duke et al., 2006). These plants grow in over 120 countries around the world (Chandra Giri et al., 2011b; Hamilton and Casey, 2016), and have adapted to life at the interface of fresh and seawater (Friess et al., 2019; Tomlinson, 1986). There is plethora of animals that depend on mangrove forests, including the Royal Bengal tiger (*Panthera tigris tigris*), sharks and rays, crabs, birds, fishes, and, of course, humans.

Humans have used mangrove ecosystems for centuries. Coastal communities benefit from a wide range of goods and services provided by mangrove forests, from aquaculture and agriculture, to wood extraction, medicines, shoreline protection and shelter from extreme weather events (FAO, 2007; Kainuma et al., 2010; Lee et al., 2014). Studies suggest that the monetary value of the goods and services that mangroves provide ranges between USD $14,000 - $194,000 per hectare, per year (Costanza et al., 2014). This means that mangrove forests are of vital importance to coastal communities and more generally to human populations, not only because mangroves protect coastlines from extreme weather events (Alongi, 2008), but also because they store large amounts of carbon.

Among tropical forests, mangroves are the most carbon dense (Donato et al., 2011; Kauffman et al., 2020), this means that they store large amounts of carbon when compared to other tropical forests. Mangroves store carbon in their biomass (i.e. leaves, trunks, and roots), but they mainly store it in the soil (Adame and Lovelock, 2011; Kauffman et al., 2020). The amount of carbon stored in these forests changes with location (e.g. continent, latitude), site (e.g. river mouth), species, water quality (e.g. turbidity, salinity), and weather (Donato et al., 2011; Lovelock et al., 2014; Sanderman et al., 2018). In general, and regardless of this variability, studies suggest that mangrove forests play a key role in the mitigation of, and adaptation to climate change either by planting new forests, protecting standing forests, and by preventing their deforestation (Duarte

et al., 2013; Gilman et al., 2008). Despite their importance, these forests face many threats, including deforestation and land use change.

Mangroves are also threatened by anthropogenic actions and the effects of climate change. Studies by Friess et al. (2019), Lovelock et al. (2015), and Rogers et al. (2019) state that mangrove ecosystems are highly threatened by sea level rise and land use change, and that the loss of these forests ranges between 1-8% per year. The main reason why mangroves are threatened by these stressors is the limited amount of land available to maintain their extent of for future expansion and migration from land cover change to aquaculture, agriculture and urban development (Friess et al., 2019). Mangroves are known to migrate landward and seaward (Asbridge et al., 2016), however, these habitats have been reduced to narrow sections of coast due to anthropogenic pressures such as agriculture, aquaculture, and urbanization (Richards and Friess, 2016). Given all these pressures, monitoring the health of mangrove forests is of prime importance to ensure the ongoing quality and quantity of goods and services provided by these ecosystems.

1.2 The importance of phenology

Phenology refers to the relationship between seasonal life cycle events of plants and animals, and cycles of abiotic factors (Annette and Menzel, 2002; Morellato et al., 2016a). For example, flowering and fruiting may be related to seasonal rainfall, or falling or rising temperatures. Flowering plants, such as mangroves, align their flowering and fruiting events with changes in temperature and moisture (Duke, 2001). At the same time, plants need to protect themselves from antagonistic insects, seed predators and other pests (Duke, 2002a; Matthews and Mazer, 2016). Plant phenology is also linked to the carbon cycle, by regulating carbon sequestration and storage. Therefore understanding plant phenology is fundamental to explain the processes governing weather, climate, and biogeochemical cycles, as well as ecosystem response to climate change and extreme weather events (Garonna et al., 2016; Peñuelas et al., 2009; Sitch et al., 2015).

There are detailed phenological descriptions for many plant species, including mangroves (Coupland et al., 2006; Duke et al., 2006; Metcalfe et al., 2011a). For example, Duke (1990) described the phenology of *Avicennia marina* mangroves and related it to temperature, rainfall,

and location along the Australian coastline. These invaluable descriptions come from small and scattered plots, but with the aid of satellite images and other tools they are used to model plant phenology over large geographical areas (e.g. 100s-1000s of km). These models of phenology help us understand global phenomena such as the carbon and water cycles, but it is important to acknowledge that these models are often biased in two main ways:

1. Most models of plant phenology are only applied to landscapes in the northern hemisphere, leaving a gap in knowledge related to the phenology of plants in the southern hemisphere (Chambers et al., 2013). This means that biogeochemical and ecosystem function models may produce results that are not representative of the global reality; and,
2. Mangroves and other tropical forests are often ignored from continental- or global-scale phenology models (see e.g. Bolton et al., (2020); Fu et al. (2014); Vogelmann et al. (2016)). Models of phenology created for temperate forests may not be applicable to mangroves or other tropical ecosystems.

To reduce these biases, and to improve global biogeochemical models, there is a need to explore plant phenology in the southern hemisphere, especially mangrove phenology. Of chief importance is the understanding of how mangrove phenology changes with location, and over time. Discerning how phenology changes with location is important because not all mangroves sequester and store the same amount of carbon (Adame and Lovelock, 2011; Kauffman et al., 2020), and learning about temporal changes could explain mangrove adaptation to a changing climate. Attaining this knowledge requires data, and data collection in mangrove forests presents a unique set of challenges, as explained below.

1.3 The challenges of monitoring mangrove forests

Usually, mangrove health, growth, and phenology are monitored in the field, and field campaigns can be challenging. To assess phenology, data collection efforts should cover, at least, one full growing cycle, but preferably more (Metcalfe et al., 2011a; Wilson and Saintilan, 2012). In Australia, most descriptions of mangrove phenology were conducted in the 1980's (Duke, 1988; Duke et al.,

1984a; Saenger and Moverley, 1985; Tomlinson, 1986). More recently, Coupland et al. (2005) and Metcalfe et al. (2011), described the phenology of several mangrove species around Darwin harbour (NT) while Wilson and Saintilan (2012) did so in the Richmond River (NSW). The information provided by these studies is very valuable, and serves as a baseline for future comparison, but data on mangrove phenology is still scarce, variables and methods are not standardized, and frequency of observation varies widely between studies. This lack of agreement only adds to the complexity of understanding mangrove phenology.

To better understand mangrove phenology, and how these forests respond to anthropogenic and natural stressors, one needs: 1) datasets that span decades; 2) to acquire data consistently over space and time; 3) collect data on a fortnightly or weekly basis; and 4) gather data over large areas instead of small plots. Satellites provide data with these characteristics, which is why remote sensing tools are emerging as indispensable tools to monitor mangrove forests at local, national, and global scales (Younes Cárdenas et al., 2017).

1.4 Remote sensing of mangrove forests

Satellites repeatedly collect data over large geographical areas, resulting in archives that can be used to monitor mangrove ecosystems worldwide. Studies have leveraged the spatial and spectral qualities of satellite sensors to create maps of mangrove forests at the global (Bunting et al., 2018; Chandra Giri et al., 2011b; Hamilton and Casey, 2016), regional (Bhattarai and Giri, 2011; Lymburner et al., 2019a), and local scales (Asbridge et al., 2018; Kovacs et al., 2001). These maps provide information on the extent, distribution of mangroves, and even Fractional Vegetation Cover (FVC), where FVC is defined as the area covered by foliage projected onto a horizontal surface (Younes et al., 2019). However, few studies have examined seasonal and long-term changes in mangrove forests.

In 2018, Pastor-Guzman et al. (2018b), used the 8-day MOD09A1 surface reflectance product from the MODIS archive (2000-2014) to examine the phenology of mangrove forests in the Yucatan Peninsula (Mexico). The authors compared four different spectral indices to temperature, rainfall, water salinity, and litterfall, and concluded that mangrove phenology in their study sites is mainly

driven by rainfall, as opposed to temperature. Similar to Pastor-Guzman et al. (2018), Songsom et al. (2019) used MODIS data (2003-2012) to examine the phenology of mangroves in Southern Thailand. The authors used the 16-day MOD13Q1 product with a spatial resolution of 250m, and found that mangroves have a distinct phenology when compared to neighbouring tropical forests. These are just two examples of studies examining mangrove phenology using satellite imagery, and there are some aspects that can be improved.

The studies by Pastor-Guzman et al. (2018) and Songsom et al. (2019), use coarse spatial resolution data (500m and 250m respectively). This means that every pixel represents not only mangrove trees from different species, but salt marshes and other plant communities associated with mangrove forests. In addition to capturing many plant communities, each pixel may also capture different land cover types such as beaches, saltpans, croplands, roads, artificial surfaces, and water. Water is omnipresent in satellite images of mangrove forests, but the effects of water in the spectral signature of mangroves remain unknown. Moreover, the contribution of water (i.e. tides) to the spectral signature of mangroves may depend on the spatial resolution of the sensor, however this also remains unexplored. The main way to prevent these mixed pixels, and explore the effects of water on the spectral reflectance of mangroves, is to use sensors with finer spatial resolution, for example, Landsat or Sentinel 2.

When compared to MODIS, the main advantage of Landsat and Sentinel 2 sensors is the finer spatial resolutions (30m and 10m respectively). Their main drawback, however, is the less frequent revisit time (8-16 days, and 3-5 days respectively). The Landsat sensors have an additional advantage in the length of its archive (32+ years) when compared to the MODIS archive (21 years), opening the opportunity to comparing past and present phenology.

Due to its geographical and temporal coverage, the Landsat archive is well suited to aid in assessing mangrove phenology and it has been used for similar purposes in a wide range of ecosystems. For example, Melaas et al. (2018) used the Landsat archive to measure intra and inter annual variations in the magnitude of the Enhanced Vegetation Index (EVI) in temperate and boreal forests of North America over 29 years. Their study suggests that eastern and western forests differ in their phenology, specifically the dates of leaf emergence and onset. Using Landsat

imagery (1985-2015), Senf et al. (2017) found that the phenology of broad-leaved forests in Germany is mainly driven by elevation, and more importantly, that the growing season is starting earlier than in the 1980's and 1990's. These and other studies demonstrate that, despite a lower temporal resolution, the Landsat archive can be used to detect seasonal and interannual changes in vegetation phenology.

Two recent studies that have used Landsat imagery to monitor seasonal changes in mangrove forests are those by Zhang et al. (2016) and Small and Sousa (2019). Zhang et al. (2016) used Landsat 5 images between 1985-2011 to explore the effects of extreme cold spells and hurricanes on the seasonal patterns of mangroves in south Florida (United States), but did not explore phenology *per se*. Small and Sousa (2019) on the other hand, examined seasonal patterns of mangrove greenness using Landsat and Sentinel 2 data over the Sundarbans region in Bangladesh. This study suggested that mangrove phenology is heavily influenced by monsoonal rainfall, and phenology seems to depend on the species composition and other environmental factors. The aforementioned studies hint at an increased interest in mangrove forests and mangrove phenology, but the following questions still remain: 1) What is the influence of water under the canopy in the spectral signature of mangroves? 2) Is mangrove phenology site dependent? 3) How do different spatial and temporal resolutions modify the observed phenology, and 4) Has mangrove phenology changed over the past 30 years?

1.5 Research Aims and objectives

Observing mangrove phenology is one way to measure vegetation response to changes in the climate. However, phenology is mostly studied in situ, at the plot level, and for short periods of time (<2 growth cycles). To examine how mangroves adapt to a changing climate, investigations spanning several decades and at different locations are needed. Satellite imagery archives hold decades-worth of data on these ecosystems around the world. In this thesis I will link field and satellite data to examine mangrove phenology. **My overarching aim is to examine temporal and spatial changes in mangrove phenology across Australia using the Landsat and Sentinel 2 archives**. To achieve this aim, I address the following objectives:

1. To investigate the effects of understory water on the estimation of Fractional Vegetation Cover in mangrove forests (Chapter 3).
2. To compare and contrast the effectiveness of different spectral indices in predicting Fractional Vegetation Cover (Chapter 3).
3. To critically evaluate the relationship between field and satellite-derived phenology in mangroves forests across Australia (Chapter 4).
4. To investigate how changes in the spatial and temporal resolution, alter the observed phenology of an ecosystem (Chapter 5).

1.6 Thesis structure

This thesis is made up of a literature review (Chapter 2), three empirical chapters (Chapters 3, 4, and 5), and a summary of the implications of this project to future work (Chapter 6). Each empirical chapter was written with the intention of being published in a peer-reviewed journal and can be read independently or in conjunction with the other chapters. Each chapter builds on the results from the previous one, creating a coherent overview of how mangrove phenology is derived from satellite imagery and how phenology changes over time and space (Figure 1). A summary of each chapter is provided in the following section.

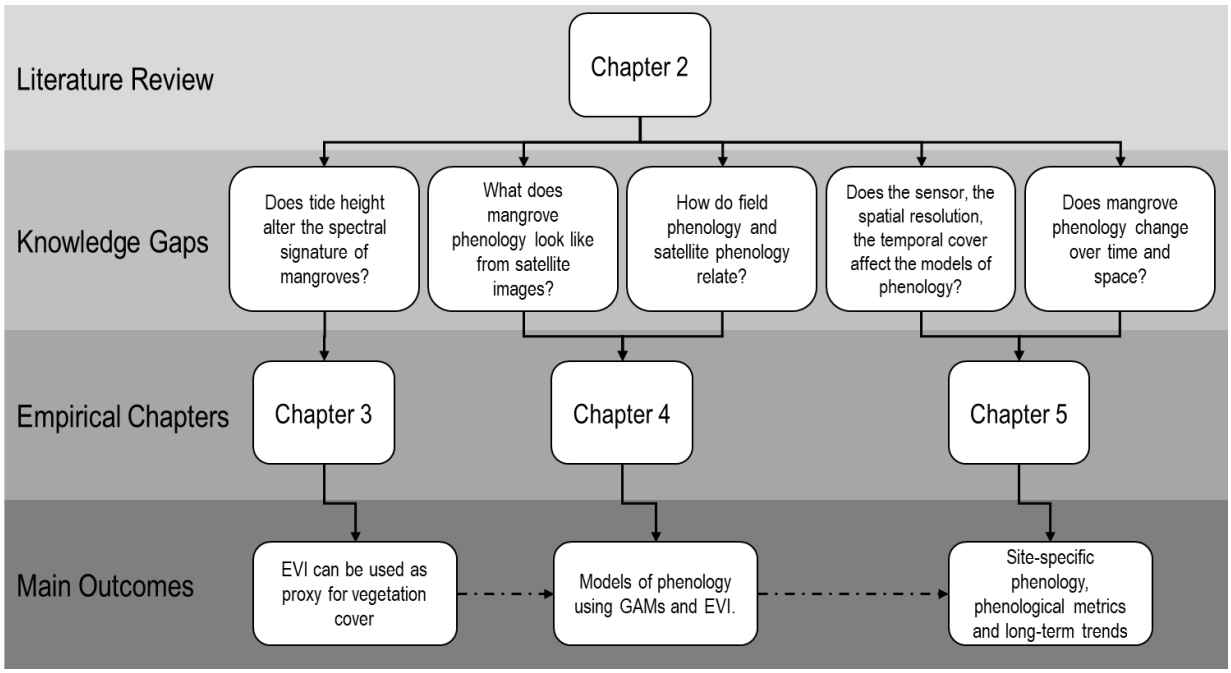

Figure 1: Thesis structure. Relationship between aims, chapters and outcomes.
Acronyms used in the figure: Enhanced Vegetation Index (EVI); Generalized Additive Models (GAMs).

1.7 Chapter synopsis

Chapter 2: Monitoring mangrove forests, are we taking advantage of technology?

In this literature review, I explore how different studies use freely available satellite imagery to monitor mangrove forests. Firstly, I look at common applications of satellite imagery in mangrove ecosystems, followed by the need for long-term studies of mangrove forests. Then I present two key gaps in using satellite imagery for mangrove research: 1) the effects of water under the canopy in the spectral signature of mangroves, and 2) the use of satellite images to detect the phenology of mangroves. The former is important because mangroves are subject to frequent inundation and thus their spectral signature may change from one observation to the next, not because of altered canopy structure, but by the presence or absence of water. The second gap is important because field descriptions of mangrove phenology are limited and there needs to be a consistent approach to monitoring phenology over time. In this chapter I argue that studies should leverage the long time series of satellite imagery to examine the phenology and trends of change in mangrove forests.

Chapter 3: The effects of water depth on estimating Fractional Vegetation Cover in mangrove forests.

Building on the results of Chapter 2, in this chapter I aim to: 1) explore the effects of understory water on estimating Fractional Vegetation Cover; and 2) compare the effectiveness of different spectral indices in predicting FVC. To achieve these aims, I designed an experiment to isolate the effect of understory water on the spectral reflectance of mangrove leaves. I used a hyperspectral pushbroom scanner to capture data to derive four spectral indices for analysis.

In this chapter I conclude that: 1) linear and non-linear models of the Enhanced Vegetation Index (EVI) produce similar predictions of FVC in mangrove forests; 2) EVI is a better predictor of FVC than the commonly used Normalized Difference Vegetation Index (NDVI); and 3) the spectral index plays a more important role than the spatial resolution when estimating FVC. The Fractional Vegetation Cover is measured at a single time step in the phenology cycle; therefore, good predictions of fractional cover over time may result in good predictions of phenology.

Chapter 4: Extracting mangrove phenology from Landsat imagery: a novel approach using Generalized Additive Models

In this chapter, I examine the relationship between satellite-derived phenology, published literature on mangrove phenology, and raw data from field observations. In contrast to previous studies, I use a data-driven approach to model phenology: Generalized Additive Models (GAMs). I evaluated six sites across Australia, and concluded that: 1) seasonal and inter-annual variations of EVI correlate well with the net leaf production, and the rate of leaf production of mangrove forests; 2) GAMs can detect one or more periods of leaf production in evergreen forests; 3) mangrove phenology is site-dependent; and 4) fully parametric methods may over-simplify the phenology of mangroves and other evergreen forests.

Chapter 5: Considerations and pitfalls in using long time series of satellite imagery for vegetation phenology investigations

This chapter builds on the results of Chapters 3 and 4; here I demonstrated how the area of interest, the sensor selection, and the data cleaning methods can change the shape of the phenology of a mangrove forest in northern Australia. To do this, I used 352 Landsat and 260 Sentinel 2 images of the Darwin harbor in Northern Australia acquired between 2010 and 2020. I conclude that, the distribution of observations over time may play a more important role on apparent phenology than the frequency of observation. Also, the apparent phenology resulting from Landsat and Sentinel 2 sensors is comparable with one another, but it is not comparable to phenology derived from MODIS due to differences in the spatial resolution of the sensors. Finally, I argue that studies must incorporate knowledge and context into their workflows to ensure *apparent* phenology resembles *true* vegetation phenology.

1.8 Research Methods

In this section, I provide a brief overview of the methods used throughout the thesis. For detailed descriptions, please refer to the corresponding section in each chapter.

1.8.1 Field Data Acquisition

For this thesis, field data collection was limited to Chapters 3 and 4. In Chapter 3, I designed an experiment to examine the effects of tidal height on the estimation of Fractional Vegetation Cover in mangrove ecosystems. I collected mature *Ceriops australis* leaves from the 'Jack Barnes Mangrove Boardwalk' in Cairns, Queensland. I inspected the leaves, and divided them intro three groups. Each group was assigned to a tidal scenario (i.e. low, transition, and high tide) and was later scanned using a hyperspectral pushbroom scanner at James Cook University in Cairns, Queensland.

The data collection for Chapter 4, was performed by Duke et al. (1999) between June 1996 and August 1998 in Curtis Island, and near the Gladstone port in central Queensland as part of an

experiment into the bioremediation of mangrove forests affected by oil spills. Importantly, for this chapter I only considered the plots not affected by the experiments, that is, the control plots. The data collected consisted of mean monthly values of six phenological variables, including the number of Leaves lost [leaves × m^{-2} × day^{-1}], Leaves gained [stipules × m^{-2} × day^{-1}], and the net leaf production [leaves gained - leaves lost × m^{-2} × day^{-1}]. I used this information to validate the phenological models generated from Landsat imagery.

1.8.2 Satellite Data Acquisition and processing

In this thesis, I used imagery from high and medium resolution satellite sensors. In Chapter 3, I used two surface reflectance images from the Worldview 3 sensor over the Cairns region, in northern Queensland. The Digital Globe Foundation provided the images that showed the study area under low and high tide conditions.

In Chapter 4, I used Landsat TM/ETM+ images, while in Chapter 5 I used Landsat TM/ETM+/OLI and Sentinel 2 images. All Landsat and Sentinel images used in this thesis were provided free of charge by the United States National Aeronautics and Space Administration (NASA) and the European Space Agency through Digital Earth Australia (DEA). DEA performed geometric, radiometric, and Nadir Bidirectional Reflectance Distribution Function (BRDF) Adjusted Reflectance (NBAR) using the methods described by Lewis et al. (2017).

1.8.3 Data Analysis

Throughout this project, I used a range of analysis and modelling techniques from the R and Python programming languages, ENVI 5.2 (Excelis Visual Information Solutions, Inc.), ArcGIS 10.3 (Environmental Systems Research Institute), and Digital Earth Australia (https://docs.dea.ga.gov.au/about/intro.html). I used satellite images and Generalized Additive Models (GAMs) to examine the phenology of mangrove forests. A python package developed by Facebook Inc. The 'Prophet' package was originally designed to detect trends in user engagement

with the social media platform (Taylor et al., 2018), but instead of looking at trends of engagement, I re-purposed the package to examine changes in EVI.

By measuring the changes in EVI, I was able to extract several phenological metrics (e.g. start, end, and length of the growing season) in different years. Moreover, GAMs allowed me to detect changes in the long-term trends of mangrove greenness, an indication that mangroves are dynamic ecosystems and are subject to the effects of long-term climate changes.

1.9 Summary of Thesis Implications

The methods used in this thesis could radically change the way we detect phenology from satellite images. In contrast to model-driven methods, I present a data-driven approach to effectively detect phenological cycles in mangrove forests. Because mangroves and other evergreen forests may have more than one period of leaf growth, sinusoidal or double logistic curves may not be good representations of the ecosystem. I have demonstrated that GAMs are able to detect these additional periods of leaf growth, as described in field observations. With the wealth of data stored in the Landsat, MODIS, and Sentinel 2 archives, data-driven models should be the norm, not the exception, when examining long term plant phenology.

While most studies focus on key phenological metrics (e.g. start of season and peak growing season dates), I argue that the shape, amplitude, and frequency of the observed phenology should also be inspected. While phenological metrics are important when examining long term changes in plant communities, limiting ourselves to these metrics means that we analyse only *some* of the data. Changes in the shape, amplitude, and frequency of the observed phenology can provide insights into ecosystem change. For example, peaks and troughs in the observed phenology may indicate a dual leaf-flush event, or understory growth. Analysing all the information is equally as important as analysing changes in key phenological metrics, especially under climate change scenarios.

I have demonstrated that small changes in the location, source data, and analysis methods can cause small - but significant - changes in the way we detect phenology and phenological metrics.

While this may seem obvious, it has far-reaching implications. The main implication is that, unless two models use the same data and parameters, they may be incomparable to one another. In other words, for any given site, two models may produce different phenological metrics because of contrasting data and methods, rather than changes in the plants themselves.

2 Monitoring mangrove forests: are we taking full advantage of technology?

A version of this chapter has been published as: **Younes Cárdenas, N**., Joyce, K. E., & Maier, S. W. (2017). Monitoring mangrove forests: Are we taking full advantage of technology? International Journal of Applied Earth Observation and Geoinformation, 63(July), 1–14. doi:10.1016/j.jag.2017.07.004

2.1 Abstract:

Mangrove forests grow in the estuaries of 124 tropical countries around the world. Because in-situ monitoring of mangroves is difficult and time-consuming, remote sensing technologies are commonly used to monitor these ecosystems. Landsat satellites have provided regular and systematic images of mangrove ecosystems for over 30 years, yet researchers often cite budget and infrastructure constraints to justify the underuse of this resource. Since 2001, over 50 studies have used Landsat or ASTER imagery for mangrove monitoring, and most focus on the spatial extent of mangroves, rarely using more than five images. Even after the Landsat archive was made free for public use, few studies used more than five images, despite the clear advantages of using more images (e.g. lower signal-to-noise ratios). The main argument of this paper is that, with freely available imagery and high performance computing facilities around the world, it is up to researchers to acquire the necessary programming skills to use these resources. Programming skills allow researchers to automate repetitive and time-consuming tasks, such as image acquisition and processing, consequently reducing up to 60% of the time dedicated to these activities. These skills also help scientists to review and re-use algorithms, hence making mangrove

research more agile. This paper contributes to the debate on why scientists need to learn to program, not only to challenge prevailing approaches to mangrove research, but also to expand the temporal and spatial extents that are commonly used for mangrove research.

2.2 Keywords:

Long-term monitoring, mangroves, tides, automation, Landsat, ASTER, programming, remote sensing.

2.3 Introduction: recalling the importance of mangroves

Mangroves are groups of trees, palms and shrubs that grow in the estuarine margins of 124 countries around the world (Duke et al., 2006; FAO, 2007), and cover between 150,000 and 188,000 km^2 (Barbier, 2015; Costanza et al., 2014). Inhabitants of mangrove forests include the Royal Bengal tiger (*Panthera tigris tigris*), crocodiles and myriad birds, reptiles, amphibians, crustaceans and, of course, humans. With so many species depending on mangrove forests, it is important to know how humans alter and use these ecosystems.

Humans use mangroves in direct (e.g.. building materials, food and medicinal purposes) and indirect ways (e.g. carbon sequestration, protection from extreme weather events, fish nurseries and land building) (Barbier, 2015; Donato et al., 2011; Kainuma et al., 2010; Lee et al., 2014). These uses and services make mangroves worth up to \$194,000 ha^{-1} yr^{-1} (Costanza et al., 2014). Despite the importance of these forests, best (and most recent) estimates declare that between 1980 and 2001 global areas of mangroves declined 30-50%, and 16% of mangrove species may be facing extinction (Donato et al., 2011; Duncan et al., 2016; FAO, 2007). Furthermore, sea level rise is expected to submerge entire forests by 2115 (Lovelock et al., 2015), which only increases the need for better management and monitoring strategies.

In-situ mangrove monitoring is a challenging task. Because these ecosystems are hard to access, surveying can be costly and time-consuming, but in-situ monitoring is still regarded as an important source of information (see e.g. Moritz-Zimmermann et al. (2002)). Remotely sensed

data provides a complementary source of information and is increasingly being used as such. For example, Lee et al. (2014) found that the Web of Science had more than 8000 indexed studies on mangroves and most of them used some sort of remotely sensed data. Their study also highlights how mangrove research is shifting from fine-scale projects (i.e. in-situ monitoring) to continental and global scale analysis. It is in the latter where remote sensing tools are most useful (see Section 2.5).

Earth observation satellites are excellent remote sensing tools for mangrove monitoring. They consistently *i)* gather information over large areas, *ii)* revisit places on a monthly, weekly, or sometimes even daily basis, and *iii)* use visible and non-visible sections of the electromagnetic spectrum to make quantitative measurements of light interactions with surface features (Chuvieco and Huete, 2010; Yang et al., 2017). Satellites also provide information and insight on spatial extent (e.g. land cover change), distribution (e.g. species), and temporal changes of mangrove forests (e.g. phenology). The collection of this information over decades is what makes satellites an invaluable tool for mangrove monitoring.

Today, more than 300 earth observation satellites from more than 15 countries are operational (Union of Concerned Scientists, 2017). Such satellites are operated by state agencies or private companies and, while many operators provide data at commercial rates, some offer their datasets free-of-charge. For example, the MODIS (Moderate Resolution Imaging Spectroradiometer) and AVHRR (Advanced Very High Resolution Radiometer) archives have been publicly available since 2001 and 1978 respectively. Although these sensors have a high spectral resolution, their spatial resolution (500m and 1.1km respectively) makes them less suitable for mangrove monitoring. In contrast, the Sentinel 2 sensor has a 10 x 10m spatial resolution in the visible and Near Infra-Red (NIR) spectral bands. Despite being publicly available since the instrument was operational in 2015, no peer-reviewed studies to date have used Sentinel 2 imagery for mangrove research. This review, however, will focus on the Landsat (free since 2008) and ASTER archives (Advanced Spaceborne Thermal Emission and Reflection Radiometer, free since 2016). While some studies have used higher spatial or spectral resolution images for mangrove research (see e.g. Heenkenda et al. 2015; Koedsin and Vaiphasa 2013; Kamal and Phinn 2011), imagery from Landsat and ASTER

is still widely used for three main reasons: 1) their worldwide coverage, 2) their archives go back to the 1980's and 1990's respectively, and 3) data is freely available to the public (Wulder et al., 2016).

Since 2000, more than 50 peer-reviewed articles have used Landsat or ASTER imagery to monitor mangroves around the world. Of these, 52% focused on just five countries (Australia, Malaysia, China, Madagascar and Mexico), while only 3% had global extent (see Table 12). The remainder of the studies focused on 19 other countries. Figure 2 shows the countries and territories where mangrove research has been done using freely available imagery from Landsat and ASTER. Only 22 countries have used freely available imagery, indicating that researchers are not taking advantage of this resource. Some of the reasons for this may include: lack of knowledge about the availability of satellite imagery, lack of interest in mangrove ecosystems, financial or data accessibility constraints and limited skills or infrastructure.

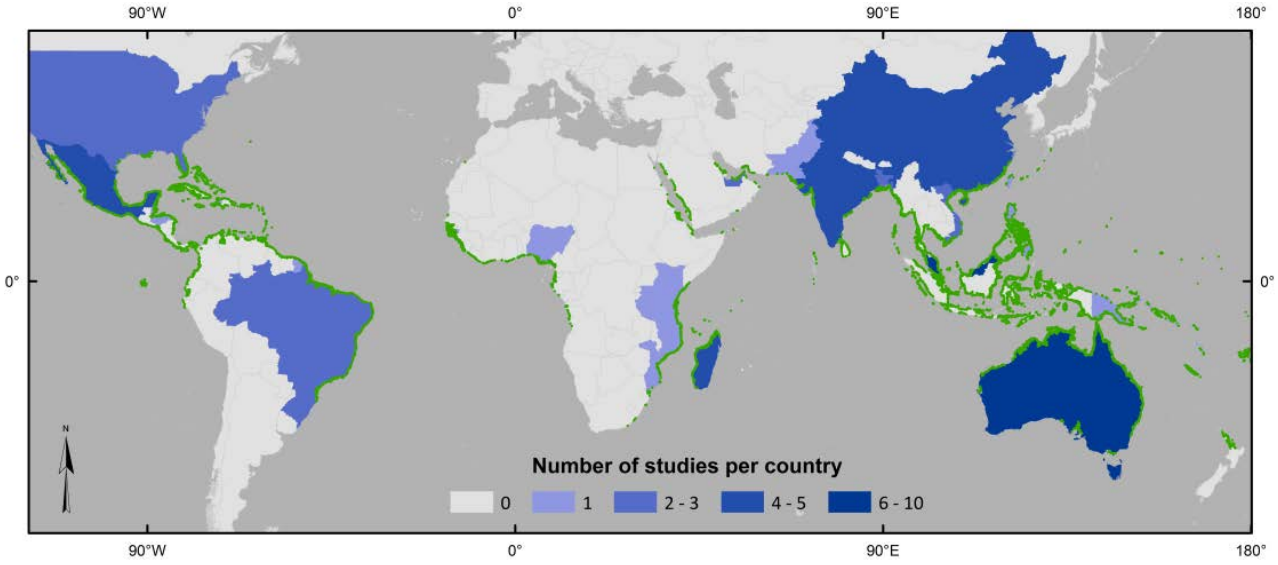

Figure 2: Number of studies per country that used Landsat imagery (2000-2016). Approximately 65% of the studies focused on mangroves in developing countries. Green areas represent the distribution mangrove forests source: Giri et al. (2013a)

This review does not intend to update the results presented by Heumann (2011) or Kuenzer and Bluemel (2011); they provide insightful reviews of methods and sensors commonly used in mangrove research. Here we intend to challenge scientists to take advantage of all available

imagery, processing facilities and datasets. This will result in examining more complex questions (e.g. seasonal and yearly changes, impacts of climate change and sea level rise), instead of focusing primarily on spatial extent.

Changes in the spatial extent of mangroves fail to represent other processes occurring in the ecosystem. Therefore, it is important to combine this information with biophysical variables such as forest density, leaf area index and chlorophyll content to gain a better understanding of how the ecosystem reacts to environmental pressures. Shifting the focus from purely spatial variables to an integrated view of the ecosystem requires additional information. This information may include meteorological, biophysical, field and citizen-collected data in various formats, resolutions and scales. Cleaning, compiling, processing and analysing larger datasets requires more processing power than ever before. Nowadays there are resources available to make this happen such as freely available imagery, enhanced storage and processing facilities (see section 2.5.3).

This review aims to: *i)* understand how researchers are currently using freely available imagery (mainly Landsat and ASTER) to study mangrove forests; *ii)* explore how long-term monitoring adds to our understanding of mangrove ecosystems; and *iii)* emphasize the need for scientists to acquire programming skills. To do this, we will revisit some of the questions being addressed and the time scales used to measure spatiotemporal changes. Next we examine the differences between high and low temporal resolution data, and suggest novel ways to process more information in less time. We then discuss how task automation needs to be incorporated into image processing and analysis and why researchers need to acquire programming skills to move mangrove research forward.

2.4 What are we looking at?

Mapping the natural extent of mangrove forests is required to quantify the services they provide as carbon sinks, fish nurseries and coastal protection (Danielsen et al., 2005; Donato et al., 2011; Lee et al., 2014). Extent mapping is also needed to analyse the threats mangroves face from climate change, deforestation and land use change (Alongi, 2008; Duke et al., 2007; FAO, 2007).

Nowadays, most maps of mangrove forests are derived from remotely sensed information and are used to represent changes in extent and land cover; examples of this are discussed below.

The vast majority of studies use remote sensing technologies to identify mangrove forests and measure their spatial extent. Many methodologies have been developed to discriminate mangrove from non-mangrove vegetation. Chuvieco and Huete (2010) and Lillesand et al. (2015) are only two of the many sources of information that describe how these methodologies work and when they should be applied. This raises the question: do we really need more methods for discriminating mangroves from other land covers? Or is it time to change the scope of research?

2.4.1 Mangroves extent and distribution

In New Zealand, Gao (1999) analysed the distribution of mangroves using SPOT XS, and Landsat TM (TM) images. He found that, despite the coarser spatial resolution, TM images resulted in a more accurate differentiation of mangroves from other land covers. This was attributed to the better spectral resolution of TM images compared to SPOT XS. In 2003, Saito et al., compared SPOT-4 and ASTER imagery of the United Arab Emirates to map mangrove forests. In this case, neither satellite proved better than the other one for delineating the extent mangrove forests, mainly due to their high spectral resolution. In China, Jia et al. (2014) used 25 Landsat images to map mangroves at the country scale. Their main objective was to update the areas presented by a 2001 study. However, they did not explain the methods of the 2001 study and only compared the areal extent of mangrove forests. The aforementioned studies indicate possible drivers of mangrove loss, but failed to analyse or provide further information on such drivers or the reasons behind the changes in mangrove distribution.

Some even more ambitious studies include species discrimination and species zonation. For example, Abdul Aziz et al., (2015) used Landsat imagery to successfully discriminate young and mature *Rhizophora* and *Avicennia-Sonneratia* forests in Malaysia. They used supervised and unsupervised classification methods, followed by segmentation of the spectral signatures of the different mangrove groups to accomplish this. In other ecosystems, using satellite images for genus identification has proven a challenging task (see e.g. Lu et al. (2004)). In mangrove

communities this process is aided by contextual information based on their distribution along estuaries and the tidal profile that leads to well-known zonation between genera (Duke et al., 2006).

Remote sensing has also been combined with other techniques to determine how mangroves change their distribution when their environment changes. The case presented by França et al., (2012) shows how Landsat imagery, paired with sediment cores and pollen analysis, can provide evidence of mangrove encroachment when the environmental conditions change. However, the authors used a single image of the Marajó Island to map the extent of mangroves, which limits the information extracted. To test how sand migration affects the mangrove ecosystem the authors could have used several Landsat or ASTER images to analyse how this process has altered mangrove habitats. With enough images, they could have created a model relating mangrove habitat to the island erosion and accretion rates to further test their hypothesis. These are just a few examples of how remote sensing technologies aid in measuring the spatial extent of mangroves. While methods vary, the result is the same: an impression of the state of the land surface at a given point in time. Conversely, the usage of two or more images of the same area results in the ability to identify changes in the landscape.

2.4.2 Thematic and biophysical variables

Identifying changes in the landscape is an important aspect of mangrove research. By using two or more remotely sensed images from different years, it is possible to identify changes in thematic and biophysical variables. These variables may be categorical or continuous and can be measured directly (e.g. land cover) or through a proxy (e.g. spectral indices). An example of how a biophysical variable may be related to a spectral index is presented by Jean-Baptiste and Jensen (2006). They used ASTER imagery to correlate in-situ measurements of canopy closure and leaf area index (LAI) with the Normalized Difference Vegetation Index (NDVI) and the Soil Adjusted Vegetation Index (SAVI). The authors found that both biophysical variables were highly correlated with the spectral indices. The main drawback of this study is the use of a single image. This provides limited results and fails to demonstrate if established relationship with the spectral indices holds true over space

or time. By using additional images, their relationships between spectral indices and biophysical variables may have been tested on different dates or study sites.

Raha et al. (2012), on the other hand, used six remotely sensed images to directly measure shoreline configuration (i.e. a thematic variable) in the Sundarbans. They found that the above-ground mangroves biomass is related to the accretion and erosion of the islands in the region. By using six satellite images, they were able to demonstrate how mangrove forests are transformed over time and the impacts this has on the ecosystem. Almost every mangrove forest around the world has been transformed in some way or another, and identifying these changes plays an important role in mangrove research.

2.4.3 Change detection

The ability to detect changes in the landscape depends mainly on the area affected and the resolution of the sensor being used. When using moderate spatial resolution sensors such as Landsat or ASTER, widespread events (e.g. defoliation) are often evident, while localized changes are difficult to detect. In eastern Africa for example, Ferreira et al., (2009) found that selective cutting and logging in the Kenya-Mozambique border cannot be detected at the pixel level using Landsat imagery due to its resolution (30 x 30 m). Importantly, the authors used methods aimed at detecting land cover changes (i.e. unsupervised classification), although sub-pixel analysis may have yielded a different result. Despite this, they did manage to quantify gains and losses when comparing images from 1995 and 2005. The losses were mostly attributed to the construction of aquaculture ponds and urban expansion, which are often bigger than a pixel and have different spectral signatures to mangroves.

Aquaculture expansion and coastal development are a threat to mangrove forests. Chen et al., (2013) and Béland et al., (2006) assessed land cover changes in Honduras and Vietnam using satellite images from the 1980s, 1990s and 2000s for their assessments. Not surprisingly, both studies correlated aquaculture expansion with mangrove loss. Despite this, some limitations need to be mentioned: *i)* both studies used images taken more than six years apart, resulting in high uncertainty and limited ability to identify other sources for land cover change; *ii)* the influence of

extreme weather events (e.g. hurricane Mitch in 1998 and typhoon Linda in 1997) is overlooked as a source of mangroves loss; and *iii)* patches of mangrove forests may have been concealed by the tidal height, or water in the ponds, which adds to the overall uncertainty in the results of these studies. The examples presented in this section show how mangrove research has been conducted thus far: focusing in the extent of mangroves and overlooking other physical variables that may influence the extent of the forests shown in satellite images.

In general, there is an abundance of studies that focus on mapping mangroves forest extent (for excellent reviews refer to Kuenzer et al. (2011) and Heumann (2011)). To map and discriminate mangroves, several image classification methodologies have been developed (e.g. object-based, pixel based, artificial neural networks). However, most studies focus on the spatial extent of mangroves, and only the location between studies seems to change. Giri et al. (2013a) and Spalding et al. (1997) have already mapped mangroves on a planetary scale, and we should leverage this information to contribute to mangrove research. Examples of knowledge gaps include: *i)* the identification of phenological changes that have occurred over past decades in mangrove ecosystems; and *ii)* how resilient are mangrove ecosystems today, compared to 30 years ago. But more importantly, we still need to determine if the tidal height, at the time of image acquisition, affects the spectral signature of mangroves. The latter is important because areas of mangrove forests may have been routinely underestimated due to the proportion of water in a pixel may influence how it is classified (see Section 2.4). Furthermore, we need to determine if the spectral bands commonly used to identify mangroves (e.g. NIR) are affected by water in the background, and the magnitude of these effects.

2.4.4 Data gaps and future research

Mangrove studies cover a wide range of topics that certainly need to be addressed; most focus their attention on changes in area, land use and land cover. However, the influence of water under the canopy (i.e. tidal height) and how it alters the spectral signature of mangroves has yet to be fully studied. Some evidence suggests that the tidal height at the time the satellite images were taken might influence mangrove classification (Adam et al., 2010; Akumu et al., 2010a; Giri et al.,

2007). If the spectral signature of mangroves indeed changes with the tidal height, mangrove classification methods and current estimates of mangrove areas would have to be revised.

To understand why this happens, we have to look into the structure of the leaves and the forest. Firstly, in the cellular structure of the leaves, the mesophyll cell layer and its internal cavities scatter the incidental light and reflect the 700 – 1100 nanometre region of the spectrum (i.e. the NIR region; Chuvieco and Huete, 2010). Secondly, from the viewpoint of a satellite, the forest structure is comprised of groups and stacks of leaves that form the canopies of trees. When leaves are stacked they reduce the backscatter of light and contribute to the overall reflected radiation; in other words, the denser the canopy, the more reflected light. In contrast, single leaves allow approximately 40% of the incident radiation to be transmitted through their structure and into the background (See, Figure 3, Dawson et al., 1998). Water is known to absorb most incident light, including the NIR and SWIR regions. During high tide, water floods the mangroves and the light that is transmitted to the background depends on the canopy density. As shown in Figure 3, when light hits a single leaf, some energy is reflected and some is transmitted; the latter is finally absorbed by the water. This scenario is common in the fringes of the forest, river margins and beaches, where canopies have a low density. Conversely, in places with denser canopies, leaves can stack and reflect more light. These differences can have a significant impact on how researchers interpret the information of a satellite image, for example when measuring the spatial extent of mangroves.

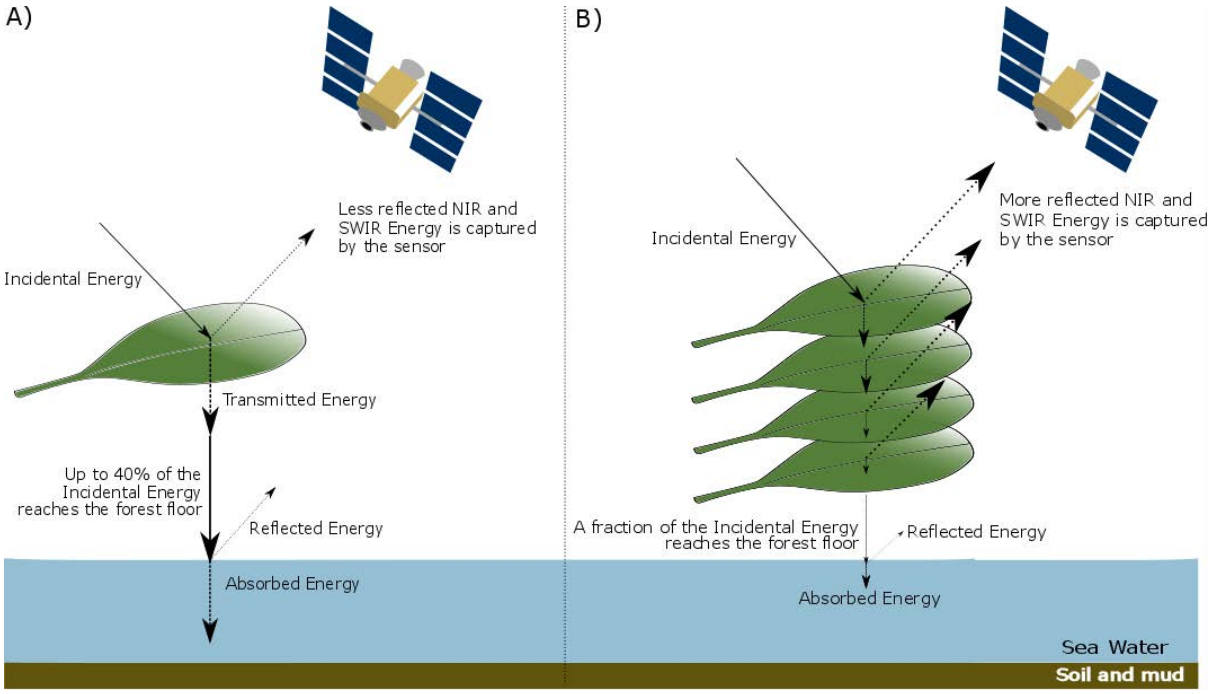

Figure 3: Interaction of electromagnetic energy with a single leaf (A) and a stack of leaves (B) (Adapted from Jong and Van der Meer, 2001, p. 118*). The higher the number of stacked leaves, the greater the NIR and SWIR energy captured by the sensor.*

Evidence that tidal height and canopy density affects the spectral signature of mangroves is presented by Saito et al. (2003). They showed abrupt declines in the NIR and SWIR spectral bands when images of *Avicennia* mangroves were taken during high tide, when compared to low tide. Although the authors do not investigate this issue further, this confirms that water in the background alters the spectral signatures of mangrove forests. A representation of how this happens is shown in Figure 4.

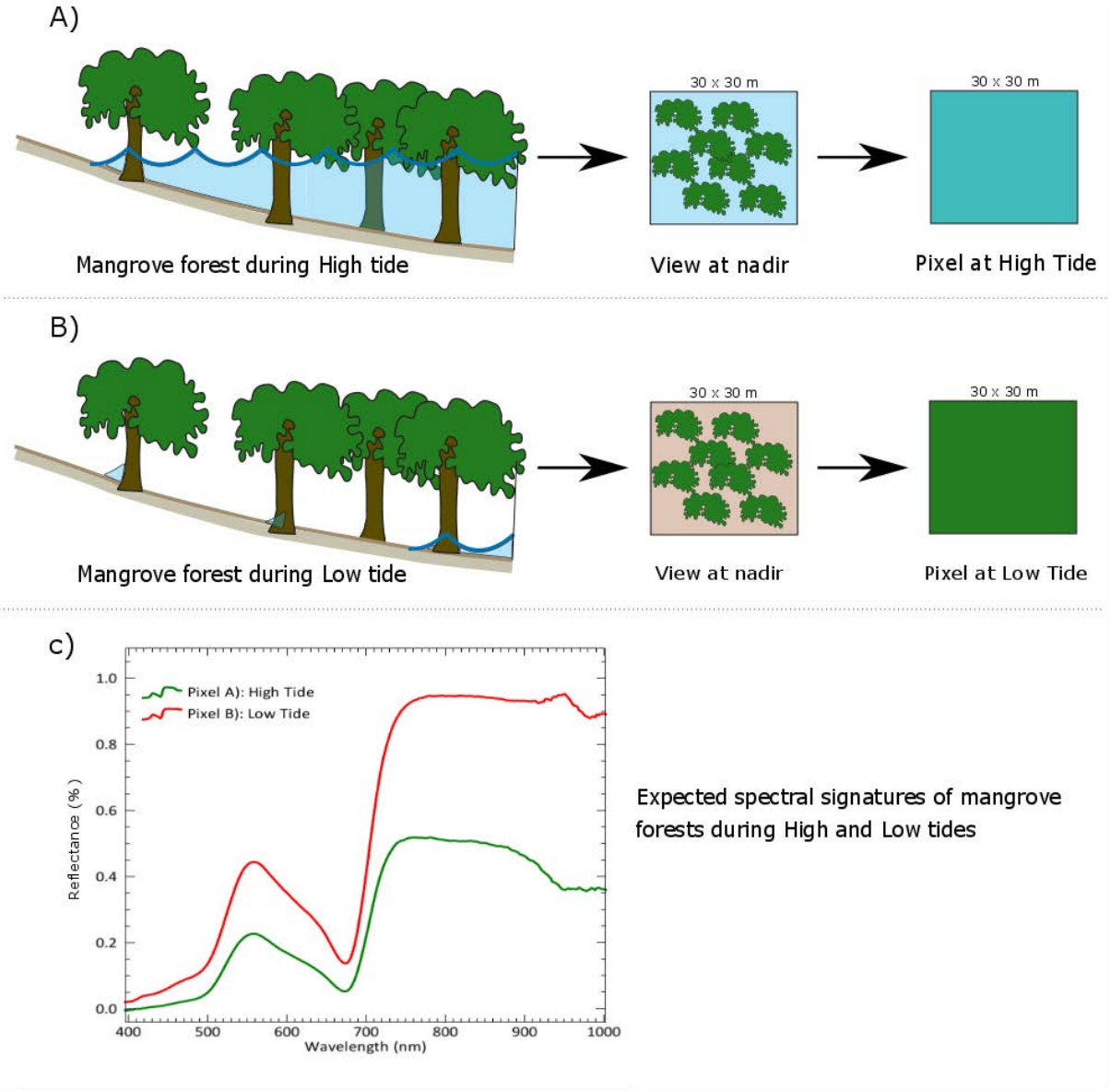

Figure 4: Conceptual figure of mangroves at high and low tides. Panel A) simulates a Landsat pixel of a mangrove forests during high tide. Here, the water in the background absorbs the NIR and the forest canopy reflects it lowering the reflectance of the pixel in all wavelengths. Panel B) simulates the same pixel during low tide; overall, more radiation is reflected in this scenario across all wavelengths. Panel C) compares the spectral signature of pixels A) and B)

This lack of understanding about how water affects the spectral signature of mangroves is a critical gap that needs further research due to the impact that it may have on the overall areas classified as 'mangroves' (Vo et al., 2013). For example, Li et al. (2013), found discrepancies in surveyed and Landsat-derived areas of mangroves in southern China. They attribute (yet do not quantify the

magnitude of) these differences to *i)* varying tidal heights in the images and during surveys; *ii)* errors in field measurements and *iii)* time gaps between imagery and surveys. All of these factors alter the classification of mangrove forests and highlight the need for a standardized way of measuring these forests, irrespective of the tidal height.

In an attempt to address this, Zhang and Tian (2013) created a Mangrove Recognition Index that includes images taken at high and low tides. The authors argue that during high tides there is a sharp decline in the spectral reflectance of mangroves, especially in the NIR and SWIR regions. While the authors state that this decline is a key element in the discrimination of mangrove from non-mangrove vegetation, they offer no explanation as to why this phenomena happens. Although the paper uses two images to discriminate mangroves at high and low tide, it fails to quantitatively address the effects of tidal height for individual spectral bands. The research would have been more relevant if a correction method (i.e. numerical relationship) for specific spectral bands had been proposed. Despite the efforts of these researchers, this index has yet to be independently tested and validated.

In summary, there are many methodologies for mangrove classification, but none consider the tidal influences. This means that biophysical and thematic variables are likely to be affected, especially in areas with big tidal fluctuations. Likewise, the thematic and biophysical changes previously identified would have to be revised. Once we account for these variations we can apply this knowledge to identifying long term changes in mangrove forests, their causes and more accurate estimates of carbon stocks (Giri, 2016; Loveland and Dwyer, 2012).

2.5 The need for long-term mangroves monitoring

2.5.1 Bi-temporal and multi-temporal analysis

The ability of satellites to systematically gather information of a given place over long periods of time makes them a valuable tool for identifying disturbances in the landscape (Loveland and Dwyer, 2012). One of the main uses of remotely sensed images has been bi-temporal analysis. Bi-temporal analysis uses two images to describe the changes in spectral or thematic characteristics

of a given environment (Hansen and Loveland, 2012). While common and simple to implement, this approach has serious limitations as it fails to describe stochastic (e.g. fire), cyclical (e.g. phenology) or long-term trends in the environment. Likewise, signal-to-noise ratios, cloud coverage and shadows may affect the interpretation of the results.

In contrast, multi-temporal analysis uses several images (often dozens) to describe not only trends in the environment, but also cyclical changes and feedback phenomena (Kennedy et al., 2014). This is where the millions of images captured by the Landsat and ASTER satellites have the potential to play a pivotal role in mangrove research. However, having the information available does not mean it is being used, and mangrove scientists are not yet fully exploiting the Landsat and ASTER archives to explore long-term changes in these fragile ecosystems.

Multi-temporal analysis is not without its challenges, one of them being (mis)registration of pixels during the calibration and validation stages of the analysis. In medium (e.g. Landsat) and coarse resolution images (e.g. MODIS) pixel alignment is key to ensure that one is tracking a single piece of land over time. Multi temporal analyses need to consider the georegistration errors inherent to the methods used, and resolution of the imagery (Claverie et al., 2018). In the best scenario, Landsat images could be up to 15m off target, while MODIS images could be off by hundreds of meters. These errors could be additive or multiplicative over time, depending on the ecosystem being examined, the number of images used, the availability of field data for validation, and the knowledge of the study site by the research team.

Here, we looked at 55 peer-reviewed journal articles published between 2001 and 2016 that used Landsat or ASTER images to map or monitor mangrove forests. Approximately 1900 satellites images were used, but most studies used three images 7 – 11 years apart (see Table 12 in Appendix 1). From 2001 to 2008, 21 studies were published and about 143 images were used, while between 2009 and 2016, more than 1700 images were used. Until 2008, budget constraints for image acquisition was a common constraint for using satellite images but, when the Landsat archive was made public a surge in their use was evident (Loveland and Dwyer, 2012; Wulder et al., 2012). This milestone has been fundamental for mangrove forest research because during and

after 2008 the total number of images used to monitor these ecosystems increased by a factor of ten (see Figure 5).

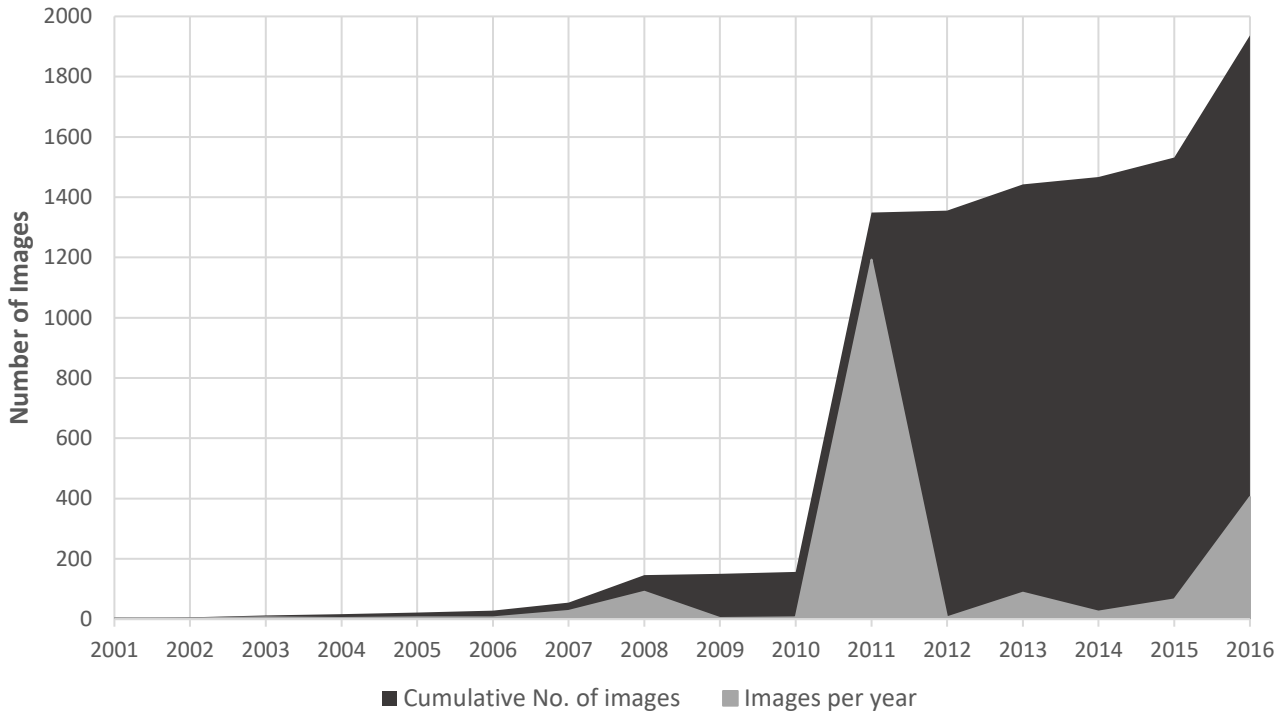

Figure 5: Cumulative number of images per year.

Monitoring mangrove forests, however, often focuses on the areal extent, rather than on long-term monitoring. After 2008 several papers had study areas larger than the footprints of a single satellite image, and hence required more images to cover their study sites. For example, Jia et al. (2014) used 25 images to map mangroves in China while Giri et al. (2011) used more than 1000 images to map mangroves worldwide. Despite the increase in the use of satellite images, most studies still use fewer than ten images (see Figure 6). This means that the full potential for the image archives is yet to be unlocked.

Recently, researchers have shown interest in using high temporal resolution data to examine how different mangrove traits change over time. For instance, Nardin et al. (2016) and (Asbridge et al.,

2016), explored canopy expansion dynamics, Zhang et al. (2016) focused on phenology and Li et al. (2013) on fragmentation. This focus shift, from forest extent to forest dynamics, is much welcomed and we expect the trend to continue.

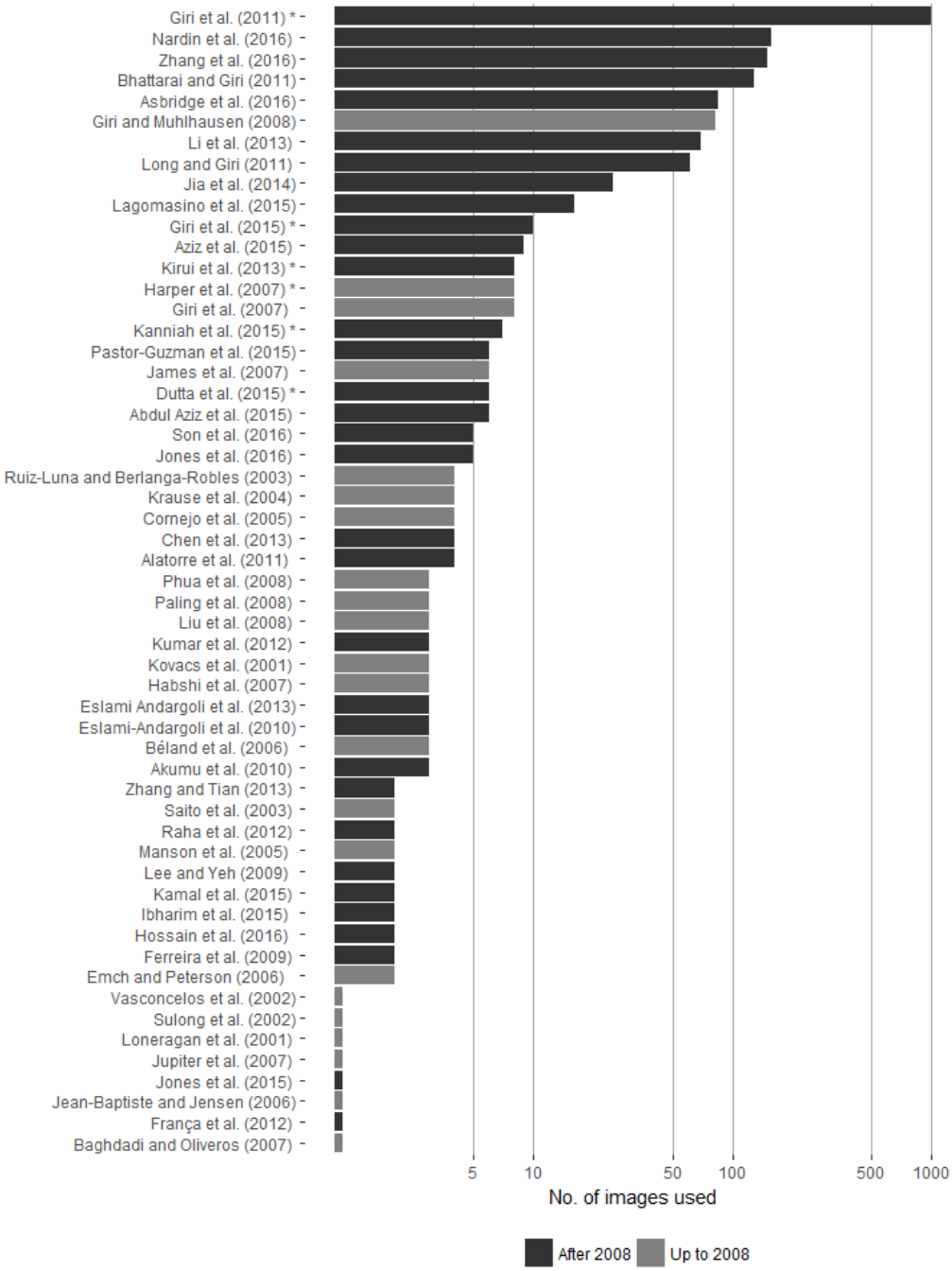

*Figure 6: Number of Landsat, ASTER images used to study mangroves since 2001. *Number of images not explicitly reported.*

2.5.2 Long-term monitoring of mangrove forests

To assess the risk of hypertension in their patients, doctors often take several blood pressure measurements in a single day. Similarly, high temporal resolution data enables a better understanding of the processes acting on an ecosystem. Long-term monitoring should be understood as systematically observing land surface dynamics using temporally dense information over a set period of time (Kuenzer et al., 2015; Lindenmayer et al., 2012). The applications of long-term monitoring range from carbon budget modelling to estimating crop yields and ecosystem management. Ultimately, the goals of long-term studies should be to support evidence-based policy decisions, and to understand the complex relationships taking place in mangrove forests.

An example of a long-term study that used high temporal resolution data of mangrove ecosystems is presented by Zhang et al. (2016). They used 150 Landsat images of southern Florida taken between 1985 and 2011 to analyse how chilling events and hurricanes affected mangrove trees. They found that shorter mangroves suffered more damage from chilling events, while taller mangroves were subject to more damage from hurricanes. They concluded that mangroves can take up to seven months to reach the lowest vegetation condition, and up to six years to fully recover after an extreme event. The case presented by Zhang et al. (2016) is relevant for two main reasons: it is a long-term study, and it uses high temporal resolution data. The former is related to the 27-year monitoring period that incorporated not only satellite imagery, but also meteorological information (i.e. temperature, humidity) and extreme weather events. The temporal resolution refers to using more than five images per year.

Going from two images per decade to five per year represents a paradigm shift in mangrove research. Long-term monitoring studies will become the new norm and regular change detection studies will become obsolete, as more images are collected and processing capabilities increase.

This is fundamental for mangrove forests, especially because this information can be further used to model how mangroves adapt to changing environmental conditions, or to value ecosystem services over time. Additionally, this opens the door to phenological research in mangrove forests.

Phenology is related to seasonal cycles of fruiting, flowering, rainfall, temperature and other factors. In mangrove ecosystems, it has been thoroughly studied in-situ, without the use of remotely sensed data (Duke et al., 2006). The spatial arrangement of mangrove forests makes them ideal targets for long-term monitoring using remote sensors. While some species can tolerate high concentrations of salt and frequent inundations, others prefer upriver locations and infrequent wetting (Duke et al., 2006). Changes in the spectral signatures and spatial configuration (or other properties) of mangroves may reveal alterations in ecological processes (Kennedy et al., 2014; Lewis III et al., 2016). For example, seasonality, disturbances and recovering ecosystems may show cyclical, abrupt decreases and steady increases respectively in the value of a given property (Figure 7). If these changes are to be noted, an adequate number of observations (i.e. satellite images) is needed (Figure 8). The ability to detect subtle or abrupt changes in mangroves can mean the difference between and timely response and a massive dieback.

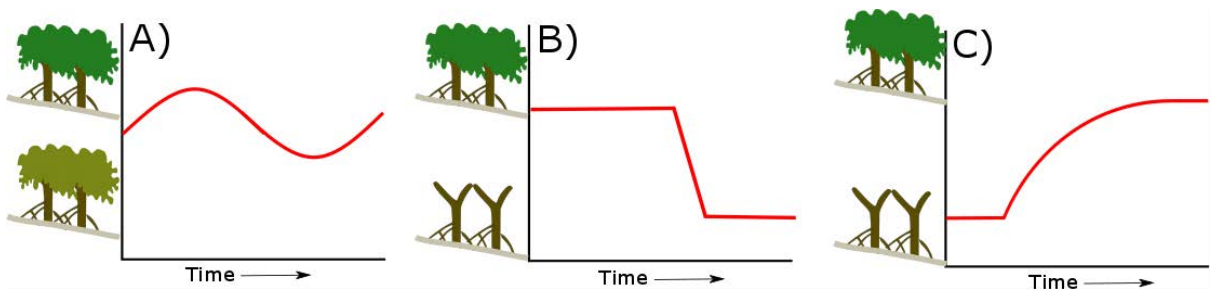

Figure 7: Conceptual diagrams of different processes in mangrove forests (adapted from Kennedy et al. (2014); Lewis III et al. (2016). Here, a mangrove ecosystem shows (A) cyclical phenological changes, (B) an abrupt disturbance and (C) a recovering phase.

The real power of remotely sensed data is that it can be traced over time at the pixel level. In north-eastern United States, for example, Zhu and Woodcock (2014) monitored land cover changes in deciduous and conifer forests using 519 Landsat images over 30 years. By using

approximately 519 observations per pixel, they established a range of values in which healthy forests should fluctuate. If an observation was outside the expected range, then the forest had changed. This method enabled them to pinpoint *when* change had occurred and measure the magnitude, frequency and intensity of that change. While this algorithm seems to be useful in detecting changes across a range of land cover classes, it has yet to be tested in mangrove forests. This would represent a challenge because of tidal variations and the corresponding changes in the spectral reflectance of mangroves. Furthermore, high numbers of false changes may arise when the algorithm classifies pixels as 'mangrove', then as 'water' and back to 'mangrove' due to changing tides.

The algorithm developed by Zhu and Woodcock (2014) used surface reflectance values as the main input, but spectral indices (e.g. NDVI) or other variables may be used. This approach was shown during the development of the algorithm (Zhu et al., 2012). Regardless of the variable, it is evident that the number of observations is of critical importance, although this may require additional processing and storage facilities (Yuan et al., 2015). To represent the importance of time density in the data, Figure 8 illustrates how an insufficient number of observations may lead to incorrect interpretation of remotely sensed information. Here, the measured variable (i.e. pixel value) changes over time and, to detect these changes, the correct number of observations (i.e. satellite images) is crucial. Panels A), B), C) and D) display changes in state, amplitude, frequency and trend of a measured variable. Too few observations lead to incorrect interpretations of the variable behaviour over time; in this case, the interpretation is that there is no change over time. In contrast, having temporally dense information provides the researcher with a more accurate perspective of the range, frequency and amplitude of a variable before and after a change. Just like doctors assessing hypertension in patients, mangrove research could benefit from having long term, temporally dense information from the Landsat and ASTER archives. Despite this, cloud cover and shadows still pose a significant challenge.

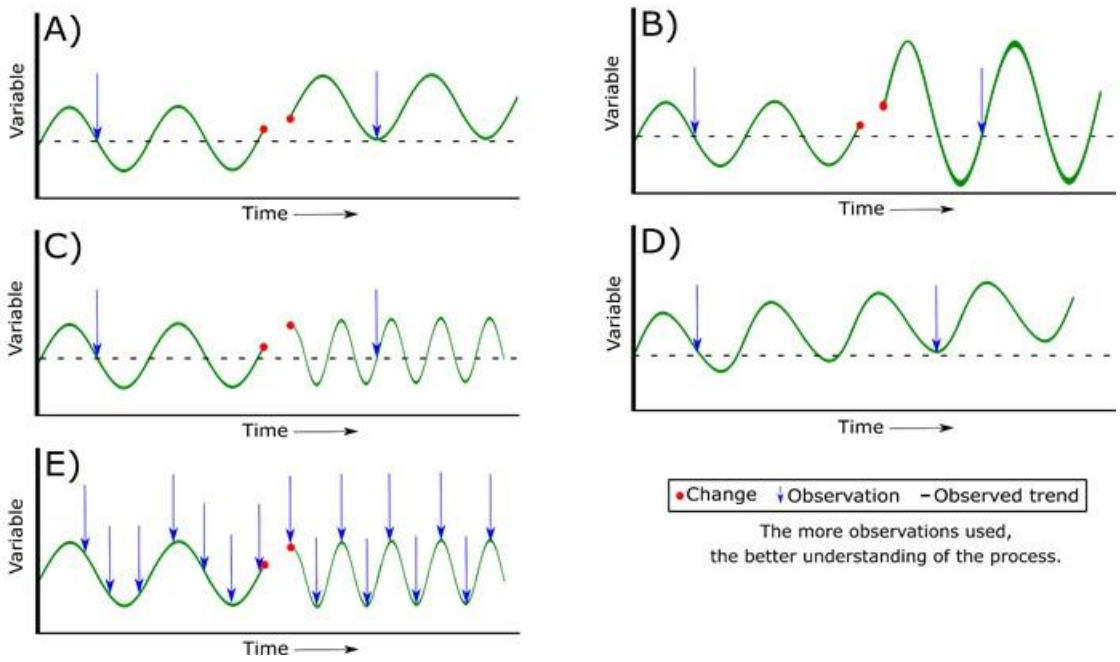

Figure 8: Change of (A) state, (B) amplitude, (C) frequency and (D) long-term trend in a variable (i.e. pixel value). The number of observations (E) allows the correct identification of the processes acting in the ecosystem (conceptual diagram, adapted from Zhu and Woodcock (2014) and Kennedy et al. (2014)*)*

Cloud cover and shadows are well-documented challenges when using satellite images (Abrams et al., 2015; Kuenzer et al., 2011; Wulder et al., 2016). Researchers usually resort to cloud-free data, regardless of the sensor, number of images or the location but this trend is changing in favour of using pixel-by-pixel observations. According to Zhu and Woodcock (2014), by discarding pixels flagged as clouds or shadows, the remainder of the pixels are used as valid observations. This also applies to gap lines in Landsat 7 images with the Scan Line Corrector off (SLC-off); the gaps are treated as masked pixels. The ability to extract information from every image is important because SLC-off images are rarely used. By enabling the usage of SLC-off images, the signal-to-noise ratio is reduced, and the number of usable images rises, resulting in more usable information and better assessment of the ecosystem.

Long-term monitoring of mangroves faces another challenge: spatial coverage. Sensors have collected different numbers of images for different geographical locations. For example, while the continental United States, Europe, Australia have more than 800 images in the Landsat archive, Africa, wester Asia, and Central America often have less than 400. The disparity of available images

makes every usable pixel very valuable, especially when there are clouded images over mangrove forests in countries with relatively few images. To overcome these limitations, researchers have various tools available that may enable the use of the whole Landsat archive for mangrove monitoring (see e.g. Braaten et al. (2015); Frantz et al. (2015); Goodwin et al. (2013); Zhe Zhu and Woodcock (2014)).

Despite our ability to use all available Landsat images, challenges remain. Selecting and validating time series methods and results depends on the environmental conditions of the study site as well as on the preferences of the researchers (Roy et al., 2015). Finally, the wealth of data required for (and generated by) long-term studies is often difficult to gather, store and process. Therefore, to unleash all the potential lying in the Landsat and ASTER archives, researchers need to take advantage of all available technology.

2.5.3 Available technologies for long-term mangrove monitoring

Most studies use images 7-11 years apart from one another (see Table 12), making it difficult to assess subtle or ongoing changes in mangrove ecosystems due to noise and low temporal resolution of the data (Kennedy et al., 2010; Zhu et al., 2012). To better understand how the ecosystem reacts to different environmental conditions (e.g. precipitation, temperature, nutrient loads), full use of the Landsat, ASTER and Sentinel 2 archives is required. This implies large dataset acquisition, storage, and processing, which are the most urgent challenges to be addressed if long-term ecosystem monitoring is to be implemented (Yang et al., 2017).

With all data available, the next challenge is the time and infrastructure required for image processing and information extraction. It is true that not all researchers have the computing power to acquire and manipulate the vast amounts of information that this represents (Wulder and Coops, 2014). Despite this, we think that long-term monitoring of mangrove forests needs to be prioritized, and thus we present some alternatives to overcome acquisition, storage and processing limitations:

Google Earth Engine (GEE, https://earthengine.google.com/) is an online platform that may be used by public and private organizations to store, process and make visualizations of large geospatial datasets. Users can upload their own images and algorithms, but GEE also features its own database of earth imagery (e.g. Landsat), processed data (e.g. Digital Elevation Models), climate, and demographic datasets (Google, 2015). All datasets and algorithms are available for approved users. While access to GEE is free, every application goes through an evaluation process and not every application is accepted. This may be due to high demand for free processing capabilities or because GEE requires research to be at a global scale. Examples of the capabilities of GEE include mapping the expansion of oil palm plantations (Lee et al., 2016) and urban settlements (Patel et al., 2015) and quantifying changes in the world's forests (Hansen et al., 2013). In mangrove research, (Giri et al., 2015) used the GEE to assess mangrove changes in Pakistan, India and Bangladesh between 1973 and 2011, but we have yet to see more uses of this platform.

Amazon Web Services (AWS, https://aws.amazon.com/) and Microsoft Azure (MA, https://azure.microsoft.com/) provide storage, processing and visualization capabilities in paid and free subscription schemes. Both services provide access to ESRI ArcGIS, provided that the user already has an active licence to run said program. ESRI has its own cloud processing platform (ArcGIS Online, https://www.arcgis.com/) that allows users to upload, process and share geospatial information using their proprietary software.

In contrast to the previous examples, the Australian Geoscience Data Cube (AGDC, http://www.datacube.org.au/) and NASA Earth Exchange (NEX, https://nex.nasa.gov/nex/) are not led by private organizations. They are government-led initiatives that provide scientists with geospatial information, algorithms and High Performance Computing (HPC) capabilities. The AGDC is hosted at the National Computing Infrastructure facility at the Australian National University (Lewis et al., 2016), and provides specialty imaging and visualization tools to its users (NCI, 2015). Likewise, the NEX platform also offers supercomputing facilities, data, algorithms and downscaled climate models to its users. Although the NEX is restricted to researchers and institutions affiliated with NASA, users can take advantage of NASA's datasets, processing algorithms and HPC facilities.

A comparison between services is presented in Table 1, but these are just a few examples. We encourage readers to look also at EarthCube (https://earthcube.org/), UCAR Unidata (http://www.unidata.ucar.edu/), European Space Agency (ESA) Grid Processing on Demand (G-POD) for Earth Observation Applications (http://gpod.eo.esa.int/) and EarthServer (http://earthserver.eu/), all of which provide varying cloud computing services for geospatial analysis. There is also one free tool specifically developed for Time Series visualization: NASA's GIOVANNI (https://giovanni.gsfc.nasa.gov/giovanni/). Despite the fact that GIOVANNI is heavily focused on atmospheric measurements, it has strong statistical and visualization tools that provide long-term data to the user.

	Google Earth Engine	NASA Earth Exchange	Australian Geoscience Data Cube	Microsoft Azure	Amazon Web Services	ArcGIS Online
HPC Capabilities	🟢	🟢	🟢	🟢	🟢	🟢
Data Storage	🟢	🟢	🟢	🟢	🟢	🟢
Preloaded Satellite Imagery	🟢	🟢	🟢	🔴	🟢	🟢
Preloaded Algorithms	🟢	🟢	🟢	🔴	🔴	🟡
Free to Access	🟢	🟢	🟢	🔴	🔴	🔴
Access Subject to Project Approval	🟡	🟡	🟡	🔴	🔴	🔴
Requires Programming Skills to Use	🟡	🟡	🟡	🟡	🟡	🟢
Provide Own Visualization Tools	🟢	🟢	🟢	🔴	🔴	🟢
Supports paid Third-Party Visualization tools.	🔴	🔴	🔴	🟢	🟢	🔴
Provide ready-to-use products (e.g. NDVI) or algorithms	🟢	🟢	🟢	🔴	🔴	🟢
User can Upload Own Imagery	🟢	🟢	🟢	🟢	🟢	🟢
User can upload/develop processing algorithms	🟢	🟢	🟢	🟢	🟢	🟢

Table 1: Comparison of available HPC resources for long-term mangrove monitoring. Symbol colour represent: Green = yes; Yellow = depends on the project; Red = no.

Although it is not the aim of this review to provide an in-depth explanation of how these platforms work, here we briefly mention four clear advantages over traditional ways of processing geospatial information (for more information see e.g. Yang et al. (2017), (2013)):

i. **Scalability**: these platforms are made to handle increasingly higher loads of data. The end user does not need to worry about expanding or upgrading memory, processors or storage because the service provider will do this as necessary.

ii. **Reliability, redundancy and maintenance**: service providers have processing and storage facilities located around the globe: if one fails, there are a number of backups that ensure processing continues (redundancy) without losing data (reliability). Also, software and hardware maintenance reduces crashes or malfunctions on the platform, allowing for peak performance and better service.

iii. **Data sharing, discovery and exchange (collaboration**): one single dataset can be used by several teams, agencies or organizations. Instead of making each research team acquire the information, it can easily be shared; this saves time and effort that can be invested in *using* the information. This applies not only to datasets but to algorithms and scripts. This is important because it makes methods reproducible by different groups.

iv. **Pay-as-you-go**: paid services charge only by amount of data processed or the time spent using the resources. Considering that 184,500 Landsat images can be processed in eight hours (Mueller et al., 2016) and some services are free-of-charge, these platforms are even more appealing.

All this means that mangrove research can process virtually unlimited amounts of data, in shorter times, for free and without data or service loss. Potential uses of these resources include near real time monitoring of land cover changes, carbon stocks and others.

In summary, future mangrove research needs to embrace cloud-computing services. They not only provide data, storage, processing and algorithms, but also enable large-scale and long-term mangrove research in an efficient, cost-effective way. Giri et al. (2013b) and Wulder and Coops (2014) have motivated researchers to use these services, but one obstacle remains: the lack of programming skills. Without them, researchers depend on manually acquiring, correcting and processing imagery, thereby limiting the spatial and temporal extent of their studies as well as the depth of questions being addressed. Once image processing is dealt with, researchers must analyse the data and, if done manually, results may be limited and superficial. Automating data analysis opens the door for continental and long term studies (see e.g. (Gill et al., 2017; Olofsson et al., 2016; Vogelmann et al., 2016a)

2.6 The need for automation: challenges and opportunities

The lack of adequate computing power is one of the main reasons cited as to why researchers are using few images, however this is changing (Giri, 2016; Wulder and Coops, 2014). We certainly

agree with Giri (2016) and Granell et al. (2016) when they state that earth observation research needs to be taken to the next level. This means using cloud computing and ever-growing data repositories, using and re-using geospatial and environmental data products and, ultimately, harnessing the capabilities of platforms like AGDC and GEE. Technology enables researchers to allocate time to data analysis, rather than to processing by automatically doing the hard work.

Labour-intensive, time-consuming tasks that require immediate action can be automated. Examples of this can be seen in stock trading (Teixeira and de Oliveira, 2010), face recognition (Jenkins and Burton, 2008) and other applications. This has also been done in earth observation applications. Researchers have been able to automate algorithms to achieve different ends. For instance, Kuleli et al. (2011) delineated shorelines of several Turkish wetlands, Barrett and Frazier (2016) linked reflectance to water quality values, while Selkowitz and Forster (2016) mapped permanent ice and snow cover over the western United States. These and many other studies automated the image pre-processing stages, cloud or water masking, index generation, thresholding and map creation, all of which are fairly straightforward but time-consuming. Despite these goals being achieved, there is room for improvement. Once an algorithm is developed, hundreds of images can automatically be downloaded and processed, greater areas can be analysed, and the process can be replicated in other ecosystems.

In mangrove forests, few authors have reported task automation. Some exceptions include Zhang et al. (2016), for instance, who automatically calculated four spectral indices (NDVIS, SAVI, EVI, NDMI) for more than 140 Landsat images through South Florida. Heenkenda et al. (2014) automated the image classification of aerial photographs and WorldView-2 imagery to distinguish mangrove species from other vegetation. Similarly, Giri and Muhlhausen (2008) used a semiautomatic technique to monitor mangrove changes in Madagascar. This shortage of examples is a reflection of the need for researchers to automate tasks if better and more complex questions are to be addressed in the near future. The use of automatic processing algorithms represents the biggest opportunity for mangrove research but, to use them, researchers need programming skills.

2.6.1 Automation requires skills

Environmental and remote sensing sciences need to leverage all technological advances, including programming (Vitolo et al., 2015). Programming has been deemed as an essential skill for the 21st century, just as important as reading or writing (Paul, 2016; Vee, 2013). However, the lack of programming skills is hampering our ability to answer complicated questions related to mangrove ecosystems. For example, we need to know more about mangrove phenology at the landscape scale, and how they respond to varying nutrient, temperature and sea level changes. Satellites generate enough information to answer these questions, but to do this we need to automate as many tasks as possible.

Automating image processing is on the rise and it can save 50-60% of the time spent on a project (Giri, 2016). The ability to sub-divide the acquisition, processing and analysis of remotely sensed data into smaller, simpler tasks that a computer can do should not require a software engineer (Paul, 2016; Wing, 2008). Scientists should be able to read and write code to make their work easier and faster.

Researchers have been developing scripts in R, Matlab, Python and other programming languages for statistical analysis and to solve complex mathematical problems (Vitolo et al., 2015). Then why are so few studies undertaking long-term projects on the dynamics of mangrove ecosystems? Reasons may differ, but some that arise from this review are *the* potential lack of knowledge of available resources and a lack of programming skills. The latter is a gap that needs urgent attention.

There are many reasons to acquire programming skills. Here we summarize some of the most important ones when related to mangrove research:

i. Fully using available computing capabilities. Be it a desktop, laptop or supercomputer, researchers often use only a small part of the processing capabilities of their machines (e.g. for word processing, and some statistical analysis). Modern computers have resources that could be used more intensively. Instead of turning off the computer during weekends or nights, researchers could automate repetitive and analytical work and dedicate their working hours to interpretation and communication of their results.

ii. Iteration over big datasets can be tedious or even impossible if done manually. Processing and analysing hundreds of images of the Landsat or ASTER archives could be done in days or weeks if automated and provide much needed information to scientists, land managers and policymakers. Considering that often data comes in different formats (e.g. images, reports, and social media) and is always growing, it becomes increasingly important to process it more efficiently. However, this is only achieved by task automation (or a very large workforce).

iii. Computational thinking and problem-solving skills go hand in hand, and many argue that programming gives researchers the ability to dissect a big problem into smaller, simpler pieces (Paul, 2016; Wing, 2008). Solving smaller problems is easier and faster than solving a single, more complex problem. Similarly, programming simple instructions is easier than creating complicated code.

We also argue that scientists should be able to create their own scripts (i.e. pieces of code that automate a task) to understand *what* the script does and *why it does it*. If researchers blindly trust the code of another person (i.e. a "black box"), confidence in the results may be greatly diminished. Researchers need to understand, correct and adapt scripts to fit their purpose, as well as audit external code for two main reasons:

1. Quality control prevents incorrect methods and results to be spread out, and entitles the researcher to make corrections. Petre and Wilson (2014) explored the benefits of the code reviewing process by involving professional software developers and scientists who had used their coding knowledge to solve a problem. The former reviewed the scripts of the latter. The authors found four main reasons for scientists to engage in code review practices, which are summarized in Figure 9.

2. Data and computer scientists have the skills to automate tasks, process information and interpret results. Because putting information into an ecological context is only a fraction of the overall workload, mangrove scientists risk being left out. In other words, the smaller the contribution of mangrove scientists, the less they will be invited to collaborate in research. The Landsat and ASTER archives house more than 5 and 2.8 million images respectively (Abrams et al., 2015; Wulder et al., 2016). Furthermore, with Sentinel 2A in orbit and Sentinel 2B expected to start operating in 2017, there is the potential to access

information up to nine times per month from medium and high spatial resolution sources. This does not include low spatial resolution sensors (e.g. MODIS), which are also freely available to users. This means that mangrove researchers need to update their skillsets or they risk becoming obsolete or irrelevant. Preventing this from happening is not easy, but it is simple: learn to code and share your code.

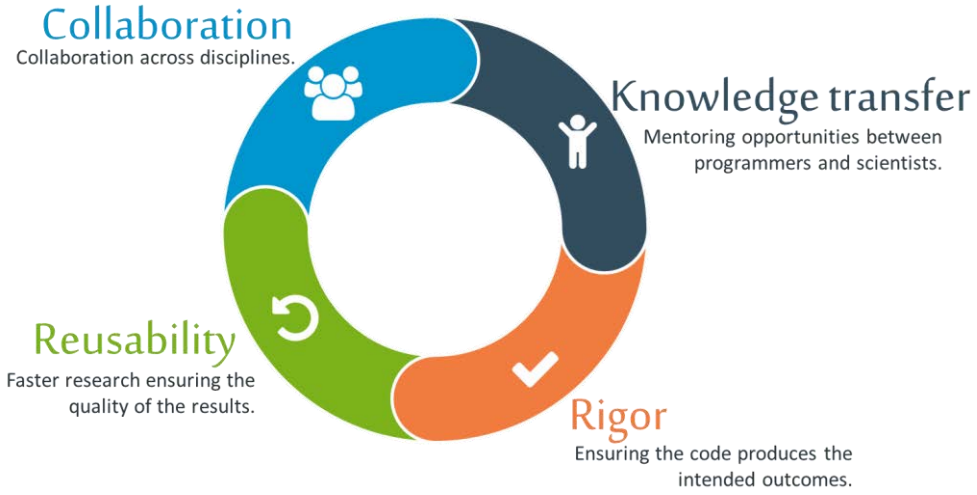

Figure 9: Main Reasons for Code Review according to Petre and Wilson (2014)

Reasons to acquire programming skills are varied (Ayer et al., 2014; Joppa et al., 2013; Trucano, 2015; Yang et al., 2013), but our aim is to encourage researchers to get skilled. Skilled researches may not only find that it is faster to automate a solution to a problem, than doing so manually. They may also find that they are more sought after for collaborations and advice. Automating tasks will make mangrove research faster, more accessible and reachable which, in turn, will attract more people into the sciences.

In summary, data resources are available for free and are collected every day, and there is no shortage of processing facilities. The link between mangrove ecosystems, data acquisition and processing is coding. The implications of coding for mangrove science are numerous: *i)* ability to address new, more complex, questions via the use of imagery, climate and other spatial datasets; *ii)* highly skilled researchers who can automate tasks and analyse information; *iii)* near-real-time data processing; *iv)* better information for mangrove management and conservation; and most

importantly *v)* scripts that are peer reviewed to ensure the quality of the methods and results is preserved.

2.7 The way forward

This review has focused on the challenges faced by mangrove research. Although the average study used 2.8 images 7-11 years apart before 2009, mangrove research is slowly changing in favour of using hundreds of images and looking at the long-term dynamics of mangrove ecosystems.

With a predicted 2% loss of mangrove forests per year (Chen et al., 2013) this change of direction is welcomed. It is safe to say that mapping the extent of these ecosystems no longer is the ultimate goal. Rather, integrating imagery and climate data is beginning to gain speed and popularity. Despite this, more work is needed to gain a greater understanding of how mangroves respond to environmental changes, especially sea level rise (Ward et al., 2016).

Tidal and hydrological regimes play a critical role in these ecosystems (Lewis III et al., 2016). To understand how they interact with mangrove forests, the information in the Landsat and ASTER archives need to be exploited. This high temporal resolution data is needed to assess long-term changes in the ecosystem. Furthermore, long-term monitoring could aid in diagnosing, and potentially preventing, massive mangrove dieback such as the events in Australia in 2016 (JCU, 2016).

Long-term monitoring of mangrove forests can only be achieved by processing large datasets, and having special infrastructure is no longer a *sine qua non* condition. This can now be achieved by using free (e.g. AGDC, NEX, GEE) or paid services (i.e. AWS, MA). These services will help make the change from local to global mangrove monitoring (Chandra Giri et al., 2011b; Wulder and Coops, 2014), but it also implies the need for researchers to acquire programming skills.

More scientists need to acquire these skills, not only for automation purposes, but to audit scripts, workflows and results (Joppa et al., 2013). This is especially true for new and early career scientists

who have grown with technology and are very comfortable with computers, internet and myriad software and hardware platforms. Researchers need not be expert programmers, but "virtual segregation" in research is a reality that should be overcome (Paul, 2016). With freely available ever-growing datasets, processing power and programming skills become a need rather than a luxury. While not every researcher will choose this path, it is in my opinion that the path that will become the rule, rather than the exception.

Finally, these skills and resources will transform data into information for management, and public awareness. But more importantly, they will help to avoid researcher obsolescence.

2.8 Acknowledgements

This work was supported by NIESGI Cia. Ltda., and a James Cook University Postgraduate Research Fellowship. We would like to thank the anonymous reviewers for their insightful comments and contributions to enhancing this manuscript. Vector illustrations of mangrove trees and mangrove leaves are courtesy of the Integration and Application Network, University of Maryland Center for Environmental Science.

3 The effects of water depth on estimating Fractional Vegetation Cover in mangrove forests

A version of this chapter has been published as: **Younes, N.,** Joyce, K. E., Northfield, T. D., & Maier, S. W. (2019). The effects of water depth on estimating Fractional Vegetation Cover in mangrove forests. International Journal of Applied Earth Observation and Geoinformation, 83, 101924. doi:https://doi.org/10.1016/j.jag.2019.101924

3.1 Abstract

Maps of mangroves have often been limited to showing the presence or absence of mangrove trees and seldom have studies shown an important indicator of ecosystem integrity such as vegetation cover. Fractional vegetation cover (FVC) is used to assess ecosystem health, land cover and carbon stocks, hence accurately measuring FVC is an important task for scientists and land managers. Many methods have been proposed to measure FVC and simple linear models are commonly used. We created an experiment that allowed us to: 1) acquire very detailed hyperspectral imagery (1mm pixel size) from a simulated mangrove forest, 2) measure the effect of water depth on FVC estimations, and 3) compare the relationship of eight spectral bands and indices with FVC using linear and non-linear models. After acquiring the imagery we corrected for dark signal and a white reference, performed spectral and spatial resampling, and created linear and non-linear models across four pixel sizes. Our results suggest that 1) linear and beta models have similar performance across all pixel sizes; 2) Soil Adjusted Vegetation Index (SAVI), Modified Soil Adjusted Vegetation Index2 (MSAVI2) and Enhanced Vegetation Index (EVI) perform better than the Normalized Difference Vegetation Index (NDVI), and, 3) our models perform better at fine pixel sizes than coarse scales. We tested our results on high-resolution satellite imagery with similar results and, therefore, recommend using SAVI, EVI or MSAVI2 when predicting FVC instead of NDVI.

Keywords: Fractional vegetation cover; beta regression; linear regression; tidal influence; tidal height; water effect size; remote sensing.

3.2 Introduction

Mangroves are among the most carbon-rich ecosystems in the tropics and provide a wide range of goods and services to human populations (Barbier, 2015; Donato et al., 2011; Kainuma et al., 2010). Mapping these ecosystems allows us to determine the amount of mangrove cover per country and serves as a basis for later comparisons. While global maps of mangroves are available (Chandra Giri et al., 2011b; Kainuma et al., 2010), these maps are often limited to show the presence or absence of mangroves but do not measure an important indicator of ecosystem integrity: fractional vegetation cover. Fractional Vegetation Cover (FVC) provides information on forest biomass, vegetation density and more (Munshi-South, 2012; Paletto and Tosi, 2009; C. Zhang et al., 2016). Fractional vegetation cover, also known as foliage projected cover, is defined as the vertical projection of foliage into a horizontal surface as a fraction per unit area. It can be estimated from aerial photographs or satellite images and is often used for assessing crop health (Boegh et al., 2002), and changes in land use and land cover (Wiesmair et al., 2016; Yang et al., 2016). FVC has been represented at different pixel sizes, and using a variety of sensors.

Fractional vegetation cover is often derived from spectral indices such as NDVI (Normalized Difference Vegetation Index), SAVI (Soil Adjusted Vegetation Index), MSAVI (Modified Soil Adjusted Vegetation Index) and others (see Table 2). Spectral indices and in turn, FVC are derived from remotely sensed information, and are often used as indicators of land condition and change (Jafari et al., 2007). As such, a well-defined relationship between spectral indices and the predicted FVC is crucial. Despite the importance of this relationship, the literature shows no consensus on how to accurately measure FVC from spectral indices due, in part, to the following four issues: *i)* The relationship between FVC and some spectral indices may be linear, non-linear, or both; *ii)* contribution of the background to the spectral reflectance of open canopy; *iii)* Spatial resolution; and *iv)* no consensus on which spectral index to use. We briefly describe these issues below.

3.2.1 The relationship of FVC with spectral indices may be linear or non-linear

Many authors have used linear relationships between spectral indices and FVC. Gutman and Ignatov (1998) were among the first to test the linear relationship between NDVI and FVC, and others have followed (see e.g. Jean-Baptiste and Jensen (2006); Montandon and Small (2008); Xiao and Moody, (2005)). Linear relationships, however, appear to be most successful in arid and semi-arid regions when compared to non-linear relationships (Camacho-De Coca et al., 2004; Jafari et al., 2007; Jia et al., 2015). Alternative studies found non-linear relationships between FVC and spectral indices: curvilinear, beta, and logistic regressions have been used to demonstrate how changes in spectral indices relate to changes in FVC (Korhonen et al., 2007; Leprieur et al., 2000; Poudel and Temesgen, 2016). This divergence in methods is further emphasized by the disagreement on which spectral indices to use, as shown in Table 2. While these relationships have been tested in an array of ecosystems, a comparison of linear and non-linear models of FVC using spectral indices has not been attempted in mangrove ecosystems.

Table 2: Examples of the various indices and modelling techniques used for estimating Fractional vegetation Cover. ARVI: Atmospherically Resistant Vegetation Index; EVI: Enhanced Vegetation Index; FVC: Fractional Vegetation Cover; GEMI: Global Environment Monitoring Index; GARI: Green Atmospherically Resistant Index; MSAVI: Modified Soil Adjusted Vegetation Index; NDVI: Normalized Difference Vegetation Index; SDVI Scaled Difference Vegetation Index; RVI: Ratio Vegetation Index; SAVI: Soil Adjusted Vegetation Index; SR: Simple Ratio Index; TCT: Tasseled Cap Transformation; TGVDI: Three-band Maximal Gradient Difference; VARI: Variably Atmospherically Resistant Index; WDVI: Weighted Difference Vegetation Index.

Index / Method used	**Modelling technique**	**Sensor(s)**	**Reference**
NDVI, TCT	Beta Regression	Landsat TM, Aerial photographs	(Coulston et al., 2012)
Top-hit Cover	Beta Regression	RapidEye	(Karl et al., 2017)
ARVI, SR, NDVI	Logistic Regression, Beta Regression	ALOS AVNIR-2, Lidar	(Korhonen et al., 2015)
LAI, NDVI	Radiative Transfer Modelling	Unspecified satellite imagery*, aerial photographs	(Carlson and Ripley, 1997)
GEMI, MSAVI2, NDVI	Curvilinear regression	AVHRR, SPOT HVR	(Leprieur et al., 2000)
NDVI	General Regression Neural Networks	Landsat TM, ETM, MODIS	(Jia et al., 2015)
NDVI	Spectral Mixture Analysis	Aerial photography, Landsat ETM	(Xiao and Moody, 2005)
NDVI, SDVI	Spectral Mixture Analysis	Spectroradiometer	(Jiang et al., 2006)
SAVI	Linear regression	Landsat TM	(Lagomasino et al., 2015)
MSAVI2, NDVI, SAVI, TSAVI	Polynomial regression	Spectroradiometer	(Purevdorj et al., 1998)
MSAVI2, NDVI	Random forest	WorldView 2	(Wiesmair et al., 2016)
NDVI, SAVI-A, TCT	Linear regression	Landsat TM	(Jafari et al., 2007)
EVI2, MSAVI2, NDVI, VARI	Linear regression	UAV	(Fang et al., 2016)
NDVI	Spectral Mixture analysis	Landsat TM	(Camacho-De Coca et al., 2004)
MSAVI2, NDVI, SNDVI, RVI	Radiative Transfer Theory modelling	Field photography, Landsat OLI	(Ding et al., 2017)
EVI, NDVI, TGVDI	Spectral Mixture Analysis	MODIS	(C. Zhang et al., 2016)
GARI, VARI	Analytical method	Spectroradiometer	(Gitelson et al., 2002)
NDVI, SAVI, SR	Linear regression	ASTER	(Jean-Baptiste and Jensen, 2006)
LAI, OSAVI, NDWI, NDVI, NDBI, GARI, NDII	Spectral Mixture analysis	Landsat 8	(Monsef and Smith, 2017)
NDVI-G, NDVI-R, NDVI-b, EVI, LAI	Analytical method	Compact Airborne Spectral Imager (CASI)	(Boegh et al., 2002)
EVI, MSAVI2, NDVI, RVI, SAVI	Linear regression	RGB Aerial Photography, Field photography, HJ 1A/1B satellites	(Chen et al., 2016)

3.2.2 Contribution of the background to spectral reflectance of open canopy vegetation

In the Sundarbans (Bangladesh), Giri et al. (2007) related mangrove FVC to NDVI using the Gutman and Ignatov model (Gutman and Ignatov, 1998). They found that NDVI values of 0.2 and 0.7 represented 'open' and 'closed' canopy mangroves respectively, and concluded that relationship was valid for each individual image but values for 'open' or 'closed' forest could change due to phenology and tidal height. The authors make no mention of the temporal and spatial variations in the background materials (e.g. mud, water) of mangroves which are known to alter the spectral signatures of mangroves (Rogers et al., 2017). Because the Sundarbans mangrove forest extends over 10,000 km^2, variations in underlying sediments and materials are inevitable and could change the relationship between FVC and NDVI. In a laboratory experiment, Meza Díaz and Blackburn (2003) tried to simulate a mangrove forest over a variety of backgrounds. The authors used *Gardenia jasminoides* (a species related to mangroves) and linear regression models to determine how different backgrounds alter the relationship between FVC and spectral indices. They concluded that the type (e.g. sand, leaves) and texture of the background materials indeed alter the spectral indices and, hence, FVC measurements. More importantly, they suggest that the relationships between FVC and some spectral indices are not necessarily linear. However, they do not suggest which type(s) of relationship could best describe FVC from spectral indices.

3.2.3 Spatial resolution

To add to the complexity of the problem, Jiang et al. (2006) stated that the relationship between FVC and NDVI was linear when the spatial resolution allowed to resolve individual elements (e.g. individual tree crowns), and non-linear when the elements could not be individually resolved. In other words, the spatial resolution or pixel size, play a crucial role in the type of relationship between FVC and NDVI. Wu and Li (2009) described the effects of scale (i.e. spatial resolution) and scaling (i.e. transferring information from one scale to another) in remote sensing scenarios. Like many others (e.g. Leprieur et al. (2000); Meza Díaz and Blackburn (2003)), Wu and Li (2009) describe how heterogeneous surfaces alter the spectral response of land surface at different pixel sizes. The authors mention two ways for reducing the influence of heterogeneity: to quantify the

intra-pixel heterogeneity or, to minimize the intra-pixel variability. While there are many methods for estimating the former (see Table 2), the latter can be achieved by using very detailed imagery.

3.2.4 No consensus on which spectral index to use

Out of all spectral indices used, one seems to appear in most studies: NDVI. The literature largely agrees that NDVI is the *de facto* index related to FVC and, while this may be true for some ecosystems, little work has been done to test other indices in mangrove forests. On the one hand, Lagomasino et al. (2015) used NDVI and SAVI to extract FVC in the Florida Everglades while Zhang et al. (2016) used NDVI, SAVI and EVI. On the other hand, Emch and Peterson (2006), Lovelock et al. (2017), Giri et al. (2007) and many others rely solely on NDVI to infer biophysical information of mangrove forests.

Up to now, we have briefly mentioned four important issues when trying to estimate FVC in mangrove ecosystems. Still, accurately measuring FVC in mangrove forests remains a challenge, because remotely sensed data is captured during varying tides. Depending on the resolution of the sensor, tidal height may alter the spectral mixture of mangrove forests in certain wavelengths, especially at the fringes of mangrove forests (Rogers et al., 2017; Saito et al., 2003). While some projects have incorporated the tidal height when mapping the presence or absence of mangroves (see e.g. Rogers et al. (2017)), none have assessed the effects of tidal height in estimating FVC (Younes Cárdenas et al., 2017).

To understand the effects of tidal height on the estimation of FVC in mangrove ecosystems we designed an experiment to compare two modelling techniques across four spatial scales using very detailed imagery. Afterwards, we contrasted our results with two high-resolution images of our study site. Knowing which combination of spectral bands or indices, modelling techniques and spatial scales yields the most accurate results will allow us to create an automated process that extracts FVC from individual images and time series datasets. With this paper, we aim to: *i)* examine the influence of water depth in the estimation of mangrove FVC, *ii)* determine which spectral band or index is the best predictor of FVC in mangrove ecosystems, and *iii)* examine the performance of the indices and bands at different spatial scales.

3.3 Materials and Methods

3.3.1 Study Area

We selected the mangroves surrounding the Cairns International Airport in northern Queensland (Australia) due to their ease of access and closeness to the James Cook University facilities. These wetlands are part of a 4,500 hectare bio-geographic region known as Trinity Inlet where the mangroves in the *Ceriops, Rhizophora, Avicennia* and *Bruguiera* genera are common (Hegerl and Davie, n.d.; Kutt, 1997). Our study site has a monsoonal climate with wet and dry winters, where temperature ranges between 20°C and 30°C and the mean annual rainfall reaches 1983 mm. The area is located 5 km north of Cairns city center, and next to the Barron River. The Barron River delta drains close to 200,000 hectares and provides a constant flow of freshwater to the study area and has six distinct habitat types (see Kutt (1997) for more information).

3.3.2 Experimental Design

Leaves were randomly selected and collected from healthy *Ceriops australis* mangrove trees in the Jack Barnes Bicentennial Mangrove Boardwalk site in Cairns (16° 52.976'S, 145° 45.663'E) (n = 96). We inspected the samples to avoid any obvious damage by insects, sunburn or disease and then placed them into coolers with ice on sealed plastic bags and taken to the remote sensing laboratory at James Cook University - Cairns. We selected this species because it is widespread throughout Australia and the size of their leaves (5.5 – 10 cm x 2.0 – 3.4 cm) was suitable for this experiment (Duke et al., 2006; Wightman et al., 2006).

The leaves were divided into three groups of 32 leaves, where each group represented a different tidal height scenario. Each group of leaves was then divided into stacks of one, three, five and seven leaves and attached to a wooden platform as shown in Figure 10. Stacks were arranged perpendicularly to each other to reduce the effects of the position of the sun, shadows or other factors when scanning. Furthermore, to reduce the effects of leaf dehydration and solar angle changes, all scenarios (i.e. 5, 15 and 30 cm of water) were scanned at the same time. Because our aim was to determine if water depth affects our ability to estimate FVC from remotely sensed data, we simulated low, transition and high tide by filling the containers with 5, 15 and 30 centimeters

of water respectively. We decided to use 5, 15 and 30 cm of water for our experiment for several reasons: *i)* we were able to replicate realistic scenarios where mangrove mud is exposed and fully covered with water; *ii)* if 15 or 30 cm of water have an effect on the spectral reflectance of mangrove leaves, a more thorough experiment should be proposed; however, if there is no effect at these depths, no effect could be expected from other tidal heights; and *iii)* the containers used limited our ability to simulate the entire tidal range of the Cairns region (i.e. 3.6m).

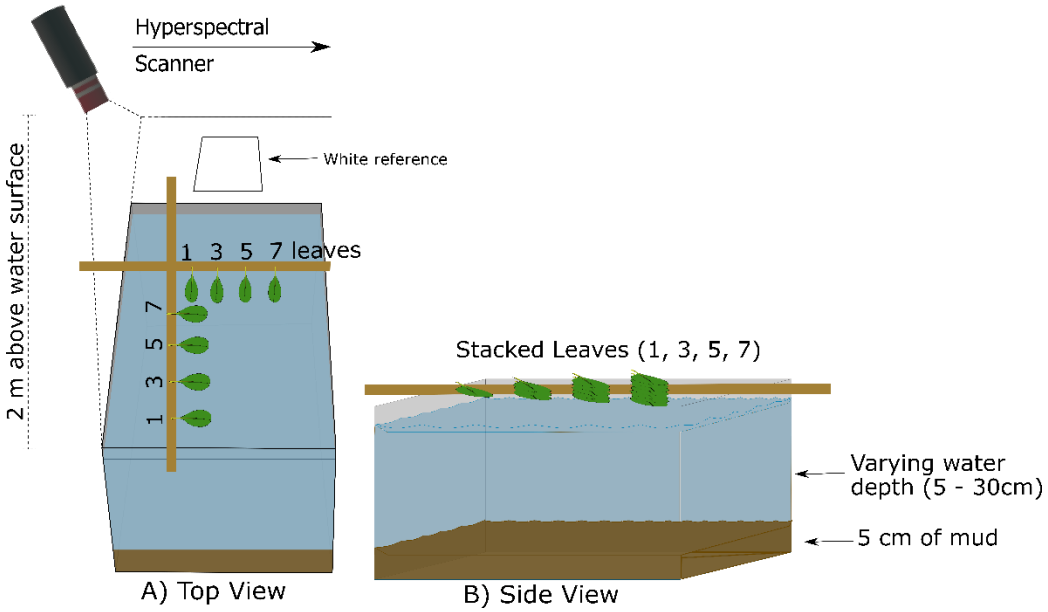

Figure 10: Experiment layout. The experiment consisted of three containers with varying water depths all of which were scanned at the same time to avoid variations in illumination. Mangrove leaves were stacked on top of each other and positioned perpendicularly from each other to better simulate a mangrove forest.

We also collected mud from the study site and used it to create a 5cm coating for the bottom of the containers. We did this for two main reasons: *i)* to better simulate the mangrove environment in our study site (turbid water) and *ii)* to prevent the bottom of the container from contributing to the spectral readings from the leaves. With the mud in place, water was poured into the container and left for 24 hours to ensure any solids would settle, though water remained turbid throughout the experiment, as it is often the case in our study area. Lastly, our design allowed us to isolate the effects of tidal height on FVC estimation from the interference of stems, branches

and dead leaves commonly found in mangrove ecosystems. We estimated FVC by performing supervised classification of the original image in ENVI and then quantifying the amount of leaf and water in each pixel using ArcGIS (Figure 11B).

3.3.3 Hyperspectral imagery acquisition and pre-processing

We obtained hyperspectral imagery over the leaf arrangement using a Headwall NANO Hyperspectral Scanner (Headwall Photonics Inc.), with a spectral resolution of 270 bands between 400 – 1000 nm (spectral bandwidth of 1.4 – 2 nm) and a Field of View equal to 15.3 degrees. The spectral range of this pushbroom scanner incorporates the visible (400-650 nm), red edge (650-750 nm) and NIR regions (750-1000 nm), which are often used to discriminate plant species. The scanner was turned on and left to warm up for 3 minutes before the first scan. Dark signal measurements were taken before and after the scans by completely covering the sensor and recording the signal in each spectral band. The samples were illuminated by direct sunlight and the scanner was positioned two meters above the samples, centered above the leaf arrangement. A 75% white Spectralon® panel was scanned alongside all images, thereby ensuring that any corrections due to changing illumination could be made during the image pre-processing stages. This set-up allowed us to *i)* reduce to the minimum any bidirectional reflectance distribution effects, *ii)* attain imagery of the mangrove leaves such that each pixel represented approximately 1x1 mm, and *iii)* isolate the effects of tidal height on mangrove leaves to assess FVC.

We selected the images that were most consistent regarding scanning speed and illumination. Out of the two selected images, one was used to create the models and the other one to test them. Images were taken five minutes apart and took approximately 40 seconds to scan. Both images were transformed to reflectance using the 'spectral math' function in ENVI (Exelis Visual Information Solutions, Inc.) in two steps: firstly, we subtracted the dark signal (S2) from the spectral measurement in each pixel (S1, equation 1). Then we divided the new spectral image (S3) by the mean spectral signature registered in the Spectralon® panel (S4, equation 2). The corrected images (S5) were used for all subsequent steps.

$$S3_{(x,y)} = S1_{(x,y)} - S2_{(x,y)} \quad (1)$$

$$S5 = \frac{S3_{(x,y)}}{S4_{(reference\ pixels)}} \quad (2)$$

where x and y are pixel coordinates, S4 represents the average over all pixels covering the reference target and $S5_{(x,y)}$ is the image reflectance.

Because we wanted to determine if the relationship between FVC and the spectral indices could be used with more freely available imagery, we resampled our hyperspectral images to match the spectral resolution of Landsat 8 (Lausch et al., 2013). We achieved this by using the 'spectral resampling' tool in ENVI. We then extracted the mangrove features from the image using a Maximum Likelihood supervised classification. Given the high spatial resolution of our images (see Figure 11), we were confident on the FVC values for each pixel thus ensuring the quality of the results.

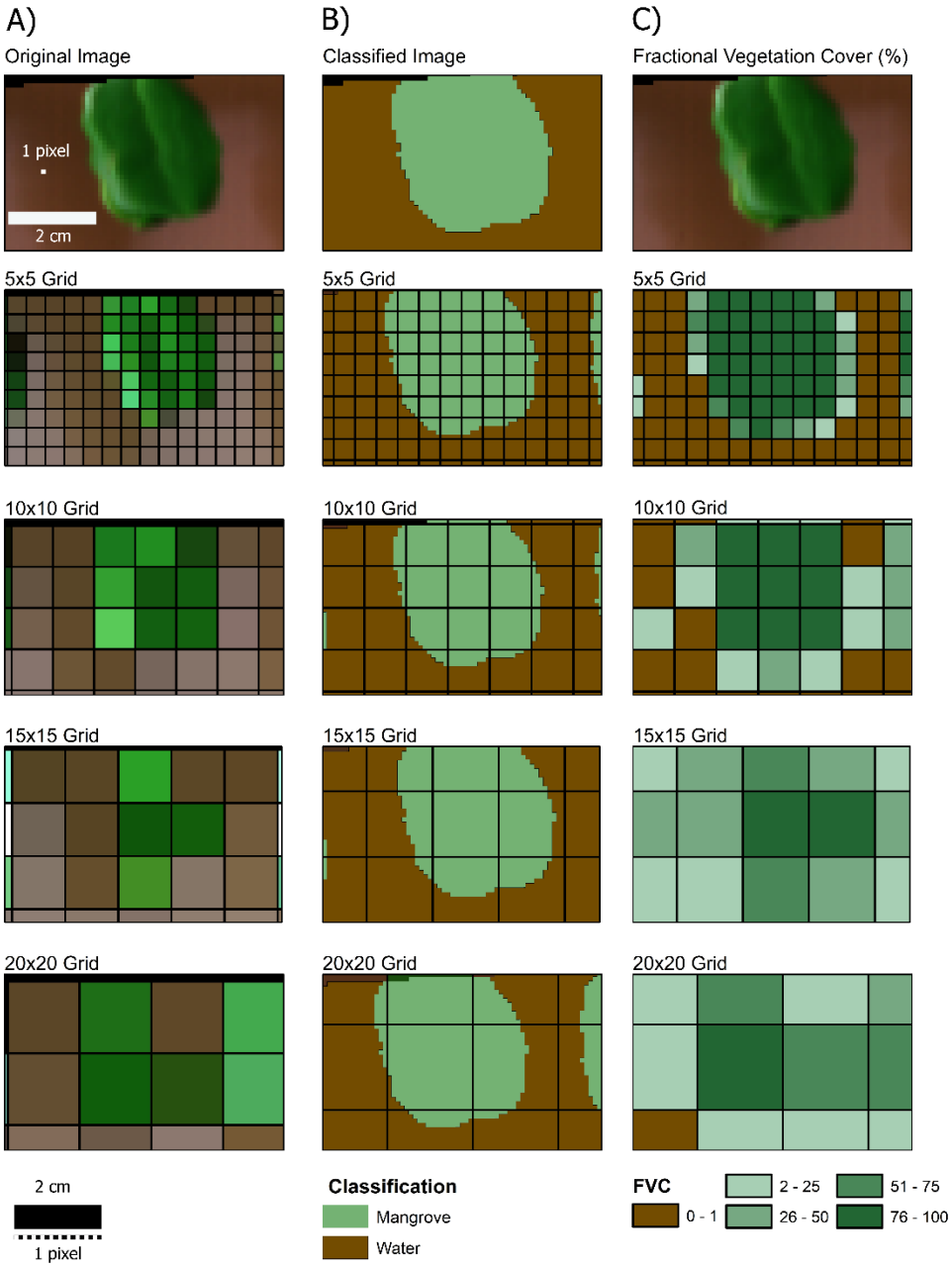

Figure 11: Original and resampled images from one leaf in our experiment. Panel A) shows the original image and the resampled images to 5 × 5, 10 × 10, 15 × 15 and 20 × 20. Panel B) shows the result from the image classification, and Panel C) shows the Fractional Vegetation Cover per pixel at all grid sizes.

3.3.4 Satellite imagery acquisition and pre-processing

The DigitalGlobe Foundation provided two Worldview 3 images of the mangrove forest that surrounds the Barnes Bicentennial Mangrove Boardwalk site in Cairns (Figure 12). The images were acquired on 31-August-2015 and 12-February-2016, have less than 20% cloud cover and a spatial resolution of 1.2m x 1.2m per pixel. Similar to our hyperspectral scanner, the Worldview 3 images capture information in the 400-1000 nm range of the electromagnetic spectrum, with the Blue (480 nm), Red (660 nm) and Near Infrared (950 nm) bands being the most relevant to this project. The images were collected at different tidal heights: 1.70m for the 2015 image and 2.4m for the 2016 image however, it is important to remember that sun-synchronous sensors rarely capture the entire tidal range as explained by Bishop-Taylor et al. (2019). Because there is a difference of only 70cm between the tides in our two satellite images, we consider that our simulation of 5, 15 and 30cm is a scenario that can truly represent a mangrove environment.

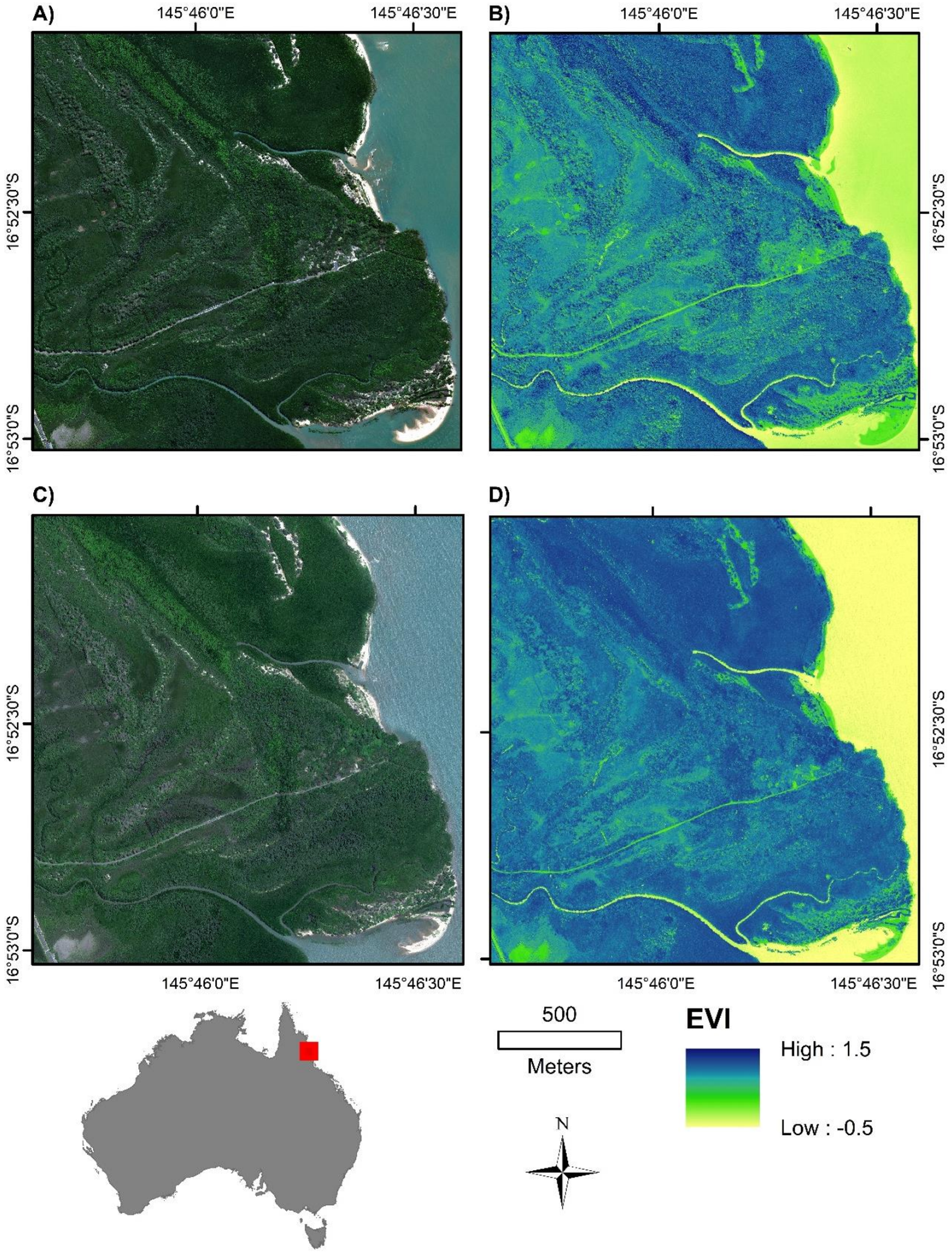

Figure 12: True colour (A, C) and EVI (B, D) images of the study area. The top row shows images of August 15th, 2015 and 1.7m tide, while the bottom row shows images of February 12th, 2016 and 2.4m tide. Worldview 3 images provided by the Digital Globe Foundation.

3.3.5 Image Analysis

In 1999, Chen (1999) demonstrated that some spectral indices were heavily affected by the pixel size of the images, something that was also re-stated by Jiang et al. (2006). We tested the effects of scale with several spectral bands and indices on four different pixel resolutions by resampling the images to 5 × 5, 10 × 10, 15 × 15 and 20 × 20 grid sizes (Figure 11). Note that as the data are not georeferenced, these grids represent counts of pixels rather than a given spatial size. Then we generated the spectral indices for each spatially resampled image and extracted the percent coverage for each grid cell. We analyzed the resulting data using the statistical software 'R' version 3.3 and 'RStudio' version 1.0.136 (R Core Development Team, 2016). This procedure was done for the calibration and the validation images, and a similar one for the satellite images (Figure 13).

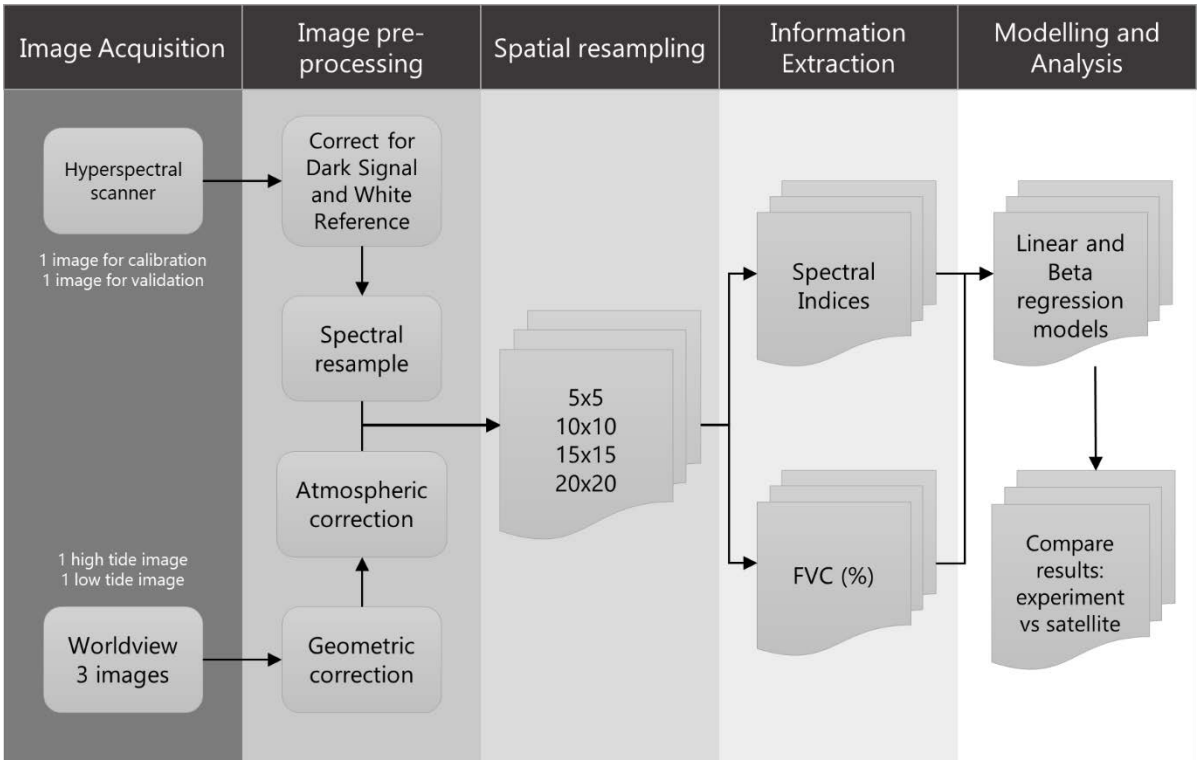

Figure 13: Data capture, pre-processing, and analysis workflow.

We used a combination of vegetation indices and individual spectral bands to examine the effect of water depth on FVC estimations (Table 3). We selected these indices mainly because they use

bands within the 400-1000nm range, but also because they account for an array of parameters that may influence the estimation of FVC. For example, SAVI and MSAVI2 account for soil influences, however MSAVI2 avoids the calculation of the soil adjustment factor (Huete, 1988; Kerr et al., 2003). In contrast to NDVI, EVI does not saturate when canopy densities are high (Huete et al., 2002). During this experiment, we decided that the soil factor (L) in the SAVI should be static at 0.5 for two reasons: firstly, the optimization of L for mangrove ecosystems is beyond the scope of this experiment. Secondly, we wanted to account for the influence of the background without adding an additional variable (i.e. L) to the models. We also tested a combination of bands in the form of a linear regression model of the Green, Red and NIR bands. We created this linear mixture model in 'R' by adding the spectral reflectance values of each spectral band as shown in Table 3.

Table 3: Spectral indices used in this manuscript.

Band or Index Name	**Reference**	**Formula**
Green band	(Barsi et al., 2014)	$Green\ reflectance = \rho_{green} = \rho_{0.533-0.590\mu m}$
Red band		$Red\ reflectance = \rho_{red} = \rho_{0.636-0.673\mu m}$
NIR band		$NIR\ reflectance = \rho_{NIR} = \rho_{0.851-0.879\mu m}$
Linear mixture		$Mixture = \rho_{green} + \rho_{red} + \rho_{NIR}$
EVI	(Huete et al., 2002)	$EVI = 2.5 * \frac{(\rho_{NIR} - \rho_{red})}{(\rho_{NIR} + 6 * \rho_{red} - 7.5 * \rho_{blue} + 1)}$
NDVI	(Tucker, 1979)	$NDVI = \frac{(\rho_{NIR} - \rho_{red})}{(\rho_{NIR} + \rho_{red})}$
SAVI	(Huete, 1988)	$SAVI = \frac{1.5 * (\rho_{NIR} - \rho_{red})}{\rho_{NIR} + \rho_{red} + 0.5}$
MSAVI2	(Kerr et al., 2003)	$MSAVI2 = \frac{2 * \rho_{NIR} + 1 - \sqrt{(2 * \rho_{NIR} + 1)^2 - 8(\rho_{NIR} - \rho_{r}}}{2}$

3.3.6 Statistical analyses and model testing

Statistically, vegetation cover is bounded between 0 and 1, it often displays the characteristics of a heteroscedastic variable and typically is not normally-distributed (Cribari-Neto and Zeileis, 2010; Karl et al., 2017). The beta distribution is defined as follows (Ferrari and Cribari-Neto, 2004):

$$\pi(y; p, q) = \frac{\Gamma(p+q)}{\Gamma(p)\Gamma(q)} y^{p-1} (1-y)^{q-1} \quad (3)$$

where y is the dependent variable and is measured continuously between 0 and 1, and the probability density function is given by:

$$f(y; \mu, \phi) = \frac{\Gamma(\phi)}{\Gamma(\mu\phi)\Gamma(1-\mu)} y^{\mu\phi-1} (1-y)^{(1-\mu)\phi-1} \quad (4)$$

where 0 < μ < 1, 0 < y < 1 and φ > 0. The mean and variance of y, respectively, are defined by:

$$E(y) = \frac{p}{p+q} = \mu, \quad (5)$$

and,

$$var(y) = \frac{pq}{(p+q)^2(p+q+1)} = \frac{\mu(1-\mu)}{(1+\phi)}. \quad (6)$$

According to Eskelson et al. (2011) and Ferrari and Cribari-Neto (2004), when y_1, … y_n are independent, random variables where y_i follows the probability density function in Equation 4, the beta regression model can be expressed in terms of:

$$g(\mu_i) = x_i^T \boldsymbol{\beta} = \eta_i \quad (5)$$

were $x_i = (x_{il}, \ldots, x_{ik})^T$ is a vector of k explanatory variables (k < n) assumed to be fixed and known, $\boldsymbol{\beta} = (\beta_l, \ldots, \beta_k)^T$ is a k x 1 vector of unknown regression parameters ($\beta \in \mathbb{R}k$), and η_i is a linear predictor. Lastly, $g(\cdot)$ is a monotonic and twice differentiable link function that maps (0, 1) into $\mathbb{R}$.

The statistical analyses were divided in three phases: *i)* Data cleaning, *ii)* measuring the effect size of water depth, *iii)* model testing. The first stage consisted of eliminating noise and data with zero FVC, which were mainly represented by pixels with 100% water. This process was done in ArcMap version 10.2 (Environmental Systems Research Institute) by inspecting all experimental and

satellite images and removing pixels without information or outside the areas of interest for this experiment.

Then we created 128 individual models, that is, a linear and beta regression model for each spectral index and band at each pixel size with and without water as a predictor of FVC. Beta regression models are well suited for situations where a response variable is bounded between 0-1 such as FVC (Ferrari and Cribari-Neto, 2004).

We used "R" (version 3.5.1) to create the models and incorporated water depth as a variable in the following way:

$$\text{model} <\text{- lm(FVC} \sim \text{Index)} \quad (7)$$

$$\text{model} <\text{- lm(FVC} \sim \text{Index + Depth)} \quad (8)$$

where:

"model" is the model name,

"FVC" is the unknown vegetation cover for each pixel,

"Index" is the known value of the spectral index for each pixel, and

"Depth" is the known depth value for each pixel.

We used the *lm* function and the *betareg* within the Betareg package in "R" to fit the linear and beta models respectively (Cribari-Neto and Zeileis, 2010; R Core Development Team, 2016). The beta regression model was developed by Ferrari and Cribari-Neto (2004) and allowed us to use the 'logit' link function to fit all models for the spectral bands and indices. The 'logit' link function accounts for the bounded nature of FVC, in other words, it limits the prediction of FVC to values between 0-1. To determine the effect size of water depth in FVC estimation, we used Cohen's d, Akaike Information Criterion and the difference in R-squared values from the models.

Finally, we tested all models to determine the strength of the relationships between FVC and the spectral indices. To measure the strength of the predictive models, we plotted the Predicted FVC

versus the Real FVC and obtained R^2 and Root Mean Squared Error (RMSE) and Mean Absolute Errors (MAE) values for that relationship.

3.4 Results

In the first instance, we acknowledge that our experimental design is a simplification of mangrove ecosystems. However, by excluding branches, stems and soil heterogeneity we *i)* isolated the tidal effects on the simulated mangrove canopy and *ii)* reduced intra-pixel heterogeneity. While the former is the main objective of this project, the latter allowed us to reduce the scaling effects introduced by heterogeneous land surfaces (Obata et al., 2012; Wu and Li, 2009a). In accordance with Lausch et al. (2013), we did not find significant differences in the maximum, minimum, median or average values of the spectral indices at the different pixel sizes neither for the experimental nor for the satellite images. Similarly, there was not a significant difference in the spectral signatures of the stacks of one, three, five and seven leaves, therefore we decided to treat them as a single unit.

3.4.1 Measuring the effect size of water depth

To measure the effect size of water depth on FVC estimations, we used linear and beta models of FVC at the 5 × 5 grid size on our training image. In Table 4 we show the results of *Cohen's d*, the difference in Akaike Information Criterion (AIC) values and the difference in R^2 values to show how water affects each spectral index and band. On our experimental images, the values for Cohen's d indicate that the effect of water depth in the linear or beta models is negligible; similarly, the models with and without water show little difference in their R^2 or pseudo-R^2 values.

Lastly, the difference in AIC values shows mixed results. On the one hand, in linear and beta models where $|\Delta AIC| < 2$, models with and without depth are considered to be similar. On the other hand, if $|\Delta AIC| > 2$, the models are considered as different. Using this reference, Table 4 would indicate that neither linear nor beta models of SAVI and MSAVI2 are influenced by water depth when

predicting FVC. However, linear and beta models that use NDVI, Red, or Green are influenced by water depth. Despite the difference in AIC values, if the predictive power (i.e. R^2 or pseudo-R^2) is invariant, and the effect size is negligible, one can assume that water depth does not influence these models when estimating FVC. To further test the influence of water depth on FVC estimation, we proceeded to create linear and beta models across all pixel sizes.

Table 4: Effect size of water depth in FVC estimation for experimental images

	Linear models			Beta models		
Band or Index	**Cohen's d**	**ΔAIC**	**R-squared Difference**	**Cohen's d**	**ΔAIC**	**R-squared Difference**
Green	0.00	-9.44	0.02	0.00	-6.79	0.01
Red	0.00	-17.26	0.03	0.01	-12.86	0.03
NIR	0.00	-4.05	0.01	0.00	-1.69	0.01
Linear Mix	0.00	-4.87	0.01	0.00	-2.06	0.01
NDVI	0.00	-30.46	0.03	-0.01	-24.14	0.03
SAVI	0.00	0.24	0.00	-0.01	1.11	0.00
MSAVI2	0.00	-0.50	0.00	-0.01	0.57	0.00
EVI	0.00	-3.92	0.01	0.00	-2.81	0.00

3.4.2 Calibration Models for experimental images

From the images of our experiment we created linear and beta models of FVC using eight spectral bands and indices across four pixel sizes to determine if water depth plays a significant role in estimating FVC in mangrove ecosystems. Evaluation of the R^2, pseudo-R^2, and RMSE values Table 5 suggests that the Red, Green, and Linear Mixture models have the lowest estimating power and highest RMSE values across all pixel sizes therefore our discussion will mostly omit these models.

Out of all the spectral bands and indices analyzed, linear models of EVI, SAVI and MSAVI2 show the highest predictive power (R^2) and the lowest RMSE values regardless of the pixel sizes. Our results indicate that these three indices outperform NDVI as predictors of FVC in mangrove ecosystems, as shown in Table 5. At the 5 × 5 pixel size, linear models of SAVI and MSAVI2 and beta models of SAVI, MSAVI and EVI are better predictors of FVC than NDVI. At the 20 × 20 pixel size, the beta model of NDVI has little predictive power (pseudo-R^2 = 0.22) whereas the models for EVI and NIR show the highest pseudo-R^2 values at 0.61 and 0.57 respectively. The linear model

of NDVI does not perform much better at this pixel size (R^2 = 0.37). Put simply, models of SAVI, EVI and MSAVI2 are more related to FVC than those of NDVI across all pixel sizes.

Models that exclude depth as a factor for estimating FVC have roughly the same predictive power when compared to those that include water depth. In our experiment, this statement holds true for linear and beta models across all pixel sizes. Our results suggest that the predictive power of the models is unaffected by the water depth across all pixel sizes tested.

Similar to the models with depth, linear and beta models of NDVI have lower predictive power than those of SAVI, EVI and MSAVI2 across all pixel sizes. The beta model of NDVI at the 20 × 20 pixel size again shows the lowest pseudo-R^2 value (0.21), even lower than the red spectral band (pseudo-R^2 = 0.23). In summary, when incorporated as a predictive variable, water depth does not influence the predictive power of linear and beta models of FVC, meaning that R^2, pseudo-R^2 and RMSE values remain mostly invariant. To test if the effect size of water depth is indeed negligible, we decided to create models with and without depth for every index on every pixel size, and we show the results in the next sections.

Table 5: Calibration and validation models of spectral bands and indices across all pixel sizes, ordered by highest R^2 or pseudo-R^2 values. The top five and all NDVI models are shown in bold lettering. Grey bars show RMSE ranking of the model against all other RMSE values.

Models with Depth

Linear Models

Grid size	Band or Index	R^2	RMSE
10x10	**SAVI**	0.73	11.89
5x5	**SAVI**	0.71	12.94
10x10	**EVI**	0.71	12.26
10x10	**MSAVI2**	0.71	12.36
20x20	**EVI**	0.71	10.55
5x5	MSAVI2	0.68	13.70
20x20	SAVI	0.67	11.25
5x5	**NDVI**	0.66	14.06
15x15	SAVI	0.65	13.11
20x20	MSAVI2	0.64	11.62
5x5	EVI	0.64	14.45
15x15	MSAVI2	0.64	13.42
15x15	EVI	0.62	13.71
20x20	NIR	0.60	12.31
10x10	NIR	0.59	14.68
10x10	**NDVI**	0.56	15.12
20x20	Linear mixture	0.52	13.48
5x5	NIR	0.51	16.91
10x10	Linear mixture	0.49	16.34
15x15	**NDVI**	0.47	16.19
15x15	NIR	0.46	16.31
20x20	**NDVI**	0.37	15.41
20x20	Green	0.36	15.50
5x5	Linear mixture	0.36	19.37
15x15	Linear mixture	0.34	18.03
10x10	Green	0.32	18.79
20x20	Red	0.20	17.42
15x15	Green	0.20	19.94
5x5	Green	0.18	21.90
10x10	Red	0.09	21.81
5x5	Red	0.08	23.21
15x15	Red	0.03	21.93

Beta Models

Grid size	Band or Index	pseudo-R^2	RMSE
10x10	**EVI**	0.68	0.11
10x10	**SAVI**	0.65	0.11
5x5	**SAVI**	0.64	0.12
10x10	**MSAVI2**	0.64	0.13
5x5	**MSAVI2**	0.62	0.12
20x20	EVI	0.61	0.10
15x15	EVI	0.61	0.13
5x5	EVI	0.60	0.12
15x15	SAVI	0.60	0.13
10x10	NIR	0.60	0.22
15x15	MSAVI2	0.59	0.13
20x20	NIR	0.57	0.11
5x5	**NDVI**	0.56	0.14
20x20	Linear mixture	0.53	0.18
20x20	SAVI	0.51	0.11
10x10	Linear mixture	0.50	0.18
20x20	MSAVI2	0.49	0.11
5x5	NIR	0.48	0.15
15x15	NIR	0.47	0.16
10x10	**NDVI**	0.41	0.15
20x20	Green	0.39	0.22
15x15	**NDVI**	0.38	0.16
15x15	Linear mixture	0.36	0.19
10x10	Green	0.34	0.20
5x5	Linear mixture	0.34	0.19
20x20	Red	0.27	0.18
20x20	**NDVI**	0.22	0.15
15x15	Green	0.21	0.15
5x5	Green	0.17	0.22
10x10	Red	0.10	0.18
5x5	Red	0.06	0.23
15x15	Red	0.04	0.22

Models without Depth

Linear Models

Grid size	Band or Index	R^2	RMSE
10x10	**SAVI**	0.73	11.90
10x10	**EVI**	0.71	12.30
20x20	**EVI**	0.71	10.57
10x10	**MSAVI2**	0.71	12.39
5x5	**SAVI**	0.70	13.28
20x20	SAVI	0.66	11.36
5x5	MSAVI2	0.66	14.08
15x15	SAVI	0.65	13.32
20x20	MSAVI2	0.64	11.73
15x15	MSAVI2	0.63	13.60
15x15	EVI	0.62	13.78
5x5	EVI	0.61	15.04
5x5	**NDVI**	0.61	15.15
20x20	NIR	0.60	12.32
10x10	NIR	0.59	14.68
10x10	**NDVI**	0.54	15.46
20x20	Linear mixture	0.52	13.58
5x5	NIR	0.49	17.24
10x10	Linear mixture	0.49	16.35
15x15	**NDVI**	0.47	16.23
15x15	NIR	0.47	16.35
20x20	**NDVI**	0.37	15.51
15x15	Linear mixture	0.35	18.03
20x20	Green	0.35	15.84
5x5	Linear mixture	0.34	19.64
10x10	Green	0.32	18.84
15x15	Green	0.20	19.98
20x20	Red	0.16	17.99
5x5	Green	0.15	22.31
10x10	Red	0.08	21.96
5x5	Red	0.02	23.90
15x15	Red	0.02	22.17

Beta Models

Grid size	Band or Index	pseudo-R^2	RMSE
10x10	**EVI**	0.68	0.11
10x10	**SAVI**	0.65	0.11
10x10	**MSAVI2**	0.64	0.11
5x5	**SAVI**	0.63	0.12
5x5	**MSAVI2**	0.61	0.12
20x20	EVI	0.61	0.10
15x15	EVI	0.60	0.13
10x10	NIR	0.60	0.13
15x15	SAVI	0.58	0.13
5x5	EVI	0.58	0.13
15x15	MSAVI2	0.58	0.13
20x20	NIR	0.57	0.11
20x20	Linear mixture	0.52	0.13
5x5	**NDVI**	0.52	0.15
20x20	SAVI	0.51	0.11
10x10	Linear mixture	0.50	0.13
20x20	MSAVI2	0.49	0.12
5x5	NIR	0.47	0.15
15x15	NIR	0.47	0.16
10x10	**NDVI**	0.40	0.15
15x15	**NDVI**	0.38	0.16
20x20	Green	0.37	0.15
15x15	Linear mixture	0.36	0.15
10x10	Green	0.34	0.20
5x5	Linear mixture	0.33	0.15
20x20	Red	0.23	0.18
15x15	Green	0.21	0.15
20x20	**NDVI**	0.21	0.15
5x5	Green	0.15	0.18
10x10	Red	0.10	0.22
15x15	Red	0.03	0.22
5x5	Red	0.02	0.24

3.4.2.1 Linear models with and without depth

All indices show a positive relationship with FVC at each the 5 × 5 grid (Figure 14) and the 20 × 20 grid (Figure 15), that is, as the index value increases FVC increases. Amongst the individual spectral bands, Green and NIR show greater correlation with FVC, while the Red band shows the weakest relationship with FVC, especially at the 20 × 20 grid (see Figure 15 and Table 5). In addition, the number of data points used to generate the models is far greater for the 5 × 5 grid than for the 20 × 20 grid (i.e. 736 and 74 respectively). This number of data points ensures the creation of robust models and solid results.

Also, most models have high intercept values; that is to say that at low index or reflectance values, predicted FVC will not necessarily be low. Put simply, these models *i)* require unrealistically low index or reflectance values to predict low FVC (0 - 35%) and *ii)* will predict FVC > 100% because the predicted variable has no boundaries. Despite this, there is one exception: NDVI. The linear model for NDVI has a low intercept value that predicts all fractions of vegetation cover (0- 100%) with values *within* the range of NDVI (see Figure 14E and Figure 15E). However, this model is far from perfect (see Section 3.3).

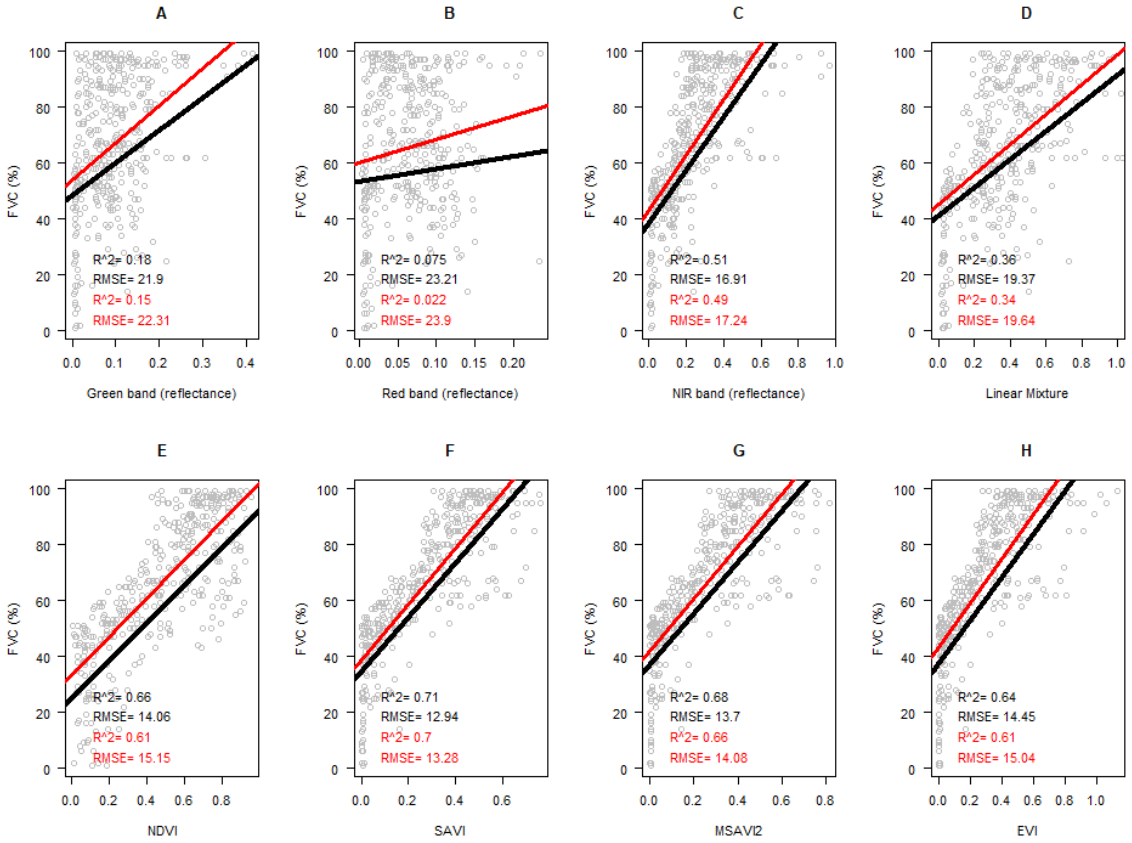

Figure 14: Linear models for individual spectral bands, band mixture and spectral indices on a 5 × 5 pixel size. Black and red lines represent models with and without depth respectively. To maintain homogeneity in the figure, values for Predicted FVC have been capped at 0% and 100%, regardless of the minimum or maximum value predicted.

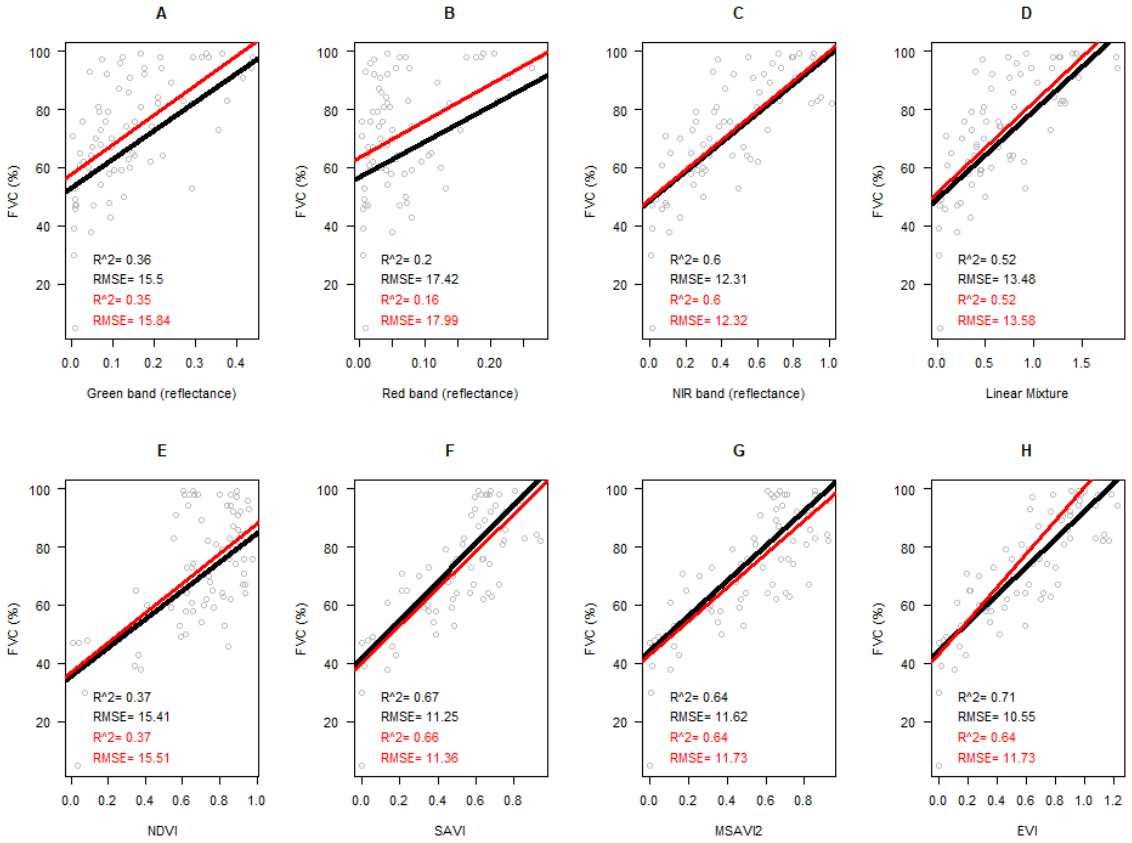

Figure 15: Linear models for individual spectral bands, band mixture and spectral indices on a 20 × 20 pixel size. Black and red lines represent models with and without depth respectively. To maintain homogeneity in the figure, values for Predicted FVC have been capped at 0% and 100%, regardless of the minimum or maximum value predicted.

When comparing the 5 × 5 and 20 × 20 grid models it is easy to see some similarities. For example, despite having fewer data points, in the 20×20 grid the distribution and spread of the data remain mostly unchanged. Another similarity between pixel sizes is that models with and without depth are very closely related to one another. In other words, intercept and slope values for models with and without depth are very similar for models with depth and without depth.

Differences between the two grid sizes include the intercept values, which are generally lower on the 5 × 5 than on the 20 × 20 grid. While on the 5 × 5 grid most models showed intercept values around 40% FVC, in the 20 × 20 grid these values are mostly above the

45% FVC mark. Another difference between pixel sizes is the range of index or reflectance values that the model uses to predict FVC. For example, the models for EVI and SAVI predict 100% FVC at 0.7 and 0.6 in the 5 × 5 grid respectively, while on the 20 × 20 values change to 1.1 and 0.9. This means that coarser grid sizes allow linear models to use a marginally wider range of measured index or reflectance values with no warranty of better a better fit.

Some linear models tend to predict FVC >100%. For instance, the models for the NIR band at the 5 × 5 grid will predict FVC >100% after reaching a reflectance value of 0.6, while linear models of MSAVI2 will do so after MSAVI2 reaches 0.59 (see Figure 14 and Figure 15). In the case of NDVI, the 5 × 5 model will predict FVC >100% starting at NDVI = 0.86, while the 20 × 20 model will predict 100% FVC only when NDVI > 1. Considering that NDVI values higher than 1 cannot exist, the bounded nature of beta models is an appealing alternative to linear models.

3.4.2.2 Beta models with and without depth

There are two main differences between the linear and beta models. The first difference is that linear models predict FVC > 100% and FVC < 0%, that is, they predict values outside the range 0-1. Alternatively, beta models always predict values between 0-1 (see Figure 16 and Figure 17). This is due to the 'logit' link function used in the beta models. The second difference is that beta models generally follow the shape of the data better than linear models. This results in more realistic estimations of FVC, especially in the middle values of the spectral indices. An example of this is shown in Figure 16 especially in the models for NDVI, EVI, SAVI and MSAVI2. These models start rising on the left-hand side of the graph where index and reflectance values are low. Then rise and become asymptotic to the horizontal axis towards the right-hand side of the graphs where index and reflectance values are higher.

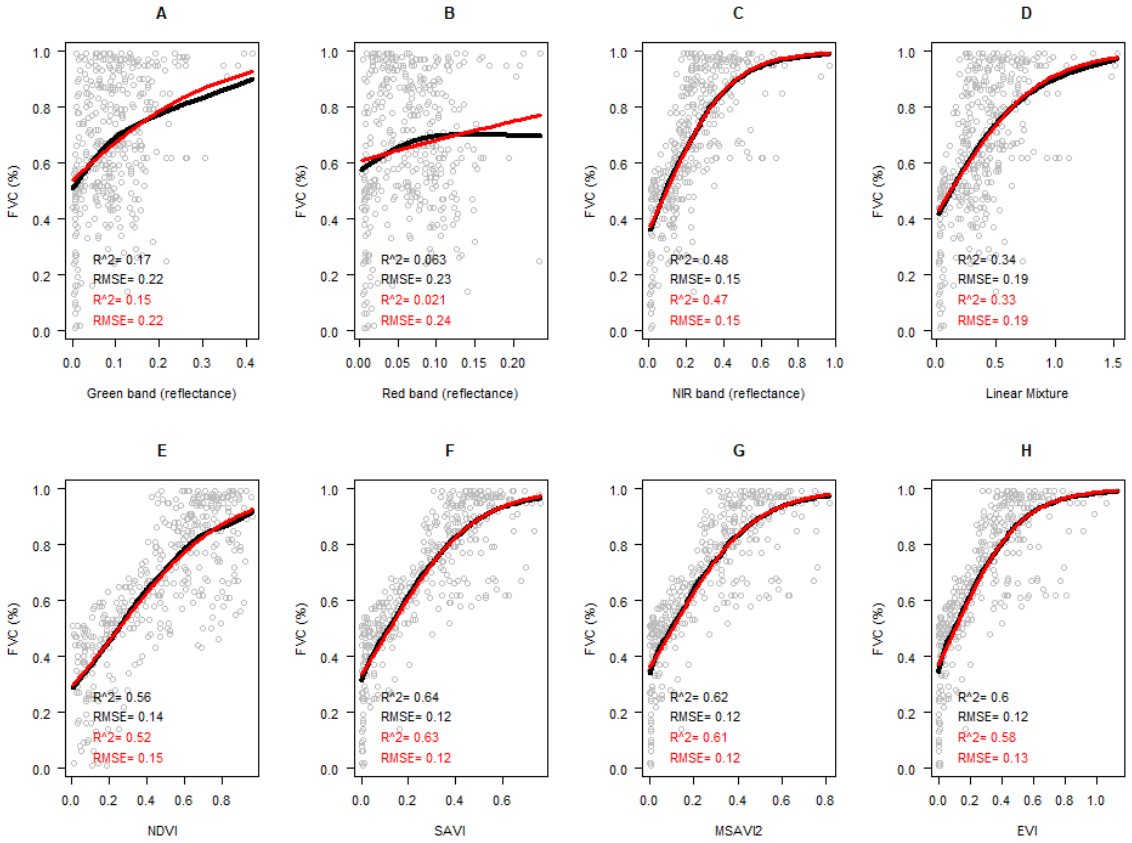

Figure 16: Beta models for individual spectral bands, band mixture and spectral indices on a 5 × 5 pixel size. FVC is represented as a fraction because beta models are bounded between 0-1.

Another difference between the linear and beta models is that beta models at the 20 × 20 grid display slightly higher intercept values than those at the 5 × 5 grid (see Figure 16 and Figure 17). It is also noticeable that, when considered individually, the green and red spectral bands do not seem to have a strong relationship with FVC. However, when combined with the NIR band the linear mixture model appears to be a closer relationship with vegetation cover across all pixel sizes (see Table 5).

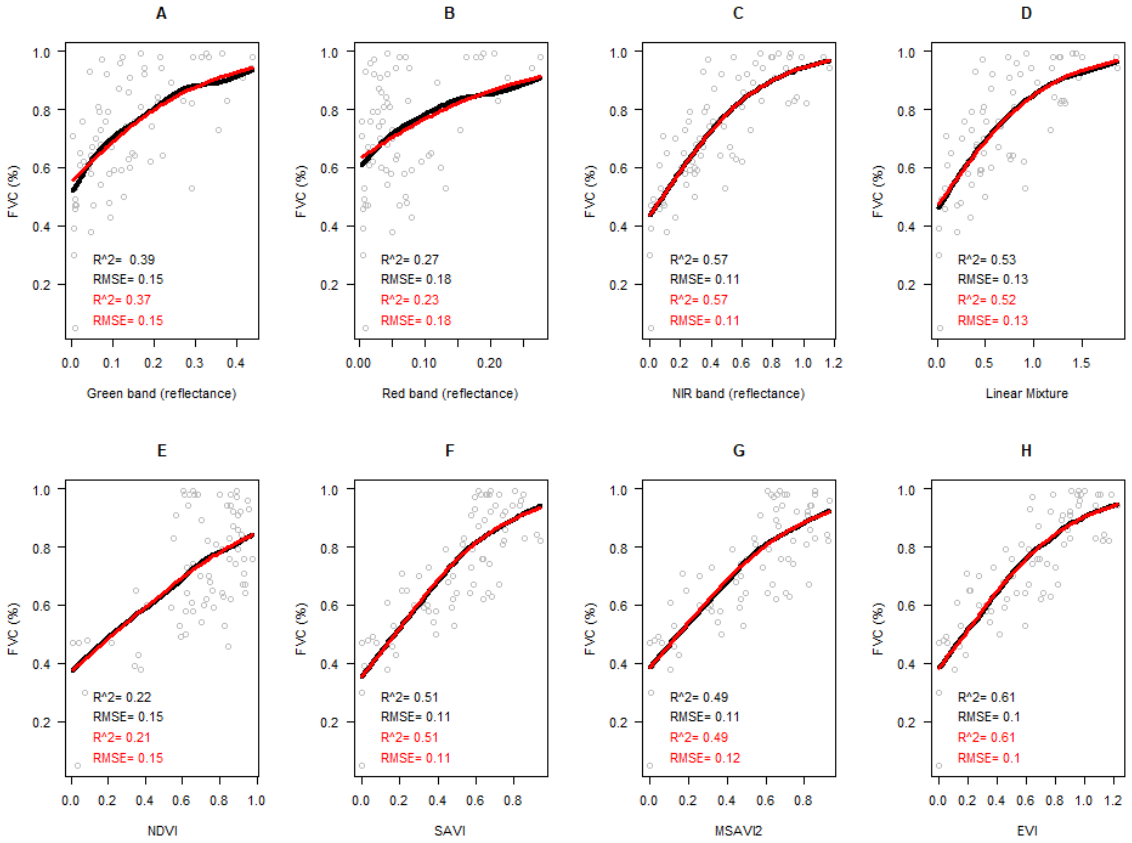

Figure 17: Beta models for individual spectral bands, band mixture and spectral indices on a 20 × 20 pixel size. FVC is represented as a fraction because beta models are bounded between 0-1.

3.4.3 Validation Models for experimental images

3.4.3.1 Linear models

After creating the models, we validated them with an independent image by comparing the true FVC against the predicted FVC. Figure 18 reveals the correlations between true and predicted FVC for the eight spectral indices and bands at the 5 × 5 scale, where black and red lines represent models with and without depth respectively. In our experiment, models without depth exhibit the same predictive power to those that include depth as a predictive factor of FVC. In Figure 18 we can see that the red band displays the lowest

correlations between true and predicted FVC, while the SAVI (R^2 = 0.71) and MSAVI2 (R^2 = 0.68) models have the highest correlations.

At the 20 × 20 the red spectral band maintains the lowest predictive power (R^2 = 0.2) while the EVI (R^2 = 0.71), SAVI (R^2 = 0.67) and MSAVI2 (R^2 = 0.65) models show the greatest correlation between real and predicted FVC (see Figure 19). At the 5 × 5 scale, NDVI is the only model that predicts FVC < 30%, while at the 20 × 20 scale none of the models can achieve this (see Figure 18 and Figure 19). The ability to estimate low FVC values is desirable, however most linear models will only produce FVC higher than 40%, even at very low true FVC values.

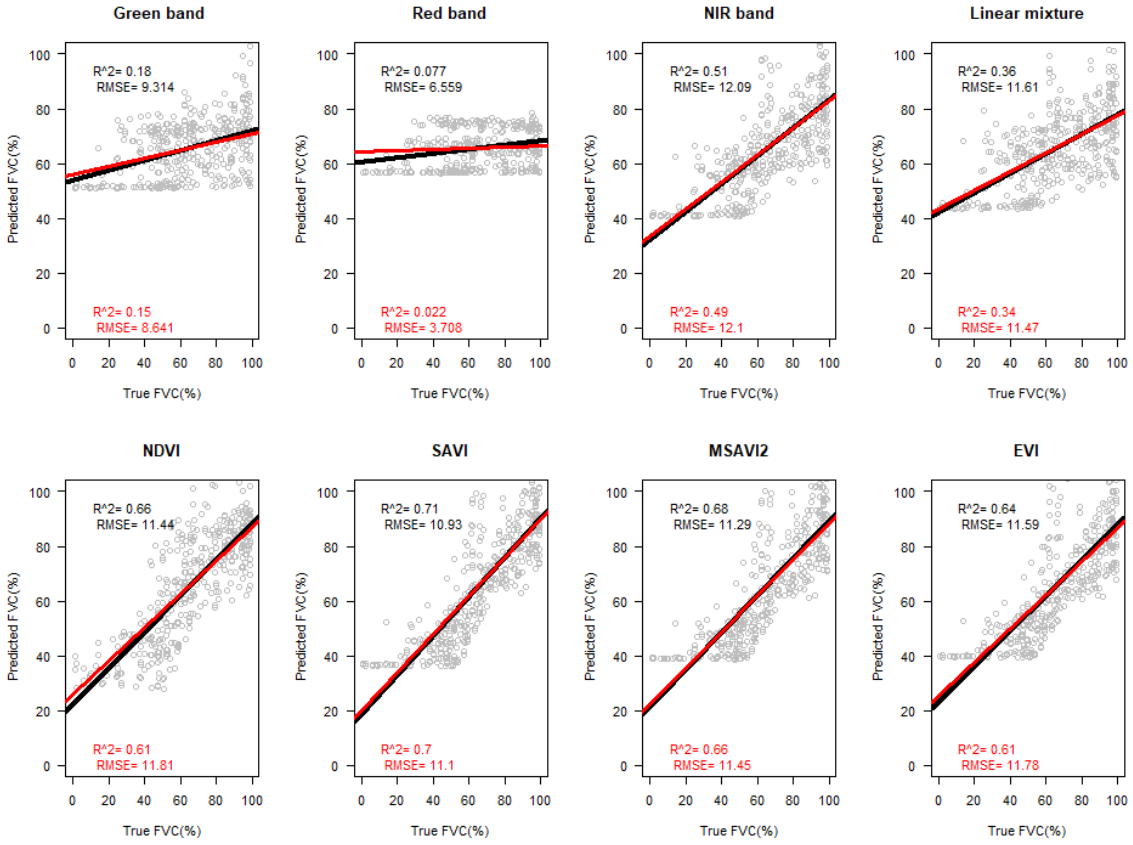

Figure 18: True versus Predicted FVC derived from linear models of individual spectral bands, band mixture and spectral indices on a 5 × 5 pixel size. Black and red lines represent models with and without depth respectively. To maintain consistency in the figure, values for Predicted FVC have been capped at 0% and 100%, regardless of the minimum or maximum value predicted.

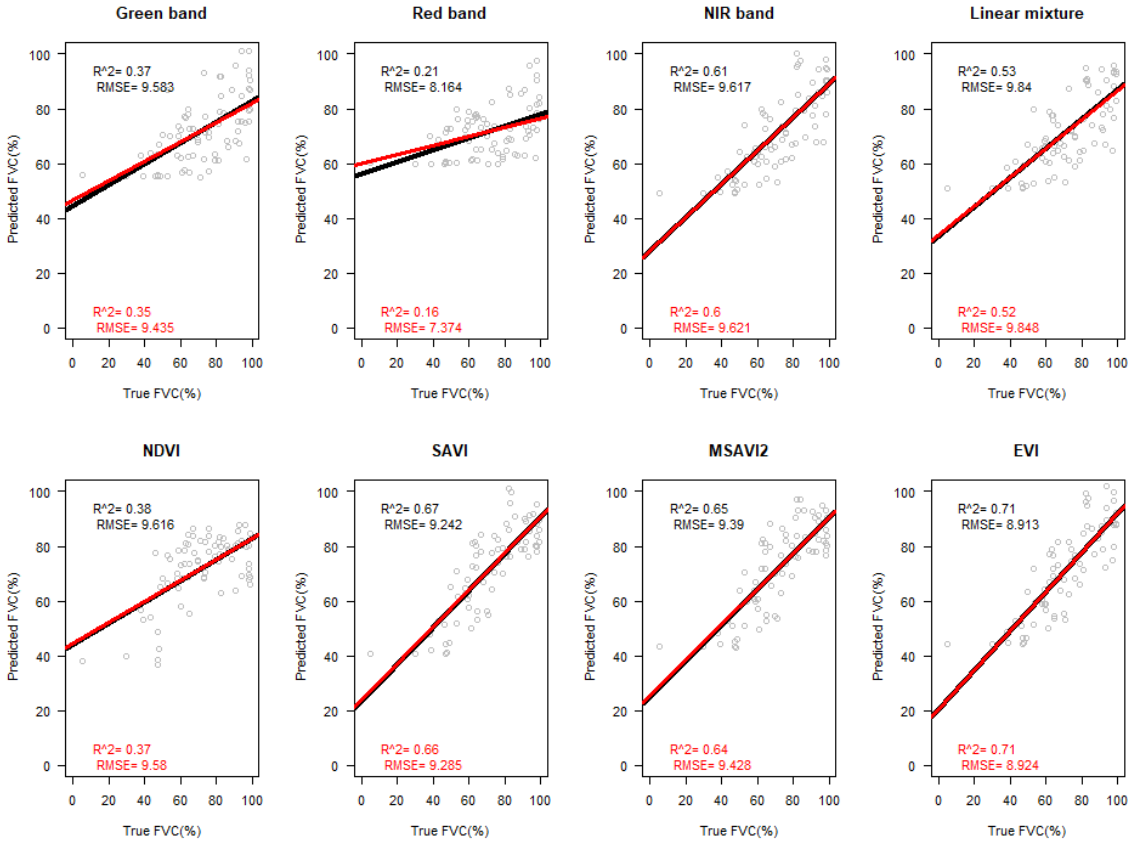

Figure 19: True versus Predicted FVC derived from linear models of individual spectral bands, band mixture and spectral indices on a 20 × 20 pixel size. Black and red lines represent models with and without depth respectively. To maintain consistency in the figure, values for Predicted FVC have been capped at 0% and 100%, regardless of the minimum or maximum value predicted.

3.4.3.2 Beta models

At the 5 × 5 grid size, the beta model for the red spectral band still has the lowest correlation between real and predicted FVC (R^2 = 0.02, see Figure 20). As with the linear models, the beta models for EVI (R^2 = 0.72), SAVI (R^2 = 0.75) and MSAVI2 (R^2 = 0.74) show the best performance whereas NDVI shows a much lower correlation between true and predicted FVC (R^2 = 0.64, see Figure 20). Given the link function used, none of the beta models predicts FVC >100% or FVC <0%, regardless of the grid size, which is one of the advantages of using this particular non-linear model.

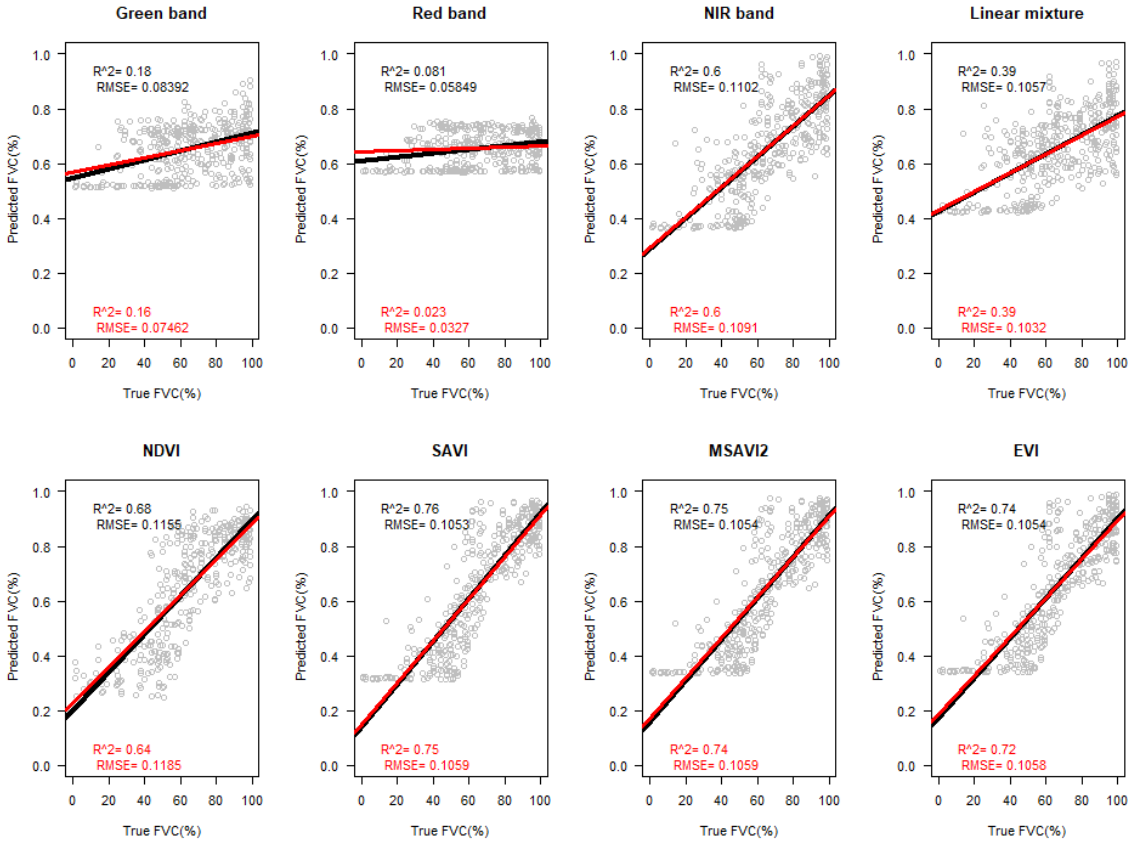

Figure 20: True versus Predicted FVC derived from beta models of individual spectral bands, band mixture and spectral indices on a 5 × 5 pixel size. Black and red lines represent models with and without depth respectively.

Similar to linear models, not all beta models are able to predict FVC < 30%. At the 5 × 5 scale the lowest predictions of FVC come from the EVI (18%), SAVI (19%) and MSAVI2 (21%). At the coarser 20 × 20 grid size, NDVI, and SAVI predict 37% and 35% FVC respectively, highlighting the difficulty of modelling this biophysical variable. Most other models retain their lower and upper limits from the 5 × 5 grid. As discussed above, the 'logit' link function in the beta regression model bounds FVC between 0 and 1, making beta models more appropriate for applications where the predicted variable is bounded between 0-1.

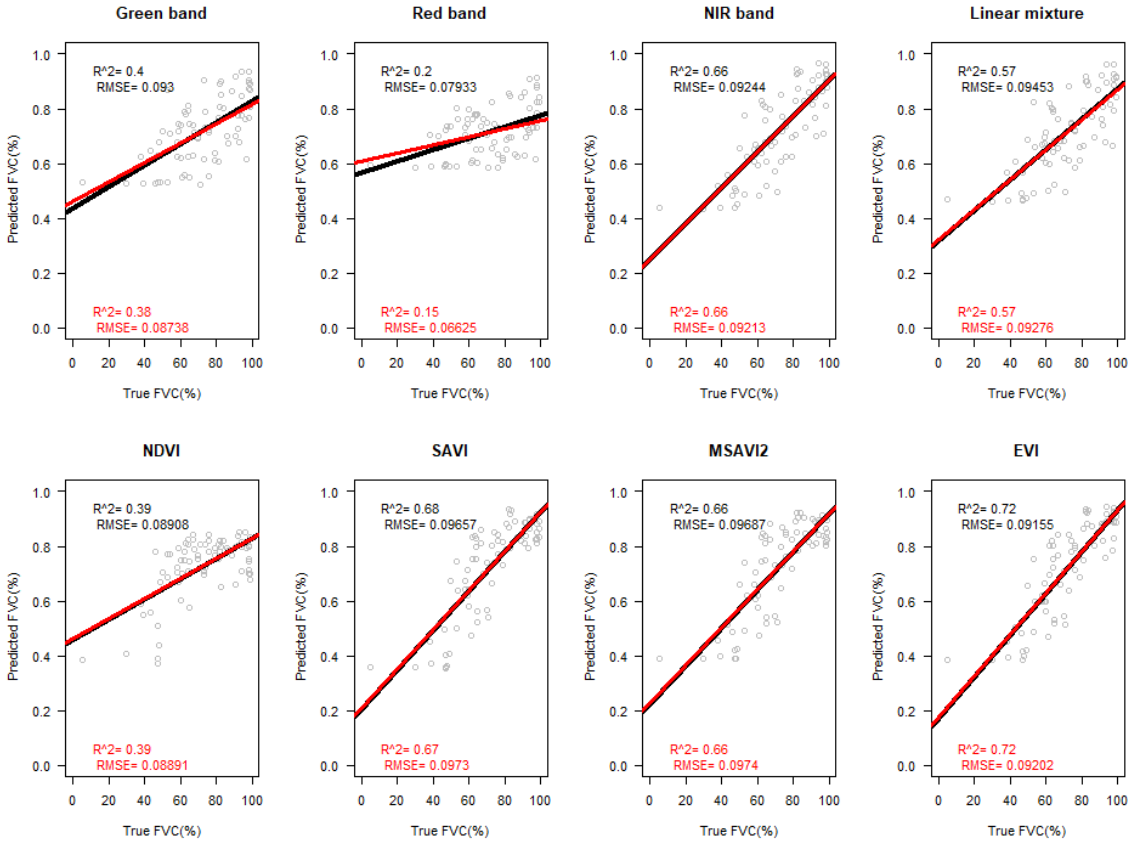

Figure 21: True versus Predicted FVC derived from beta models of individual spectral bands, band mixture and spectral indices on a 20 × 20 pixel size. Black and red lines represent models with and without depth respectively.

Regarding the different pixel sizes used, Table 6 shows a comparison of RMSE values for spectral indices across all pixel sizes, while Table 7 compares MAE values. In general, EVI, SAVI and MSAVI2 produce the models with the lowest RMSE values regardless of the type of model or the inclusion depth as a predictive variable. Notably, models that use NDVI present higher RMSE values across pixel sizes and modelling techniques when compared to EVI, SAVI and MSAVI2. Also, RMSE values were higher for linear and beta models at 5 × 5 scale than those at the 20 × 20 scale, however with only four pixel sizes tested we cannot make a generalization of a trend.

When looking at the models with and without depth, we can see that linear models that include depth have marginally lower RMSE values than those without depth (see Table 6).

This trend is reversed on beta models where models without depth present the lower RMSE values. As shown in Table 5 and Table 6, the predictive power and RMSE of each index is similar across pixel sizes. In other words, if the appropriate index is selected the predictive power and RMSE are of the models should not change drastically if the data is up-scaled (Lausch et al., 2013).

Table 6: Comparison of RMSE values across all pixel sizes.

RMSE values for linear models

	With Depth				Without Depth			
	5x5	**10x10**	**15x15**	**20x20**	**5x5**	**10x10**	**15x15**	**20x20**
EVI	14.45	12.26	13.71	10.55	15.04	12.30	13.78	10.57
Green	21.90	18.79	19.94	15.50	22.31	18.84	19.98	15.84
Linear mixture	19.37	16.34	18.03	13.48	19.64	16.35	18.03	13.58
MSAVI2	13.70	12.36	13.42	11.62	14.08	12.39	13.60	11.73
NDVI	14.06	15.12	16.19	15.41	15.15	15.46	16.23	15.51
NIR	16.91	14.68	16.31	12.31	17.24	14.68	16.35	12.32
Red	23.21	21.81	21.93	17.42	23.90	21.96	22.17	17.99
SAVI	12.94	11.89	13.11	11.25	13.28	11.90	13.32	11.36

RMSE values for beta models

	With Depth				Without Depth			
	5x5	**10x10**	**15x15**	**20x20**	**5x5**	**10x10**	**15x15**	**20x20**
EVI	0.12	0.11	0.13	0.10	0.13	0.11	0.13	0.10
Green	0.22	0.20	0.15	0.22	0.18	0.20	0.15	0.15
Linear mixture	0.19	0.18	0.19	0.18	0.15	0.13	0.15	0.13
MSAVI2	0.12	0.13	0.13	0.11	0.12	0.11	0.13	0.12
NDVI	0.14	0.15	0.16	0.15	0.15	0.15	0.16	0.15
NIR	0.15	0.22	0.16	0.11	0.15	0.13	0.16	0.11
Red	0.23	0.18	0.22	0.18	0.24	0.22	0.22	0.18
SAVI	0.12	0.11	0.13	0.11	0.12	0.11	0.13	0.11

Another measurement that shows little variation when data are up-scaled is the Mean Absolute Error (MAE, see Table 7). We used MAE to determine the average magnitude of the errors in our models and found two main things: firstly, there is little difference in the

MAE values for models with depth and without depth. Secondly, most models show a marginally lower MAE value at coarser pixel sizes than at finer ones.

Table 7: Comparison of MAE values across all pixel sizes.

MAE values for linear models

	With Depth				Without Depth			
	5x5	**10x10**	**15x15**	**20x20**	**5x5**	**10x10**	**15x15**	**20x20**
EVI	11.35	9.32	10.10	8.21	11.55	9.20	10.30	8.26
Green	17.95	15.40	15.64	12.58	18.20	15.39	15.69	12.68
Linear mixture	15.68	13.14	13.57	10.80	15.58	13.12	13.57	10.85
MSAVI2	10.63	9.56	10.24	9.43	10.75	9.51	10.53	9.50
NDVI	11.40	12.14	12.92	12.83	12.05	12.36	12.94	12.91
NIR	13.46	11.58	12.02	9.66	13.34	11.54	12.07	9.65
Red	19.36	18.25	18.24	14.44	20.02	18.40	18.27	14.53
SAVI	10.04	9.24	9.99	9.26	10.14	9.22	10.34	9.43

MAE values for beta models

	With Depth				Without Depth			
	5x5	**10x10**	**15x15**	**20x20**	**5x5**	**10x10**	**15x15**	**20x20**
EVI	0.10	0.08	0.10	0.08	0.10	0.08	0.10	0.08
Green	0.18	0.15	0.16	0.12	0.18	0.15	0.16	0.12
Linear mixture	0.15	0.12	0.13	0.10	0.15	0.12	0.13	0.10
MSAVI2	0.09	0.09	0.10	0.09	0.09	0.09	0.11	0.10
NDVI	0.11	0.12	0.13	0.13	0.12	0.12	0.13	0.13
NIR	0.12	0.10	0.11	0.09	0.12	0.10	0.11	0.09
Red	0.19	0.18	0.18	0.15	0.20	0.19	0.18	0.15
SAVI	0.09	0.09	0.10	0.09	0.09	0.09	0.11	0.10

In summary, our results show that when using spectral bands or indices in the 400-100nm range of the spectrum: *i*) water depth has a negligible effect on the estimation of FVC, *ii*) SAVI, MSAVI2 and EVI are better predictors of FVC than NDVI and, *iii*) the selection of the index and modelling technique seem to have greater effect on FVC prediction than the pixel size.

3.4.4 The effect size of water depth using satellite imagery

To determine if the results from our experiment held true in a mangrove ecosystem, we followed the workflow in Figure 13 to create linear and beta models for the two satellite images from our study site. In Figure 22, we show a false color composite of the low tide image at its original resolution (i.e. 1.2m x 1.2m) and resampled to 5x5 and 20x20 cells along their corresponding EVI and FVC.

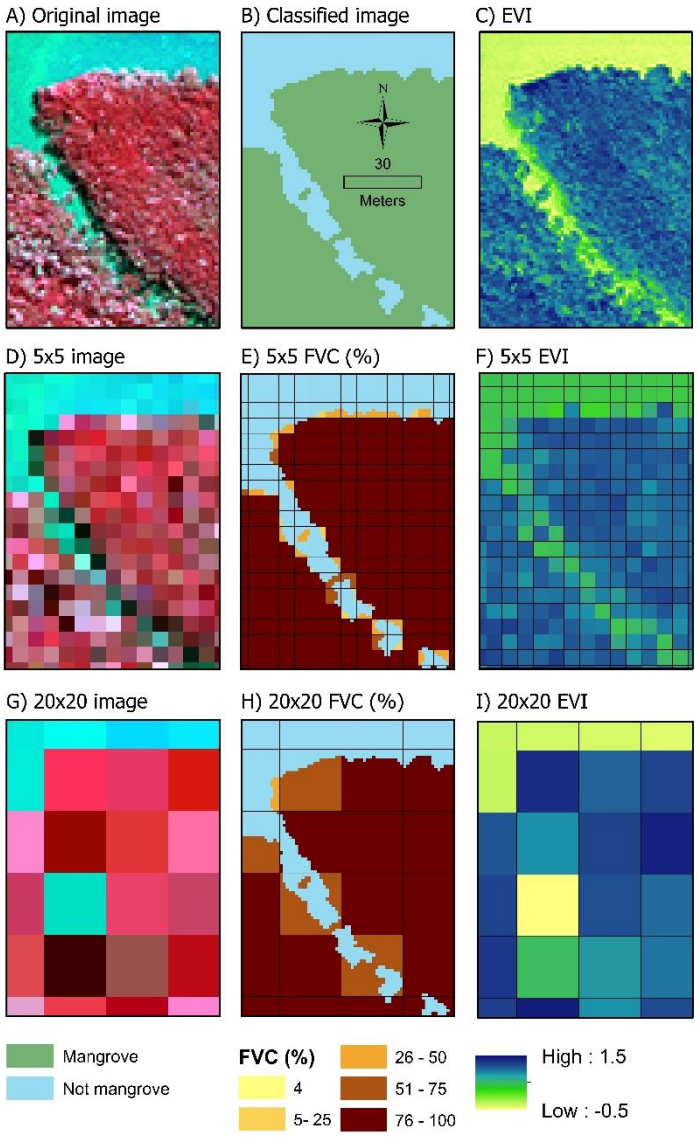

Figure 22: Original and resampled satellite images from our study site for low tide image (August 2015). False colour composite, supervised classification and EVI are shown in panels A, B, C respectively. False colour composite, FVC and EVI for the 5x5 and 20x20 grids are shown in panels D through I respectively.

After estimating the true FVC from each image, we used the spectral indices to create linear and beta models that of FVC. We selected pixels with mangroves from both images and

created a training and testing dataset with a 75%-25% split. Finally, we used Cohen's d, the difference in AIC values and R^2 values to compare the models that included depth with those that excluded depth as a modelling factor. In Table 8 we show the results of such comparison for the low and high tide images. For brevity we will only show the results for EVI, however all indices show similar outcomes. While there is variation in the AIC values between the models, the predictive power of the models remains the same. In other words, by including water depth as a factor to predict FVC does not imply the models will have better predictive power (i.e. R^2). In summary, the effect of water depth is negligible when estimating FVC regardless of the scale or modelling technique.

Table 8: Effect size of water depth in FVC estimation from satellite images

	Linear models			Beta models		
EVI	Cohen's d	ΔAIC	R-squared Difference	Cohen's d	ΔAIC	R-squared Difference
5x5	-0.01	-68.8	0.00	-0.02	78.9	0.00
10x10	0.04	-38.4	0.00	0.02	49.9	0.00
15x15	0.01	-24.6	0.00	0.00	32.4	0.00
20x20	0.02	-22.0	0.01	0.02	28.0	0.01

3.5 Discussion

Accurately predicting fractional vegetation cover in mangrove ecosystems remains an unresolved issue. Here, we designed an experiment to determine the influence of tidal height in estimating FVC using linear and non-linear models of eight spectral indices and bands. We later compared our experimental results to satellite images of mangroves under different tidal regimes and found that tidal height does not influence the estimation of FVC, regardless of the spectral index used.

Of all spectral indices used to estimate FVC, NDVI seems to be the most common. Leprieur et al. (2000) for example, used NDVI and MSAVI to predict FVC in the arid grasslands of the Niger region in West Africa. While the authors hint that NDVI may be a better predictor of low FVC, they did not fully validate their claim. They argue that sharp increases in the index values in response to vegetation are enough to support their results. In contrast, Jean-Baptiste and Jensen (2006) used linear regression models in a mangrove ecosystem to predict percent

canopy closure from field and satellite data. The authors state that their linear models reach R^2 = 0.82, their field data points (n = 32) only cover areas with measured vegetation ranging from 25% - 90%, ignoring areas with lover FVC. This omission is important because areas with FVC < 25% are found mostly in the fringes of mangrove forests alongside estuaries where intra-pixel heterogeneity may changes with the tidal height. Whereas Leprieur et al. (2000) focus on areas with low FVC and produced a curvilinear relationship, Jean-Baptiste and Jensen (2006) rely on high FVC to produce a linear model that predicts FVC outside the 0-1 range. These two studies, as well as those mentioned in Table 2, are only a sample of the many show the disagreement on the linearity or non-linearity of the NDVI-FVC relationship.

In our study, some linear models predict FVC values higher than 100%. This too was observed by Gutman and Ignatov (1998), Ding et al. (2017) and Meza Díaz and Blackburn (2003). The latter also found that the brightness of the background saturated some indices and altered their predictive power. Aside from index saturation, the relationship between FVC and spectral indices appears to affected by other factors and is less likely to be linear (Huete, 1988; Meza Díaz and Blackburn, 2003). Specifically, Jiang et al. (2008) stated that the relationship between NDVI and FVC can be linear *and* non-linear depending on the spatial scale. The authors mention that shadows and the brightness of the soil play an important role in the linearity of the relationship. The effects of soil brightness on the estimations of FVC were also observed by (Meza Díaz and Blackburn, 2003), who indicate that NDVI and SAVI are heavily affected by soil background, including sediment-laden water. Our results are consistent with those of Meza Díaz and Blackburn (2003) in the sense that other spectral indices outperform NDVI in predictive power and lower errors. In our case, EVI, SAVI and MSAVI2 are better predictors of FVC than NDVI when using linear and non-linear models.

Similar to the findings by Eskelson et al. (2011), our results demonstrate that beta models can be used as an alternative to simple linear models for FVC. Some authors have compared beta models with other, more complex and computationally intensive methods to predict FVC. For example, Coulston et al. (2012) compared beta models with a random forest classification method to predict FVC in the continental United States. They found that the random forest classification method produced better results than the beta regression models. Nonetheless, they also acknowledge that the random forest methodology requires *i)* more computational

power, *ii)* spectral normalization between images and, *iii)* that each explanatory variable is tested for significance. The advantages of using beta models are twofold: firstly, FVC will be predicted within its true range (i.e. 0-1), and secondly, it can be easily computed from different spectral bands and indices such as EVI or NDVI.

Although NDVI has been commonly used to predict FVC in various ecosystems, some studies suggest that SAVI and MSAVI provide equal or better results than NDVI (Ding et al., 2017; Kerr et al., 2003; Korhonen et al., 2015). Here, we found that EVI, SAVI and MSAVI2 are better predictors of FVC than NDVI. One reason for this is background heterogeneity. The background of the vegetation often alters NDVI values by introducing 'noise', especially when FVC < 60% (Kerr et al., 2003; Meza Díaz and Blackburn, 2003) and because NDVI often saturates when FVC ≥ 80% (Ding et al., 2017). Because we measured the reflectance at all vegetation fractions (i.e. 1 – 100%) we were able to determine that most spectral bands and indices will read zero at FVC<30%. In other words, most indices and bands only measure vegetation fractions higher than 30% when water dominates the background (see Figure 14-7). This phenomenon, when coupled with the known saturation of NDVI at high FVC could explain why the images at the 10 × 10 pixel size outperform the others. Still, we advise caution when comparing different pixel sizes.

Comparing spectral indices across spatial scales is an issue of debate. Many authors, including Wu and Li (2009), Jiang et al. (2008) and Lausch et al. (2013) have discussed the issue at length and all suggest caution when comparing up-scaled or down-scaled spatial data. While Jiang et al. (2008) state that NDVI across different spatial scales is not comparable, Lausch et al. (2013) say that up-scaled datasets 'inherit' the heterogeneity characteristics and features making them similar to the original data. Both Wu and Li (2009) and Jiang et al. (2008) make the case that changes in scale may affect the linearity of the response of NDVI to vegetation, however we could not confirm that statement with our experiment or using satellite imagery.

One of the limitations of our study is that we only used data in the 400 – 1000 nm region, meaning that indices that use short wave infrared bands were not tested. Despite this, our study is relevant to sensors with high spatial resolution that do not register longer wavelengths or provide them separately and at a fee. Another limitation of our study is the fact that we only tested two modelling techniques. While there are other, more complex models, we tested the

linear and non-linear response of the spectral indices to FVC, a matter of much debate. Finally, the code used to create a linear and a beta model in 'R' is freely available through GitHub alongside some of the data used in this project (see (Younes Cárdenas, 2018)).

3.6 Conclusions

In this study we used linear and non-linear models to *i)* examine the influence of water depth in estimating mangrove FVC, and *ii)* determine which spectral bands or indices are good predictors of FVC in mangrove ecosystems. By using very detailed imagery we have demonstrated that the effect size of water depth is negligible, at least under the conditions tested here. Our results also indicate that SAVI, MSAVI2 and EVI are better predictors of vegetation cover than NDVI given their better predictive power and lower errors. We also used high-resolution satellite imagery at two different tidal regimes to validate our experimental results and found that models with and without water as factor as essentially the same according to Cohens'd and the differences in R^2 values. Further research is needed to understand the implications of using EVI, SAVI and MSAVI2 (instead of NDVI) in different inversion models to estimate FVC in mangrove ecosystems. The results from our experiment suggest three main things:

1. Linear and beta models produce similar results when predicting FVC from spectral bands or indices particularly at fine spatial resolutions. Although beta regression is seldom used to relate FVC to spectral indices, it should be considered as robust alternative to linear models.

2. Spectral bands and indices other than NDVI should be considered when predicting FVC using remotely sensed imagery in mangrove environments. More specifically SAVI, MSAVI2 and EVI are suitable replacements for NDVI as they outperform the latter index across all pixel sizes. Our results demonstrated that, under the evaluated conditions, NDVI is not the best predictor of FVC. While other studies have suggested this, we have systematically demonstrated it using highly detailed imagery in a controlled environment and validated it using high-resolution satellite imagery.

3. Although not directly comparable, finer pixel sizes (i.e. 5 × 5 and 10 × 10) provide the best relationships between predicted and true FVC than coarse pixel sizes (i.e. 15 × 15 and 20

× 20). This indicates that, under certain conditions, the selection of the spectral index for estimating FVC plays a more important role than the pixel size used.

Based on these findings, our next steps include using beta regression models over broad scale mangrove ecosystems and obtain a measure of FVC change over time.

3.7 Acknowledgements

This work was supported by NIESGI Cia. Ltda., James Cook University Postgraduate Research Fellowship, and a Wet Tropics Management Authority Student Research Grant. We would like to thank the Digital Globe Foundation for providing the satellite imagery used in this study and the anonymous reviewers for their insightful comments and contributions to enhancing this manuscript.

4 Extracting mangrove phenology from Landsat imagery: a novel approach using Generalized Additive Models

A version of this chapter is currently in press in 'Remote Sensing'.

4.1 Graphical Abstract

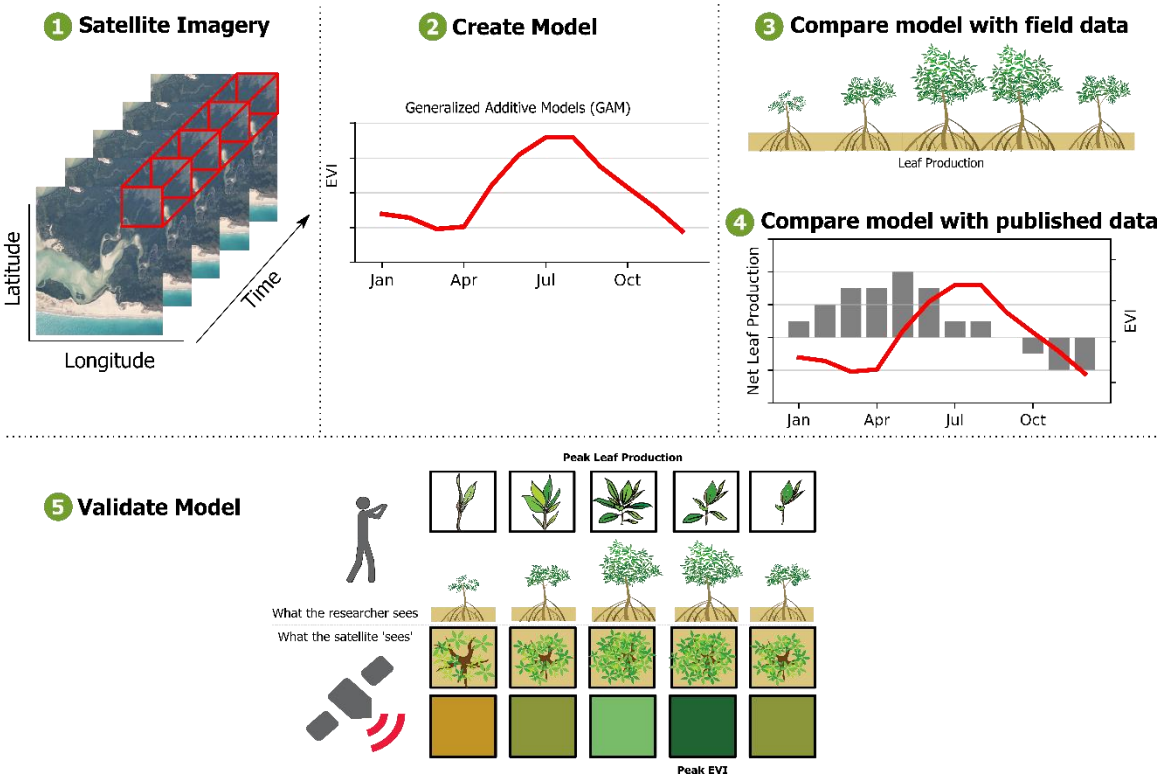

4.2 Abstract

Around the world, the effects of changing plant phenology are evident in many ways: from earlier and longer growing seasons to altering the relationships between plants and their natural pollinators. Plant phenology is often monitored using satellite images and parametric methods. Parametric methods assume that ecosystems have unimodal phenologies and that the phenology model is invariant through space and time. In evergreen ecosystems such as mangrove forests, these assumptions may not hold true. Here we present a novel, data-driven

approach to extract plant phenology from Landsat imagery using Generalized Additive Models (GAMs). Using GAMs, we created models for six different mangrove forests across Australia. In contrast to parametric methods, GAMs let the data define the shape of the phenological curve, hence showing the unique characteristics of each study site. We found that the Enhanced Vegetation Index (EVI) model is related to leaf production rate (from in situ data), leaf gain and net leaf production (from published literature). We also found that EVI does not respond immediately to leaf gain in most cases, but has a two- to three-month lag. We also identified the start of season and peak growing season dates at our field site. The former occurs between September and October and the latter May and July. The GAMs allowed us to identify dual phenology events in our study sites, indicated by two instances of high EVI and two instances of low EVI values throughout the year. We contribute to a better understanding of mangrove phenology by presenting a data driven method that allows us to link physical changes of mangrove forests with satellite imagery. In the future, we will use GAMs to 1) relate phenology to environmental variables (e.g. temperature and rainfall) and 2) predict phenological changes.

Keywords: GAMs; Generalized Additive Models; EVI; Landsat; Mangrove forests; Phenology; Time Series Analysis;.

4.3 Introduction

Around the world, the effects of changing plant phenology are evident in many ways: from earlier and longer growing seasons to altering the relationships between plants and their natural pollinators (Chambers et al., 2013; Garonna et al., 2016; Morellato et al., 2016a). Remote sensing techniques allow us to detect subtle changes in plant phenology, and here we present a novel approach to describe phenological cycles of mangrove ecosystems. We contribute to a better understanding of mangrove phenology by investigating physical changes of mangrove ecosystems and how the evidence of change is captured by satellite images. Accurately modelling and predicting mangrove phenology will help us understand not only the seasonal variations, but also the long-term trends in natural cycles of these forests. New models, such as the one presented here, will advance our understanding of how drought, heat waves and other extreme weather events affect mangrove health and growth. Similar to using

sea temperature to predict coral bleaching events, we could use phenology to predict mangrove dieback events akin to those of 2015 and 2016 in the Gulf of Carpentaria in northern Australia.

Phenology is related to the life cycle events of plants and animals and their relationship to climatic and other abiotic factors (Menzel, 2002; Morellato et al., 2016). Plant phenology also plays an important role in the carbon cycle in the form of sequestration and storage. Phenological cycles of plants ensure that leafing, flowering and fruiting events occur during the most appropriate season to achieve maximum growth and reproductive success. Mangrove phenology is often described at the species level by relating the time of year when trees flower, fruit or defoliate with suspected drivers like temperature and rainfall (Duke et al., 2006; Tomlinson, 1986). For example, Duke (1990) described the phenology and distribution of *Avicennia marina* mangroves along the Australian coastline, and Metcalfe et al. (2011) described the flowering and leafing phenologies of mangroves in the Darwin region. While these descriptions provide a very valuable baseline for comparison, they often lack the spatial extent and frequency needed for phenological studies (Younes Cárdenas et al., 2017).

We can monitor mangrove phenology using remote sensing or we can collect *in situ* data. The main advantage of *in situ* monitoring is that it provides information at the tree and species level, where observations can be very detailed over a wide range of variables. However, *in situ* monitoring is challenging, time-consuming and variation in methods and survey effort can make it difficult to compare results (Cresswell and Semeniuk, 2011). In contrast, the remote sensing approach provides information at the landscape and continental scales and is consistently acquired over time and space (Younes Cárdenas et al., 2017). While there are many studies that used spaceborne sensors to map mangroves at the global (Ciri et al., 2011; Hamilton and Casey, 2016), continental (Lymburner et al., 2019b; Rogers et al., 2017), and local scales (Asbridge et al., 2016), few have used these sensors to monitor mangrove phenology. (Pastor-Guzman et al., 2018) used MODIS (Moderate Resolution Imaging Spectroradiometer) data between 2000-2014 to detect mangrove phenology using four different spectral indices in the Yucatan peninsula in Mexico. Similarly, (Songsom et al., 2019) compared the phenology of mangroves to that of the surrounding forests using MODIS imagery. While the temporal resolution of the MODIS sensors is very high (1-2 days), the spatial resolution is coarse (250-

500m). Landsat satellites offer a better spatial resolution at the cost of a lower temporal resolution. Despite this trade-off, the Landsat archive is key to using remote sensing to monitor mangrove phenology as it provides more than 30 years of imagery at a spatial resolution of 30 m x 30 m and a temporal resolution of 8 – 16 days (Dhu et al., 2017).

To date, most studies on plant phenology have used fully parametric models, mainly in the form of double logistic or sinusoidal functions (Broich et al., 2015; Pastor-Guzman et al., 2015; Zhang et al., 2014). These functions may perform well in deciduous or temperate forests, where there is a single, well defined period of leaf production, and a single, well defined period of leaf senescence (Melaas et al., 2016; White et al., 2009), but these methods may not be well suited for mangroves and other evergreen forests. When detecting phenology, one of the main limitations of parametric models (e.g. logistic functions) is that they fail to detect asymmetric trends in leaf growth or senescence (Melaas et al., 2016). Considering that the growing season of some evergreen forests consists of two periods of leaf growth and death, fully parametric (or model-driven) models have the potential to oversimplify the phenology of these ecosystems. Other, more complex models have also been used to examine plant phenology, mainly in the form of artificial neural networks, however these methods are known to have mostly been used in croplands (Xin et al., 2020) . Semi parametric (or data-driven) models, on the other hand, may be better suited for this task as they do not necessarily assume that there will be a single peak or trough in leaf growth or death. Rather, semi parametric models use the data to determine the shape of the phenology.

Studies have documented the dual phenology of mangroves (Tomlinson, 1986) and other evergreen forests (Liu et al., 2013) in the field, but this dual phenology has not been recorded using satellite imagery. Dual phenology refers to two periods of leaf growth; unlike deciduous forests which grow their leaves during the spring, some evergreen forests have two periods of leaf growth every year. In mangrove forests these events have never been documented using satellite imagery, probably due to the use of fully parametric models to detect phenology, or because *in situ* data collection focuses mainly on litter fall rather than leaf production. The novelty of this study is that, we use a semi-parametric method to model mangrove phenology and in doing that we present, for the first time, these two distinct periods of leaf growth described in the literature. Generalized Additive Models (GAMs) are commonly used in ecology

and climate sciences, to examine non-linear relationships between response and independent variables. Here we present a novel, data-driven method to extracting mangrove phenology from a series of Landsat images. We use discrete observations of mangrove forests (i.e. satellite images) and Generalized Additive Models (GAMs) to create a continuous curve of phenology over time, without assuming a certain shape, amplitude, or frequency. Our aims are to: 1) Use a semi-parametric approach (GAMs) to examine if seasonal changes in biophysical variables are related to seasonal changes in the spectral reflectance of mangrove forests;; 2) Compare the satellite-derived phenology with a set of field observations and measurements; 3) Compare the satellite-derived phenology to peer-reviewed literature describing the phenology of mangrove forests; and 4) Determine how the Enhanced Vegetation Index (EVI) responds to leaf gain, leaf fall or net leaf production in mangrove ecosystems across Australia. This manuscript is organized in the following way: firstly, we describe the site and methods used to collect the field data. Then we describe how we use the literature to create a proxy for mangrove phenology. Afterwards, we describe the use of GAMs and satellite images to detect the apparent phenology of mangroves across northern Australia. Having done this, we present the models of apparent phenology and compare them with the data collected in the field, and the proxies from the literature. Finally, we discuss the results, limitations, and future work.

4.4 Materials and Methods

We selected six study sites across Australia to evaluate mangrove phenology from satellite imagery using GAMs. One site corresponds to field observations collected in the Gladstone region (Queensland) in the late 1990's, and the remaining sites (n=5) correspond to qualitative data extracted from peer-reviewed publications (Figure 23). In this section we first describe the field site followed by the peer-reviewed studies, the image acquisition process, and the time series analysis using GAMs. Finally, we describe the phenology model validation.

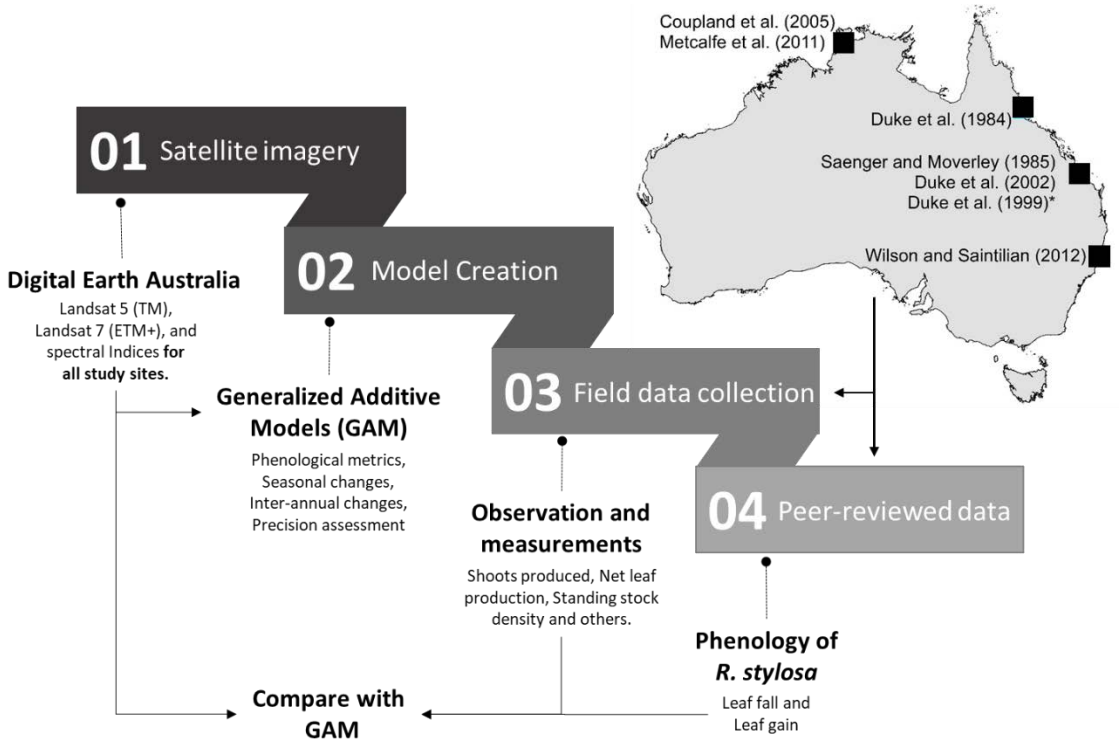

*Figure 23: Workflow and location of the study sites used to validate the phenology model. * shows the location of the field site* (Duke et al., 1999) *and two other published studies used.*

4.4.1 Field Site Description

The Gladstone region in central Queensland is home to over 100,000 ha of intertidal wetlands, out of which 30% are mangrove forests (Trewin, 2013). The annual mean temperature ranges between 18.4°C and 27.5°C, the mean annual rainfall is 874 mm, and the semi-diurnal tides often range from 1.5 – 3.5 m but reach up to 6 m. In this region, mangroves of the *Rhizophora, Avicenna*, and *Ceriops* genera are among the most common (Duke et al., 2006; Trewin, 2013). The field data were collected between July 1996 and August 1998 in two plots located in Fisherman's Landing and one plot on Curtis Island (Figure 24). The sites were dominated by *Rhizophora stylosa* trees and located within the Landsat World Reference System 2 (WRS-2) path 91 and rows 76 and 77.

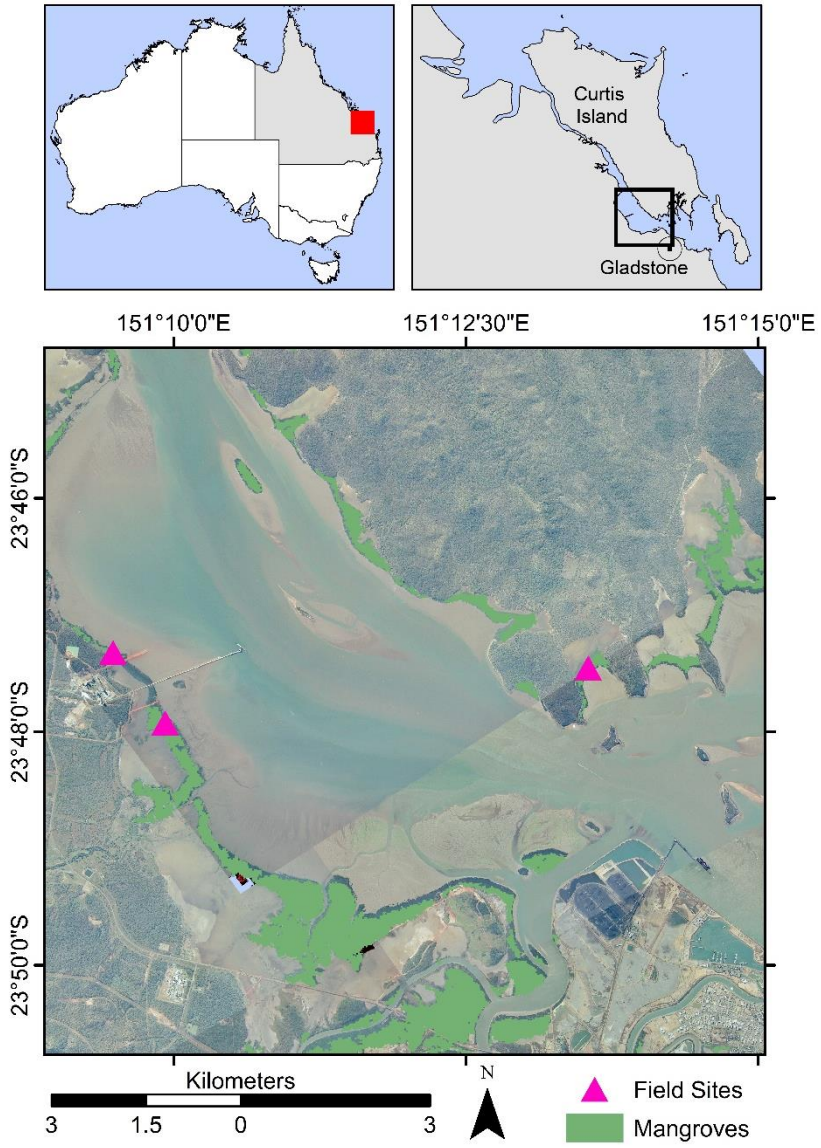

Figure 24: Location of the field sites and mangrove patches in the Gladstone region, Queensland. Aerial images of the study site for 1996, provided by the State of Queensland (QAP5402131/47)

4.4.2 Field Observations and Measurements

The data were collected by (Duke et al., 1999) in the following way: in each plot, the authors selected mature *R. stylosa* trees between 4-9 meters tall and tagged 21 leafy shoots in the upper two meters of the canopy. They conducted monthly inspections and recorded the shoot status, number of leaves, reproductive parts and number of branch shoots. To measure the amount of litter fall, the authors suspended litter traps (1m^2 in area) under the selected trees. The traps were suspended above the high tide mark and litter was collected, sorted and weighted on a monthly basis. During the data collection period the average tide height was

2.49 m according to historical records for the site (TMR - Queensland Dept. of Transport and Main Roads, n.d.). Importantly, Duke et al. (1999) never intended to validate satellite imagery with their data, therefore these data are completely independent of our EVI model. The data consist of the mean monthly values of six phenological variables, however, we selected the three that were more relevant for our study (see (Duke et al., 1999) for details). The selected biophysical variables are:

Leaves lost [leaves × m^{-2} × day^{-1}]: The number of leaves that fell into the litter traps.

Leaves gained [stipules × m^{-2} × day^{-1}]: The number of interpetiolar stipules that fell into the litter traps. This variable serves as a proxy for the number of leaves produced in a tree.

Net leaf production [leaves gained - leaves lost]: The difference between leaves gained and fallen leaves. This measure is an indication the net balance of leaves in the canopy with more or less leaves as leaves appear or fall, leaving the canopy in either debit (=stressed), credit (=growth) or neutral condition.

4.4.3 Published literature on the phenology of R. stylosa

To compare the phenology model (i.e. from the GAMs) to other sources of information, we gathered a set of peer-reviewed papers that included *R. stylosa* as target species. The reasons for selecting this species were twofold: 1) it is common throughout northern Australia; and 2) a number of studies have described its phenology over a wide geographic area across the Indo West Pacific region. We looked for papers that had a graphical interpretation of leaf fall and/or leaf gain over time and we found six examples (Table 9). We used the published graphical interpretations of leaf fall and leaf gain to determine, in a qualitative way, the times of the year where most leaves grew or fell. All published graphs show 'Time' on the horizontal axis and a measure of leaf fall or gain on the vertical axis. In each study, we divided the vertical axis into five equidistant categories (i.e. very low, low, medium, high, very high) and recoded the category for each month (not shown). Finally, we calculated the net leaf production from each study by subtracting the leaf fall from leaf gain values and then compared the three variables with the EVI models of each site (Table 9).

Table 9: Peer-reviewed studies used for the qualitative comparison.

Reference	Target species	Leaf fall or Leaf Gain	Study duration	Observation frequency	Location
(Duke et al., 1984a)	*C. tagal var. tagal* *B. gymnorhiza* *R. apiculata* *R. stylosa* *R. X lamarckii*	LF, LG	1975 - 1978	Monthly	Hinchinbrook Island, QLD
(Saenger and Moverley, 1985)	*A. annulata* *A. corniculaturn* *A. marina* *C. tagal* *E. agallocha* *L. racemosa* *O. octodonta* *R. stylosa* *X australasicus*	LF, LG	1979 - 1982	Monthly	Gladstone and Proserpine, QLD
(Duke, 2002a)*	*R. stylosa*	LF, LG	1996 - 1998	Monthly	Gladstone, QLD
(Coupland et al., 2005)	*A. marina* *C. australis* *R stylosa* *S. alba*	LF, LG	1999 - 2001	Monthly	Darwin Harbor, NT
(Metcalfe et al., 2011a)	*A. marina* *B. exaristata* *C. schultzii* *C. australis* *E. ovalis* *L. racemosa* *R. stylosa* *S. alba*	LF	1997 - 2000	Monthly	Darwin Harbor, NT
(Wilson and Saintilan, 2012)	*R. stylosa*	LF, LG	2002 - 2004	73 days	South West Rocks Creek, Richmond River, Brunswick River, NSW

**Same location as Duke et al. (1999).*

From Table 9 one can see that the studies by (Duke et al., 1984b) and (Saenger and Moverley, 1985) pre date the time where Landsat imagery was collected. Between 1974 and 1989, cyclones Dawn (March 1976), Keith (January 1977), Gordon (January 1979), and Kerry (March 1979) affected Hinchinbrook Island, Gladstone, or Proserpine in Queensland. Neither (Duke et al., 1984b) nor (Saenger and Moverley, 1985) mention the effects of cyclones, drought on their respective study sites, either because the field campaigns happened before the cyclones, or there was no significant damage to the trees. While there is no certainty about the effects of extreme weather events for those studies, here we assume that the phenology observed by the authors did not change until satellite imagery was acquired.

4.4.4 Landsat image acquisition and processing

Digital Earth Australia holds a copy of the Landsat archive (1987 – present) for the whole of Australia (Dhu et al., 2017; Lewis et al., 2016). Digital Earth Australia provided all images (n=787) of our sites between 1987 and 2006 for the Landsat 5 (TM) and Landsat 7 (ETM+) sensors, and performed 1) geometric, 2) atmospheric and 3) Nadir-adjusted Bidirectional reflectance distribution function Reflectance (NBAR) corrections. Digital Earth Australia uses the 'Pixel Quality Assessment' algorithm (Dhu et al., 2017) to remove pixels with clouds and cloud shadows, and we used the resulting product to extract the Enhanced Vegetation Index (EVI) (Huete et al., 2002). EVI is commonly used to assess phenology using remote sensing (Broich et al., 2014; Pastor-Guzman et al., 2018; Songsom et al., 2019), it rarely saturates with high-density vegetation, and has demonstrated to perform better than other spectral indices in mangrove ecosystems (Younes et al., 2019).

Our study leverages the high temporal density of the Landsat archive, and the overlapping footprints of two or more Landsat scenes, hence increasing the number of usable pixels in a given area. To compare the GAMs with peer-reviewed literature, we selected a period equal to the time of the data collection plus and minus one year, thereby ensuring that the models had enough input data. In the cases where studies were dated before 1987, we used the first three years of available imagery of the area to create the GAM. We estimated the location of the studies from the site descriptions in each publication and created a region of interest of approximately 17 ha of mangrove forests surrounding the study area. Afterwards, we masked

out pixels with no mangroves and applied the GAM to every mangrove pixel within our region of interest. This approach ensured that we captured the phenology of the mangrove community instead of a small plot.

4.4.5 Time Series Analysis using Generalized Additive Models

With all images pre-processed, georeferenced and sorted by time of acquisition, we proceeded to create a model of phenology for every available pixel in our study sites using GAMs. Like other statistical methods for time series analysis, GAMs decompose a noisy time series (e.g. satellite images) into three main constituents: a seasonal component, a trend component and a residual component. Here, we will only focus on the *seasonal component* (i.e. phenology), which refers to a change or fluctuation in a series that occurs periodically one or more times per year (Hyndman and Athanasopoulos, 2018)

Contrary to linear additive models, GAMs are statistical models in which the relationship of predictor and response variables is captured by smooth functions instead of coefficients (Hastie and Tibshirani, 1986). Equations 1 and 2 show the respective linear and generalized additive relationships between one response variable (Y) and two predictor variables (X_i) for i observations (Jones and Almond, 1992):

$$Y = \beta_0 + \beta_1 X_{i1} + \beta_2 X_{i2} + \varepsilon \quad (1)$$

$$Y = \beta_0 + f_1(X_{i1}) + f_2(X_{i2}) + \varepsilon \quad (2)$$

Noticeably, there is no change in the form of the model. However, there is no assumption that the relationship between predictor and response variables is linear. In equation (1) an additive linear relationship between Y and X_i is captured by the slope terms β_1 and β_2, while in equation (2) the additive relationship is captured by the 'smooth' functions $f_1(\cdot)$ and $f_2(\cdot)$. The shape of the 'smooth' functions ($f_n(\cdot)$) is determined during the computation in an iterative way and can take many forms (Jones and Almond, 1992; Zuur, 2012). Another characteristic of GAMs is that measurements do not need to be evenly spaced in time (Taylor and Letham, 2018). This works well in our case for two reasons: 1) pixels with clouds, shadows and other errors are

flagged as invalid observations leading to time series with random gaps in both length and timing; and 2) areas where the footprints of two or more scenes overlap will have more observations than areas with no overlap.

To detect mangrove phenology from a satellite-derived data series, we used the python programming language and the 'Prophet' package (version 0.3.post2) developed by Facebook (Taylor and Letham, 2018). Facebook designed this package to analyze user engagement with the social network at different time scales, and to investigate how periodic events such as holidays affect that engagement. Similar to mangrove phenology, user engagement on the social media platform is affected by regular and irregular events such as weekends (i.e. regular events) and public holidays, which change every year (Taylor and Letham, 2018). In a similar fashion, mangroves are affected by regular changes in temperature and rainfall (i.e. seasons) and irregular events such as cyclones or drought. While the time scales may differ, the concept of tracing an event (e.g. phenology or user engagement) over time remains the same. We selected this package due to its ease of use and re-purposed it to extract seasonal variations in greenness and phenological metrics from satellite images of mangrove forests.

I chose 'Prophet' because when I started this thesis chapter it was (to the best of my knowledge) the only python package that had the capability to generate GAMs in the python programming language. The other main reason to use prophet is that the developers of the packages had already published a peer-reviewed paper showing the use, capabilities, and some results of the package, therefore providing me with a high degree of certainty that the package was valid and functional. Since then, and especially since 2019, other libraries and packages have added GAMs to their repertoire of statistical functions, however most are still in 'beta' versions and testing is ongoing. In addition, 'Prophet' allows me to analyse the seasonal patterns, and the overall trend separately from one another, thereby giving me a lot of flexibility in the analysis and interpretation of the results.

4.4.6 Phenological metrics

With the data ingested, Prophet separates the seasonal components of the time series from the trend and the residual components. Prophet then uses GAMs, a Fourier series and a matrix of seasonality vectors to model periodic events in a time series (Taylor and Letham, 2018). The

seasonal component of the GAMs is used as an approximation of phenological cycles and several techniques can be adapted to extract the start, end, and duration of the mangrove 'green-up' season. In this study, we adopted similar definitions to those by (Restrepo-Coupe et al., 2015) to identify the Start of Season, End of Season and Peak Growing Season, however, as our study does not involve a sinusoidal curve the definitions vary slightly. For simplicity, we define the start of season and end of season as the lowest points, and peak growing season as the highest points of the de-trended time series (Figure 25). We also define the Length of the growing season as the time between the start of season and end of season. Because we use start of season, end of season and peak growing season as phenological metrics of the landscape, they do not represent individual species.

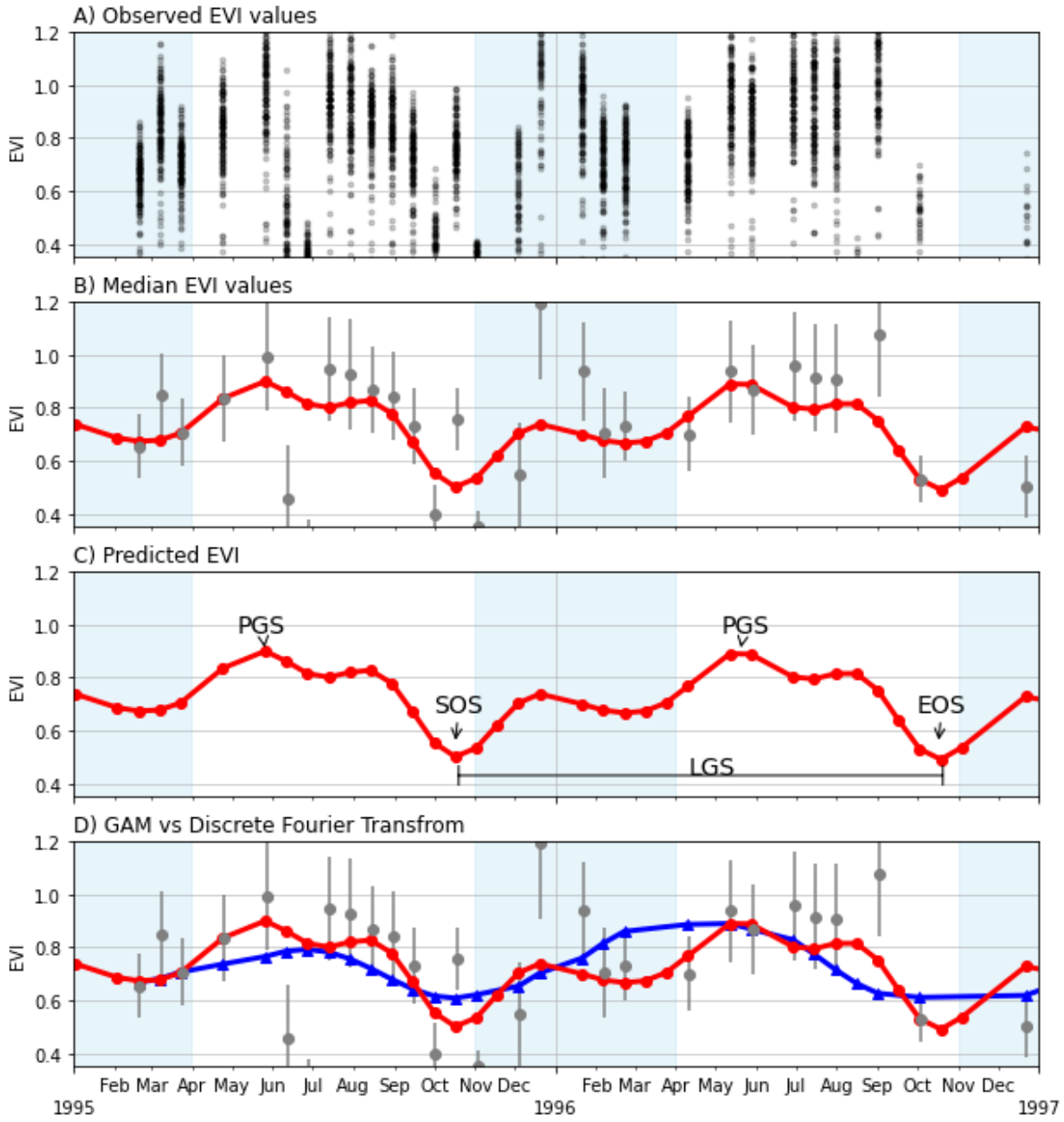

Figure 25: Panel A) shows every available EVI observation for every pixel in the 17 ha region of interest from February 1995 to December 1996 for the Gladstone region. Panel B) shows the median and standard deviation of the observed EVI values in grey dots and lines respectively, and the EVI model (i.e. GAM) in red. Panel C) shows the EVI model, the definitions of: start and end of season (SOS, EOS), peak growing season (PGS) and length of the growing season (LGS). Shaded areas represent the wet season months. Panel D) shows the apparent phenology resulting from the GAM (red) versus the apparent phenology resulting from using a Discrete Fourier Transform (blue).

We extracted the start of season and peak growing season for each pixel in our field study site in the following way: from the seasonal component, we selected the predicted index values from the GAMs that were lower or higher than the 5 or 95 percentile as potential start of season or peak growing season dates, respectively (Figure 25C). Then we selected the median

of the image acquisition dates as the start of season, peak growing season and end of season dates. In case the selected date was not a date in which an image was acquired, we searched for the image with the closest date and used that date instead.

Because we wanted to determine if the GAMs were correlated with biophysical processes described in the literature (i.e. leaf gain, leaf loss, net leaf production), we decided to shift the models (i.e. displace the models along the time axis) by one, two and three months. We then examined if the EVI response was immediate or delayed. An immediate response of EVI to a biophysical process would imply that remote sensing techniques could be used for real-time monitoring. In contrast, a delayed response would help us understand which processes drive the changes in EVI. After comparing the biophysical processes to the EVI, we examined their relationship using linear regressions.

For the purposes of this thesis, we decided that the Discrete Fourier Transform was not an adequate method to detect phenology because it does not fit the real data as well as the GAMs. In Figure 25D we present a simple comparison between the apparent phenology resulting from using Prophet, and the apparent phenology from using a Discrete Fourier Transform using the ScyPy package for python. While the Fourier transform is aesthetically more pleasing, is it evident that it misses many of the median and standard deviation values of EVI.

4.4.7 Validation of the GAMs

We assessed the precision of our model by running linear regressions between the EVI model and 1) observed EVI values; 2) *in situ* data from (Duke et al., 1999); and 3) leaf fall, leaf gain and net leaf production values from published literature.

4.5 Results

4.5.1 Time Series Analysis using GAMs – Mangrove phenology

We found that some Australian mangroves display a bimodal seasonality with two periods of high EVI values and two periods of low EVI values, as shown in Figure 25 and Figure 26. In the Gladstone region, the highest EVI values are recorded between May and August ('Peak

growing season' in Figure 25), which are immediately followed by the lowest EVI values between September and November ('Start of season/End of season' in Figure 25). During the wet season, EVI values exhibit a second, less pronounced peak between December and January followed by a subtle drop between February and April. This bimodal seasonality refers to two different peaks in leaf production (Tomlinson, 1986) and is also seen through time, with EVI values in mid-year being higher than those at the beginning or end of the year (wet season).

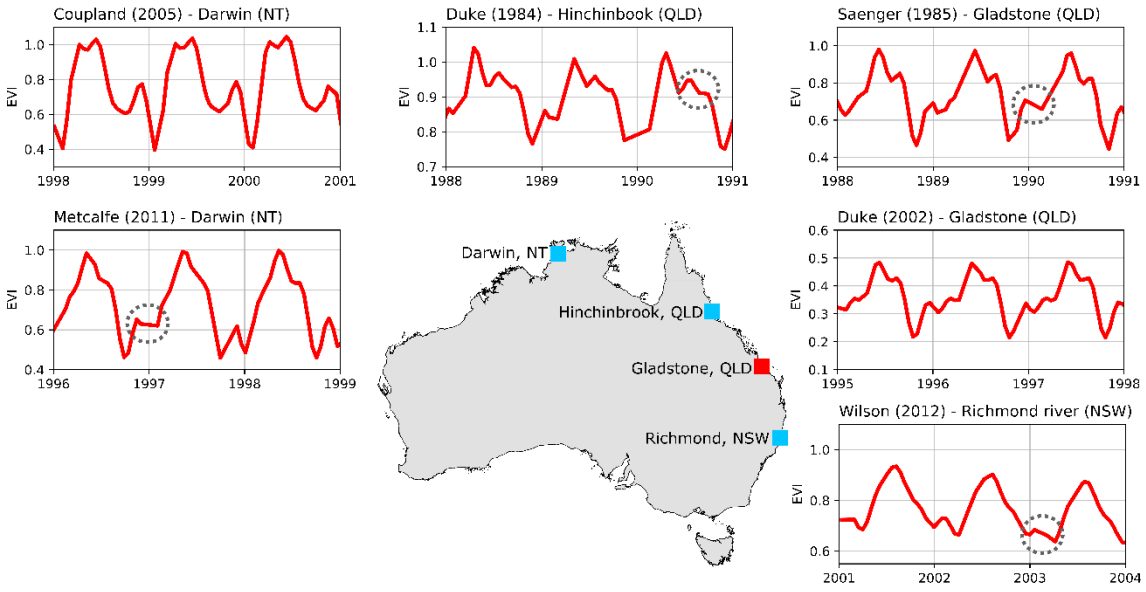

Figure 26: EVI model of phenology for each study site. Blue squares represent locations where only published literature was used, while the red square represents the location of the field data site and where published literature was used. Grey dashed circles show examples of year-to-year variations in the EVI model.

Figure 26 shows the average phenology model of all the pixels in each study site and highlights the fact that mangrove phenology varies with location and through time. For example, both Gladstone sites display similar phenology models despite being years apart. When compared to the Hinchinbrook site, however, the models are somewhat different, especially when looking immediately before and after the highest EVI values (i.e. peak growing season). On a greater scale, the phenology models across states differ greatly from one another. The site located in New South Wales has a distinctly smooth phenology curve while the Queensland sites show jagged features and the Northern Territory is in between.

Temporally, GAMs reveals subtle year-to-year differences in the phenology model that cannot be seen with fully parametric models as the latter over-simplify the phenology from satellite images. Grey circles in Figure 26 focus on certain features in the phenology models that change from year to year. Since we created the GAMs on a pixel-by-pixel basis, we can examine each pixel individually and determine the causes of such variations.

4.5.2 GAMs and Field Data

In Figure 27 we show the EVI model and the *in situ* data from (Duke et al., 1999). We can see that each field variable has a marked seasonal pattern, where the values of the variable increase and decrease at certain times of the year (see below). Similarly, the EVI models show a seasonal pattern with higher values between May and September and lower values between October and April. Both the monthly mean and the chronological EVI models seem to describe some variables better than others as explained below (see Section 4.6).

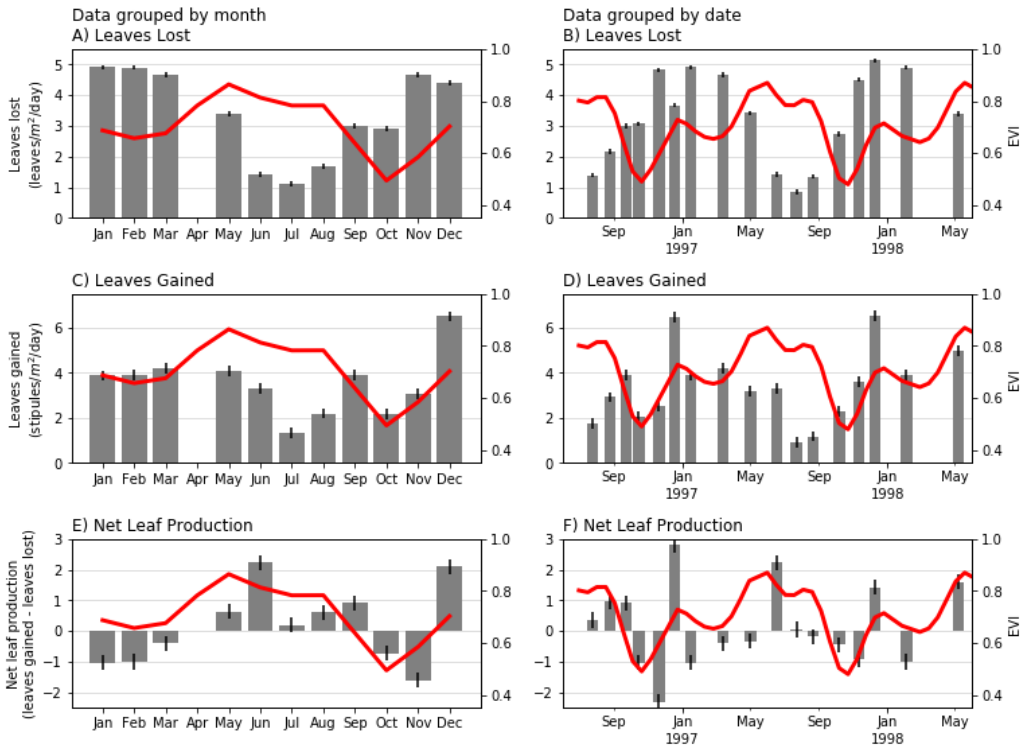

Figure 27: Predicted EVI vs in situ data from (Duke et al., 1999). *Red line represents the EVI model for the Gladstone area (1995-1999). Grey bars and black lines represent the values for each variable and standard error respectively. On the left panel, the data are grouped by month and on the right panel the data are presented in chronological order. No in situ data were recorded for April during the experiment.*

4.5.2.1 EVI model and leaves lost

Visually, the EVI model appears to have an inverse relationship with the number of leaves lost. Between November and March, when the number of leaves lost is high (≥3 leaves/m^2/day), EVI values are often low. In contrast, EVI values are often high between May and October when fewer leaves are lost. This relationship is evident in Figure 27A/B.

4.5.2.2 EVI model and leaves gained

From Figure 27 C/D we see that the EVI model has a closer relationship with the number of leaves gained than with the number of leaves lost. Visually, this relationship is very strong, especially in the second half of the year. Between October and December the number of leaves gained rises to its maximum value; this number then drops and remains stable until May. Similarly, in October, EVI rises steadily from its lowest value until December where it remains stable until March before rising to its maximum values between May and June before dropping again and restarting the cycle. In Figure 27D the EVI model shows peaks that coincide with periods of high number of leaves produced (e.g. January 1997, December 1997, and May 1998). The same can be said about the troughs in the EVI model, which coincide with lower values of leaves produced (e.g. October 1996 and 1997).

4.5.2.3 EVI model and Net Leaf Production

Net leaf production presented by (Duke et al., 1999) shows two distinct peaks (i.e. June and December) and two troughs (i.e. January and November) that coincide with the peaks and troughs of the EVI model (Figure 27E). When the data are aggregated by month (Figure 27E), the relationship between EVI and the net leaf production is clear. Similarly, when the data are presented in chronological order, the months where net leaf production is highest (or lowest) coincide with months of high (or low) EVI values (Figure 27F). In some cases, high and low EVI values precede the highest and lowest values of net leaf production by about a month, however this is not consistent over time.

4.5.3 GAMs and Published Literature

Similar to our field data site, the GAMs showed a bimodal phenology curve across all sites described in the selected literature (Table 9, Figure 28). In general, the phenology models have either 1) an inverse relationship or 2) a time lag with respect to the intensity of leaf fall reported in the literature. Most studies report higher leaf fall rates between October and March and lower leaf fall rates between April and September (Figure 28), which denotes an inverse relationship with EVI. By shifting the models by three months, the visual relationship between leaf fall and EVI becomes stronger, especially for the data presented by (Coupland et al., 2005; Duke, 2002a) and (Metcalfe et al., 2011a).

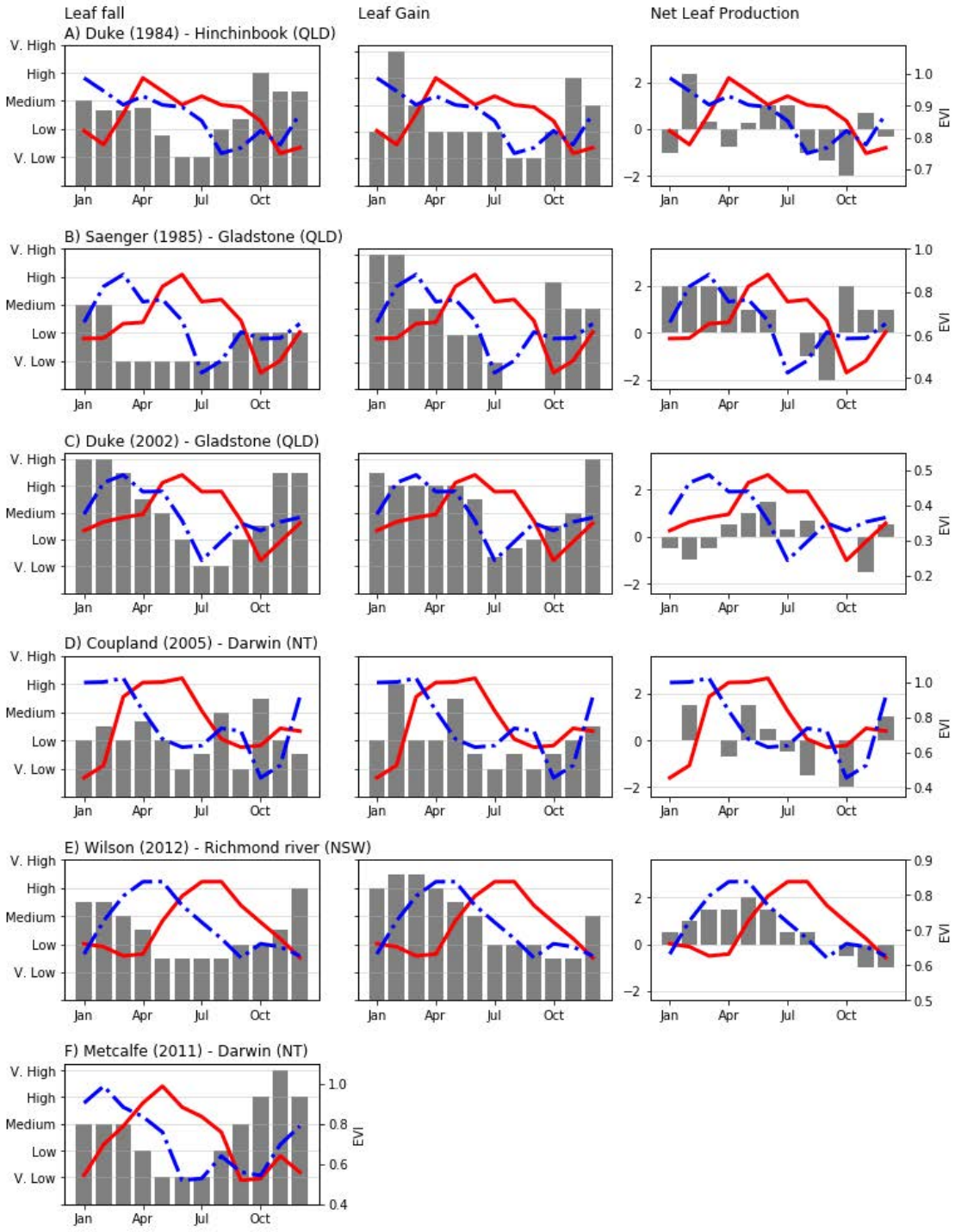

Figure 28: Left, centre and right show a qualitative measure of Leaf fall, Leaf gain and Net Leaf Production for each study site. The red line represents the monthly value of the predicted EVI from the GAMs and the blue dotted line represents the predicted EVI shifted by three months.

Models of EVI seem to be better predictors of leaf gain intensity when compared to leaf fall intensity. On most sites, leaf gain intensity is highest between November and April and lowest between May and October. Higher values of leaf gain intensity relate well with high values of

EVI. However, their timing does not match exactly. Visually, the shifted EVI models show a much closer relationship with leaf gain intensity across all sites than the models with no time shift (Figure 28). Regarding net leaf production, sites in Gladstone (QLD) and Darwin (NT) show that the peaks and troughs of the EVI model coincide with the highest and lowest values of leaf production (Figure 28C/D.) In contrast, the shifted models shown in Figure 28A/B/E have a better visual relationship with net leaf production.

4.5.4 Validation: Predicted EVI vs published data

With the exception of Duke et al. (1984a), all sites have higher correlation values with leaf gain or net leaf production when the EVI model is shifted by two or three months. For example, the EVI model correlates better with leaf gain values shifted by two months in the case of (Duke, 2002a) and (Nicholas C Wilson and Saintilan, 2012) and tree months in the case of (Saenger and Moverley, 1985) and (Coupland et al., 2005). The high R^2 values in Table 10 demonstrate that, in mangrove forests, the EVI response to leaf gain intensity and net leaf production is not immediate but delayed by two to three months.

Table 10: Correlation coefficients of the EVI model versus Net leaf production, leaf fall and leaf gain for each site. Highest R^2 values per site are shown in bold.

Site	Shift (months)	Leaf Fall R^2	Leaf Fall p value	Leaf Gain R^2	Leaf Gain p value	Net leaf production R^2	Net leaf production p value
Duke_1984	-3	0.01	0.75	0.24	0.11	0.15	0.22
	-2	0.24	0.11	0.17	0.18	0.00	0.93
	-1	0.33	0.05	0.24	0.10	0.00	0.91
	0	0.33	0.05	**0.47**	**0.01**	0.05	0.49
Saegner_1985	-3	0.11	0.29	0.54	0.01	**0.55**	**0.01**
	-2	0.16	0.19	0.43	0.02	0.36	0.04
	-1	0.21	0.13	0.35	0.04	0.23	0.12
	0	0.41	0.02	0.35	0.04	0.14	0.23
Duke_2002	-3	0.38	0.03	0.53	0.01	0.01	0.81
	-2	0.74	0.00	**0.90**	**0.00**	0.04	0.53
	-1	0.71	0.00	0.36	0.04	0.43	0.02
	0	0.25	0.10	0.02	0.70	0.51	0.01
Coupland_2005	-3	0.04	0.52	**0.39**	**0.03**	0.15	0.22
	-2	0.07	0.42	0.05	0.49	0.00	0.98
	-1	0.08	0.38	0.08	0.38	0.00	0.90
	0	0.06	0.46	0.00	0.87	0.01	0.71
Wilson_2012	-3	0.02	0.63	0.42	0.02	**0.75**	**0.00**
	-2	0.06	0.45	0.71	0.00	0.53	0.01
	-1	0.33	0.05	0.66	0.00	0.16	0.20
	0	0.71	0.00	0.37	0.04	0.00	0.83
Metcalfe_2011	-3	0.06	0.46	-	-	-	-
	-2	0.55	0.01	-	-	-	-
	-1	**0.79**	**0.00**	-	-	-	-
	0	0.61	0.00	-	-	-	-

In summary: 1) the EVI models resulting from the GAMs are good predictors of leaf gain and net leaf production across our study sites; and 2) EVI does not respond immediately to leaf gain and in most cases has a two- to three-month delay after mangrove forests show signs of leaf gain or increased net leaf production.

4.5.5 Phenological Metrics

After analyzing every pixel in the Landsat images from our field site, we found that the growing season starts and ends between Day of Year (DOY) 280 and 316, that is between September and October each year (Figure 29A). The peak growing season occurs most frequently between May and July (i.e. DOY 137-165, Figure 29B). The start of season and peak growing season

usually occur before and after the wet season respectively, however establishing a relationship between the two events is beyond the scope of this study. See the Discussion section for more on the bimodal seasonality of mangrove ecosystems.

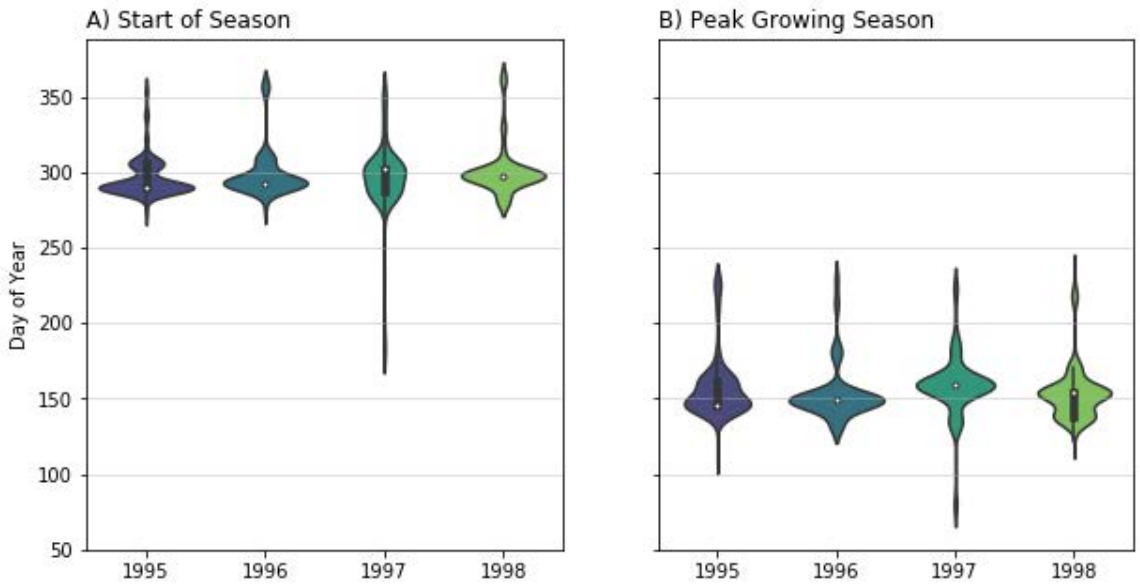

Figure 29: Start of Season and Peak of Growing Season for mangroves in the Gladstone region (QLD) between 1995-1999, as determined by the EVI model.

4.6 Discussion

Extracting phenological metrics of mangrove forests from satellite images is an ongoing field of research. We contribute to this field by 1) presenting a novel, data-driven method to extracting phenology from satellite imagery; and 2) applying the method in evergreen forests across Australia. Importantly, with the use of satellite images we have demonstrated that plots with similar species can have different phenologies. Phenology is, in turn, site dependent and hence should not be described using a single logistic or sinusoidal curve.

4.6.1 The phenology of Rhizophora stylosa

Authors have described, in situ, the phenological traits of R. stylosa around the world, however few have attempted to compare mangrove phenology across regions. (Pastor-Guzman et al., 2018), for example, used satellite imagery and a sinusoidal model to describe seasonal

variations of mangrove forests in the Yucatan peninsula in Mexico. They found that the spectral index values are lower during the dry season and higher during the wet season, an outcome that differs from our findings. Across all our study sites, we found lower EVI values during the wet season and higher EVI values during the dry season. These differences may be due to the geographical location and the species composition of both studies. R. mangle, Laguncularia, racemosa, Avicennia germinans and Conocarpus erectus dominated their study site, while R. stylosa, A. marina and C. tagal dominated ours. Despite R. stylosa being the dominant species in our site, several species of mangroves may contribute to the apparent phenology of each pixel given the resolution of the Landsat images (i.e. 30m). Determining the contribution of each species to the apparent phenology is an ongoing field of research.

Another big difference between our study and that of (Pastor-Guzman et al., 2018) is that the species that dominate mangrove forests in their study sites show a unimodal phenology response across the Yucatan peninsula. In contrast, we found bimodal phenology signals in our field study site as well as in the sites described in the peer-reviewed literature (Figure 26). This bimodal phenology is not new. Duke et al. (1984) , and later Tomlinson (1986) described *R. stylosa* and other mangrove species as having two distinct periods of leaf growth each year. Descriptions at the plot level certainly help us understand the bimodal response of EVI over time, however the number of leaves that a tree produces might not be the only explanation for a bimodal response in EVI.

Recently, Smith et al. (2019) suggested that the seasonal response of EVI in an evergreen forest was bimodal due to layers of the canopy responding in opposing seasonal patterns. When there is decrease in leaf area index of the upper canopy, the lower canopy takes advantage of the extra light to increase its leaf area. Following the findings by Wu et al. (2016), Smith et al. (2019) propose that the seasonal response of EVI comes from variations in leaf area index and photosynthetic capacity (i.e. younger, more efficient leaves), rather than from climate and weather patterns alone. Indeed, leaf ontogeny, demography and longevity could influence satellite observations, with leaves of different ages having varying amounts of chlorophyll, carotenoids, and water, resulting in slightly different spectral signatures. These assertions need to be tested in mangrove ecosystems, to determine if the bimodal response of EVI is related to the canopy structure or net leaf production.

In this study we have demonstrated that seasonal and inter-annual changes in leaf gain and net leaf production are related to changes in EVI. Coupland et al. (2005) suggested that leaf production of *R. stylosa* in Northern Australia is most evident during the wet season (December through May), however this species produces new leaves throughout the year. Similarly, Wilson and Saintilan (2012) found that *R. stylosa* has the highest values of leaf production and leaf fall between December and April. The authors also indicated that this species has a net leaf gain between January and August, and a net leaf loss between September and December, which coincides with upward and downward trends in the EVI model for that site (Figure 28E). Despite the strength of the EVI-net leaf production relationship, when using satellite imagery, there are other factors that affect the phenology response of mangrove forests.

Environmental and biological factors such as cyclones, rainfall and tree age are known to alter the phenology and spectral response of mangrove ecosystems (Kovacs et al., 2001; Lovelock et al., 2015; Pastor-Guzman et al., 2018). With the help of satellite imagery and GAMs, we can now look at inter-annual changes in mangrove phenology (e.g. Figure 26) and relate them to environmental or biological factors. Because these factors may change one by one, or several at a time, inter-annual predictions of mangrove phenology are difficult. A way to improve the prediction of seasonal and inter-annual phenology is to include past and present observations of these factors during the creation of the GAMs. GAMs create a numerical relationship between each factor and the phenology model to determine how influential is the former over the latter.

For example, there seems to be an inverse relationship between apparent phenology and temperature (Figure 30). EVI reaches its highest values at the same time when temperature is low and vice versa. On the other hand, EVI seems to be correlated with rainfall, with EVI displaying increasing values after periods of high or continuous rainfall. In *R. stylosa* and other mangrove species the inverse relationship between phenology and temperature has also been noted by Duke (2002), and Pastor-Guzman et al. (2018), but does not seem to be the case everywhere (Duke et al., 1984). While not investigated here, the year-to-year variability in temperature and rainfall is also evident in Figure 30. Between November 1995 and March 1996, there were more episodes of rainfall, combined with higher maximum temperatures when

compared to subsequent years. Year-to-year variations in weather and climate patterns are likely to play a role in long-term changes in mangrove phenology. Given that GAMs allow us to examine long term trends in phenology, linking trends in phenology with changes temperature and rainfall is a natural next step for this research.

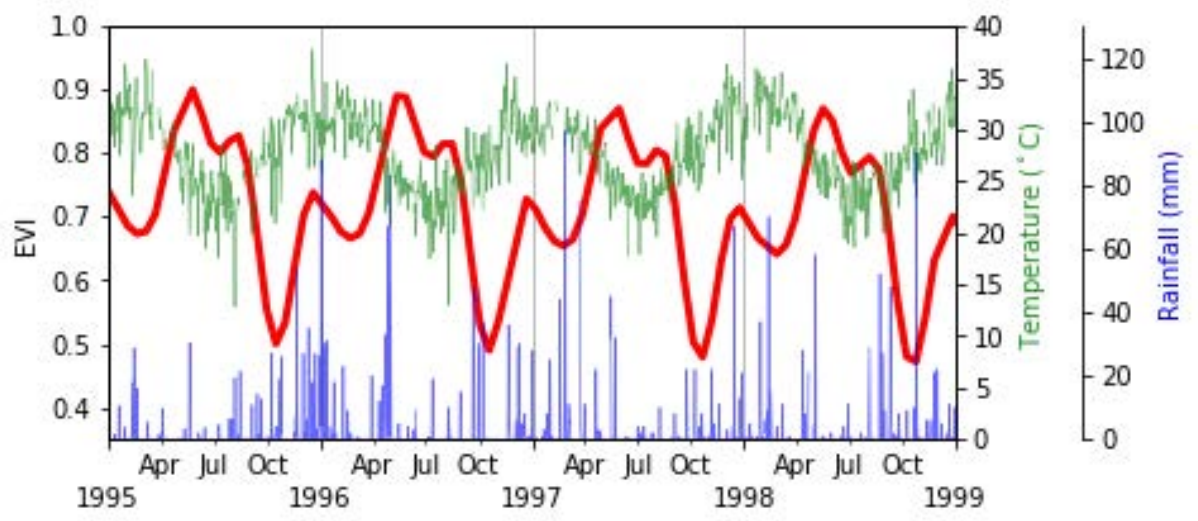

Figure 30: Apparent phenology from the GAMs for the Gladstone site is shown in red. The maximum daily temperature (°C,), and the daily rainfall (mm) for the Gladstone Airport weather station between 1995 and 1999 are shown in green and blue respectively.

Similarly, biological variables such as species composition, growth rate and forest maturity may also affect the spectral response of mangroves, and thus, any model derived from satellite sensors. A mature, dense forest will have a different response to a newly-planted mangrove patch or one that is recovering from a natural or manmade disaster (Chandra Giri et al., 2011a). Because relating 30 years of satellite observations to biological processes requires that *in situ* data is collected frequently and over long periods, the need for long-term (five or more years) monitoring sites in mangrove forests is evident. Long-term monitoring of mangrove ecosystems is important, especially when relating variations in spectral indices, to changes in tree growth and temperature such as those presented by Coldren et al. (2016) and Coldren et al. (2018).

4.6.2 GAMs vs parametric methods

Our ability to detect and forecast mangrove phenology improves our understanding of the ecosystem (Chambers et al., 2013), and our approach greatly differs from others, more commonly used (Helman, 2018). For example, Zhang et al. (2003) derived a mathematical function that resembles the phenological phases of forests in the northeastern United States. Their aim was to use satellite images to monitor vegetation dynamics at the landscape level, and one of their biggest achievements was that the method did not require any fixed constants or thresholds to be applicable. This method has been used at the local (Fisher et al., 2006) and global scales (White et al., 2009), however the premise that a parametrized mathematical curve fits every plot of land has remained unchanged. The method derived by Zhang et al. (2003) assumes that the selected model of phenology is: 1) correct, 2) already known and 3) is invariant through space and time (Jones and Almond, 1992; Yee and Mitchell, 1991). Even recent studies (Songsom et al., 2019) insist on these assumptions when applying smoothers and filter to the data prior to detecting the phenology without considering that the data they discard may provide insights into the phenomenon their trying to model (i.e. phenology). We, on the other hand, used semiparametric GAMs as an estimation method to describe the changing relationship between mangrove phenology and EVI. GAMs let the data define the shape of the phenology curve, allowing for bimodality and skewness to be detected and modelled (Yee and Mitchell, 1991).

As shown above, the relationship between EVI and mangrove phenology changes with space and time. The main limitation of parametric approaches is that those methods are constrained to the particular models evaluated (e.g. Pasquarella et al. (2018), Zhang et al. (2003), Zhu et al. (2012)). That is to say, parametric methods assume that the shape of the phenological curve remains invariant and only variations in the frequency and amplitude of the signals are allowed.

In contrast to parametric methods, GAMs use the data itself (in this case EVI values from satellite imagery) to determine the shape of the relationship. Because the relationship between the predictor and response variable is unknown beforehand, GAMs apply a series of smooth functions and use the data to determine which function is the best fit for a given dataset. This data-driven approach enabled us to demonstrate three key things: 1) the phenology response of mangroves forests dominated by *R. stylosa* is not unimodal, but often bimodal across our

study sites; 2) the second leaf growth phase varies in intensity depending on the site. For example the second leaf flush is much lower in New South Wales (Figure 28E) than in Queensland and the Northern Territory (Figure 28B/D). The reasons behind these differences are not fully understood but may be due, in part, to differences in air temperature, rainfall and water temperature; 3) the phenology response of mangrove ecosystems is site dependent and GAMs allow us to see small seasonal and inter-annual variations that are otherwise impossible to detect using fully parametric methods. However, to provide a better, more accurate, description of mangrove phenology we need ecophysiological descriptions that span more than 18 – 24 months to compare to satellite-derived phenology.

Field descriptions of phenology longer than two years will also help inform apparent phenology models in different ways. For example, here we found that there is a 2-3 month lag between *in situ* phenology and apparent phenology. These lags need to be validated with field data, and across different sites. One way of examining these relationships could include the comparison of parametric and semi-parametric methods for detecting phenology from satellite images. If the lag between higher net leaf production and higher EVI is real, then it should show regardless of the method used. Moreover, these lags should also be evident while using sensors with different spatial and temporal resolutions. This hypothesis was not tested here but it poses a set of research questions worth exploring.

4.6.3 Validation of the GAMs

Peer-reviewed literature of phenological models often lacks a description of the methods used to validate the models, making it difficult to compare the performance of the GAMs versus other approaches. Despite this limitation, we validated our EVI model using three different, independent sources of information and found that GAMs are good tools to extract the phenology response of mangrove forests from satellite images.

Linear regressions between Observed and Predicted EVI values showed a good model fit, with $R^2 > 0.40$ in half of our study sites despite variations in the raw EVI values (see Figure 41). Correlation values between the GAM and *in situ* data were low (as expected), but there are valid reasons for this. The study by Duke et al. (1999) focused on three sites in the Gladstone region in Queensland, and aimed at examining potential bioremediation strategies in case an

oil spill hit the Queensland coast. The authors never intended to use the field data to validate satellite imagery, hence the difficulties in correlating one with the other. Furthermore, the dataset consisted of one value per date per site i.e. only three data points per date, and some dates had no values (e.g. April 1997), which reduced the potential for correlation even more. Lastly, the study only gathered data over an 18-month period, limiting our information to one and a half growing seasons. Having only one full season of information limits the number of links we could create between the EVI model and the field data. We need longer field studies to understand fully the phenology curves extracted from satellite imagery and to examine the response of mangrove forests to changes in weather and climate patterns.

The validation process of the EVI model with peer-reviewed literature provided us with two important pieces of information: 1) our models correlate well with the leaf gain intensity and net leaf production reported in the literature, regardless of the year in which those data were acquired; and 2) EVI has a two- to three-month lag with leaf gain intensity in most of our study sites. The former is important because it highlights the usefulness of GAMs. The latter tells us that, from a biophysical perspective, EVI responds to the canopy elements that absorb red light for photosynthesis and scatter near infra-red light, while field phenology traces leaf formation and drop. The delayed response of EVI is expected for two reasons: 1) the time it takes newly formed leaves to reach their maximum size, and 2) the net leaf production varies throughout the year. In Figure 31 we show an example of this. At 't1' leaves are scarce and bud breaking, net leaf production and chlorophyll content are low but positive and the satellite captures mainly the background of the mangrove tree (i.e. exposed soil and understory water). At 't2' leaves are growing and new leaves are bud breaking. At 't3', net leaf production peaks, meaning that there are many leaves growing and bud breaking, the satellite captures mainly green material, including chlorophyll, thus EVI is high as well. When 't4' arrives EVI is still high, more leaves are dropping than bud breaking, but leaves from 't3' are still growing and reaching maturity (i.e. high chlorophyll content) hence the lag between peak EVI and peak leaf gain/production. Finally, the tree loses more leaves and the background in the satellite images starts to show again ('t5') and the cycle starts again. The implications of this delayed response of EVI need to be explored because the growth/recovery rate after a natural disaster may not be as evident from satellite imagery as previously thought (Chandra Giri et al., 2011a).

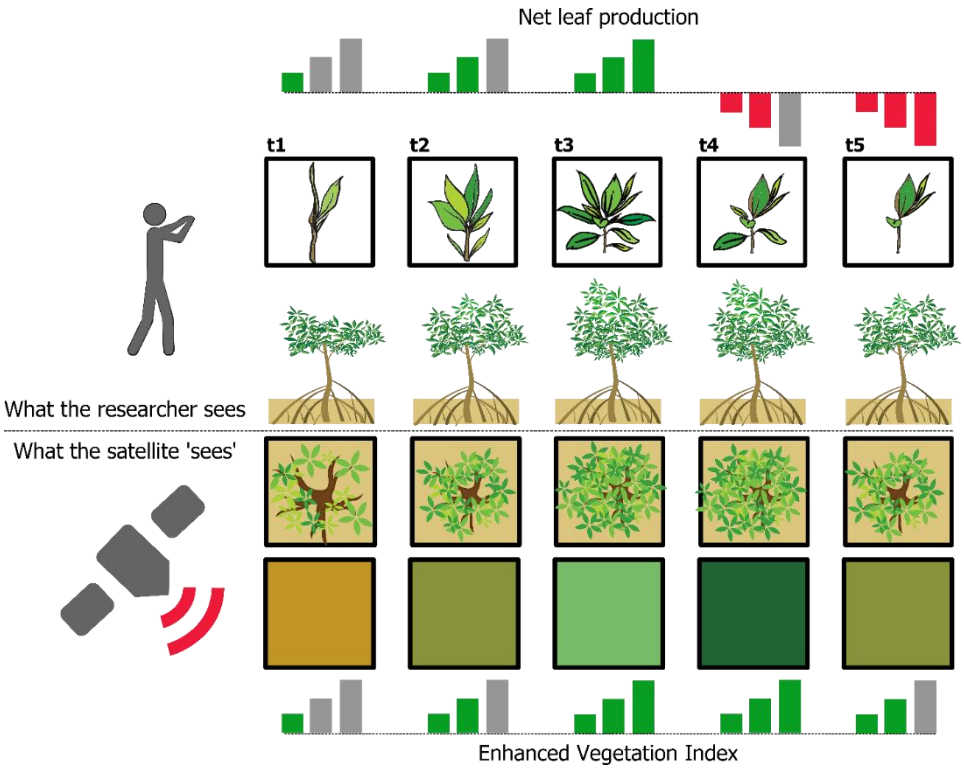

Figure 31: Time difference between peak leaf production and peak EVI during a given year for a simulated mangrove tree.

Apparent phenology can be detected using a variety of spectral indices, and EVI is only one of several that has been used for coastal ecosystem investigations (Murray et al., 2019; Pastor-Guzman et al., 2018; Rogers et al., 2017). Future studies could use EVI in combination with other spectral indices to improve the detection of phenological events such as accurate measurement of leaf production and different stages of leaf growth. It would also be important to assess whether other spectral indices also display a time lag with relation to net leaf production, and whether other phenology models show this temporal shift as well. For example, spectral indices that use the short-wave infra-red region of the spectrum could provide information on water content and indirectly inform the number of leaves in the forest. Establishing this relationship is important, especially in scenarios where mangroves are at risk of massive diebacks such as drought and heat waves.

Besides temperature, rainfall, and other climate data, other sources of information that can potentially provide additional insights to our model: 1) Fractional Vegetation cover, and 2) radar imagery from Sentinel 1 or Advanced Land Observing Satellite (ALOS) sensors. The use of Radar datasets to monitor mangrove forests has been increasing in the past few years,

mainly providing insights on mangrove zonation (Held et al., 2003; Worthington et al., 2020), canopy structure and height (Simard et al., 2019), while Fractional Vegetation Cover informs mangrove dynamics (Lymburner et al., 2019). The spatial resolution of many of these sensors, including Landsat, does not allow the discrimination of species, however, estimating general trends in mangrove phenology could be more important to protect these forests rather than species-specific values.

4.7 Conclusions

In this paper, we demonstrated that GAMs help us detect seasonal and inter-annual changes in mangrove phenology by using 787 satellite images of different study sites across Australia. We compared our model to field and published data. When compared to field data, we found that seasonal and inter-annual variations of EVI correlate well with the leaf production rate, net leaf production of mangrove forests. When compared to published data, we found that there is a time lag between leaf gain and the EVI. Overall, leaf gain and net leaf production are more closely related to higher EVI values than leaf fall. Regarding the phenological metrics, in our Gladstone site, start of season occurs more frequently between September and October each year and peak growing season between May and July.

Rather than imposing a parameterized mathematical curve to the data, our study leverages the ability of GAMs to let the data determine the type of relationship between a given spectral index and plant phenology. This data-driven approach helped us detect a bimodal phenology in mangrove forests dominated by *R. stylosa;* bimodal phenology has been reported in the literature but it has never been seen with remote sensing techniques. More importantly, GAMs allowed us to determine that mangrove phenology is site-dependent. Fully parametric methods, when applied to remotely sensed data, have over-simplified the phenology of mangrove ecosystems and other evergreen forests worldwide.

By understanding how phenology changes from site to site, and year to year, this study provides a tool for regional and continental-scale assessments of mangrove phenology. We expect to see an increase in the use of GAMs, especially in conjunction with the Landsat and other long-term, worldwide imagery archives.

4.8 Acknowledgements

This project is supported by NIESGI Cia. Ltda., James Cook University Postgraduate Research Fellowship, Wet Tropics Management Authority Student Research Grant, National Environment Science Program (NESP) Tropical Water Quality (TWQ) Hub research Grant, and a Centre for Tropical Water & Aquatic Ecosystem Research (TropWater) Student Research Grant.

5 All models of satellite-derived phenology are wrong, but some are useful.

A version of this chapter is currently in review in 'International Journal of Applied Earth Observations and Geoinformation'.

5.1 Graphical Abstract

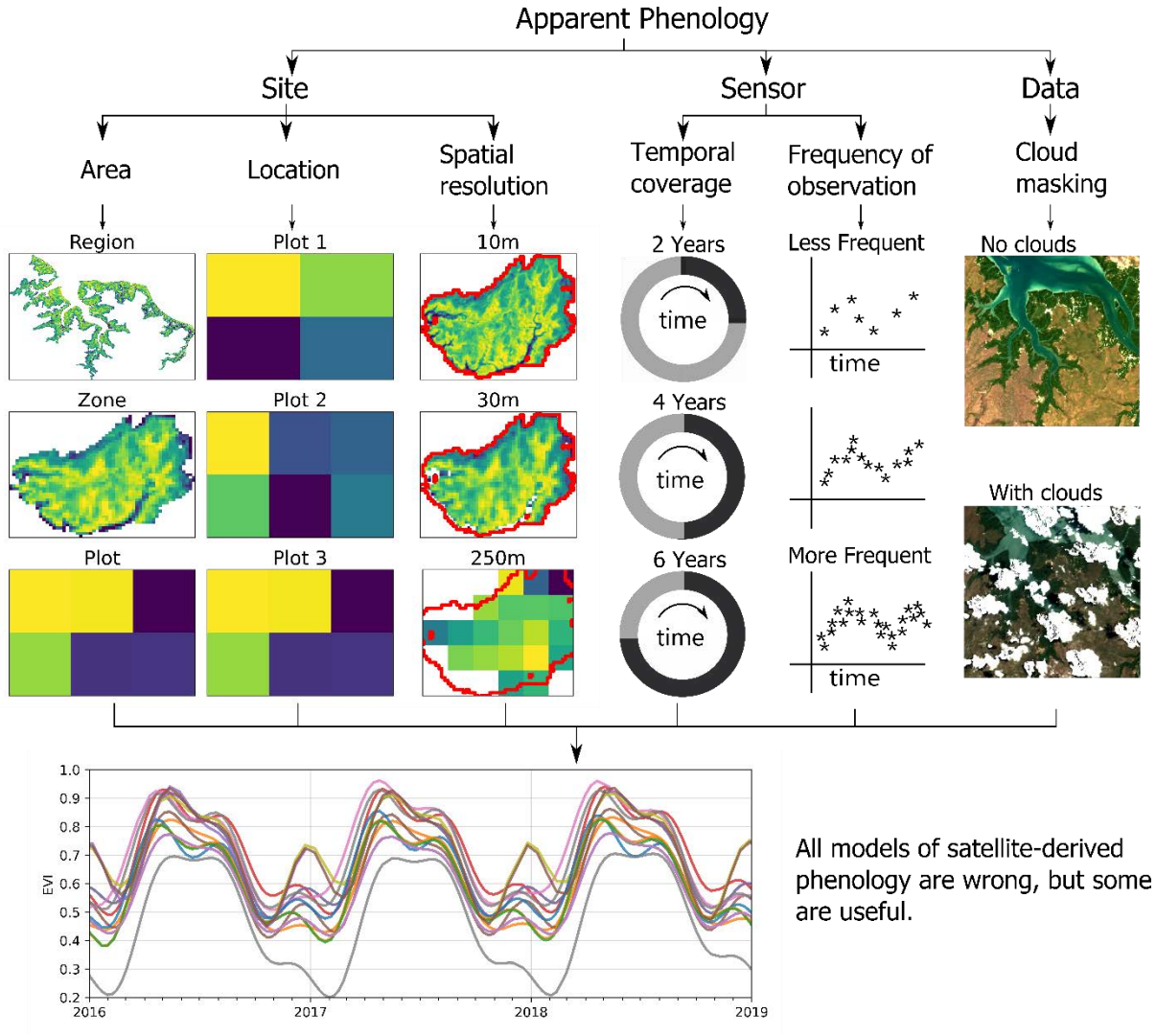

5.2 Abstract

Satellite-derived phenology (or apparent phenology) is frequently used to illustrate changes in plant phenology (i.e. true phenology) and the effects of climate forcing. However, each study uses a different method to detect phenology. Plant phenology refers to the relationship between the life cycle of plants and weather and climate events. Phenology is often studied in the field, but recently studies have transitioned towards using satellite images to monitor phenology at the plot, country, and continental scales. The problem with this approach is that there is an ever-increasing variety of earth observation satellites collecting data with different spatial, spectral, and temporal characteristics. In this paper we ask if studies that detect phenology using different sensors over the same site produce comparable results. Mangrove forests are one example where different methods have been used to examine their apparent phenology. In general, plant phenology, including mangroves, is described using few individual plants, but continental-scale descriptions of phenological events are scarce or inexistent. Few attempts have been made to describe the phenology of mangroves using satellite imagery, and each study presents a different method. We hypothesize that apparent phenology changes with: 1) areal extent; 2) site location; 3) frequency of observation; 4) spatial resolution; 5) temporal coverage; and 6) the number of cloud contaminated observations. Intuitively, one would assume that these hypotheses hold true, yet few studies have investigated this. For example, one would expect that clouds change the observed phenology of vegetation, that the number of species captured at spatial resolution will impact the apparent phenology, or that mangroves in different places display different phenologies, but how are these changes represented in the apparent phenology? We use the Enhanced Vegetation Index (EVI) to examine the changes in the start of season and peak growing season dates, as well as the shape and amplitude of the apparent phenology in each hypothesis. We use Landsat and Sentinel 2 imagery over the mangrove forests in Darwin Harbour (Northern Territory, Australia) as a case study, and found that apparent phenology does change with the sensor, site, and cloud contamination. Importantly, the apparent phenology is comparable between Landsat and Sentinel 2 sensors, but it is not comparable to phenology derived from MODIS. This is due to differences in the spatial resolution of the sensors. Cloud contamination also significantly changes the apparent phenology of vegetation. In this paper we expose the

complexity of modelling phenology with remote sensing and help guide future phenology investigations.

Keywords: Landsat, Sentinel 2, phenology, Time Series Analysis, Generalized Additive Models, apparent phenology, mangroves.

5.3 Introduction

Phenology is the branch of science that relates the life-cycle events of organisms to the biotic and abiotic events that cause them (Cerdeira et al., 2018); for example, plants losing their leaves in autumn and growing them in spring. Plant phenology is usually studied in the field. Field observations allow researchers to closely examine the life cycles of plants; however, these studies are often limited to small areas and to short periods of observation. In addition, historical records of plant phenology are limited in their geographical extent, number of species, and availability. Recently, studies have used satellite images to examine plant phenology at larger scales and over longer periods of time (Broich et al., 2014; Verbesselt et al., 2010; White et al., 2009). Here we use the term 'apparent phenology' to refer to satellite-derived phenology to discriminate it from the phenology observed in the field. The advantages of using satellites for studying phenology are threefold: 1) there are decades worth of images for most places on earth; 2) satellites collect data at periodic intervals over large areas; and 3) all images are collected in the same way, thereby ensuring the data collection remains consistent over space and time. These advantages imply that we can assess phenology over large areas and retrospectively, however satellite images are just a tool to detect plant phenology, and, like any other tool, these images can be used in several ways.

From entire continents, to individual countries and small regions, satellite images are *the* preferred tool to detect plant phenology at different spatial scales (Czernecki et al., 2018; Pastor-Guzman et al., 2018; White et al., 2002). Like other tools, satellite images have different characteristics depending on the sensor that collects the data. Two important characteristics of satellite images that relate to the sensor are the spatial resolution and the temporal resolution. The spatial resolution refers to the land surface area covered by each pixel (i.e. pixel

size), and the temporal resolution refers to the frequency with which the satellite visits a given site. Each sensor has a unique combination of spatial and temporal resolution, and the most frequently used sensors to detect plant phenology are Landsat, Sentinel 2, and MODIS (Moderate Resolution Imaging Spectroradiometer) (Bolton et al., 2020; Fu et al., 2014b; Melaas et al., 2018). But detecting phenology not only depends on the sensor, it also depends on the amount of data available for the study site, and environmental factors such as cloud cover.

Many ecosystems are covered by clouds throughout the year, therefore obtaining cloud-free satellite images from those regions is rare. In other occasions, the target feature or phenomenon occurs when clouds are prevalent and, therefore, they are hidden from satellite view. When presented with these circumstances, researchers interested in phenology have resorted to using methods such as compositing to remove the effects of clouds in their data (e.g. (Griffiths et al., 2019)). Such approaches, however, may remove important within-year phenological features, making them less than ideal in many cases. More often than not, studies resort to masking algorithms to remove pixels marked as clouds, or cloud shadows; however, these algorithms are not perfect and can remove valid observations (i.e. commission errors), or keep invalid data (i.e. omission errors) (Ernst et al., 2018). The effects of clouds and cloud shadows on the satellite-derived (i.e. apparent) phenology of ecosystems are yet to be explored. One advantage of using cloud masking algorithms is that they remove unwanted data from the dataset, however this also reduces the number of usable observations to detect phenology.

The number of observations available for any given site is known as the time series, and it varies from sensor to sensor. Because detecting plant phenology requires (at least) one year of observations, the length of the time series plays an important role not only in detecting phenology, but also in evaluating changes over time (Garonna et al., 2016; Melaas et al., 2013; Vogelmann et al., 2016b). Changes in plant phenology serve as indicators of alterations in weather and climate patterns (Garonna et al., 2016; Peñuelas et al., 2009; Sitch et al., 2015). However, there is no consensus on the most effective methods or models to detect these changes.

When referring to the ability of a model to represent the exact behaviour of a system, George Box famously stated the '*all models are wrong, but some are useful*' (Box, 1979, 1976). This

assertion seems to hold true for phenology investigation, where studies have used wide range of models across different ecosystems, spanning different decades, and using different sensors. Because of this variation in methods and inputs, comparing the phenology from two or more studies remains a challenging endeavour.

Vegetation phenology has been studied at different spatial scales and over different landscapes (Melaas et al., 2018; Pastor-Guzman et al., 2018). Broich et al. (2014) studied the phenology across Australia, and found stark differences between landscapes. Plant communities in central Australia, where rain is scarce, displayed small variations in greenness and, in some cases, seemed to skip the growing season altogether due to the lack of available water. The apparent (i.e. satellite-derived) phenology showed by the authors corresponds, to some degree, to the real phenology of the vegetation. However, the variability in the vegetation within a 500m pixel could be influencing the signal captured by the model. These, and many other models are wrong. They are wrong not because they lack merit or scientific validity, but because are incapable of representing the exact behaviour of the ecosystem.

But these models are also very useful. These models provide a good starting point for plant phenology investigations, but with an ever-increasing variety of earth observation satellites, it is important to raise the question: when two studies use different sensors to detect phenology over the same site, are their models comparable to one another? Our aim is to answer this question. To determine if satellite-derived phenology is comparable between studies, we evaluate if: 1) the size of the study site, 2) the location of the study site, 3) the frequency of observation, 4) the spatial resolution, 5) the temporal coverage, and 6) the data pre-processing methods change the apparent phenology of the study area. We test these hypotheses using mangrove forests as an example, but these considerations also apply to other intertidal ecosystems, inland wetlands, and tropical evergreen forests.

5.4 Methods

5.4.1 Study Area

For this study we selected the mangroves that surround the city of Darwin, in Australia's Northern Territory because their phenology and distribution are well-known (Coupland et al., 2005; Metcalfe et al., 2011a; Rogers et al., 2017). Darwin Harbour is comprised by three main

sections or 'arms': the western arm, the central arm, and the eastern arm, which borders Darwin city. Within Darwin Harbour we selected one large area of the central arm (4,500ha, Figure 32A), one smaller area covering 140ha (Figure 32B), and three small plots (1ha each, Figure 32B), as study sites. To avoid confusion, we will refer to them as 'region', 'zone', and 'plots' respectively.

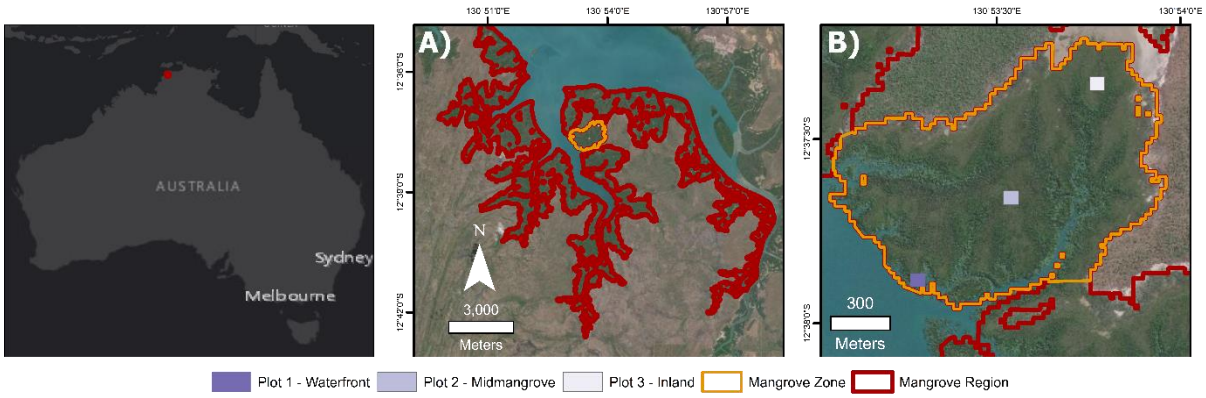

Figure 32: Study area and selected sites. Panel A) shows the central arm of Darwin Harbour and the mangrove Region and mangrove Zone. Panel B) shows the mangrove Zone and the three mangrove plots (i.e. plot 1, plot 2, and plot 3). Basemap source: Esri.. Mangrove polygon source: "Mangrove canopy cover" version 2.0.2 (Lymburner et al., 2019a)

Darwin harbour has an approximate area of 450 km2, out of which 190 km2 are covered by mangrove forests (Metcalfe et al., 2011). This region has a monsoonal climate and experiences maximum daily temperatures surrounding 32°C all year long, while minimum temperatures vary between 18°C and 25 °C. Precipitation is seasonal, with January, February and March being the months with highest rainfall, averaging 1105 mm; the drier months see around 8 mm. This region is also prone to tropical cyclones. According to the Australian Bureau of Meteorology Tropical Cyclone Data Portal (accessed 22/11/2020), since the 2009-2010 season over 14 tropical cyclones have been within a 300km radius of Darwin Harbor, and several made landfall. Mangrove zonation in this region is highly dependent on tidal elevation due to an abrupt elevation 2 m rise from the coastal fringes. Mangrove diversity in Darwin harbour is high, with 48 mangrove species identified (Moritz-Zimmermann et al., 2002, p. 6); the species that dominate the seaward margin are mainly *Rhizophora stylosa* and *Sonneratira alba*, and *Ceriops australis* dominate the mid and upper tidal flats (Metcalfe et al., 1999, p. 16).

5.4.2 Data acquisition and processing

In this project we used 352 Landsat and 260 Sentinel 2 images, collected over our study area between January 2010 and January 2020. Landsat satellites collect data every 8-16 days in the visible and near infra-red regions of the electromagnetic spectrum at 30m, while the Sentinel 2 sensors collect data every 5-10 days at 10m resolution in similar spectral regions. Also, Landsat imagery for the Australian mainland goes back to 1987 but only to 2015 for Sentinel 2 sensors. All images were georegistered, atmospherically corrected, and grouped into tiles with a defined equal area projection by Geoscience Australia and loaded into the Digital Earth Australia platform (Dhu et al., 2017; Lewis et al., 2017; Roberts et al., 2017). We used Digital Earth Australia to load all satellite images, aggregate the data, and remove all pixels that did not correspond to mangrove forests using the mangrove extent data from the National Map (https://nationalmap.gov.au/, dataset "Mangrove canopy cover" version 2.0.2). We calculated the Enhanced Vegetation Index (EVI) (Huete et al., 2002) for every mangrove pixel in every image; we selected EVI because it is known to be effective in mangrove and phenology investigations (Pastor-Guzman et al., 2018; Younes et al., 2019). To test hypothesis 4, we used Sentinel 2 images and resampled them to 30m and 250m to simulate the spatial resolution of the Landsat and MODIS sensors (see Section 5.4.3.4 for details).

We used Generalized Additive Models (GAMs) to represent the phenology of our mangrove sites and to calculate two commonly-used metrics: Start of Season (SOS) and Peak of Growing Season (PGS) (Figure 33). Importantly, while GAMs can be used to model phenology on a pixel by pixel basis, for simplicity, we aggregated the data in the following way: first, we grouped all images by date of image acquisition, and then we extracted the median EVI of all pixels in the area under analysis (Figure 33). The result of this aggregation is a singe EVI value per site per date. We selected the geometric median because it produces statistically representative results, and can be used for time series investigations (Roberts et al., 2017).

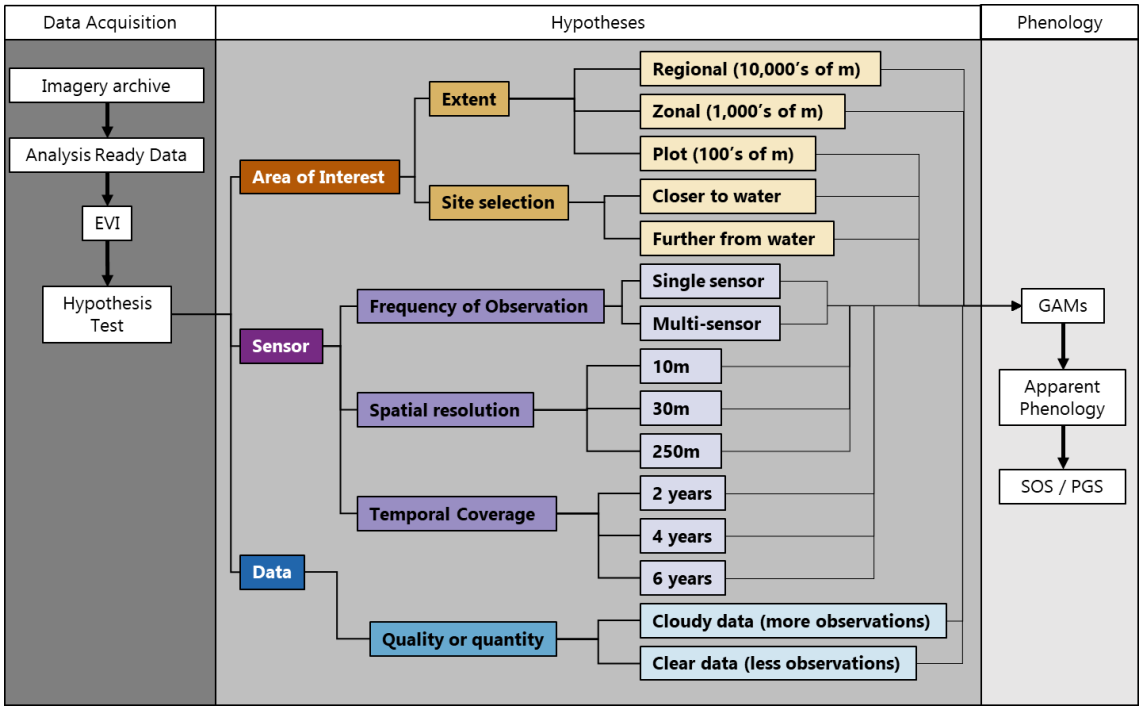

Figure 33: Conceptual diagram of the hypotheses tested. From the apparent phenology we derived the following metrics: Start of Season (SOS) and Peak of Growing Season (PGS) represent the lowest and highest EVI values in the apparent phenology curve. Sentinel 2 data were resampled to obtain 250m resolution imagery.

5.4.3 Data analysis

Vegetation phenology can be studied at the continental, regional, or plot level. Some studies look at vegetation phenology at the pixel level while others perform temporal or spatial aggregations to generate landscape averages (Czernecki et al., 2018; White et al., 2009). In this study we use three spatial scales (i.e. region, zone, plot) and aggregate the data for each spatial scale as shown in Figure 33. We mainly used the 'Xarray' (Hoyer and Hamman, 2017) and 'Prophet' (version 0.6, Taylor and Letham, 2018) packages for Python to create the models of apparent phenology for each analysis, and all model parameters remained unchanged throughout the analyses. As a result, any differences in the apparent phenology are derived from changes in the input data, not from changes in the model parameters. From the models of phenology, we derived the SOS and PGS days, defined as the median of the days of the year with the lowest and highest 5% of EVI values in the apparent phenology, respectively. In each hypothesis, we compared the following aspects of apparent phenology: number of peaks, number of troughs, median SOS date, median PGS date, maximum EVI, and minimum EVI, as well as the shape of the apparent phenology curve and the trend.

Importantly, we tested only one hypothesis at a time, meaning that there was no interaction between different areas, locations, frequencies of observation, spatial resolutions, time coverage, or cloud contamination. For most hypotheses we used all available Landsat images between 2010 and 2020, and cloud masked following Dhu et al. (2017) and Li et al. (2012). However, to test some hypotheses we used Sentinel 2 images, or a different time frame (see below). Furthermore, most scientific studies related to plant phenology rely on spectral indices such as EVI, rather than using individual spectral bands, therefore we do not investigate the effects of the spectral characteristics of the sensor on apparent phenology. We used Digital Earth Australia to test our six hypotheses, and below is a brief description of each analysis.

5.4.3.1 Hypothesis 1: Influence of size of area under investigation on apparent phenology.

To examine if the size of the study site changes the apparent phenology, we used all available Landsat images and compared models at the regional, zonal, and plot scales between the years 2010 and 2020 (Figure 33). Here we define regional, zonal, and plots, as spaces covering thousands of hectares, hundreds of hectares, and 10 hectares or less respectively. To detect the apparent phenology, we used the median EVI of each site as input data for the GAMs.

5.4.3.2 Hypothesis 2: Influence of location on apparent phenology

When assessing the phenology of mangroves and other intertidal ecosystems, the site selection may play a crucial role in the results. To test our hypothesis, we compared three plots of the same size (3 x 2 pixels), located within 500m of each other, as shown in Figure 32B. One plot was located next to the high tide mark, one plot was located 300m from the observable water edge, and the last plot was located (500m from the observable water). Phenology was extracted from all Landsat 5/7/8 sensors for years 2010 to 2020.

5.4.3.3 Hypothesis 3: Influence of frequency of observation on apparent phenology

This hypothesis arises from the fact that each Landsat satellite (i.e. Landsat 7, and Landsat 8) has a temporal resolution of 16 days, but when combined, the temporal resolution of these sensors is reduced to eight days. Similarly, the Sentinel 2 sensors revisit frequency is 10 days, but only five when combined (Li and Roy, 2017). To investigate how the frequency of

observations affects the observed phenology of mangrove forests, we compared the apparent phenology using all available observations from two individual sensors (i.e. Landsat 8 and Sentinel 2A), and of two families of sensors (i.e. Landsat and Sentinel 2) over the same period of time (i.e. 2015 – 2020). We selected these years because it is when both families of sensors have two operational satellites. All data was kept at native resolution, that is, 30m for Landsat images, and 10m for Sentinel 2 images. As a result, four models were generated: 1) Landsat 8; 2) Sentinel 2A; 3) Landsat 7/8; and 4) Sentinel 2A/B.

5.4.3.4 Hypothesis 4: Influence of spatial resolution on apparent phenology

We examined the effects of the spatial resolution on the apparent phenology of mangroves by using all available Sentinel 2 observations between 2010 and 2020. To simulate the spatial resolution of Landsat and MODIS sensors, we used analysis-ready Sentinel 2 images (Dwyer et al., 2018), we resampled the surface reflectance images to 30m, and 250m, and from the resampled images we derived the EVI. This resulted in three datasets for the selected area (i.e. 10m, 30m, and 250m). Finally, we used GAMs to detect the apparent phenology.

5.4.3.5 Hypothesis 5: Influence of temporal coverage on apparent phenology

To examine how the length of a time series changes the apparent phenology of mangroves we used Landsat 8 observations of the study zone Figure 32B) to create models spanning different lengths of time. To simulate different temporal coverages, we subset the Landsat 8 archive in the following way: one dataset spanning two years (2013-205), one dataset spanning four years (2013-2017), and one dataset using all data (2013-2020). We fitted the GAMs to each dataset and compared the results.

5.4.3.6 Hypothesis 6: Influence of cloud contamination on apparent phenology

To explore the extent to which apparent phenology is affected by cloud-contaminated observations, we compared two phenology models using all Landsat 5/7/8 observations over the mangrove region between 2010 and 2020 (Figure 32A). As described by Lewis et al. (2017), Digital Earth Australia creates a 'Pixel Quality' band for each observation that results from testing each pixel for the presence of clouds or cloud shadows, radiometric saturation and

zero values. This band allows the user to select or remove pixels that are relevant for their study. In our case, we used the 'Pixel Quality' band to remove observations tagged as clouds or cloud shadows from each image for the first model. For the second model, we did not remove the pixels tagged as clouds. Under the assumption that the 'Pixel Quality' band had few commission and omission errors, one model had fewer, but higher quality, mangrove observations, while the other model had more observations, but with lower quality overall.

5.5 Results

In Table 11 we show the median SOS and PGS, as well as the maximum and minimum EVI for each apparent phenology model in each hypothesis. We chose the midmangrove plot (i.e. Plot 2) to test several hypotheses because it is less influenced by water under the canopy, and edge effects from being close to other vegetation communities. These results suggest that mangroves around Darwin Harbour reach the PGS between Day of Year (DOY) 110 (April) and 144 (May), that is to say, within a 34-day window. The SOS is more variable. Some models show the SOS on DOY 288 (October) while others show it on DOY 56 (February). The shape of the apparent phenology also changes within, and between hypotheses, with some alterations being more evident than others. Figure 34 shows the apparent phenology curves from all models created here, and highlights two that are more dissimilar from the rest. The trend (i.e. the general increase or decrease over time) of most models did not show significant changes, except in Hypothesis 5, therefore, we rarely refer to it in the text. In the following sections we describe the changes to the apparent phenology curve, the SOS and PGS arising from each hypothesis tested.

Table 11: Compilation of median SOS and PGS, maximum and minimum EVI for each hypothesis tested.

Hypothesis	Site	Resolution (m)	Sensors	Median SOS	Median PGS	Maximum EVI	Minimum EVI
Hypothesis 1: Influence of size of area under investigation on apparent phenology	Region	30	Landsat 5/7/8	35	134	0.81	0.41
	Zone	30	Landsat 5/7/8	29	136	0.87	0.42
	Plot 2	30	Landsat 5/7/8	299	136	0.95	0.48
Hypothesis 2: Influence of location on apparent phenology	Plot 1	30	Landsat 5/7/8	35	123	0.97	0.39
	Plot 2	30	Landsat 5/7/8	299	136	0.95	0.48
	Plot 3	30	Landsat 5/7/8	299	136	0.90	0.41
Hypothesis 3: Influence of frequency of observations on apparent phenology	Plot 2	10	Sentinel 2A	306	110	0.96	0.48
	Plot 2	10	Sentinel 2A/B	302	115	0.93	0.51
	Plot 2	30	Landsat 8	288	131	0.94	0.45
	Plot 2	30	Landsat 7/8	35	134	0.81	0.41
Hypothesis 4: Influence of spatial resolution on apparent phenology	Zone	250	Sentinel 2A/B	297	112	0.86	0.44
	Zone	30	Sentinel 2A/B	26	116	0.84	0.38
	Zone	10	Sentinel 2A/B	27	116	0.83	0.38
Hypothesis 5: Influence of temporal coverage on apparent phenology	Plot 2 (2 years)	30	Landsat 8	56	136	1.16	0.39
	Plot 2 (4 years)	30	Landsat 8	299	139	1.04	0.45
	Plot 2 (6 years)	30	Landsat 8	296	134	1.01	0.45
Hypothesis 6: Influence of cloud contamination on apparent phenology	Region (with cloud mask)	30	Landsat 5/7/8	35	134	0.81	0.41
	Region (without cloud mask)	30	Landsat 5/7/8	33	144	0.76	0.20

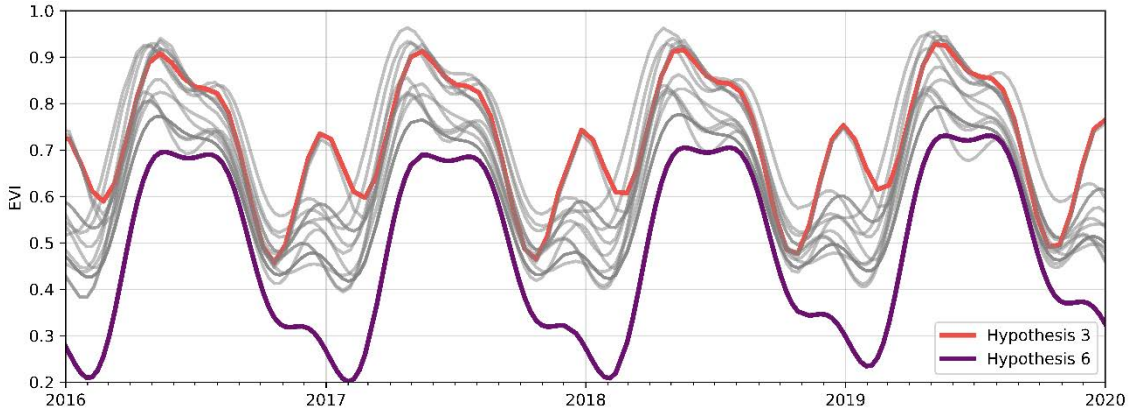

Figure 34: Comparison of the apparent phenology models from all hypotheses (grey lines). Highlighted in red (Hypothesis 3) and purple (Hypothesis 6) are two models that show dissimilar patterns to other models. The trends of each model are not shown.

5.5.1 Extent and Site Selection

5.5.1.1 Hypothesis 1: Influence of site size on apparent phenology

The size of the site does change the apparent phenology. However, the models display some similarities. From Figure 35 it is clear that the apparent phenology for the three sites has a single peak and two troughs. The apparent phenology of the sites shows that the PGS occurs on similar DOY. For the region, zone, and plot the PGS is at DOY 134, 136, and 136 respectively. According to the models, the median SOS for the region and the mangrove zone occurs early in the year (DOY 35 and 29 respectively), but the median SOS for the plot happens on DOY 299. This difference can also be seen in Figure 35G. Another difference in the models is the range of EVI values. EVI ranges from 0.41-0.81 and 0.42-0.87 for the region and zone respectively, but those values change for the plot (i.e. 0.48-0.95).

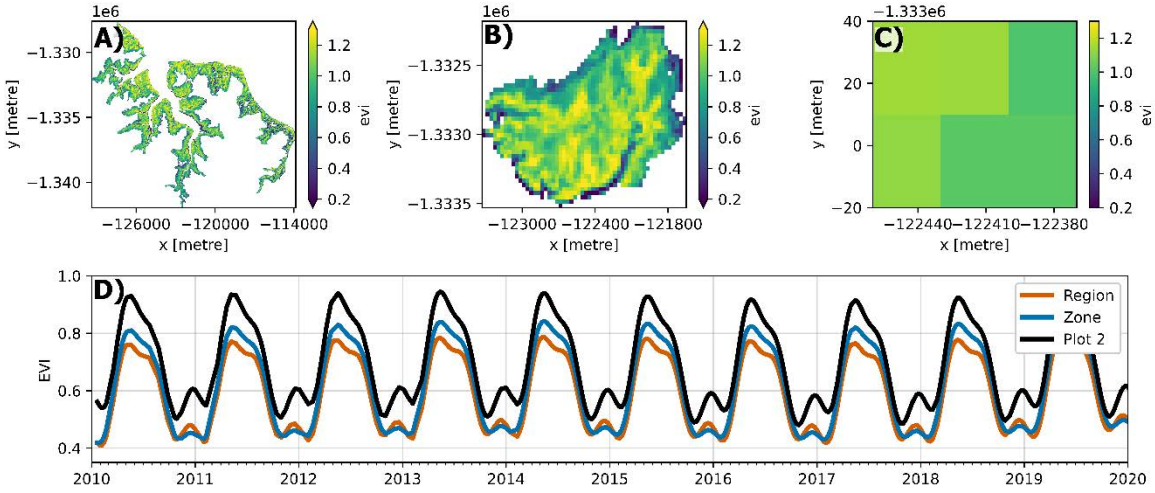

Figure 35: Spatial representation and apparent phenology of mangroves at three different spatial scales: A) mangrove region, B) mangrove zone, C) mangrove plot 2 (midmangrove), and D) apparent phenology from the mangrove region, zone and plot 2. Note that the pixel size is the same across all samples. Median values are shown in all panels.

5.5.1.2 Hypothesis 2: Influence of location on apparent phenology

Figure 36 shows the apparent phenology for three plots located in three different intertidal zones, and, overall, the apparent phenology is similar across them. At the beginning of the calendar year, the three curves in Figure 36 show a trough, followed by a well-defined peak; after this peak, the curves show a second trough followed by a smaller peak in EVI values.

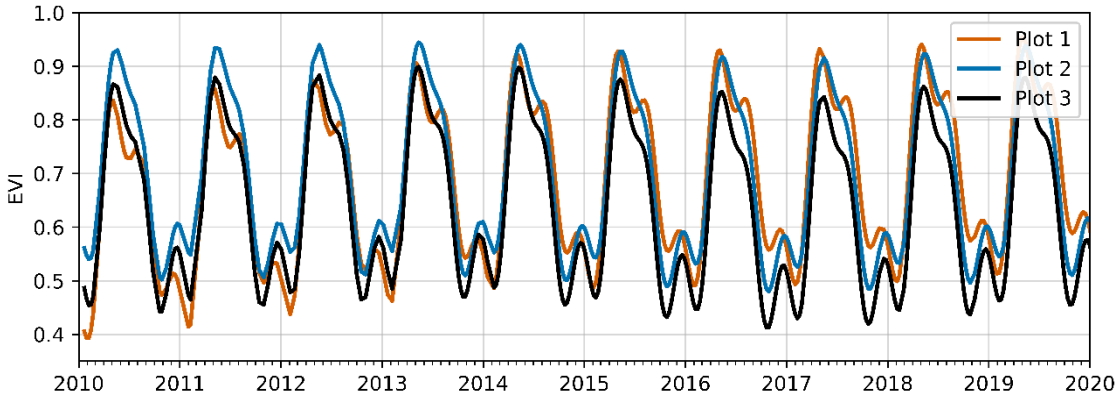

Figure 36: Apparent phenology of three mangrove plots in different intertidal zones. Plot 1, Plot 2, and Plot 3 correspond to the waterfront, midmangrove, and inland plots respectively. The lines for plot 3 (black) and plot 2 (blue) sites have similar SOS and PGS dates over the years, but different EVI magnitudes. The apparent phenology of plot 1 (orange) has different SOS dates when compared to the other two sites.

Mangroves in different intertidal zones display similar PGS dates, but different SOS dates. For example, the median PGS for plot 1 is 123, while the PGS for plot 2 and plot 3 is 136, and 136 respectively, resulting in a 13-day difference. In contrast, the median SOS occurs on DOY 35, 299, and 299 for plot 1, plot 2, and plot 3 respectively. For instance, the lines for plot 3 (black) and plot 2 (blue) in Figure 36 display the lowest values in late 2010, while the line for plot 1 (orange) only shows a small trough. The lowest point of the phenology curve of plot 1 is reached in early 2011, as stated before, a recurring pattern between 2010 and 2020. Figure 36 also shows that the EVI range for plot 1 changed from 0.39-0.86 in the 2010-2011 period, to 0.50-0.95 between 2018-2019. Plots 2 and 3 also display changes in their EVI range during different periods. We do not attempt to analyze the factors leading to these variations in the EVI. Given that the model parameters to detect phenology of the three plots remained unchanged, our results support the idea PGS dates are comparable between plots, but the SOS dates are not comparable.

5.5.2 Sensor Selection

5.5.2.1 Hypothesis 3: Influence of frequency of observation on apparent phenology

With a higher revisit time, there are approximately 51% more Sentinel 2A images of Darwin Harbour between 2015 and 2020 (n=159), when compared to Landsat 8 (n=105). Figure 37 clearly shows that the frequency of observation changes the apparent phenology of plot 2, when comparing the apparent phenology from the Sentinel 2A and Landsat 8 sensors. The median PGS from Sentinel 2A occurs in DOY 110 (Figure 37A), while the median PGS of the Landsat 8 model happens in DOY 131 (Figure 37B). Regarding the SOS, the Sentinel 2A model shows that the lowest EVI values happen in DOY 306, while the phenology derived from only Landsat 8 images shows that the median SOS occurs in 288 (Figure 37B). When comparing Figure 37A to Figure 37B, it is clear that there are differences in the shape of the curves. The Sentinel 2A model displays a single, well-defined peak in EVI values, while the Landsat 8 model shows two peaks, one in May, and one in December. This demonstrates that the frequency of observation does change the apparent phenology of mangroves.

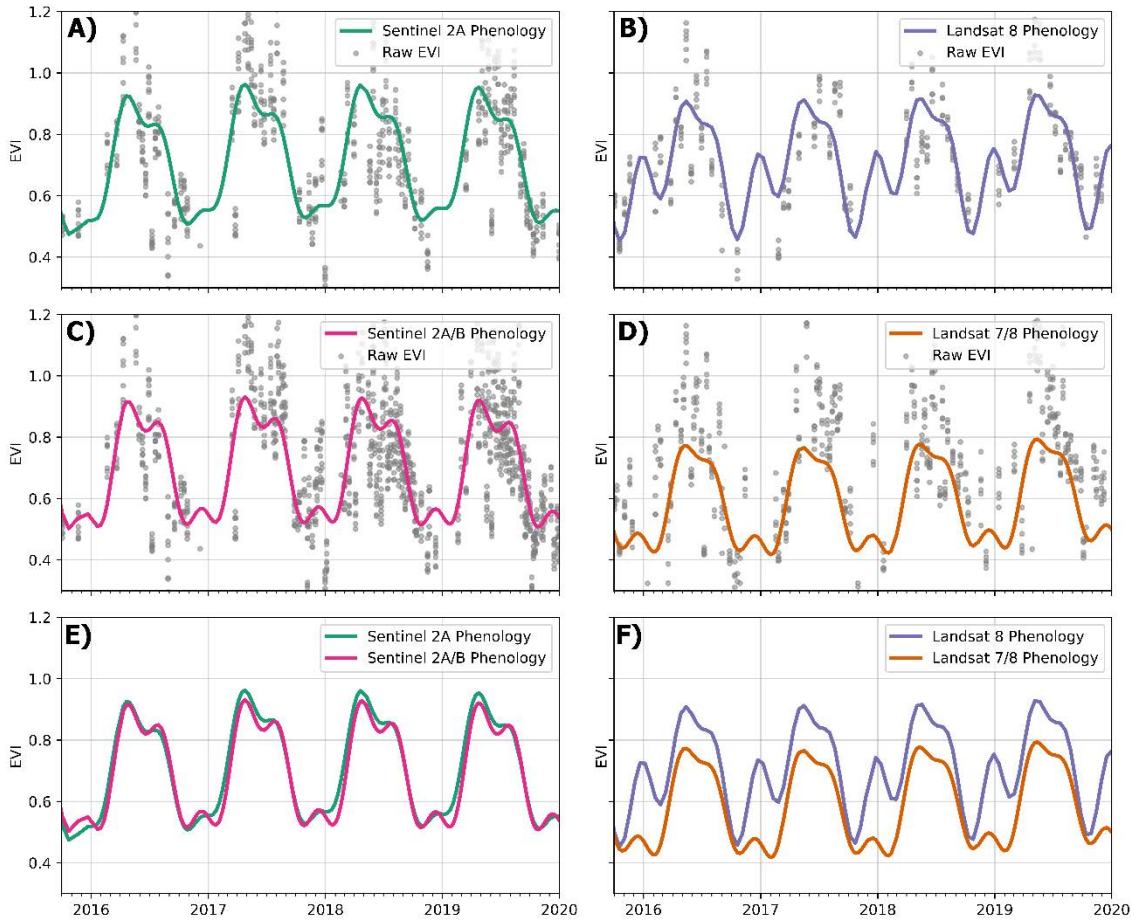

Figure 37: Observation frequency and phenology from Sentinel 2A (A), Landsat 8 (B), Sentinel 2A/B (C), and Landsat 7/8 (D). Panels E) and F) compare the apparent phenology from the Sentinel and Landsat families for sensors respectively. For display purposes we only show the 2016-2020 period. Sentinel 2B was launched in September 2015.

When all Sentinel 2A/B images are considered (n=260, Figure 37C), the apparent phenology of plot 2 changes slightly when compared to the apparent phenology of detected when only using Sentinel 2A images (Figure 37C). The shape of both models is similar, while the EVI range varies slightly between the two models (0.48-0.96 for the Sentinel 2A, and 0.51-0.93 for the Sentinel 2A/B models). When the two Sentinel satellites gather information, the median PGS and SOS happen in DOY 115, and 302 respectively.

In sharp contrast to the Sentinel 2A/B case, when all Landsat 7/8 images are used (n=207), the apparent phenology of plot 2 changes significantly when compared to the Landsat 8 phenology. Mainly, the December peak in EVI values changes to a trough, thereby moving the median SOS date from DOY 288 to DOY 35 (Figure 37D/F). The median PGS experiences almost no change, occurring on DOY 134.

An important distinction between these models is the distribution of images over time. As shown by the Landsat 8 models (Figure 37B), there are more observations between March and October, than between November and February each year. This results in a data void that the GAMs need to fill. The situation is similar for the Landsat 7/8 model (Figure 37D) where, despite having double the observations, there are few data points between December and February. In contrast, the images used for the Sentinel 2A and Sentinel 2A/B model are more evenly distributed throughout the year, hence the apparent phenology resulting from these models is more similar to those presented in the previous hypotheses.

5.5.2.2 Hypothesis 4: Influence of spatial resolution on apparent phenology

In Figure 38 we demonstrate how the spatial resolution of the sensor changes the apparent phenology of the mangrove zone. The number of observations remains unchanged, therefore changes in the apparent phenology are related to the number of pixels and their EVI value in each scenario. For example, at the 10m (Figure 38A/B) and 30m resolutions (Figure 38C/D), the apparent phenology of the zone is almost identical. EVI ranges between 0.38-0.83, and 0.38-0.84 for the 30m and 10m models respectively, and the median SOS and PGS occur at approximately the same times: DOY 27 and 116 respectively for the 10m model, and DOY 26 and 116 for the 30m model (Figure 38G). At these two resolutions, apparent phenology models are comparable with one another.

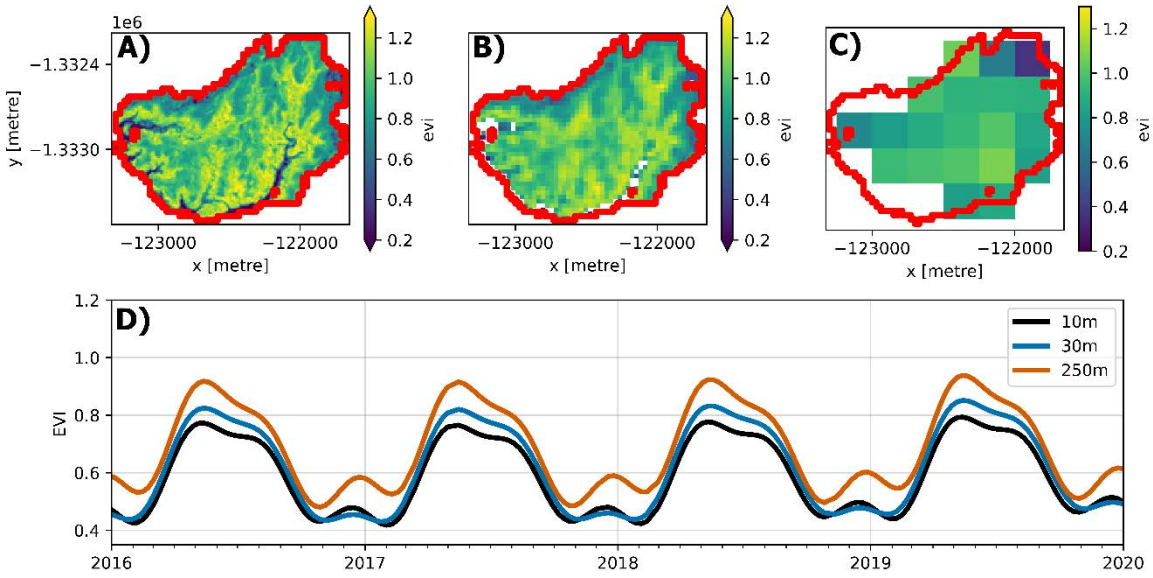

Figure 38: Spatial representation and apparent phenology of the study zone from Sentinel 2 data. Panel A): Sentinel 2 data at native spatial resolution (10m). Panel B) Sentinel 2 data resampled to match the spatial resolution of Landsat (30m). Panel C): Sentinel 2 data resampled to match the spatial resolution of MODIS (250m). Panel D): comparison of the apparent phenology of the study zone at three different spatial resolutions.

In contrast to the 10m and 30m resolutions, the EVI range for the 250m resolution model ranges between 0.44-0.86, displaying a change in the amplitude of the model (Figure 38E/F). The median PGS for the 250m model occurs on DOY 112, however the median SOS occurs on DOY 297 (October), as opposed to January like in the finer resolution models.

5.5.2.3 Hypothesis 5: Influence of temporal coverage on apparent phenology

The amount of data used by phenology studies alters the shape, amplitude, and apparent phenology metrics. Using Landsat 8 as an example, in Figure 39we demonstrate how the length of the time series changes the shape and amplitude of the apparent phenology, as well as changes in the trends in EVI values. Figure 39A shows the apparent phenology of the two-year, four-year, and six-year models, as well as the raw EVI values (gray dots). It is easy to see that the range of EVI values for the two-year model of phenology is larger (0.39-1.16) than the EVI range for the four- and six-year models (0.45-1.04, and 0.45-1.01 respectively). Using only two years of observations (n=38), the GAM tries to accommodate for all the peaks and troughs in the data, hence creating a model with a large amplitude. In this model, the median SOS and PGS occur on DOY 56 and 136 respectively.

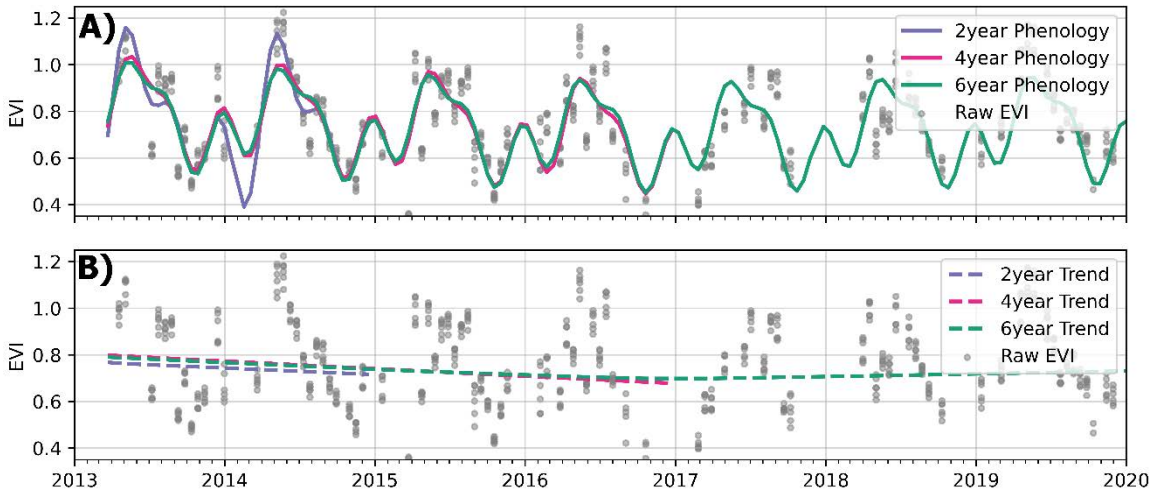

Figure 39: Panel A) shows the apparent phenology curves using 2, 4, and 6 years of Landsat 8 observations. Panel B) shows the trends of apparent phenology from using 2, 4, and 6 years of Landsat 8 data.

With four years of data (n=83), the EVI range is reduced, but the overall shape of the phenology is kept. The median PGS dates remain unchanged, but the median SOS moves to DOY 299. The model that used six years of data (n=136) is very similar to the four-year model. Maximum and minimum EVI values, including the intermediate peaks and troughs, do not show significant changes when compared to the four-year model, and the median SOS and PGS occur on DOY 296 and 134 respectively.

Regarding the trends in EVI values, the two- and four-year models show a downward trend, indicating that EVI values decrease each year, however, with only few years of data this should be interpreted with caution. The six-year model shows a downward trend EVI values between 2013 and early 2016, which is consistent with the previous two models. After 2017, the downward trend in the six-year model is replaced by an increasing trend, demonstrating that the temporal coverage alters the slope of the trend and the apparent phenology of mangrove forests.

5.5.3 Data and Data Processing

5.5.3.1 Hypothesis 6: Influence of cloud contamination on apparent phenology

We created two models of phenology using all Landsat 5/7/8 observations over the mangrove region between 2010 and 2020. The first difference between the models is the amount of data fed to the GAMs. As shown in Figure 40A, the total number of usable pixels for the model *with* cloud masking is lower when compared to the number of usable pixels used for the model *without* cloud masking. The majority of the pixels masked by the algorithm have EVI values lower than 0.4, which correspond mostly, but not always, to clouds and cloud shadows. By removing these pixels the GAM has fewer input data, meaning that 1) there is less bias towards pixels with low EVI values, and 2) less variance in the data (see Section 5.6.3). The effects of reducing the bias and variances are clearly reflected in the apparent phenology (Figure 40B).

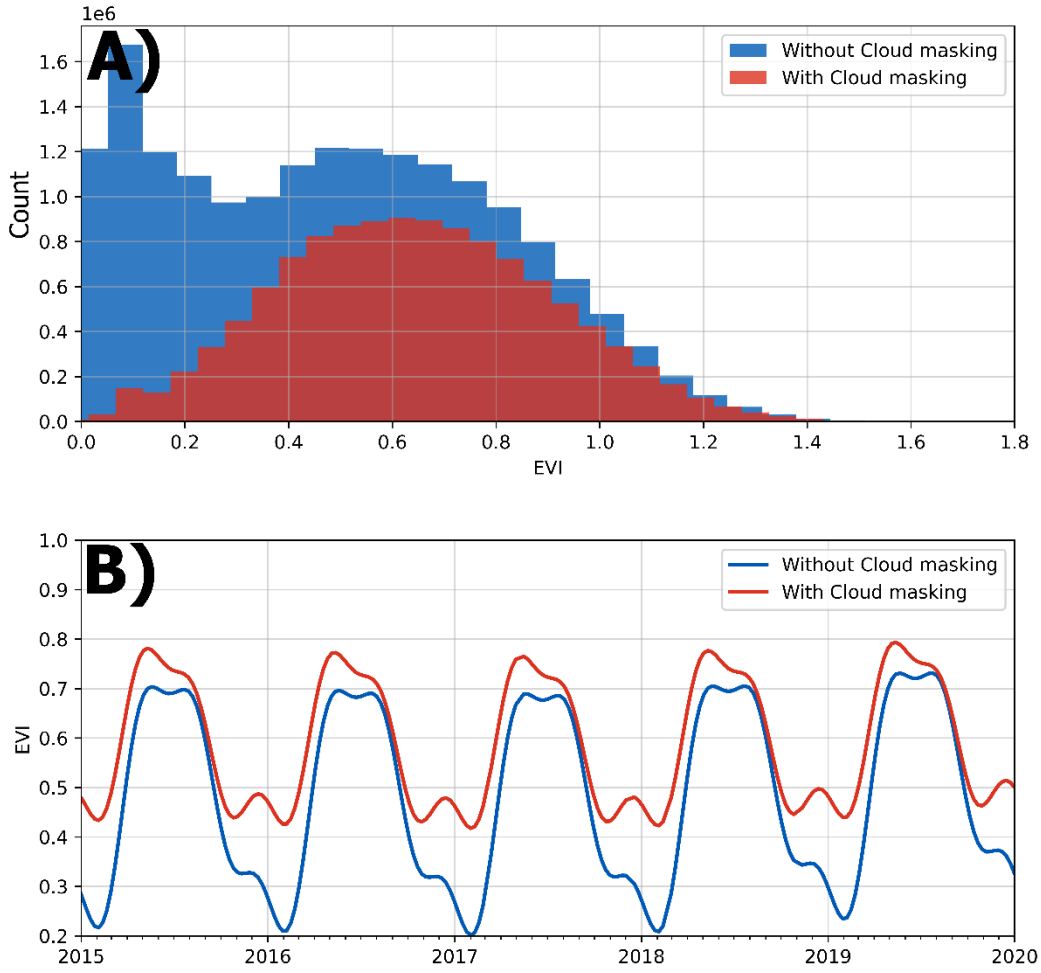

Figure 40: Panel A) shows the apparent phenology of the mangrove zone when using data with cloud masking, and data without cloud masking. Panel B) shows a histogram of the distribution of pixel values (i.e. EVI) used to detect the apparent phenology (2010-2020).

With respect to the median SOS, the models display similar dates: DOY 34 and 33 for the models *with* and *without* cloud masking respectively (Figure 40B). The median PGS however, shows a wider gap between the models. The model *with* cloud masking shows this event on DOY 134, while in the model *without* cloud masking the PGS occurs on DOY 144. From Figure 40B it is easy to see that the amplitude of the model *without* cloud masking is greater (EVI between 0.20-0.76) than the amplitude of the apparent phenology model *with* cloud masking (EVI between 0.41-0.81).

5.6 Discussion

Studies that analyze plant phenology using satellite images are more common than ever before. However, these studies use a wide range of sensors, look at different sites, and process their data in different ways. The idea that "*all models are wrong, but some are useful*" (Box, 1979) is put to the test by asking: if two studies use different sensors to detect phenology over the same site, do they produce comparable results? We answer this question by testing six hypotheses related to the area of interest, the sensor selection, and the data pre-processing over an Australian mangrove forest (Figure 33). Under certain circumstances, we found that studies may produce comparable phenology models, as explained below.

5.6.1 Area of interest (Extent and Site Selection)

When studies perform spatial aggregation on sites that differ significantly in their areal extent (i.e. one order of magnitude or more), comparison is not advisable, mainly because of differences in the species composition, species richness, plant growth stages. All these factors can influence the shape and amplitude of the apparent phenology, as well as the SOS and PGS dates. Differences in SOS and PGS dates, as well as in EVI values support the idea that the size of the area of interest changes the apparent phenology of an ecosystem. Therefore, studies comparing sites of different areal extents may not be comparable with one another, even if data are spatially aggregated. Spatial aggregations are good for making generalizations over

selected areas, however they come with their own set of challenges (Jelinski and Wu, 1996a; Wu and Li, 2009b; Younes et al., 2019), including changing apparent phenology of vegetation. In our case, the apparent phenology curves were similar in shape, but the phenology metrics were different. The similarity in the shape of the three curves is not entirely surprising because 1) the region is dominated by mangroves of the *Ceriops* and *Rhizophora* genera (Metcalfe et al., 2011a); 2) by using the median value of all pixels we capture the general trends in pixel values (Roberts et al., 2017); and 3) all models were created using the same number of input EVI values (i.e. the median EVI per date), which reduces the model variance. Despite these similarities, there are important differences in the apparent phenology of the mangrove region, zone, and plot.

Here, we have demonstrated that spatial aggregation of data results in changes to the SOS by more than 60 days and PGS. Our results agree with those of van Bussel et al. (2011), who conclude that spatial aggregations 1) can change the phenological metrics of crops by more than 10 days, and 2) they average the values of apparent phenology, thereby reducing natural variation and presenting a smoother phenology signal. Importantly, phenological metrics are key variables in assessing how an ecosystem responds to variations in the climate and, if these metrics are subject to change due to spatial averaging, they become unreliable, and potentially misleading.

Regarding the different locations, the models of apparent phenology shown here seem to coincide with the PGS dates, but not always with the SOS dates. These differences may be due to:

1. The species represented at the sites are slightly different and thus their phenology differs from one another. In other words, the dominant species in each site may change from site to site, therefore the phenology captured by the model differs.
2. The tidal height may play a role changing the apparent phenology of plot 1. Changes in apparent phenology may be due to variable tide heights, when the satellite image captures more water per pixel in plot 1 when compared to plots 2 and 3. In 2019, (Younes et al., 2019) described how different tidal heights might change the spectral signature of mangrove forests. The study concluded that, when using high spatial resolution imagery (1.4m), the spectral signatures of mangrove forests does not change

during high tide when compared to low tide. However, that study failed to examine the influence of the tides when a mixed pixel is more likely to occur. Further, in 2019 (Bishop-Taylor et al., 2019) demonstrated that optical sun-synchronous satellites fail to capture the entire tidal range in the Australian mainland. As a result, if the satellite consistently captures the higher tides, models of phenology at the fringes of mangroves may be biased towards lower values due to a larger proportion of water in each pixel (thus a smaller proportion of vegetation). Conversely, if the satellite captures the lower end of the tidal range, each pixel would have more vegetation exposed and thus, a more accurate phenology model.

Here, it is unclear if the tides have any real effect on the phenology model of plots 1 and 2, or if the mangrove species in each plot have slightly different phenologies. However, we demonstrated that while the phenology curves are similar between plots, the location of the site does play a role in the apparent phenology. If the areal extent of the sites remains similar, apparent phenologies should be comparable between studies, assuming other factors remain equal (i.e. sensor and data processing).

5.6.2 Sensor Selection (Frequency of Observation, Spatial Resolution, and Temporal Coverage)

Understanding the needs of the phenological study is crucial to selecting the frequency of observations. For example, a study looking at crops may require a higher frequency of observations to examine the dates where leaf-growing occurs or when dormancy starts. In contrast, examining broad trends of leaf production and leaf fall in evergreen forests may require a lower frequency of observation. The frequency of observation is a recurring topic in phenology investigations. For example, Melaas et al. (2018b) and Kowalski et al. (2020) leverage the frequency of observation of Landsat or Sentinel 2 sensors, but also the overlapping footprints of the images. It is easy to understand that, if there are more images available for a given time of year, the apparent phenology will be better represented than if there are fewer images. But if we have many images for one season (e.g. winter) and few, or none, for another (e.g. summer), the apparent phenology might not be well represented. In Section 5.5.2.1 we showed that, with more observations between September and April, the

Landsat 7/8 model was more similar to the Sentinel 2 models than to the Landsat 8 model. With a higher temporal resolution, Sentinel 2 sensors have more useful (i.e. with no clouds) observations when compared to Landsat sensors, and this is directly related to the distribution of observations through time (Figure 37). Here, we demonstrated that the frequency of observation changes the apparent phenology of a mangrove forest, but we also showed that the distribution of images over time is also an important factor. Recently, Kowalski et al. (2020) found that the frequency and distribution of observations changed the SOS dates throughout Germany, while Zhou et al. (2019) had similar findings in north American grasslands. Although their temporal and spatial scales differ from ours, our results align.

Turning to the spatial resolution of the sensor, to date, most studies on phenology have used sensors with a spatial resolution of 250m, or coarser, particularly MODIS (see e.g. (Czernecki et al., 2018; White et al., 2009). This is too coarse to examine the phenology of a particular community, plot or species. It has been demonstrated the heterogeneous surfaces have different spectral responses at different spatial scales (Wu and Li, 2009), and that there are ways of minimizing this effect: either quantify the intra-pixel heterogeneity, or to use higher spatial resolution imagery (Younes et al., 2019). Considering that many studies of phenology use sensors with pixels that measure 250m or more, it is inevitable to think that these models cannot accurately describe the phenology of a particular vegetation type. Using Box's words coupled with the findings by Wu and Li (2009), models that use large pixel sizes are more wrong than models that use smaller pixels sises. Regardless of the pixel size, these models provide useful hints regarding the apparent phenology of the landscape.

Lately, the trend is to use Landsat or Sentinel 2 imagery individually or in combination. With higher spatial resolution than MODIS products, one would assume lower intra-pixel heterogeneity in Landsat and Sentinel 2 imagery, and thus, an apparent phenology that is less wrong. Despite this, a higher resolution means that one is not necessarily looking at the phenology of the landscape, but at the phenology of a plot or stand, turning this into a classic example of the modifiable area unit problem (Jelinski and Wu, 1996). Our results suggest that the spatial resolution of the sensor can change the apparent phenology of the ecosystem being investigated. Therefore, images with similar resolutions (i.e. 10m and 30m) produce apparent phenologies that are comparable with one another. Under the conditions tested

here, the apparent phenology of our study zone is almost identical between the 10m and 30m resolution images. In other words, the models of apparent phenology from Landsat and Sentinel 2 sensors are comparable with one another.

In 2018, Pastick et al. combined Landsat and Sentinel 2 observations to detect the apparent phenology of dryland ecosystems in the western United States. To validate their models of phenology they compared the apparent phenology detected at 30m to MODIS NDVI (Normalized Difference Vegetation Index) data collected at 250m. At their native resolutions these two are not comparable, therefore the authors downscaled the 250m data to 30m, and they upscaled the 30m data to 250m. Similarly, when Claverie et al. (2018) describe the Harmonized Landsat and Sentinel dataset, they hint caution when comparing the 30m data to the 250m data. We too advise against the comparison of phenology models from 10m or 30m to those of 250m or coarser because of changes in the EVI range, and SOS dates.

Lastly, the effects of temporal coverage on apparent phenology are related to changes in the amplitude of the model (i.e. shape) and the SOS. Some studies look at plant phenology using a single year of data (Kowalski et al., 2020), but others examine the apparent phenology over decades (Garonna et al., 2016; Melaas et al., 2018). A single year of satellite images may give an idea of what the ecosystem is doing and when; however, examining one or two years of apparent phenology may not provide the full picture. Studies have demonstrated the difficulties in making generalizations of phenological cycles due to inter- and intra-annual variability in apparent phenology. For example Broich et al. (2014) used satellite imagery between 2000 and 2013 to examine apparent phenology across Australia. The authors conclude that, in some ecosystems of the Australian interior, the PGS varies by over a month from one year to the next, driven by rainfall patterns and atmospheric circulation. In comparison, our study site has a fairly regular phenology and, despite this, the apparent phenology of the mangroves from two years of data had considerable differences when compared to the four- and six-year models. Considering this, we advise caution when using less than four years of satellite imagery to detect apparent phenology, and we encourage incorporating contextual information in the analysis (e.g. weather and climate data) before comparing studies that span different periods.

Four years of data provide a more informative version of the phenology of the landscape than just one or two years, but it certainly does not allow for a comprehensive understanding of phenological events. As show by Broich et al. (2014) year-to-year variations in weather and climate patterns can, and often do, change the phenology of different vegetation types. In Australia, El Nino Southern Oscillation, the Julian-Madden Oscillation, and the Indian Ocean Dipole, control the amount of water contained in the atmosphere, and thus, precipitation over the continent. Precipitation, in turn, is a driver of vegetation phenology, making phenology susceptible to the aforementioned phenomena. Because one cannot assume that climate patterns are stable through time, one should not assume a stable phenology either. Under the conditions tested here, the shape of the four-year and six-year phenology curves and the long term trends are similar, but not identical. Feeding more data to the GAMs does change the output, and these differences should be tested with longer time series.

5.6.3 Data and Data Processing

We detected apparent phenology from a dataset that includes cloudy observations, and a dataset that removes most of the pixels affected by clouds and cloud shadows. Here, we demonstrate that the apparent phenology is, indeed, affected by clouds and cloud shadows (see also Section 5.6.5). While it is unlikely that many studies will use satellite images without any type of cloud removal, there are two main reasons why knowing how clouds affect apparent phenology is important: knowledge and context (Comber and Wulder, 2019).

Knowledge refers to understanding the *true* phenology of the study site, regardless of the vegetation type (e.g. crops, wetlands, or forests). For example, *when* the SOS and PGS happen and *how* they are expressed on the ground. Context, on the other hand, refers to the ability of the user to make informed decisions based on the apparent phenology. When knowledge and context are integrated, they allow the user to assess whether the apparent phenology is within an expected range of values (e.g. $0.4 < EVI < 1.2$) or if it affected by clouds or cloud shadows (e.g. $EVI < 0.4$). After comparing the true and apparent phenologies (i.e. using context and knowledge), the user can: 1) further clean the data, 2) tune or change the model, or 3) change the workflow (e.g. sensor fusion), to ensure that the apparent phenology is representative of the true phenology.

Moreover, many tropical ecosystems have prevalent cloud cover, which limits the number of clear observations in a year. Adding to this, the Landsat archive does not provide the same number of images over all continents (Wulder et al., 2016). Examples of areas that have persistent cloud cover and low number of images include the upper guinea forest in west Africa, the tropical rainforests of Central and South America. Due to the lack of clear observations, phenology investigations in these areas may resort to using cloud masks (or algorithms) with larger omission errors to ensure more cloud-free observations are available for analysis, therefore prior knowledge about the effects of clouds and cloud shadows in phenology are important.

5.6.4 The definition of Start of Season

In this study we showed that the area and sensor(s) selected will change, to some degree, the shape, amplitude, and metrics of the apparent phenology. Our results indicate that the SOS is the metric most subject to change, and there are two main reasons for that: 1) the method used for representing apparent phenology, and 2) the definition of SOS. Here, we used GAMs to represent apparent phenology from satellite images, but most studies of phenology use fully parametric methods for this purpose. Studies that use fully parametric methods to represent phenology assume, among other things, that phenology can be represented by a model with a single peak and a single trough. This assumption may not hold true for mangroves and other evergreen forests, given that studies have demonstrated that some mangrove species display multimodal vegetative phenologies (Duke, 1990b; Duke et al., 1984a; Tomlinson, 1986). By using GAMs, we do not assume that there is a single peak or trough in the phenology of mangroves, and we let the data define the number, frequency and magnitude of the peaks and troughs. Also, to prevent overfitting, we constrained the number of seasonal components in the 'Prophet' package. This means that, despite fitting a curve with fewer peaks and troughs, most models still display two peaks and two troughs in EVI values. Some of the changes in the SOS dates (e.g. in section 5.5.1.1) may be due to the use of the median values for each date. By aggregating the data, we tend to capture the trend of the region or zone, in detriment of the natural variation of smaller plots. Given that we make no

assumption about the number or magnitude of the peaks and troughs in the apparent phenology, PGS and SOS dates are subject to change (see Section 5.5).

The second reason that makes the SOS change is the way in which we defined it. We defined the SOS as the median of the lowest five percent of EVI values in a growth cycle. Others define SOS as the midpoint between the minimum spectral index value and the maximum green-up rate (Restrepo-Coupe et al., 2015). Broich et al. (2014), for example, defined the SOS as the date where the EVI values reached 20% of the phenology curve amplitude, and tested their method on several vegetation types across Australia. Before fitting a double logistic curve to the data, the authors used a Savitzky–Golay filter to reduce the variability in EVI values. In doing so, the authors alter the data to fit a unimodal model of phenology, and therefore, the SOS dates. Under the conditions tested here, neither of the previous definitions may be adequate given that the data shows two periods of low EVI with an intermediate peak of varying magnitude. A new definition of SOS may be required to accommodate for unimodal and multimodal phenologies in different environments.

5.6.5 Uncertainties and limitations

In this document, we used Darwin Harbor as a case study for examining the influence that the site, sensor, and data have on apparent phenology. While we have tried to isolate every element to demonstrate its influence, there are some limitations that need to be acknowledged.

Firstly, we may not be looking at the same site every time. Most methods for geocoding satellite images are subject to errors of up to half a pixel, therefore using Sentinel or Landsat images implies that each pixel might be off target by up to 6 and 18 meters respectively (Claverie et al., 2018). If, like here, one is aggregating the data before applying the model, these errors might be reduced because the aim is to capture the phenology of an area larger than one pixel. Conversely, if the aim is to examine the phenology of every pixel, geo-location errors must be acknowledged, and cautious interpretation is advised.

Secondly, no cloud-masking algorithm is perfect. There will be omission and commission errors associated with each algorithm, and interpretation of phenology models needs to accommodate for such errors. Despite new methods being developed for cloud and cloud

shadow detection for Landsat and Sentinel datasets (Candra et al., 2020; Ernst et al., 2018; Mateo-García et al., 2018), the user must acknowledge that abnormally low or high values may result from omitted clouds or shadows. In our case, some omission and commission errors were evident in the Landsat images despite masking the clouds and cloud shadows. We reduced these errors by aggregating the data, and using the median values for each date. Nevertheless, the user may decide not to do any spatial aggregations, and must acknowledge the limitations of cloud-masking algorithms. But pixel values are not only affected by clouds or shadows, they can be affected by vegetation migration.

Mangroves are dynamic ecosystems; they are known to migrate in response to changes in environmental conditions (Asbridge et al., 2015; Rogers et al., 2017; Saintilan et al., 2014). This implies that models of phenology may not only reflect annual cycles in the trees, but also plant migration, colonization, or dieback. Recently, Lymburner et al. (2019) mapped the extent of mangrove forests across Australia on a yearly basis. This information, coupled with high-resolution imagery, phenocams, and other ancillary datasets may provide insights as to the processes driving the phenology of a particular pixel, plot, or region (Moore et al., 2016).

While the claims that satellites collect data consistently over space and time are true, modifications in the sensor characteristics and orbit may show as changes in phenology. For example, Roy et al. (2016), and Zhang and Roy (2016) attributed some changes in surface reflectance to variations in orbits, sensing geometries, and spectral characteristics of the Landsat 5, Landsat 7 and Landsat 8 sensors. Considering that these changes are small, but potentially significant, data harmonization should be considered when analysing a time series from these sensors.

There are also limitations related to GAMs, for example, their tendency to overfit the data. To overcome this, 'Prophet' and other packages offer the ability to limited the number of knots and penalizing models in favour of simpler ones. As a result, our models captured the principal features of the phenology without overfitting the data. There are, however, ways to improve upon the method used here. For example, combining the advanced capabilities of the 'mgcv' package to select different smooth functions, and Bayesian stochastic simulation (Wood, 2017).

Lastly, we used GAMs as a way to examine phenology from satellite imagery, while others have used fully parametric methods (Pasquarella et al., 2018; Verbesselt et al., 2010). Because the mechanisms behind the models differ from one another, phenology models may not be directly comparable unless the site, sensor, and data are the same (see e.g. Atkinson et al. (2012)). Here we demonstrated the usefulness of GAMs as a tool for detecting mangrove phenology in Northern Australia, however our intention is not to compare this method to other methods or sites. Indeed, a comparison between parametric and semi-parametric methods is needed, not only in the context of assessing phenology, but also to determine if different sites and sensors alter the apparent phenology equally. Atkinson et al. (2012) compared several fully parametric algorithms used to detect phenology, but did not incorporate GAMs or other semi-parametric models. Change detection algorithms are often based on the vegetation changes over time (i.e. phenology), however they are rarely used for phenology investigations. Yan et al. (2019), for example, compared 'Prophet' (the algorithm used here) to other, commonly-used, algorithms for land cover change detection. The authors found that the algorithm that used 'Prophet' was able to accurately capture subtle changes in land cover, as well as the direction and rate of change. The performance of GAMs could be compared to change detection models (Yan et al., 2019) especially in the context of climate forcing and its effects on phenological cycles.

5.6.6 Future directions

To date, most remote sensing studies on phenology have used MODIS, with fewer studies using Landsat or Sentinel data. Currently, there are several methods to harmonize Landsat and Sentinel-2 data to study phenology, however they focus mainly in dryland ecosystems (Pastick et al., 2018; Zhou et al., 2019). Data harmonization of these two families of sensors will improve phenology investigations in several ways, including: 1) near real-time monitoring of phenology, 2) increased frequency of observations, 3) more evenly distributed usable observations throughout the year, and 4) increased number of cloud-free observations in mangrove and other evergreen forests. With this wealth of methods and data, phenology investigations can move from examining past phenology to forecasting future phenology. Forecasting phenology will allow us to assess future carbon budgets, and select the

ecosystems that will help mitigate the effects of increased concentration of carbon dioxide in the atmosphere.

5.7 Conclusions

In this paper we ask if studies that detect phenology using different sensors on the same site produce comparable results, and often the result is: no. We explored different area sizes, using one versus many sensors, and removing clouds. Each maintained some characteristics of the apparent phenology, but not all. Our intention is not to prescribe a method for modelling phenology, but to expose the complexity of the process and help guide future phenology investigations. We conclude that: 1) the areal extent and the location of the study site change the apparent phenology of the vegetation; 2) the distribution of observations over time may play a more important role on apparent phenology than the frequency of observation; 3) the apparent phenology resulting from Landsat and Sentinel 2 sensors is comparable with one another, but it is not comparable to phenology derived from MODIS due to differences in the spatial resolution of the sensors; 4) the length of the time series has more impact on the trend of the phenology than on the apparent phenology itself; and 5) cloud contamination significantly changes the apparent phenology of vegetation, therefore, studies must incorporate knowledge and context into their workflows to ensure apparent phenology resembles true vegetation phenology. Reflecting on what George Box said, the models tested here are able to represent behaviour of a mangrove ecosystem and, like many other models of phenology, the ones presented here are wrong. They are wrong because we are not certain about the miniscule and specific changes that take place in the ecosystem, or when they take place, or if they take place at the same time throughout the landscape. But the models are certainly useful. The usefulness of these models comes from their ability to represent data and its variations. From these models we can examine seasonal variations and long term trends, and eventually compare those variations to other biophysical drivers. In conclusion, each combination of sensor, site, and data will produce a unique apparent phenology model, therefore, all models of apparent phenology are wrong, but some are useful.

5.8 Acknowledgements

This project is supported by NIESGI Cia. Ltda., James Cook University Postgraduate Research Fellowship, Wet Tropics Management Authority Student Research Grant, National Environment Science Program (NESP) Tropical Water Quality (TWQ) Hub research Grant, and a Centre for Tropical Water & Aquatic Ecosystem Research (TropWater) Student Research Grant. We would like to acknowledge NASA, the USGS and ESA for making all Landsat and Sentinel images freely available. This research was undertaken with the assistance of resources from Digital Earth Australia (DEA).

6 Synthesis and Implications

The overarching aim of this thesis was **to examine temporal and spatial changes in mangrove phenology across Australia using the Landsat and Sentinel 2 archives**. I achieved this by completing a literature review (Chapter 2), and through three empirical chapters (Chapters 3, 4, and 5). Specifically, I:

1. Reviewed the literature on the options to process large datasets of satellite imagery (Chapter 2),
2. Investigated the effects of understory water on the estimation of Fractional Vegetation Cover in mangrove forests (Chapter 3),
3. Compared the effectiveness of different spectral indices in predicting Fractional Vegetation Cover in a simulated, and a real mangrove forest (Chapter 3),
4. Evaluated the relationship between field and satellite-derived phenology in mangroves forests across Australia (Chapter 4), and
5. Investigated how changes in the spatial and temporal resolution, alter the observed phenology of a mangrove ecosystem (Chapter 5).

Each of the previous chapters in this thesis has its own discussion and conclusions. However, here I summarize the key findings of this thesis, put these findings into context, and discuss the implications for future phenology investigations. Importantly, my intention with this thesis is not to prescribe semi-parametric or data-driven models for all phenological investigations, but to present a different approach to monitor phenology that will show, in more detail, the phenology of different plant communities, when compared to fully parametric models.

6.1 Summary of Key Findings

6.1.1 Key findings of Chapter 2: Monitoring mangrove forests: are we taking full advantage of technology?

- Satellite images are commonly used to detect changes in mangrove forests. These changes are often related to their extent (e.g. logging), land cover change (e.g. mangrove to aquaculture farms).

- Until recently, most studies relied on two to five images, due to computational and data storage constraints.
- There has been an increase in the number of images used for analysis due to the availability of images from different sources (e.g. Landsat and Sentinel 2 archives). This, couples with cloud computation and storage resources implies that researchers now have the ability to process thousands of images at a time.
- Considering the amount of data stored in the Landsat, MODIS, Sentinel 2, and other satellite archives, manually analysing each image is no longer viable. Fully automating the analysis of satellite imagery is becoming the norm rather than the exception, therefore researchers and students alike are encouraged to acquire any level of programming skills.

When I wrote chapter in 2016, few studies had used more than 10 images to monitor mangrove forests, and nowadays studies using long time series are more common than ever before (Pastor-Guzman et al., 2018; Songsom et al., 2019; K. Zhang et al., 2016). Coding skills, coupled with freely available data and computational resources, have allowed an explosion of studies that look at spatiotemporal changes over entire continents at a time. Where before studies used tens of images, now they use thousands; and where before studies looked at sites now they look at continents. The way we do these spatiotemporal analyses, including detecting phenology, has radically changed in the past decade and will continue to evolve in the following years. Coding is now an essential skill for students and researchers alike, not only for phenology investigations, but for many spatiotemporal analyses.

Phenology investigations require hundreds, and potentially thousands, of images over the selected study site. It is, therefore imperative to change the way we process these images, from a manual process to a fully automated process or using Analysis Ready Data (Dwyer et al., 2018; Ernst et al., 2018). More and more imagery archives are moving to cloud storage, and allowing users to perform analyses on the spot rather than forcing them to download all required images, process, and analyse them one by one (Dhu et al., 2017; Gorelick et al., 2017). Platforms like Digital Earth Australia and Google Earth Engine are making phenology investigations more accessible, not only by providing free access to data and processing capabilities, but also because they allow the users to create their own algorithms. Users are

now responsible for gaining new insights as to how ecosystems have changed over space and time at the local, regional, and continental scales.

6.1.2 Key findings of Chapter 3: The effects of water depth on estimating Fractional Vegetation Cover in mangrove forests

- The spectral indices EVI, MSAVI, and MASVI2 are better predictors of vegetation fraction when compared to NDVI.
- When high resolution imagery (<1.4m) is used, water under the canopy of mangrove forests does not impact estimations of FVC.
- The spectral index selected for estimating FVC is more important than the spatial resolution of the image.

One of the knowledge gaps identified in Chapter 2 was that water under the canopy may alter the spectral signature of mangrove forests because of the absorption of near-infrared light. This gap was addressed in this thesis using very detailed (1mm) imagery over a simulated mangrove forests, and high resolution (1.2m) satellite imagery over a real mangrove ecosystem. The effect of water depth on the spectral signature of mangroves remains untested when using the short-wave infrared region of the spectrum, and in medium resolution imagery (i.e. 10m or 30m). In 2017, Sagar et al., developed an algorithm that allows the user to create composite images using tidal height instead of the time as compositing dimension. In other words, instead of creating a yearly composite, one can create a composite of all images at high, or low tide regardless of the date of image acquisition. Recently, Bishop-Taylor et al. (2019) successfully used this method to delineate spatiotemporal changes of the Australian coastline over the past 30 years. This algorithm could be used to test if tidal height changes the spectral signature of mangroves when using the visible, near infrared, and shortwave infrared regions of the spectrum. I did not use this algorithm in this thesis for two main reasons: firstly, the algorithm was made available after I had completed this chapter; and secondly, I only had two high resolution (1.2m) satellite images donated by the Digital Globe Foundation, therefore I could not create a composite.

Findings of this chapter have been corroborated in phenology investigations. For example, Kowalski et al., (2020) also found that EVI is better suited for investigations of vegetation

fraction, and hence phenology, than NDVI. The authors compared the phenology of temperate broadleaf forests in Germany and made similar conclusions to the ones one this chapter. Firstly, they found that that the apparent phenology from EVI was more correlated with true phenology when compared to the apparent phenology from NDVI. Secondly, they too conclude that the spectral index used is more important than the spatial resolution of the images, when comparing the apparent phenology using Landsat and Sentinel 2 imagery. I further explored the spatial resolution claim in Chapter 5. It is important to remember that apparent phenology is, at least in part, a function of FVC (i.e. more leaves in a tree equate to increased FVC), therefore EVI can be used as a proxy for FVC and phenology. Findings from this chapter served as steppingstones for the next chapter in this thesis.

6.1.3 Key findings of Chapter 4: Extracting mangrove phenology from Landsat imagery: a novel approach using Generalized Additive Models

- Phenology is site dependent, irrespective of the dominant species at each site.
- Generalized Additive Models (GAMs) are a data-driven approach capable of detecting phenology.
- Satellite images capture changes in greenness and those changes are related to leaf growth and net leaf production.

Mangroves grow along most of the Australian coastline, but their distribution is dictated, in part, by the climate, geomorphology, and lithology (Lymburner et al., 2019a). Therefore it is to be expected that each mangrove community displays a different phenology. Despite having the same dominant species at each of the study sites, I have demonstrated that each site displays a different phenology. These differences in phenology may be related to the species composition and richness, the growth stage of the trees, the number of trees in each pixel, or the number of layers in the forest canopy. The importance of this finding is that phenology is linked to carbon stocks (Richardson et al., 2009; Saitoh et al., 2015), therefore the amount of carbon that mangroves store (or release), depends on factors such as: the phenological phase of the trees, the species composition and richness of the site, age of the mangrove forest, and others. This link between carbon stocks and phenology implies that we need to: 1) extend research efforts into understanding the phenology of evergreen forests; 2) include phenology

investigations in the methods for estimating carbon stocks and budgets, and more importantly; 3) adapt and update national and international policies (e.g. International Treaty on Wetlands (Ramsar Treaty), or the Commonwealth Environment Protection and Biodiversity Conservation Act 1999) to account for changes in the phenology of evergreen forests and wetlands due to changing climate conditions (Rogers et al., 2016).

6.1.4 Key findings of Chapter 5: All models of satellite-derived phenology are wrong, but some are useful.

- The apparent phenology resulting from Landsat and Sentinel 2 sensor observations is comparable with one another, but it is not comparable to phenology derived from MODIS.
- The length of the time series has more impacts on the trend of the phenology than on the apparent phenology itself.
- The distribution of observations over time may play a more important role on apparent phenology than the frequency of observation.

In Chapter 4 I demonstrated that mangrove phenology is site dependent, and in this chapter I demonstrate that there are many factors that influence apparent phenology, including the location, the spatial and temporal resolution, and cloud contamination. Phenological patterns are set to be disrupted, especially in Europe, Asia, Australasia and North America by the effects of climate change (Field et al., 2014), and to assess how, and when these changes take place, it is important to establish a baseline of what phenology looks like. Satellite images often aid in this effort, especially those images from the 1970's and 1980's. From these images, studies can establish a baseline of phenological patterns, mainly the start of season, peak growing season, and the length of the growing season. Past and current patterns in plant phenology can be studied to assess if changes have occurred, but before those assessments are made, one needs to ensure that these phenological patterns are, in fact, comparable.

In this Chapter I have demonstrated that apparent phenology changes with the following factors: spatial resolution, cloud contamination, and the frequency of observations. The main implication for phenology investigations is that, unless the spatial resolution of the images used, and the processing techniques are similar, the detected phenologies may not be

comparable. By ensuring that changes in apparent phenology are real, and not an artefact of the data or analysis method, studies can accurately track the response of plants to climate forcing. There are guidelines that describe how to detect and validate phenology observations (e.g. Restrepo-Coupe et al. (2015)), but with many studies using different data and methods, comparing changes in plant phenology remains a challenge.

6.2 Implications for future work

6.2.1 Theoretical implications

One of the main implications of this thesis is that models of phenology developed for temperate or deciduous forests may not be directly transferable to mangrove forests. Plant phenology is often modelled using temperate or deciduous forests from the northern hemisphere. As a result, most models of phenology assume that plants follow a unimodal cycle with a single, well-defined peak in leaf production, and a single, well-defined trough that represents leaf senescence. In some cases, sinusoidal or double logistic curves can be used to represent phenology. Tropical evergreen forests such as mangroves do not necessarily follow a yearly cycle, or have single, well-defined, period of leaf growth or leaf fall, and neither do drylands (Broich et al., 2014). As a result, researchers need to re-think their assumptions when using remotely sensed data to detect phenology in these ecosystems. In other words, the assumption that tropical evergreen forests, or drylands, will always display a unimodal phenology may result in models that are not representative of true phenology.

Another important lesson from this thesis is that phenology is site specific, in the sense that each individual patch of mangrove forest (represented by a pixel) presents a unique phenology curve. This is especially important because mangrove forests are dynamic ecosystems known to expand landward and seawards (Asbridge et al., 2018; Lymburner et al., 2019a), and phenology investigations must take these migrations into account. Firstly, the apparent phenology of a pixel that represents a stable mangrove patch over time will differ from that of a pixel that changes from representing a mud flat to one colonized by mangroves. Secondly, keeping track of landward and seaward migrations will allow future investigations to couple changes in phenology with changes in land cover. Linking phenology with mangrove migration

(i.e. land cover) will provide insights into the response of the ecosystem to changes in weather and climate patterns.

Lastly, future work must debate the application of model- and data-driven approaches to detecting phenology. Model driven approaches are commonly used to detect phenology from satellite images (Broich et al., 2014; Melaas et al., 2018; Pastor-Guzman et al., 2018), but these approaches oversimplify the apparent phenology of vegetation. Studies have compared the performance and suitability of model-driven methods for phenology investigations (Atkinson et al., 2012; Hird and McDermid, 2009), and data-driven methods have been largely ignored. In this thesis I challenge the *status quo* and demonstrate that data-driven approaches are well suited for detecting phenology using satellite imagery. The importance of this demonstration is that future work can use data-driven methods not only to detect phenology, but to forecast it. Forecasting phenology under different climate change scenarios is important for estimating carbon stocks and budgets in the near and distant futures. Moreover, GAMs allow the identification of the contribution of each explanatory variable and its importance in the prediction of phenology (e.g. the influence of rainfall or temperature).

6.2.2 Analytical implications

The main analytical implication arising from this thesis is that GAMs can be used on gridded datasets. In other words, we can generate an individual, data-driven model for each pixel in a time series of satellite images, without the need to aggregate the data spatially or temporally. This itself is not new; the novelty is that GAMs allow each model of phenology (i.e. pixel) to have its own set of explanatory variables. These variables can be independent from each other, or they can interact with each other to present a more coherent phenology-climate change connection (Kennedy et al., 2014; Morisette et al., 2009). This is useful especially when considering continuous variables such as temperature or rainfall, and discrete variables such as land use. While neighbouring pixels might have explanatory variables with similar values, subtle changes in these variables could trigger changes in phenology. For example, we could use time series of mangrove EVI, precipitation, and temperature to: 1) detect phenology, 2) examine the influence of precipitation and temperature on phenology for every pixel in the study site, and 3) forecast phenology. To date, most studies that have modelled apparent

phenology from satellite imagery have modelled explanatory variables separately from the imagery (Melaas et al., 2018; Pastor-Guzman et al., 2018). In contrast, GAMs perform these three operations in a single step, and for every pixel, thereby removing the need to model the influence of the predictor variables as a separate operation. By modelling each pixel independently, studies could gain a deeper understanding of the drivers of mangrove phenology and their importance in the apparent phenology at a resolution never attempted before.

Future work on phenology must also consider the advantages and disadvantages of using GAMs versus other modelling methods. Some advantages of GAMs over model driven approaches, are that they do not depend on an accurate description of the process (i.e. minimal number of assumptions made), and that the process itself does not need to be known to create a model (i.e. phenology of mangrove forests). Model driven approaches do need accurate descriptions of the process (i.e. several assumptions are made), and, if the process is unknown, it is difficult to represent. GAMs, however, do have some drawbacks when compared to model driven methods. For example, GAMs are computationally intensive, take longer to fit a model, and may require large training datasets, whereas model driven methods are fast and simple to interpret. High performance computing environments such as Digital Earth Australia and Google Earth Engine, take advantage of parallelization packages (e.g. Dask Development Team (2016)) that distribute the computations over the total number of processing nodes in the environment. As a result, GAMs can be applied to many pixels at once, rather than one at a time, thereby optimizing the resources and reducing the overall time required to model phenology over large areas.

Finally, GAMs allow users to forecast phenology. There are over 30 years of satellite images of mangrove forests, temperature, rainfall, and other biophysical data from land and spaceborne sensors. These data, along with predictions of future climate conditions could be included in the GAMs as explanatory variables and help researchers forecast mangrove phenology. Forecasting phenology is important for several reasons, including its link to carbon stocks (Morisette et al., 2009), and the uncertainty of the impacts of climate change in tropical regions of Australia (Turton, 2017). Forecasting phenology can help us understand the effects of rising

temperatures, increased atmospheric moisture, and erratic rainfall patters in vegetation communities, and consequently, in human populations that live in coastal environments.

6.2.3 Implications for field work and long-term monitoring

My experience doing this research has shown that there are few, long-term (>1.5 years) field studies on mangrove forests throughout Australia, and each study collects data in a slightly different way, hence comparing studies becomes a complicated task. In addition, there are no long-term sites for constant monitoring of mangroves and their phenology. This hampers the ability to validate satellite-derived phenology investigations in these ecosystems. As a result, there are two main recommendations for field work arising from this research. Firstly, standardising phenological field data collection is imperative. Specifically, the variables to be collected (e.g. leaf growth, net leaf production, leaf area index), the frequency of observations (e.g. monthly), the number of trees per species, and the number of replicate plots. Ancillary data (e.g. temperature, humidity), are also key for phenology investigations in the field, and from satellite imagery.

Secondly, establishing long-term field monitoring site(s) in mangrove forests will help us understand the link between mangrove phenology, biogeochemical cycles, and the effects of cyclones, rising sea level, and heatwaves on mangrove forests. These sites, in conjunction with satellite imagery would allow researchers to measure the effects of extreme weather events, climate forcing, and anthropogenic pressures on mangroves ecosystems.

6.3 Directions for future work

In this thesis I focused on detecting the phenology of mangrove forests from a time series of satellite images, using sites located in Queensland and the Northern Territory of Australia. The work presented in this document does not end here, and some work is still ongoing. While beyond the scope of this thesis, I am continuing to examine the influence of temperature, rainfall, and other biophysical variables on the phenology of mangroves. Ideally, the next step would be to use GAMs, all available Landsat imagery, and Digital Earth Australia to create a phenology product for mangrove ecosystems. This product would complement the one

created by Broich et al. (2015), by presenting a longer view of phenology at a finer spatial resolution, and be specific to mangrove forests. Beyond this, I present four key questions related to phenology that can help guide future work:

1. Can we integrate optical, radar, and LiDAR information to better understand mangrove phenology? Given that the Sentinel 1 (European Space Agency) and GEDI (NASA) sensors are currently operating and will collect data over several years, these three datasets could be integrated to provide a comprehensive view of mangrove growth, structure, and phenology.
2. I have demonstrated that apparent phenology is correlated to net leaf production, leaf growth, and leaf fall. These variables are key in carbon sequestration models. This raises the question: can we improve current models of carbon sequestration by using the phenological cycles of mangroves?
3. Species identification using 30m resolution imagery is a complicated task at the best of times. Can we use pixel-wise phenology in combination with harmonized Landsat and Sentinel 2 data to aid in species identification in mangrove forests?
4. Can we use the phenology as an indicator of stress for mangrove ecosystems? Similar to seagrass dieback and coral bleaching, mangroves suffer from massive dieback events. Establishing when and where these lethal (i.e. dieback) and sub-lethal (e.g. stress due to drought) events happen, are key to understanding the conditions leading to them. Spatiotemporal changes in phenology may be used as early indicators of stress due to alterations in their environmental conditions.

7 References

Abdul Aziz, A., Phinn, S., Dargusch, P., Omar, H., Arjasakusuma, S., 2015. Assessing the potential applications of Landsat image archive in the ecological monitoring and management of a production mangrove forest in Malaysia. Wetl. Ecol. Manag. 23, 1049–1066. doi:10.1007/s11273-015-9443-1

Abrams, M., Tsu, H., Hulley, G., Iwao, K., Pieri, D., Cudahy, T., Kargel, J., 2015. The Advanced Spaceborne Thermal Emission and Reflection Radiometer (ASTER) after fifteen years: Review of global products. Int. J. Appl. Earth Obs. Geoinf. 38, 292–301. doi:http://dx.doi.org/10.1016/j.jag.2015.01.013

Adam, E., Mutanga, O., Rugege, D., 2010. Multispectral and hyperspectral remote sensing for identification and mapping of wetland vegetation: A review. Wetl. Ecol. Manag. 18, 281–296. doi:10.1007/s11273-009-9169-z

Adame, M.F., Lovelock, C.E., 2011. Carbon and nutrient exchange of mangrove forests with the coastal ocean. Hydrobiologia 663, 23–50. doi:10.1007/s10750-010-0554-7

Akumu, C.E., Pathirana, S., Baban, S., Bucher, D., 2010a. Modeling Methane Emission from Wetlands in North-Eastern New South Wales, Australia Using Landsat ETM+. Remote Sens. 2, 1378.

Akumu, C.E., Pathirana, S., Baban, S., Bucher, D., 2010b. Monitoring coastal wetland communities in north-eastern NSW using ASTER and Landsat satellite data. Wetl. Ecol. Manag. 18, 357–365. doi:10.1007/s11273-010-9176-0

Alatorre, L.C., Sánchez-Andrés, R., Cirujano, S., Beguería, S., Sánchez-Carrillo, S., 2011. Identification of Mangrove Areas by Remote Sensing: The ROC Curve Technique Applied to the Northwestern Mexico Coastal Zone Using Landsat Imagery. Remote Sens. 3. doi:10.3390/rs3081568

Alongi, D.M., 2008. Mangrove forests: Resilience, protection from tsunamis, and responses to global climate change. Estuar. Coast. Shelf Sci. 76, 1–13. doi:10.1016/j.ecss.2007.08.024

Annette, M., Menzel, A., 2002. Phenology: Its Importance To the Global Change Community. Clim. Change 54, 379–385. doi:10.1023/A:1016125215496

Asbridge, E., Lucas, R., Accad, A., Dowling, R., 2015. Mangrove response to environmental changes predicted under varying climates: Case studies from Australia. Curr. For. Reports 1, 178–194. doi:10.1007/s40725-015-0018-4

Asbridge, E., Lucas, R., Rogers, K., Accad, A., 2018. The extent of mangrove change and potential for recovery following severe Tropical Cyclone Yasi, Hinchinbrook Island, Queensland, Australia. Ecol. Evol. 8, 10416–10434. doi:10.1002/ece3.4485

Asbridge, E., Lucas, R., Ticehurst, C., Bunting, P., 2016. Mangrove response to environmental change in Australia's Gulf of Carpentaria. Ecol. Evol. 6, 3523–3539. doi:10.1002/ece3.2140

Atkinson, P.M., Jeganathan, C., Dash, J., Atzberger, C., 2012. Inter-comparison of four models for smoothing satellite sensor time-series data to estimate vegetation phenology. Remote Sens. Environ. 123, 400–417. doi:10.1016/j.rse.2012.04.001

Ayer, V.M., Miguez, S., Toby, B.H., 2014. Why scientists should learn to program in Python - [WWW Document]. Powder Diffr. doi:DOI: 10.1017/S0885715614000931

Aziz, A.A., Phinn, S., Dargusch, P., 2015. Investigating the decline of ecosystem services in a production mangrove forest using Landsat and object-based image analysis. Estuar. Coast. SHELF Sci. 164, 353–366. doi:10.1016/j.ecss.2015.07.047

Baghdadi, N., Oliveros, C., 2007. Potential of ASAR/Envisat Data for Mud Bank Monitoring in French Guiana Compared to ASTER Imagery. J. Coast. Res. 23, 1509–1517. doi:10.2112/05-0477.1

Barbier, E.B., 2015. The protective service of mangrove ecosystems: A review of valuation methods. Marine Pollution Bulletin special issue: "Turning the tide on mangrove loss." Mar. Pollut. Bull. 109, 676–681. doi:10.1016/j.marpolbul.2016.01.033

Barrett, D., Frazier, A., 2016. Automated Method for Monitoring Water Quality Using Landsat Imagery. Water 8, 257.

Barsi, A.J., Lee, K., Kvaran, G., Markham, L.B., Pedelty, A.J., 2014. The Spectral Response of the Landsat-8 Operational Land Imager. Remote Sens. doi:10.3390/rs61010232

Béland, M., Goïta, K., Bonn, F., Pham, T.T.H., 2006. Assessment of land-cover changes related to shrimp aquaculture using remote sensing data: a case study in the Giao Thuy District,

Vietnam. Int. J. Remote Sens. 27, 1491–1510. doi:10.1080/01431160500406888

Bhattarai, B., Giri, C., 2011. Assessment of mangrove forests in the Pacific region using Landsat imagery. J. Appl. Remote Sens. 5. doi:10.1117/1.3563584

Bishop-Taylor, R., Sagar, S., Lymburner, L., Beaman, R.J., 2019. Between the tides: Modelling the elevation of Australia's exposed intertidal zone at continental scale. Estuar. Coast. Shelf Sci. doi:https://doi.org/10.1016/j.ecss.2019.03.006

Boegh, E., Soegaard, H., Broge, N., Hasager, C.B., Jensen, N.O., Schelde, K., Thomsen, A., 2002. Airborne multispectral data for quantifying leaf area index, nitrogen concentration, and photosynthetic efficiency in agriculture. Remote Sens. Environ. 81, 179–193. doi:http://dx.doi.org/10.1016/S0034-4257(01)00342-X

Bolton, D.K., Gray, J.M., Melaas, E.K., Moon, M., Eklundh, L., Friedl, M.A., 2020. Continental-scale land surface phenology from harmonized Landsat 8 and Sentinel-2 imagery. Remote Sens. Environ. 240, 111685. doi:https://doi.org/10.1016/j.rse.2020.111685

Box, G.E.P., 1979. Robustness in the strategy of scientific model building, in: Robustness in Statistics. Academic Press, pp. 201–236.

Box, G.E.P., 1976. Science and Statistics. J. Am. Stat. Assoc. 71, 791–799. doi:10.1080/01621459.1976.10480949

Braaten, J.D., Cohen, W.B., Yang, Z., 2015. Automated cloud and cloud shadow identification in Landsat MSS imagery for temperate ecosystems. Remote Sens. Environ. 169, 128–138. doi:10.1016/j.rse.2015.08.006

Broich, M., Huete, A., Paget, M., Ma, X., Tulbure, M., Coupe, N.R., Evans, B., Beringer, J., Devadas, R., Davies, K., Held, A., 2015. A spatially explicit land surface phenology data product for science, monitoring and natural resources management applications. Environ. Model. Softw. 64, 191–204. doi:https://doi.org/10.1016/j.envsoft.2014.11.017

Broich, M., Huete, A., Tulbure, M.G., Ma, X., Xin, Q., Paget, M., Restrepo-Coupe, N., Davies, K., Devadas, R., Held, A., 2014. Land surface phenological response to decadal climate variability across Australia using satellite remote sensing. Biogeosciences 11, 5181–5198. doi:10.5194/bg-11-5181-2014

Bunting, P., Rosenqvist, A., Lucas, M.R., Rebelo, L.-M., Hilarides, L., Thomas, N., Hardy, A., Itoh, T., Shimada, M., Finlayson, M.C., 2018. The Global Mangrove Watch—A New 2010 Global Baseline of Mangrove Extent. Remote Sens. . doi:10.3390/rs10101669

Camacho-De Coca, F., Garcia-Haro, F.J., Gilabert, M.A., Melia, J., 2004. Vegetation cover seasonal changes assessment from TM imagery in a semi-arid landscape. Int. J. Remote Sens. 25, 3451–3476. doi:10.1080/01431160310001618761

Candra, D.S., Phinn, S., Scarth, P., 2020. Cloud and cloud shadow masking for Sentinel-2 using multitemporal images in global area. Int. J. Remote Sens. 41, 2877–2904. doi:10.1080/01431161.2019.1697006

Carlson, T.C., Ripley, D. a., 1997. On the relationship between NDVI, fractional vegetation cover, and leaf area index. Remote Sens. Environ. 62, 241–252. doi:10.1016/S0034-4257(97)00104-1

Cerdeira, M.L.P., Katharine, A., Irene, M., 2018. Rethinking tropical phenology: insights from long-term monitoring and novel analytical methods. Biotropica 50, 371–373. doi:10.1111/btp.12562

Chambers, L.E., Altwegg, R., Barbraud, C., Barnard, P., Beaumont, L.J., Crawford, R.J.M.M., Durant, J.M., Hughes, L., Keatley, M.R., Low, M., Morellato, P.C., Poloczanska, E.S., Ruoppolo, V., Vanstreels, R.E.T.T., Woehler, E.J., Wolfaardt, A.C., 2013. Phenological Changes in the Southern Hemisphere. PLoS One 8, e75514. doi:10.1371/journal.pone.0075514

Chen, C.C.C.C., Son, N.N., Chang, N.N., Chen, C.C.C.C., Chang, L.-Y., Valdez, M., Centeno, G., Thompson, C.A., Aceituno, J.L., 2013. Multi-Decadal Mangrove Forest Change Detection and Prediction in Honduras, Central America, with Landsat Imagery and a Markov Chain Model. Remote Sens. 5, 6408–6426. doi:10.3390/rs5126408

Chen, J., Yi, S., Qin, Y., Wang, X., 2016. Improving estimates of fractional vegetation cover based on UAV in alpine grassland on the Qinghai-Tibetan Plateau. Int. J. Remote Sens. 37, 1922–1936. doi:10.1080/01431161.2016.1165884

Chen, J.M., 1999. Spatial Scaling of a Remotely Sensed Surface Parameter by Contexture. Remote Sens. Environ. 69, 30–42. doi:10.1016/S0034-4257(99)00006-1

Chuvieco, E., Huete, A., 2010. Fundamentals of satellite remote sensing. CRC Press, Boca Raton FLA.

Claverie, M., Ju, J., Masek, J.G., Dungan, J.L., Vermote, E.F., Roger, J.-C., Skakun, S. V, Justice, C., 2018. The Harmonized Landsat and Sentinel-2 surface reflectance data set. Remote Sens. Environ. 219, 145–161. doi:https://doi.org/10.1016/j.rse.2018.09.002

Coldren, G.A., Barreto, C.R., Wykoff, D.D., Morrissey, E.M., Langley, J.A., Feller, I.C., Chapman, S.K., 2016. Chronic warming stimulates growth of marsh grasses more than mangroves in a coastal wetland ecotone. Ecology 97, 3167–3175. doi:10.1002/ecy.1539

Coldren, G.A., Langley, J.A., Feller, I.C., Chapman, S.K., 2018. Warming accelerates mangrove expansion and surface elevation gain in a subtropical wetland. J. Ecol. 0. doi:10.1111/1365-2745.13049

Comber, A., Wulder, M., 2019. Considering spatiotemporal processes in big data analysis: Insights from remote sensing of land cover and land use. Trans. GIS 0. doi:10.1111/tgis.12559

Cornejo, R.H., Koedam, N., Luna, A.R., Troell, M., Dahdouh-Guebas, F., 2005. Remote sensing and ethnobotanical assessment of the mangrove forest changes in the Navachiste-San Ignacio-Macapule Lagoon Complex, Sinaloa, Mexico. Ecol. Soc. 10, 16. doi:10.5751/ES-01286-100116

Costanza, R., Groot, de R.S., Sutton, P., Ploeg, van der S., Anderson, S.J., Kubiszewski, I., Farber, S., Turner, R.K., 2014. Changes in the global value of ecosystem services. Glob. Environ. Change 26, 152–158. doi:10.1016/j.gloenvcha.2014.04.002

Coulston, J.W., Moisen, G.G., Wilson, B.T., Finco, M. V, Cohen, W.B., Brewer, C.K., 2012. Modeling percent tree canopy cover: A pilot study. Photogramm. Eng. Remote Sensing 78, 715–727.

Coupland, G.T., Paling, E.I., McGuinness, K.A., 2006. Floral abortion and pollination in four species of tropical mangroves from northern Australia. Aquat. Bot. 84, 151–157. doi:10.1016/j.aquabot.2005.09.003

Coupland, G.T., Paling, E.I., McGuinness, K.A., 2005. Vegetative and reproductive phenologies of four mangrove species from northern Australia. Aust. J. Bot. 53, 109–117. doi:10.1071/BT04066

Cresswell, I.D., Semeniuk, V., 2011. Mangroves of the Kimberley coast: Ecological patterns in a tropical Ria coast setting. J. R. Soc. West. Aust. 94, 213–237.

Cribari-Neto, F., Zeileis, A., 2010. Beta regression in R. J. Stat. Softw.

Czernecki, B., Nowosad, J., Jabłońska, K., 2018. Machine learning modeling of plant phenology based on coupling satellite and gridded meteorological dataset. Int. J. Biometeorol. 62, 1297–1309. doi:10.1007/s00484-018-1534-2

Danielsen, F., Sørensen, M.K., Olwig, M.F., Selvam, V., Parish, F., Burgess, N.D., Hiraishi, T., Karunagaran, V.M., Rasmussen, M.S., Hansen, L.B., Quarto, A., Suryadiputra, N., 2005. The Asian Tsunami: A Protective Role for Coastal Vegetation. Science (80-.). 310, 643. doi:10.1126/science.1118387

Dask Development Team, 2016. Dask: Library for dynamic task scheduling.

Dawson, T.P., Curran, P.J., Plummer, S.E., 1998. LIBERTY—Modeling the Effects of Leaf Biochemical Concentration on Reflectance Spectra. Remote Sens. Environ. 65, 50–60. doi:http://dx.doi.org/10.1016/S0034-4257(98)00007-8

Dhu, T., Dunn, B., Lewis, B., Lymburner, L., Mueller, N., Telfer, E., Lewis, A., McIntyre, A., Minchin, S., Phillips, C., 2017. Digital earth Australia – unlocking new value from earth observation data. Big Earth Data 1, 64–74. doi:10.1080/20964471.2017.1402490

Ding, Y., Zhang, H., Zhao, K., Zheng, X., 2017. Investigating the accuracy of vegetation index-based models for estimating the fractional vegetation cover and the effects of varying soil backgrounds using in situ measurements and the PROSAIL model. Int. J. Remote Sens. 38, 4206–4223. doi:10.1080/01431161.2017.1312617

Donato, D.C., Kauffman, J.B., Murdiyarso, D., Kurnianto, S., Stidham, M., Kanninen, M., 2011. Mangroves among the most carbon-rich forests in the tropics. Nat. Geosci. 4, 293–297. doi:10.1038/ngeo1123

Duarte, C.M., Losada, I.J., Hendriks, I.E., Mazarrasa, I., Marbà, N., 2013. The role of coastal plant communities for climate change mitigation and adaptation. Nat. Clim. Chang. 3, 961–968. doi:10.1038/nclimate1970

Duke, N.C., 2002a. Sustained high levels of foliar herbivory of the mangrove Rhizophora stylosa

by a moth larva Doratifera stenosa (Limacodidae) in north-eastern Australia. Wetl. Ecol. Manag. 10, 403–419.

Duke, N.C., 2002b. Sustained high levels of foliar herbivory of the mangrove Rhizophora stylosa by a moth larva Doratifera stenosa (Limacodidae) in north-eastern Australia. Wetl. Ecol. Manag. 10, 403–419. doi:10.1007/BF03263357

Duke, N.C., 2001. Mangrove phenologies and the factors influencing them in the Australasian region, in: de Lacerda, L.D. (Ed.), Mangrove Ecosystems: Function and Management. Springer-Verlag, Berlin, pp. 217–233.

Duke, N.C., 1990a. Phenological Trends with Latitude in the Mangrove Tree Avicennia Marina. J. Ecol. 78, 113–133. doi:10.2307/2261040

Duke, N.C., 1990b. Phenological Trends with Latitude in the Mangrove Tree Avicennia Marina. J. Ecol. 78, 113. doi:10.2307/2261040

Duke, N.C., 1988. Phenologies and Litter Fall of Two Mangrove Trees, Sonneratia alba Sm. And S. caseolaris (L.) Engl., And Their Putative Hybrid, S. × Gulngai N.C. Duke. Aust. J. Bot. 36, 473–482.

Duke, N.C., Bunt, J.S., Williams, W.T., 1984a. Observations on the Floral and Vegetative Phenologies of North-Eastern Australian Mangroves. Aust. J. Bot. 32, 87–99.

Duke, N.C., Bunt, J.S., Williams, W.T., 1984b. Observations on the floral and vegetative phenologies of north- eastern Australian mangroves. Aust. J. Bot. 32, 87–99.

Duke, N.C., Burns, K.A., Swannell, R.P.J., 1999. Research into the Bioremediation of Oil Spills in Tropical Australia: with particular emphasis on oiled mangrove and salt marsh habitat, Sources, Fates and Consequences of Pollutants in the Great Barrier Reef and Torres Strait.

Duke, N.C., Kleine, D., University of, Q., 2006. Australia's mangroves: the authoritative guide to Australia's mangrove plants. University of Queensland, Brisbane.

Duke, N.C., Meynecke, J.O., Dittmann, S., Ellison, A.M., Anger, K., Berger, U., Cannicci, S., Diele, K., Ewel, K.C., Field, C.D., Koedam, N., Lee, S.Y., Marchand, C., Nordhaus, I., Dahdouh-Guebas, F., 2007. A World without Mangroves? Science (80-.). 317, 41–42. doi:10.1126/science.317.5834.41b

Duncan, C., Primavera, J.H., Pettorelli, N., Thompson, J.R., Loma, R.J.A., Koldewey, H.J., 2016. Rehabilitating mangrove ecosystem services: A case study on the relative benefits of abandoned pond reversion from Panay Island, Philippines. Mar. Pollut. Bull. 109, 772–782. doi:10.1016/j.marpolbul.2016.05.049

Dutta, D., Das, P.K., Paul, S., Sharma, J.R., Dadhwal, V.K., 2015. Assessment of ecological disturbance in the mangrove forest of Sundarbans caused by cyclones using MODIS time-series data (2001–2011). Nat. Hazards 79, 775–790. doi:10.1007/s11069-015-1872-x

Dwyer, J.L., Roy, D.P., Sauer, B., Jenkerson, C.B., Zhang, H.K., Lymburner, L., 2018. Analysis Ready Data: Enabling Analysis of the Landsat Archive. Remote Sens. 10. doi:http://dx.doi.org/10.3390/rs10091363

Emch, M., Peterson, M., 2006. Mangrove Forest Cover Change in the Bangladesh Sundarbans from 1989-2000: A Remote Sensing Approach. Geocarto Int. 21, 5–12. doi:10.1080/10106040608542368

Ernst, S., Lymburner, L., Sixsmith, J., 2018. Implications of Pixel Quality Flags on the Observation Density of a Continental Landsat Archive. Remote Sens. doi:10.3390/rs10101570

Eskelson, B.N.I., Madsen, L., Hagar, J.C., Temesgen, H., 2011. Estimating riparian understory vegetation cover with beta regression and copula models. For. Sci. 57, 212–221.

Eslami-Andargoli, L., Dale, P.E.R., Sipe, N., Chaseling, J., 2010. Local and landscape effects on spatial patterns of mangrove forest during wetter and drier periods: Moreton Bay, Southeast Queensland, Australia. Estuar. Coast. Shelf Sci. 89, 53–61. doi:10.1016/j.ecss.2010.05.011

Eslami-Andargoli, L., Dale, P.A.T., Sipe, N., 2013. Does spatial scale affect the pattern of mangrove change under different rainfall regimes? An example in southeast Queensland, Australia. Austral Ecol. 38, 208–218. doi:10.1111/j.1442-9993.2012.02393.x

Fang, S., Tang, W., Peng, Y., Gong, Y., Dai, C., Chai, R., Liu, K., 2016. Remote Estimation of Vegetation Fraction and Flower Fraction in Oilseed Rape with Unmanned Aerial Vehicle Data. Remote Sens. 8. doi:10.3390/rs8050416

FAO, 2007. The world's mangroves 1980-2005. Food and Agriculture Organization, Rome, Italy.

Ferrari, S.L.P., Cribari-Neto, F., 2004. Beta regression for modelling rates and proportions. J. Appl. Stat. 31, 799–815. doi:10.1080/0266476042000214501

Ferreira, M.A., Andrade, F., Bandeira, S.O., Cardoso, P., Mendes, R.N., Paula, J., 2009. Analysis of cover change (1995-2005) of Tanzania/Mozambique trans-boundary mangroves using Landsat imagery. Aquat. Conserv. Mar. Freshw. Ecosyst. 19, S38–S45. doi:10.1002/aqc.1042

Field, C.B., Barros, V.R., Dokken, D.J., Mach, K.J., Mastrandrea, M.D., Bilir, T.E., Chatterjee, M., Ebi, K.L., Estrada, Y.O., Genova, R.C., Girma, B., Kissel, E.S., Levy, A.N., MacCracken, S., Mastrandrea, P.R., White, L., 2014. IPCC, 2014a: Climate Change 2014: Impacts, Adaptation, and Vulnerability. Part A: Global and Sectoral Aspects. Cambridge University Press, Cambridge.

Fisher, J.I., Mustard, J.F., Vadeboncoeur, M.A., 2006. Green leaf phenology at Landsat resolution: Scaling from the field to the satellite. Remote Sens. Environ. 100, 265–279. doi:https://doi.org/10.1016/j.rse.2005.10.022

França, M.C., Francisquini, M.I., Cohen, M.C.L., Pessenda, L.C.R., Rossetti, D.F., Guimarães, J.T.F., Smith, C.B., 2012. The last mangroves of Marajó Island - Eastern Amazon: Impact of climate and/or relative sea-level changes. Rev. Palaeobot. Palynol. 187, 50–65. doi:10.1016/j.revpalbo.2012.08.007

Frantz, D., Roder, A., Udelhoven, T., Schmidt, M., 2015. Enhancing the Detectability of Clouds and Their Shadows in Multitemporal Dryland Landsat Imagery: Extending Fmask. IEEE Geosci. Remote Sens. Lett. 12, 1242–1246. doi:10.1109/LGRS.2015.2390673

Friess, D.A., Rogers, K., Lovelock, C.E., Krauss, K.W., Hamilton, S.E., Lee, S.Y., Lucas, R., Primavera, J., Rajkaran, A., Shi, S., 2019. The State of the World's Mangrove Forests: Past, Present, and Future. Annu. Rev. Environ. Resour. 44, 89–115. doi:10.1146/annurev-environ-101718-033302

Fu, Y., Zhang, H., Dong, W., Yuan, W., 2014a. Comparison of Phenology Models for Predicting the Onset of Growing Season over the Northern Hemisphere. PLoS One 9, e109544. doi:10.1371/journal.pone.0109544

Fu, Y., Zhang, H., Dong, W., Yuan, W., 2014b. Comparison of Phenology Models for Predicting

the Onset of Growing Season over the Northern Hemisphere 9. doi:10.1371/journal.pone.0109544

Gao, J., 1999. A comparative study on spatial and spectral resolutions of satellite data in mapping mangrove forests. Int. J. Remote Sens. 20, 2823–2833. doi:10.1080/014311699211813

Garonna, I., de Jong, R., Schaepman, M.E., 2016. Variability and evolution of global land surface phenology over the past three decades (1982-2012). Glob. Chang. Biol. 22, 1456–1468. doi:10.1111/gcb.13168

Gill, T., Johansen, K., Phinn, S., Trevithick, R., Scarth, P., Armston, J., 2017. A method for mapping Australian woody vegetation cover by linking continental-scale field data and long-term Landsat time series. Int. J. Remote Sens. 38, 679–705. doi:10.1080/01431161.2016.1266112

Gilman, E.L., Ellison, J., Duke, N.C., Field, C., 2008. Threats to mangroves from climate change and adaptation options: A review. Aquat. Bot. 89, 237–250. doi:10.1016/j.aquabot.2007.12.009

Giri, C., 2016. Observation and Monitoring of Mangrove Forests Using Remote Sensing: Opportunities and Challenges. Remote Sens. 8, 783.

Giri, C., Long, J., Abbas, S., Murali, R.M., Qamer, F.M., Pengra, B., Thau, D., 2015. Distribution and dynamics of mangrove forests of South Asia. J. Environ. Manage. 148, 101–111. doi:http://dx.doi.org/10.1016/j.jenvman.2014.01.020

Giri, Chandra, Long, J., Tieszen, L., 2011a. Mapping and Monitoring Louisiana's Mangroves in the Aftermath of the 2010 Gulf of Mexico Oil Spill. J. Coast. Res. 27, 1059–1064.

Giri, C., Muhlhausen, J., 2008. Mangrove forest distributions and dynamics in Madagascar (1975-2005). Sensors 8, 2104–2117. doi:10.3390/s8042104

Giri, C., Ochieng, E., Tieszen, L.L., Zhu, Z., Singh, A., Loveland, T., Masek, J., Duke, N.C., 2013a. Global Mangrove Forests Distribution, 2000 (Dataset). doi:http://dx.doi.org/10.7927/H4J67DW8

Giri, Chandra, Ochieng, E., Tieszen, L.L., Zhu, Z., Singh, A., Loveland, T., Masek, J., Duke, N.C.,

2011b. Status and distribution of mangrove forests of the world using earth observation satellite data. Glob. Ecol. Biogeogr. 20, 154–159. doi:10.1111/j.1466-8238.2010.00584.x

Giri, C., Ochieng, E., Tieszen, L.L., Zhu, Z., Singh, A., Loveland, T., Masek, J., Duke, N.C., 2011. Status and distribution of mangrove forests of the world using earth observation satellite data. Glob. Ecol. Biogeogr. 20, 154–159. doi:10.1111/j.1466-8238.2010.00584.x

Giri, C., Pengra, B., Long, J., Loveland, T.R., 2013b. Next generation of global land cover characterization, mapping, and monitoring. Int. J. Appl. Earth Obs. Geoinf. 25, 30–37. doi:http://dx.doi.org/10.1016/j.jag.2013.03.005

Giri, C., Pengra, B., Zhu, Z., Singh, A., Tieszen, L.L., 2007. Monitoring mangrove forest dynamics of the Sundarbans in Bangladesh and India using multi-temporal satellite data from 1973 to 2000. Estuar. Coast. Shelf Sci. 73, 91–100. doi:10.1016/j.ecss.2006.12.019

Gitelson, A.A., Kaufman, Y.J., Stark, R., Rundquist, D., 2002. Novel algorithms for remote estimation of vegetation fraction. Remote Sens. Environ. 80, 76–87. doi:10.1016/S0034-4257(01)00289-9

Goodwin, N.R., Collett, L.J., Denham, R.J., Flood, N., Tindall, D., 2013. Cloud and cloud shadow screening across Queensland, Australia: An automated method for Landsat TM/ETM+ time series. Remote Sens. Environ. 134, 50–65. doi:10.1016/j.rse.2013.02.019

Google, 2015. Google Earth Engine: A planetary-scale geospatial analysis platform [WWW Document]. URL https://earthengine.google.com

Gorelick, N., Hancher, M., Dixon, M., Ilyushchenko, S., Thau, D., Moore, R., 2017. Google Earth Engine: Planetary-scale geospatial analysis for everyone. Remote Sens. Environ. 202, 18–27. doi:https://doi.org/10.1016/j.rse.2017.06.031

Granell, C., Havlik, D., Schade, S., Sabeur, Z., Delaney, C., Pielorz, J., Usländer, T., Mazzetti, P., Schleidt, K., Kobernus, M., Havlik, F., Bodsberg, N.R., Berre, A., Mon, J.L., 2016. Future Internet technologies for environmental applications. Environ. Model. Softw. 78, 1–15. doi:http://dx.doi.org/10.1016/j.envsoft.2015.12.015

Griffiths, P., Nendel, C., Hostert, P., 2019. Intra-annual reflectance composites from Sentinel-2 and Landsat for national-scale crop and land cover mapping. Remote Sens. Environ. 220, 135–151. doi:https://doi.org/10.1016/j.rse.2018.10.031

Gutman, G., Ignatov, A., 1998. The derivation of the green vegetation fraction from NOAA/AVHRR data for use in numerical weather prediction models. Int. J. Remote Sens. 19, 1533–1543. doi:10.1080/014311698215333

Habshi, A. Al, Youssef, T., Aizpuru, M., Blasco, F., 2007. New mangrove ecosystem data along the UAE coast using remote sensing. Aquat. Ecosyst. Health Manag. 10, 309–319. doi:10.1080/14634980701512525

Hamilton, S.E., Casey, D., 2016. Creation of a high spatio-temporal resolution global database of continuous mangrove forest cover for the 21st century (CGMFC-21). Glob. Ecol. Biogeogr. 25, 729–738. doi:10.1111/geb.12449

Hansen, M.C., Loveland, T.R., 2012. A review of large area monitoring of land cover change using Landsat data. Remote Sens. Environ. 122, 66–74. doi:10.1016/j.rse.2011.08.024

Hansen, M.C., Potapov, P. V, Moore, R., Hancher, M., Turubanova, S.A., Tyukavina, A., Thau, D., Stehman, S. V, Goetz, S.J., Loveland, T.R., Kommareddy, A., Egorov, A., Chini, L., Justice, C.O., Townshend, J.R.G., 2013. High-Resolution Global Maps of 21st-Century Forest Cover Change. Science (80-.). 342, 850–853. doi:10.1126/science.1244693

Harper, G.J., Steininger, M.K., Tucker, C.J., Juhn, D., Hawkins, F., 2007. Fifty years of deforestation and forest fragmentation in Madagascar. Environ. Conserv. 34, 325–333. doi:10.1017/S0376892907004262

Hastie, T., Tibshirani, R., 1986. Generalized Additive Models. Stat. Sci. 1, 297–318.

Heenkenda, M.K., Joyce, K.E., Maier, S.W., Bartolo, R., 2014. Mangrove species identification: comparing WorldView-2 with aerial photographs.

Heenkenda, M.K., Maier, S.W., Bruin, de S., Joyce, K.E., 2015. Quantifying mangrove chlorophyll from high spatial resolution imagery. ISPRS J. Photogramm. Remote Sens. 108, 234–244. doi:10.1016/j.isprsjprs.2015.08.003

Hegerl, E.J., Davie, J.D.S., n.d. THE MANGROVE FORESTS OF CAIRNS, NORTHERN AUSTRALIA. Mar. Res. Indones. Vol 18 (1977)DO - 10.14203/mri.v18i0.360.

Helman, D., 2018. Land surface phenology: What do we really 'see' from space? Sci. Total Environ. 618, 665–673. doi:10.1016/j.scitotenv.2017.07.237

Heumann, B.W., 2011. Satellite remote sensing of mangrove forests: Recent advances and future opportunities. Prog. Phys. Geogr. 35, 87–108. doi:10.1177/0309133310385371

Hird, J.N., McDermid, G.J., 2009. Noise reduction of NDVI time series: An empirical comparison of selected techniques. Remote Sens. Environ. 113, 248–258. doi:10.1016/j.rse.2008.09.003

Hossain, M.S., Bujang, J.S., Zakaria, M.H., Hashim, M., 2016. Marine and human habitat mapping for the Coral Triangle Initiative region of Sabah using Landsat and Google Earth imagery. Mar. Policy 72, 176–191. doi:10.1016/j.marpol.2016.07.003

Hoyer, S., Hamman, J.J., 2017. xarray: N-D labeled Arrays and Datasets in Python. J. open Res. Softw. 5. doi:10.5334/jors.148

Huete, A., Didan, K., Miura, T., Rodriguez, E.., Gao, X., Ferreira, L.., 2002. Overview of the radiometric and biophysical performance of the MODIS vegetation indices. Remote Sens. Environ. 83, 195–213. doi:10.1016/S0034-4257(02)00096-2

Huete, A.R., 1988. A soil-adjusted vegetation index (SAVI). Remote Sens. Environ. 25, 295–309. doi:http://dx.doi.org/10.1016/0034-4257(88)90106-X

Hyndman, R.J., Athanasopoulos, G., 2018. Forecasting: Principles and Practice, 2nd ed. Otexts, Australia.

Ibharim, N.A., Mustapha, M.A., Lihan, T., Mazlan, A.G., 2015. Mapping mangrove changes in the Matang Mangrove Forest using multi temporal satellite imageries. Ocean Coast. Manag. 114, 64–76. doi:10.1016/j.ocecoaman.2015.06.005

Jafari, R., Lewis, M.M., Ostendorf, B., 2007. Evaluation of vegetation indices for assessing vegetation cover in southern arid lands in South Australia. Rangel. J. 29, 39–49. doi:10.1071/RJ06033

James, G.K., Adegoke, J.O., Saba, E., Nwilo, P., Akinyede, J., 2007. Satellite-Based Assessment of the Extent and Changes in the Mangrove Ecosystem of the Niger Delta. Mar. Geod. 30, 249–267. doi:10.1080/01490410701438224

JCU, 2016. Large-scale mangrove dieback "unprecedented" [WWW Document]. TropWATER - Trop. Water Aquat. Ecosyst. Res. URL https://research.jcu.edu.au/tropwater/news-and-

events/large-scale-mangrove-dieback-unprecedented

Jean-Baptiste, N., Jensen, J.R., 2006. Measurement of Mangrove Biophysical Characteristics in the Bocozelle Ecosystem in Haiti Using ASTER Multispectral Data. Geocarto Int. 21, 3–8. doi:10.1080/10106040608542397

Jelinski, D.E., Wu, J., 1996a. The modifiable areal unit problem and implications for landscape ecology. Landsc. Ecol. 11, 129–140. doi:10.1007/BF02447512

Jelinski, D.E., Wu, J., 1996b. The modifiable areal unit problem and implications for landscape ecology. Landsc. Ecol. 11, 129–140. doi:10.1007/BF02447512

Jenkins, R., Burton, A.M., 2008. 100% Accuracy in Automatic Face Recognition. Science (80-.). 319, 435. doi:10.1126/science.1149656

Jia, K., Liang, S., Liu, S., Li, Y., Xiao, Z., Yao, Y., Jiang, B., Zhao, X., Wang, X., Xu, S., Cui, J., 2015. Global Land Surface Fractional Vegetation Cover Estimation Using General Regression Neural Networks From MODIS Surface Reflectance. IEEE Trans. Geosci. Remote Sens. doi:10.1109/TGRS.2015.2409563

Jia, M., Wang, Z., Li, L., Song, K., Ren, C., Liu, B., Mao, D., 2014. Mapping China's mangroves based on an object-oriented classification of Landsat imagery. WETLANDS 34, 277–283. doi:10.1007/s13157-013-0449-2

Jiang, Z., Huete, A.R., Chen, J., Chen, Y., Li, J., Yan, G., Zhang, X., 2006. Analysis of NDVI and scaled difference vegetation index retrievals of vegetation fraction. Remote Sens. Environ. 101, 366–378. doi:10.1016/j.rse.2006.01.003

Jiang, Z., Huete, A.R., Didan, K., Miura, T., 2008. Development of a two-band enhanced vegetation index without a blue band. Remote Sens. Environ. 112, 3833–3845. doi:http://dx.doi.org/10.1016/j.rse.2008.06.006

Jones, K., Almond, S., 1992. Moving out of the Linear Rut: The Possibilities of Generalized Additive Models. Trans. Inst. Br. Geogr. 17, 434. doi:10.2307/622709

Jones, T., Glass, L., Gandhi, S., Ravaoarinorotsihoarana, L., Carro, A., Benson, L., Ratsimba, H., Giri, C., Randriamanatena, D., Cripps, G., 2016. Madagascar's Mangroves: Quantifying Nation-Wide and Ecosystem Specific Dynamics, and Detailed Contemporary Mapping of

Distinct Ecosystems. Remote Sens. 8, 106.

Jones, T.G., Ratsimba, H.R., Ravaoarinorotsihoarana, L., Glass, L., Benson, L., Teoh, M., Carro, A., Cripps, G., Giri, C., Gandhi, S., Andriamahenina, Z., Rakotomanana, R., Roy, P.-F., 2015. The Dynamics, Ecological Variability and Estimated Carbon Stocks of Mangroves in Mahajamba Bay, Madagascar. J. Mar. Sci. Eng. 3, 793–820. doi:10.3390/jmse3030793

Jong, S.M. de, Van der Meer, F., 2001. Imaging spectrometry: basic principles and prospective applications .

Joppa, L.N., McInerny, G., Harper, R., Salido, L., Takeda, K., O'Hara, K., Gavaghan, D., Emmott, S., 2013. Troubling Trends in Scientific Software Use. Science (80-.). 340, 814–815. doi:10.1126/science.1231535

Jupiter, S.D., Potts, D.C., Phinn, S.R., Duke, N.C., 2007. Natural and anthropogenic changes to mangrove distributions in the Pioneer River Estuary (QLD, Australia). Wetl. Ecol. Manag. 15, 51–62. doi:10.1007/s11273-006-9011-9

Kainuma, M., Spalding, M., Collins, L., 2010. World Atlas of Mangroves. Earthscan, London.

Kamal, M., Phinn, S., 2011. Hyperspectral data for mangrove species mapping: A comparison of pixel-based and object-based approach. Remote Sens. 3, 2222–2242. doi:10.3390/rs3102222

Kamal, M., Phinn, S., Johansen, K., 2015. Object-Based Approach for Multi-Scale Mangrove Composition Mapping Using Multi-Resolution Image Datasets. Remote Sens. 7, 4753. doi:10.3390/rs70404753

Kanniah, K., Sheikhi, A., Cracknell, A., Goh, H., Tan, K., Ho, C., Rasli, F., 2015. Satellite Images for Monitoring Mangrove Cover Changes in a Fast Growing Economic Region in Southern Peninsular Malaysia. Remote Sens. 7, 14360.

Karl, J.W., McCord, S.E., Hadley, B.C., 2017. A comparison of cover calculation techniques for relating point-intercept vegetation sampling to remote sensing imagery. Ecol. Indic. 73, 156–165. doi:10.1016/j.ecolind.2016.09.034

Kauffman, J.B., Adame, M.F., Arifanti, V.B., Schile-Beers, L.M., Bernardino, A.F., Bhomia, R.K., Donato, D.C., Feller, I.C., Ferreira, T.O., del Carmen Jesus Garcia, M., MacKenzie, R.A.,

Megonigal, J.P., Murdiyarso, D., Simpson, L., Hernández Trejo, H., Jesus Garcia, M. del C., MacKenzie, R.A., Megonigal, J.P., Murdiyarso, D., Simpson, L., Hernández Trejo, H., 2020. Total ecosystem carbon stocks of mangroves across broad global environmental and physical gradients. Ecol. Monogr. n/a. doi:10.1002/ecm.1405

Kennedy, R.E., Andréfouët, S., Cohen, W.B., Gómez, C., Griffiths, P., Hais, M., Healey, S.P., Helmer, E.H., Hostert, P., Lyons, M.B., Meigs, G.W., Pflugmacher, D., Phinn, S.R., Powell, S.L., Scarth, P., Sen, S., Schroeder, T.A., Schneider, A., Sonnenschein, R., Vogelmann, J.E., Wulder, M.A., Zhu, Z., 2014. Bringing an ecological view of change to Landsat-based remote sensing. Front. Ecol. Environ. doi:10.1890/130066

Kennedy, R.E., Yang, Z., Cohen, W.B., 2010. Detecting trends in forest disturbance and recovery using yearly Landsat time series: 1. LandTrendr — Temporal segmentation algorithms. Remote Sens. Environ. 114, 2897–2910. doi:10.1016/j.rse.2010.07.008

Kerr, Y.H., Huete, A.R., Qi, J., Sorooshian, S., Chehbouni, A., 2003. A modified soil adjusted vegetation index. Remote Sens. Environ. 48, 119–126. doi:10.1016/0034-4257(94)90134-1

Kirui, K.B., Kairo, J.G., Bosire, J., Viergever, K.M., Rudra, S., Huxham, M., Briers, R.A., 2013. Mapping of mangrove forest land cover change along the Kenya coastline using Landsat imagery. Ocean Coast. Manag. 83, 19–24. doi:10.1016/j.ocecoaman.2011.12.004

Koedsin, W., Vaiphasa, C., 2013. Discrimination of tropical mangroves at the species level with EO-1 hyperion data. Remote Sens. 5, 3562–3582. doi:10.3390/rs5073562

Korhonen, L., Ali-Sisto, D., Tokola, T., 2015. Tropical forest canopy cover estimation using satellite imagery and airborne lidar reference data. SILVA Fenn. 49. doi:10.14214/sf.1405

Korhonen, L., Korhonen, K.T., Stenberg, P., Maltamo, M., Rautiainen, M., 2007. Local models for forest canopy cover with beta regression. Silva Fenn. doi:10.14214/sf.275

Kovacs, J.M., Wang, J., Blanco-Correa, M., 2001. Mapping Disturbances in a Mangrove Forest Using Multi-Date Landsat TM Imagery. Environ. Manage. 27, 763–776. doi:10.1007/s002670010186

Kowalski, K., Senf, C., Hostert, P., Pflugmacher, D., 2020. Characterizing spring phenology of temperate broadleaf forests using Landsat and Sentinel-2 time series. Int. J. Appl. Earth

Obs. Geoinf. 92, 102172. doi:https://doi.org/10.1016/j.jag.2020.102172

Krause, G., Bock, M., Weiers, S., Braun, G., 2004. Mapping Land-Cover and Mangrove Structures with Remote Sensing Techniques: A Contribution to a Synoptic GIS in Support of Coastal Management in North Brazil. Environ. Manage. 34, 429–440. doi:10.1007/s00267-004-0003-3

Kuenzer, C., Bluemel, A., Gebhardt, S., Quoc, T.V., Dech, S., 2011. Remote Sensing of Mangrove Ecosystems: A Review. Remote Sens. 3, 878. doi:doi:10.3390/rs3050878

Kuenzer, C., Dech, S., Wagner, W., Land, R., Dynamics, S., 2015. Remote Sensing Time Series Revealing Land Surface Dynamics. Springer International Publishing, S.l. doi:10.1007/978-3-319-15967-6

Kuleli, T., Guneroglu, A., Karsli, F., Dihkan, M., 2011. Automatic detection of shoreline change on coastal Ramsar wetlands of Turkey. Ocean Eng. 38, 1141–1149. doi:http://dx.doi.org/10.1016/j.oceaneng.2011.05.006

Kumar, T.S., Mahendra, R.S., Nayak, S., Radhakrishnan, K., Sahu, K.C., 2012. Identification of hot spots and well managed areas of Pichavaram mangrove using Landsat TM and Resourcesat—1 LISS IV: an example of coastal resource conservation along Tamil Nadu Coast, India. J. Coast. Conserv. 16, 1–12. doi:10.1007/s11852-011-0162-3

Kutt, A.S., 1997. Terrestrial vertebrate survey in the coastal wetlands surrounding Cairns International Airport, North Queensland. Aust. Zool. 30, 300–309.

Lagomasino, D., Price, R.M., Whitman, D., Melesse, A., Oberbauer, S.F., 2015. Spatial and temporal variability in spectral-based surface energy evapotranspiration measured from Landsat 5TM across two mangrove ecotones. Agric. For. Meteorol. 213, 304–316. doi:10.1016/j.agrformet.2014.11.017

Lausch, A., Pause, M., Doktor, D., Preidl, S., Schulz, K., 2013. Monitoring and assessing of landscape heterogeneity at different scales. Environ. Monit. Assess. 185, 9419–9434. doi:10.1007/s10661-013-3262-8

Lee, J.S.H., Wich, S., Widayati, A., Koh, L.P., 2016. Detecting industrial oil palm plantations on Landsat images with Google Earth Engine. Remote Sens. Appl. Soc. Environ. 4, 219–224. doi:http://dx.doi.org/10.1016/j.rsase.2016.11.003

Lee, S.Y., Hamilton, S., Barbier, E.B., Primavera, J., Lewis, R.R., 2019. Better restoration policies are needed to conserve mangrove ecosystems. Nat. Ecol. Evol. doi:10.1038/s41559-019-0861-y

Lee, S.Y., Primavera, J.H., Dahdouh-Guebas, F., McKee, K., Bosire, J.O., Cannicci, S., Diele, K., Fromard, F., Koedam, N., Marchand, C., Mendelssohn, I., Mukherjee, N., Record, S., 2014. Ecological role and services of tropical mangrove ecosystems: a reassessment. Glob. Ecol. Biogeogr. 23, 726–743. doi:10.1111/geb.12155

Lee, T.-M., Yeh, H.-C., 2009. Applying remote sensing techniques to monitor shifting wetland vegetation: A case study of Danshui River estuary mangrove communities, Taiwan. Ecol. Eng. 35, 487–496. doi:10.1016/j.ecoleng.2008.01.007

Leprieur, C., Kerr, Y.H., Mastorchio, S., Meunier, J.C., 2000. Monitoring vegetation cover across semi-arid regions: Comparison of remote observations from various scales. Int. J. Remote Sens. 21, 281–300. doi:10.1080/014311600210830

Lewis, A., Lymburner, L., Purss, M.B.J., Brooke, B., Evans, B., Ip, A., Dekker, A.G., Irons, J.R., Minchin, S., Mueller, N., Oliver, S., Roberts, D., Ryan, B., Thankappan, M., Woodcock, R., Wyborn, L., 2016. Rapid, high-resolution detection of environmental change over continental scales from satellite data – the Earth Observation Data Cube. Int. J. Digit. Earth 9, 106–111. doi:10.1080/17538947.2015.1111952

Lewis, A., Oliver, S., Lymburner, L., Evans, B., Wyborn, L., Mueller, N., Raevksi, G., Hooke, J., Woodcock, R., Sixsmith, J., Wu, W., Tan, P., Li, F., Killough, B., Minchin, S., Roberts, D., Ayers, D., Bala, B., Dwyer, J., Dekker, A., Dhu, T., Hicks, A., Ip, A., Purss, M., Richards, C., Sagar, S., Trenham, C., Wang, P., Wang, L.-W., 2017. The Australian Geoscience Data Cube — Foundations and lessons learned. Remote Sens. Environ. 202, 276–292. doi:https://doi.org/10.1016/j.rse.2017.03.015

Lewis III, R.R., Milbrandt, E.C., Brown, B., Krauss, K.W., Rovai, A.S., Beever Iii, J.W., Flynn, L.L., 2016. Stress in mangrove forests: Early detection and preemptive rehabilitation are essential for future successful worldwide mangrove forest management. Mar. Pollut. Bull. 109, 764–771. doi:http://dx.doi.org/10.1016/j.marpolbul.2016.03.006

Li, F., Jupp, D.L.B., Thankappan, M., Lymburner, L., Mueller, N., Lewis, A., Held, A., 2012. A

physics-based atmospheric and BRDF correction for Landsat data over mountainous terrain. Remote Sens. Environ. 124, 756–770. doi:https://doi.org/10.1016/j.rse.2012.06.018

Li, J., Roy, D.P., 2017. A Global Analysis of Sentinel-2A, Sentinel-2B and Landsat-8 Data Revisit Intervals and Implications for Terrestrial Monitoring. Remote Sens. . doi:10.3390/rs9090902

Li, M.S., Mao, L.J., Shen, W.J., Liu, S.Q., Wei, A.S., 2013. Change and fragmentation trends of Zhanjiang mangrove forests in southern China using multi-temporal Landsat imagery (1977-2010). Estuar. Coast. Shelf Sci. 130, 111–120. doi:10.1016/j.ecss.2013.03.023

Lillesand, T.M., Kiefer, R.W., Chipman, J.W., 2015. Remote sensing and image interpretation. John Wiley & Sons, Inc, Hoboken, N.J.

Lindenmayer, D.B., Likens, G.E., Andersen, A., Bowman, D., Bull, C.M., Burns, E., Dickman, C.R., Hoffmann, A.A., Keith, D.A., Liddell, M.J., 2012. Value of long-term ecological studies. Austral Ecol. 37, 745–757.

Liu, K., Li, X., Shi, X., Wang, S., 2008. Monitoring mangrove forest changes using remote sensing and GIS data with decision-tree learning. WETLANDS 28, 336–346. doi:10.1672/06-91.1

Liu, L.Y., Tang, H., Caccetta, P., Lehmann, E.A., Hu, Y., Wu, X.L., 2013. Mapping afforestation and deforestation from 1974 to 2012 using Landsat time-series stacks in Yulin District, a key region of the Three-North Shelter region, China. Environ. Monit. Assess. 185, 9949–9965. doi:10.1007/s10661-013-3304-2

Loneragan, N.R., McLeod, I.M., Kenyon, R.A., 2001. Assessing techniques for estimating the extent of mangroves: topographic maps, aerial photographs and Landsat TM images. Mar. Freshw. Res. 52, 787–792. doi:10.1071/MF00052

Long, J.B., Giri, C., 2011. Mapping the Philippines' mangrove forests using Landsat imagery. Sensors 11, 2972–2981. doi:10.3390/s110302972

Loveland, T.R., Dwyer, J.L., 2012. Landsat: Building a strong future. Remote Sens. Environ. 122, 22–29. doi:10.1016/j.rse.2011.09.022

Lovelock, C.E., Adame, M.F., Bennion, V., Hayes, M., O'Mara, J., Reef, R., Santini, N.S., 2014. Contemporary Rates of Carbon Sequestration Through Vertical Accretion of Sediments in

Mangrove Forests and Saltmarshes of South East Queensland, Australia. Estuaries and Coasts 37, 763–771. doi:10.1007/s12237-013-9702-4

Lovelock, C.E., Cahoon, D.R., Friess, D.A., Guntenspergen, G.R., Krauss, K.W., Reef, R., Rogers, K., Saunders, M.L., Sidik, F., Swales, A., Saintilan, N., Thuyen, L.X., Triet, T., 2015. The vulnerability of Indo-Pacific mangrove forests to sea-level rise. Nature 526, 559-U217. doi:10.1038/nature15538

Lovelock, C.E., Feller, I.C., Reef, R., Hickey, S., Ball, M.C., 2017. Mangrove dieback during fluctuating sea levels. Sci. Rep. 7, 1–8. doi:10.1038/s41598-017-01927-6

Lu, D., Mausel, P., Brondízio, E., Moran, E., 2004. Relationships between forest stand parameters and Landsat TM spectral responses in the Brazilian Amazon Basin. For. Ecol. Manage. 198, 149–167. doi:http://dx.doi.org/10.1016/j.foreco.2004.03.048

Lymburner, L., Bunting, P., Lucas, R., Scarth, P., Alam, I., Phillips, C., Ticehurst, C., Held, A., 2019a. Mapping the multi-decadal mangrove dynamics of the Australian coastline. Remote Sens. Environ. 238, 111185. doi:10.1016/j.rse.2019.05.004

Lymburner, L., Bunting, P., Lucas, R., Scarth, P., Alam, I., Phillips, C., Ticehurst, C., Held, A., 2019b. Mapping the multi-decadal mangrove dynamics of the Australian coastline. Remote Sens. Environ. 238, 111185. doi:https://doi.org/10.1016/j.rse.2019.05.004

Manson, F.J., Loneragan, N.R., Harch, B.D., Skilleter, G.A., Williams, L., 2005. A broad-scale analysis of links between coastal fisheries production and mangrove extent: A case-study for northeastern Australia. Fish. Res. 74, 69–85. doi:10.1016/j.fishres.2005.04.001

Mateo-García, G., Gómez-Chova, L., Amorós-López, J., Muñoz-Marí, J., Camps-Valls, G., 2018. Multitemporal Cloud Masking in the Google Earth Engine. Remote Sens. . doi:10.3390/rs10071079

Matthews, E.R., Mazer, S.J., 2016. Historical changes in flowering phenology are governed by temperature × precipitation interactions in a widespread perennial herb in western North America. New Phytol. 210, 157–167. doi:10.1111/nph.13751

Melaas, E.K., Friedl, M.A., Zhu, Z., 2013. Detecting interannual variation in deciduous broadleaf forest phenology using Landsat TM/ETM+ data. Remote Sens. Environ. 132, 176–185. doi:10.1016/j.rse.2013.01.011

Melaas, E.K., Sulla-Menashe, D., Friedl, M.A., 2018. Multidecadal Changes and Interannual Variation in Springtime Phenology of North American Temperate and Boreal Deciduous Forests. Geophys. Res. Lett. 45, 2679–2687. doi:10.1002/2017GL076933

Melaas, E.K., Sulla-Menashe, D., Gray, J.M., Black, T.A., Morin, T.H., Richardson, A.D., Friedl, M.A., 2016. Multisite analysis of land surface phenology in North American temperate and boreal deciduous forests from Landsat. Remote Sens. Environ. 186, 452–464. doi:https://doi.org/10.1016/j.rse.2016.09.014

Menzel, A., 2002. Phenology : Its Importance To the. Clim. Chang. 54, 379–385.

Metcalfe, K., Harbour, D., Territory, N., n.d. MANGROVE LITTER PRODUCTION DARWIN HARBOUR , NORTHERN TERRITORY A study of litter fall as a measure of primary productivity in the mangrove communities of Darwin Harbour MANGROVE LITTER PRODUCTION.

Metcalfe, K.N., Franklin, D.C., McGuinness, K.A., 2011a. Mangrove litter fall: Extrapolation from traps to a large tropical macrotidal harbour. Estuar. Coast. Shelf Sci. 95, 245–252. doi:10.1016/j.ecss.2011.09.006

Metcalfe, K.N., Franklin, D.C., McGuinness, K.A., 2011b. Mangrove litter fall: Extrapolation from traps to a large tropical macrotidal harbour. Estuar. Coast. Shelf Sci. 95, 245–252. doi:10.1016/j.ecss.2011.09.006

Meza Díaz, B., Blackburn, G.A., 2003. Remote sensing of mangrove biophysical properties: Evidence from a laboratory simulation of the possible effects of background variation on spectral vegetation indices. Int. J. Remote Sens. 24, 53–73. doi:10.1080/01431160305012

Monsef, H.A.-E., Smith, S.E., 2017. A new approach for estimating mangrove canopy cover using Landsat 8 imagery. Comput. Electron. Agric. 135, 183–194. doi:http://dx.doi.org/10.1016/j.compag.2017.02.007

Montandon, L.M., Small, E.E., 2008. The impact of soil reflectance on the quantification of the green vegetation fraction from NDVI. Remote Sens. Environ. 112, 1835–1845. doi:10.1016/j.rse.2007.09.007

Moore, C.E., Brown, T., Keenan, T.F., Duursma, R.A., Van Dijk, A.I.J.M., Beringer, J., Culvenor, D., Evans, B., Huete, A., Hutley, L.B., Maier, S., Restrepo-Coupe, N., Sonnentag, O., Specht, A.,

Taylor, J.R., Van Gorsel, E., Liddell, M.J., Lawrence Berkeley National Lab. (LBNL) CA (United States), B., 2016. Reviews and syntheses: Australian vegetation phenology: New insights from satellite remote sensing and digital repeat photography. Biogeosciences. doi:10.5194/bg-13-5085-2016

Morellato, L.P.C., Alberton, B., Alvarado, S.T., Borges, B., Buisson, E., Camargo, M.G.G., Cancian, L.F., Carstensen, D.W., Escobar, D.F.E.E., Leite, P.T.P.P., Mendoza, I., Rocha, N.M.W.B.W.B., Soares, N.C., Silva, T.S.F., Staggemeier, V.G., Streher, A.S., Vargas, B.C., Peres, C.A., Cerdeira, M.L.P., Katharine, A., Irene, M., 2016a. Linking plant phenology to conservation biology. Biol. Conserv. 195, 60–72. doi:10.1016/j.biocon.2015.12.033

Morellato, L.P.C., Alberton, B., Alvarado, S.T., Borges, B., Buisson, E., Camargo, M.G.G., Cancian, L.F., Carstensen, D.W., Escobar, D.F.E.E., Leite, P.T.P.P., Mendoza, I., Rocha, N.M.W.B.W.B., Soares, N.C., Silva, T.S.F., Staggemeier, V.G., Streher, A.S., Vargas, B.C., Peres, C.A., Cerdeira, M.L.P., Katharine, A., Irene, M., 2016b. Linking plant phenology to conservation biology. Biol. Conserv. 195, 60–72. doi:10.1016/j.biocon.2015.12.033

Morisette, J.T., Richardson, A.D., Knapp, A.K., Fisher, J.I., Graham, E.A., Abatzoglou, J., Wilson, B.E., Breshears, D.D., Henebry, G.M., Hanes, J.M., Liang, L., 2009. Tracking the rhythm of the seasons in the face of global change: phenological research in the 21st century. Front. Ecol. Environ. 7, 253–260. doi:10.1890/070217

Moritz-Zimmermann, A., Comely, B., Lewis, D., Environment., D. of I.P. and, 2002. Darwin harbour mangrove monitoring methodology. Northern Territory Government, Department of Infrastructure Planning and Environment.

Mueller, N., Lewis, A., Roberts, D., Ring, S., Melrose, R., Sixsmith, J., Lymburner, L., McIntyre, A., Tan, P., Curnow, S., Ip, A., 2016. Water observations from space: Mapping surface water from 25 years of Landsat imagery across Australia. Remote Sens. Environ. 174, 341–352. doi:http://dx.doi.org/10.1016/j.rse.2015.11.003

Munshi-South, J., 2012. Urban landscape genetics: canopy cover predicts gene flow between white-footed mouse (Peromyscus leucopus) populations in New York City. Mol. Ecol. 21, 1360–1378. doi:10.1111/j.1365-294X.2012.05476.x

Nardin, W., Locatelli, S., Pasquarella, V., Rulli, M.C., Woodcock, C.E., Fagherazzi, S., 2016.

Dynamics of a fringe mangrove forest detected by Landsat images in the Mekong River Delta, Vietnam: Dynamics of Mangrove Forest Detected by Landsat Images in Vietnam. Earth Surf. Process. Landforms 41, 2024–2037. doi:10.1002/esp.3968

NCI, 2015. National Computational Infrastructure [WWW Document]. URL https://nci.org.au/

Obata, K., Miura, T., Yoshioka, H., 2012. Analysis of the Scaling Effects in the Area-Averaged Fraction of Vegetation Cover Retrieved Using an NDVI-Isoline-Based Linear Mixture Model. Remote Sens. 4, 2156–2180. doi:10.3390/rs4072156

Olofsson, P., Holden, C.E., Bullock, E.L., Woodcock, C.E., 2016. Time series analysis of satellite data reveals continuous deforestation of New England since the 1980s. Environ. Res. Lett. doi:10.1088/1748-9326/11/6/064002

Paletto, A., Tosi, V., 2009. Forest canopy cover and canopy closure: comparison of assessment techniques. Eur. J. For. Res. 128, 265–272. doi:10.1007/s10342-009-0262-x

Paling, E.I., Kobryn, H.T., Humphreys, G., 2008. Assessing the extent of mangrove change caused by Cyclone Vance in the eastern Exmouth Gulf, northwestern Australia. Estuar. Coast. Shelf Sci. 77, 603–613. doi:10.1016/j.ecss.2007.10.019

Pasquarella, V.J., Holden, C.E., Woodcock, C.E., 2018. Improved mapping of forest type using spectral-temporal Landsat features. Remote Sens. Environ. 210, 193–207. doi:10.1016/j.rse.2018.02.064

Pastick, J.N., Wylie, K.B., Wu, Z., 2018. Spatiotemporal Analysis of Landsat-8 and Sentinel-2 Data to Support Monitoring of Dryland Ecosystems. Remote Sens. . doi:10.3390/rs10050791

Pastor-Guzman, J., Atkinson, P.M., Dash, J., Rioja-Nieto, R., 2015. Spatiotemporal Variation in Mangrove Chlorophyll Concentration Using Landsat 8. Remote Sens. 7, 14530–14558. doi:10.3390/rs71114530

Pastor-Guzman, J., Dash, J., Atkinson, P.M., 2018. Remote sensing of mangrove forest phenology and its environmental drivers. Remote Sens. Environ. 205, 71–84. doi:10.1016/j.rse.2017.11.009

Patel, N.N., Angiuli, E., Gamba, P., Gaughan, A., Lisini, G., Stevens, F.R., Tatem, A.J., Trianni, G.,

2015. Multitemporal settlement and population mapping from Landsat using Google Earth Engine. Int. J. Appl. Earth Obs. Geoinf. 35, Part B, 199–208. doi:http://dx.doi.org/10.1016/j.jag.2014.09.005

Paul, A.M., 2016. The Coding Revolution. Sci. Am. 315, 42–49. doi:10.1038/scientificamerican0816-42

Peñuelas, J., Rutishauser, T., Filella, I., 2009. Phenology Feedbacks on Climate Change. Science (80-.). 324, 887 LP – 888.

Petre, M., Wilson, G., 2014. PLOS/Mozilla Scientific Code Review Pilot: Summary of Findings 4. doi:https://arxiv.org/pdf/1407.5648v2.pdf

Phua, M.-H., Tsuyuki, S., Furuya, N., Lee, J.S., 2008. Detecting deforestation with a spectral change detection approach using multitemporal Landsat data: A case study of Kinabalu Park, Sabah, Malaysia. J. Environ. Manage. 88, 784–795. doi:10.1016/j.jenvman.2007.04.011

Poudel, P.K., Temesgen, H., 2016. Developing Biomass Equations for Western Hemlock and Red Alder Trees in Western Oregon Forests. Forests. doi:10.3390/f7040088

Purevdorj, T.S., Tateishi, R., Ishiyama, T., Honda, Y., 1998. Relationships between percent vegetation cover and vegetation indices. Int. J. Remote Sens. 19, 3519–3535. doi:10.1080/014311698213795

R Core Development Team, 2016. R: A language and environment for statistical computing.

Raha, A., Das, S., Banerjee, K., Mitra, A., 2012. Climate change impacts on Indian Sunderbans: a time series analysis (1924–2008). Biodivers. Conserv. 21, 1289–1307. doi:10.1007/s10531-012-0260-z

Restrepo-Coupe, N., Huete, A., Davies, K., 2015. Satellite Phenology Validation, in: Held, A., Phinn, S., Soto-Berelov, M., Jones, S. (Eds.), AusCover Good Practice Guidelines: A Technical Handbook Supporting Calibration and Validation Activities of Remotely Sensed Data Product. TERN AusCover, pp. 155–157.

Richards, D.R., Friess, D.A., 2016. Rates and drivers of mangrove deforestation in Southeast Asia, 2000–2012. Proc. Natl. Acad. Sci. doi:10.1073/pnas.1510272113

Richardson, A.D., Hollinger, D.Y., Dail, D.B., Lee, J.T., Munger, J.W., O'keefe, J., 2009. Influence of spring phenology on seasonal and annual carbon balance in two contrasting New England forests. Tree Physiol. 29, 321–331. doi:10.1093/treephys/tpn040

Roberts, D., Mueller, N., McIntyre, A., 2017. High-Dimensional Pixel Composites from Earth Observation Time Series. IEEE Trans. Geosci. Remote Sens. 55, 6254–6264. doi:10.1109/TGRS.2017.2723896

Rogers, K., Boon, P.I., Branigan, S., Duke, N.C., Field, C.D., Fitzsimons, J.A., Kirkman, H., Mackenzie, J.R., Saintilan, N., 2016. The state of legislation and policy protecting Australia's mangrove and salt marsh and their ecosystem services. Mar. POLICY. doi:10.1016/j.marpol.2016.06.025

Rogers, K., Kelleway, J.J., Saintilan, N., Megonigal, J.P., Adams, J.B., Holmquist, J.R., Lu, M., Schile-Beers, L., Zawadzki, A., Mazumder, D., Woodroffe, C.D., 2019. Wetland carbon storage controlled by millennial-scale variation in relative sea-level rise. Nature 567, 91–95. doi:10.1038/s41586-019-0951-7

Rogers, K., Lymburner, L., Salum, R., Brooke, B.P., Woodroffe, C.D., 2017. Mapping of mangrove extent and zonation using high and low tide composites of Landsat data. Hydrobiologia 803, 49–68. doi:10.1007/s10750-017-3257-5

Roy, D.P., Kovalskyy, V., Zhang, H., Yan, L., Kommareddy, I., 2015. The utility of landsat data for global long term terrestrial monitoring. Remote Sens. Digit. Image Process. 22, 289–305. doi:10.1007/978-3-319-15967-6_14

Roy, D.P., Kovalskyy, V., Zhang, H.K., Vermote, E.F., Yan, L., Kumar, S.S., Egorov, A., 2016. Characterization of Landsat-7 to Landsat-8 reflective wavelength and normalized difference vegetation index continuity. Remote Sens. Environ. 185, 57–70. doi:https://doi.org/10.1016/j.rse.2015.12.024

Ruiz-Luna, A., Berlanga-Robles, C.A., 2003. Land use, land cover changes and coastal lagoon surface reduction associated with urban growth in northwest Mexico. Landsc. Ecol. 18, 159–171. doi:10.1023/A:1024461215456

Saenger, P., Moverley, J., 1985. Vegetative phenology of mangroves along the Queensland coastline. Proc. Ecol. Soc. Aust. 13, 257–265.

Sagar, S., Roberts, D., Bala, B., Lymburner, L., 2017. Extracting the intertidal extent and topography of the Australian coastline from a 28year time series of Landsat observations. Remote Sens. Environ. 195, 153–169. doi:https://doi.org/10.1016/j.rse.2017.04.009

Saintilan, N., Wilson, N.C., Rogers, K., Rajkaran, A., Krauss, K.W., 2014. Mangrove expansion and salt marsh decline at mangrove poleward limits. Glob. Chang. Biol. 20, 147–157. doi:10.1111/gcb.12341

Saito, H., Bellan, M.F., Al-Habshi, A., Aizpuru, M., Blasco, F., 2003. Mangrove research and coastal ecosystem studies with SPOT-4 HRVIR and TERRA ASTER in the Arabian Gulf. Int. J. Remote Sens. 24, 4073–4092. doi:10.1080/0143116021000035030

Saitoh, T.M., Nagai, S., Yoshino, J., Kondo, H., Tamagawa, I., Muraoka, H., 2015. Effects of canopy phenology on deciduous overstory and evergreen understory carbon budgets in a cool-temperate forest ecosystem under ongoing climate change. Ecol. Res. 30, 267–277. doi:10.1007/s11284-014-1229-z

Sanderman, J., Hengl, T., Fiske, G., Solvik, K., Adame, M.F., Benson, L., Bukoski, J.J., Carnell, P., Cifuentes-Jara, M., Donato, D., Duncan, C., Eid, E.M., Ermgassen, P. zu, Lewis, C.J.E., Macreadie, P.I., Glass, L., Gress, S., Jardine, S.L., Jones, T.G., Nsombo, E.N., Rahman, M.M., Sanders, C.J., Spalding, M., Landis, E., 2018. A global map of mangrove forest soil carbon at 30 m spatial resolution. Environ. Res. Lett. 13, 55002. doi:10.1088/1748-9326/aabe1c

Selkowitz, D.J., Forster, R.R., 2016. Automated mapping of persistent ice and snow cover across the western U.S. with Landsat. ISPRS J. Photogramm. Remote Sens. 117, 126–140. doi:http://dx.doi.org/10.1016/j.isprsjprs.2016.04.001

Senf, C., Pflugmacher, D., Heurich, M., Krueger, T., 2017. A Bayesian hierarchical model for estimating spatial and temporal variation in vegetation phenology from Landsat time series. Remote Sens. Environ. 194, 155–160. doi:https://doi.org/10.1016/j.rse.2017.03.020

Sitch, S., Friedlingstein, P., Gruber, N., Jones, S.D., Murray-Tortarolo, G., Ahlström, A., Doney, S.C., Graven, H., Heinze, C., Huntingford, C., Levis, S., Levy, P.E., Lomas, M., Poulter, B., Viovy, N., Zaehle, S., Zeng, N., Arneth, A., Bonan, G., Bopp, L., Canadell, J.G., Chevallier, F., Ciais, P., Ellis, R., Gloor, M., Peylin, P., Piao, S.L., Le Quéré, C., Smith, B., Zhu, Z., Myneni, R., 2015. Recent trends and drivers of regional sources and sinks of carbon dioxide.

Biogeosciences. doi:10.5194/bg-12-653-2015

Small, C., Sousa, D., 2019. Spatiotemporal Characterization of Mangrove Phenology and Disturbance Response: The Bangladesh Sundarban. Remote Sens. (Basel, Switzerland) 11, 2063. doi:10.3390/rs11172063

Smith, M.N., Stark, S.C., Taylor, T.C., Ferreira, M.L., de Oliveira, E., Restrepo-Coupe, N., Chen, S., Woodcock, T., dos Santos, D.B., Alves, L.F., Figueira, M., de Camargo, P.B., de Oliveira, R.C., Aragão, L.E.O.C.O.C., Falk, D.A., McMahon, S.M., Huxman, T.E., Saleska, S.R., 2019. Seasonal and drought related changes in leaf area profiles depend on height and light environment in an Amazon forest. New Phytol. 0, 0–3. doi:10.1111/nph.15726

Son, N.T., Thanh, B.X., Da, C.T., 2016. Monitoring Mangrove Forest Changes from Multi-temporal Landsat Data in Can Gio Biosphere Reserve, Vietnam. WETLANDS 36, 565–576. doi:10.1007/s13157-016-0767-2

Songsom, V., Koedsin, W., Ritchie, J.R., Huete, A., 2019. Mangrove Phenology and Environmental Drivers Derived from Remote Sensing in Southern Thailand. Remote Sens. doi:10.3390/rs11080955

Spalding, M., Blasc, o F., Field, C., 1997. World Mangrove Atlas (Dataset). Okinawa, Japan.

Sulong, I., Mohd-Lokman, H., Mohd-Tarmizi, K., Ismail, A., 2002. Mangrove Mapping Using Landsat Imagery and Aerial Photographs: Kemaman District, Terengganu, Malaysia. Environ. Dev. Sustain. 4, 135–152. doi:10.1023/A:1020844620215

Taylor, S.J., Letham, B., 2018. Forecasting at Scale. Am. Stat. 72, 37–45. doi:10.1080/00031305.2017.1380080

Taylor, S.J., Letham, B., Taylor, S.J., Letham, B., 2018. Forecasting at Scale. Am. Stat. 72, 37–45. doi:10.1080/00031305.2017.1380080

Teixeira, L.A., de Oliveira, A.L.I., 2010. A method for automatic stock trading combining technical analysis and nearest neighbor classification. Expert Syst. Appl. 37, 6885–6890. doi:http://dx.doi.org/10.1016/j.eswa.2010.03.033

TMR - Queensland Dept. of Transport and Main Roads, n.d. 1998-1999—Fishermans Landing tide gauge archived interval recordings [WWW Document]. Queensl. Dep. Transp. Main

Roads. URL https://www.data.qld.gov.au/dataset/fishermans-landing-tide-gauge-archived-interval-recordings/resource/ef1d0409-06ee-498d-83a0-649f8478a786 (accessed 11.15.20).

Tomlinson, P.B., 1986. The botany of mangroves .

Trewin, C., 2013. Mangrove & Saltmarsh Monitoring: Literature Review. Sinclair Kn. Merz Gladstone Ports Corp. CA120019 R, 53.

Trucano, M., 2015. Research questions about technology use in education in developing countries. infoDev / World Bank.

Tucker, C.J., 1979. Red and photographic infrared linear combinations for monitoring vegetation. Remote Sens. Environ. doi:10.1016/0034-4257(79)90013-0

Turton, S.M., 2017. Expansion of the tropics: revisiting frontiers of geographical knowledge. Geogr. Res. 55, 3–12. doi:10.1111/1745-5871.12230

Union of Concerned Scientists, 2017. Satellite Database 1-1-17.

van Bussel, L.G.J., Ewert, F., Leffelaar, P.A., 2011. Effects of data aggregation on simulations of crop phenology. Agric. Ecosyst. Environ. 142, 75–84. doi:https://doi.org/10.1016/j.agee.2010.03.019

Vasconcelos, M.J.P., Mussá Biai, J.C., Araújo, A., Diniz, M.A., 2002. Land cover change in two protected areas of Guinea-Bissau (1956-1998). Appl. Geogr. 22, 139–156. doi:10.1016/S0143-6228(02)00005-X

Vee, A., 2013. Understanding Computer Programming as a Literacy. Lit. Compos. Stud. 1.

Verbesselt, J., Hyndman, R., Newnham, G., Culvenor, D., 2010. Detecting trend and seasonal changes in satellite image time series. Remote Sens. Environ. 114, 106–115. doi:10.1016/j.rse.2009.08.014

Vitolo, C., Elkhatib, Y., Reusser, D., Macleod, C.J.A., Buytaert, W., 2015. Web technologies for environmental Big Data. Environ. Model. Softw. 63, 185–198. doi:http://dx.doi.org/10.1016/j.envsoft.2014.10.007

Vo, Q.T., Oppelt, N., Leinenkugel, P., Kuenzer, C., 2013. Remote sensing in mapping mangrove ecosystems - an object-based approach. Remote Sens. 5, 183–201.

doi:10.3390/rs5010183

Vogelmann, J.E., Gallant, A.L., Shi, H., Zhu, Z., 2016a. Perspectives on monitoring gradual change across the continuity of Landsat sensors using time-series data. Remote Sens. Environ. doi:10.1016/j.rse.2016.02.060

Vogelmann, J.E., Gallant, A.L., Shi, H., Zhu, Z., 2016b. Perspectives on monitoring gradual change across the continuity of Landsat sensors using time-series data. Remote Sens. Environ. doi:10.1016/j.rse.2016.02.060

Ward, R.D., Friess, D.A., Day, R.H., MacKenzie, R.A., 2016. Impacts of climate change on mangrove ecosystems: a region by region overview. Ecosyst. Heal. Sustain. 2, n/a-n/a. doi:10.1002/ehs2.1211

White, M.A., De Beurs, K.M., Didan, K., Inouye, D.W., Richardson, A.D., Jensen, O.P., O'keefe, J., Zhang, G., Nemani, R.R., Van Leeuwen, W.J.D., Brown, J.F., De Wit, A., Schaepman, M., Lin, X., Dettinger, M., Bailey, A.S., Kimball, J., Schwartz, M.D., Baldocchi, D.D., Lee, J.T., Lauenroth, W.K., 2009. Intercomparison, interpretation, and assessment of spring phenology in North America estimated from remote sensing for 1982–2006. Glob. Chang. Biol. 15, 2335–2359. doi:10.1111/j.1365-2486.2009.01910.x

White, M.A., Nemani, R.R., Thornton, P.E., Running, S.W., 2002. Satellite evidence of phenological differences between urbanized and rural areas of the eastern United States deciduous broadleaf forest. Ecosystems 5, 260–273. doi:10.1007/s10021-001-0070-8

Wiesmair, M., Feilhauer, H., Magiera, A., Otte, A., Waldhardt, R., 2016. Estimating Vegetation Cover from High-Resolution Satellite Data to Assess Grassland Degradation in the Georgian Caucasus. Mt. Res. Dev. 36, 56–65. doi:10.1659/MRD-JOURNAL-D-15-00064.1

Wightman, G.M., Andrews, M., Northern Territory. Dept. of Infrastructure, P. and E., 2006. Mangroves of the Northern Territory, Australia: identification and traditional use.

Wilson, Nicholas C, Saintilan, N., 2012. Growth of the mangrove species Rhizophora stylosa Griff. at its southern latitudinal limit in eastern Australia. Aquat. Bot. 101, 8–17. doi:10.1016/j.aquabot.2012.03.011

Wilson, Nicholas C., Saintilan, N., 2012. Growth of the mangrove species Rhizophora stylosa Griff. at its southern latitudinal limit in eastern Australia. Aquat. Bot. 101, 8–17.

doi:10.1016/j.aquabot.2012.03.011

Wing, J.M., 2008. Computational thinking and thinking about computing. Philos. Trans. R. Soc. A Math. Phys. Eng. Sci. doi:10.1098/rsta.2008.0118

Wood, S., 2017. Generalized Additive Models An Introduction with R, Second Edi. ed. Chapman and Hall/CRC, NEW YORK. doi:https://doi.org/10.1201/978131537027

Wu, H., Li, Z.-L., 2009a. Scale issues in remote sensing: A review on analysis, processing and modeling. Sensors. doi:10.3390/s90301768

Wu, H., Li, Z.-L.L., 2009b. Scale issues in remote sensing: A review on analysis, processing and modeling. Sensors 9, 1768–1793. doi:10.3390/s90301768

Wu, J., Albert, L.P., Lopes, A.P., Restrepo-Coupe, N., Hayek, M., Wiedemann, K.T., Guan, K., Stark, S.C., Christoffersen, B., Prohaska, N., Tavares, J. V, Marostica, S., Kobayashi, H., Ferreira, M.L., Campos, K.S., da Silva, R., Brando, P.M., Dye, D.G., Huxman, T.E., Huete, A.R., Nelson, B.W., Saleska, S.R., 2016. Leaf development and demography explain photosynthetic seasonality in Amazon evergreen forests. Science (80-.). 351, 972 LP – 976. doi:10.1126/science.aad5068

Wulder, M.A., Coops, N.C., 2014. Satellites: Make Earth observations open access. Nature 513, 30–31.

Wulder, M.A., Masek, J.G., Cohen, W.B., Loveland, T.R., Woodcock, C.E., 2012. Opening the archive: How free data has enabled the science and monitoring promise of Landsat. Remote Sens. Environ. 122, 2–10. doi:10.1016/j.rse.2012.01.010

Wulder, M.A., White, J.C., Loveland, T.R., Woodcock, C.E., Belward, A.S., Cohen, W.B., Fosnight, E.A., Shaw, J., Masek, J.G., Roy, D.P., 2016. The global Landsat archive: Status, consolidation, and direction. Remote Sens. Environ. 185, 271–283. doi:10.1016/j.rse.2015.11.032

Xiao, J., Moody, A., 2005. A comparison of methods for estimating fractional green vegetation cover within a desert-to-upland transition zone in central New Mexico, USA. Remote Sens. Environ. 98, 237–250. doi:10.1016/j.rse.2005.07.011

Xin, Q., Li, J., Li, Z., Li, Y., Zhou, X., 2020. Evaluations and comparisons of rule-based and

machine-learning-based methods to retrieve satellite-based vegetation phenology using MODIS and USA National Phenology Network data. Int. J. Appl. Earth Obs. Geoinf. 93, 102189. doi:https://doi.org/10.1016/j.jag.2020.102189

Yan, J., Wang, L., Song, W., Chen, Y., Chen, X., Deng, Z., 2019. A time-series classification approach based on change detection for rapid land cover mapping. ISPRS J. Photogramm. Remote Sens. 158, 249–262. doi:https://doi.org/10.1016/j.isprsjprs.2019.10.003

Yang, C., Xu, Y., Nebert, D., 2013. Redefining the possibility of digital Earth and geosciences with spatial cloud computing. Int. J. Digit. Earth 6, 297–312. doi:10.1080/17538947.2013.769783

Yang, C., Yu, M., Hu, F., Jiang, Y., Li, Y., 2017. Utilizing Cloud Computing to address big geospatial data challenges. Comput. Environ. Urban Syst. 61, Part B, 120–128. doi:http://dx.doi.org/10.1016/j.compenvurbsys.2016.10.010

Yang, L., Jia, K., Liang, S., Liu, J., Wang, X., 2016. Comparison of Four Machine Learning Methods for Generating the GLASS Fractional Vegetation Cover Product from MODIS Data. Remote Sens. doi:10.3390/rs8080682

Yee, T.W., Mitchell, N.D., 1991. Generalized Additive Models in Plant Ecology. J. Veg. Sci. 2, 587–602. doi:10.2307/3236170

Younes Cárdenas, N., 2018. Linear and Beta regression models to predict Fractional Vegetation Cover. doi:http://doi.org/10.5281/zenodo.1195576

Younes Cárdenas, N., Joyce, K.E., Maier, S.W., 2017. Monitoring mangrove forests : Are we taking full advantage of technology? Int J Appl Earth Obs Geoinf. 63, 1–14. doi:10.1016/j.jag.2017.07.004

Younes, N., Joyce, K.E., Northfield, T.D., Maier, S.W., 2019. The effects of water depth on estimating Fractional Vegetation Cover in mangrove forests. Int. J. Appl. Earth Obs. Geoinf. 83, 101924. doi:https://doi.org/10.1016/j.jag.2019.101924

Yuan, Y., Meng, Y., Lin, L., Sahli, H., Yue, A., Chen, J., Zhao, Z., Kong, Y., He, D., 2015. Continuous change detection and classification using hidden Markov model: A case study for monitoring urban encroachment onto farmland in Beijing. Remote Sens. 7, 15318–15339.

doi:10.3390/rs71115318

Zhang, C., Lu, D., Chen, X., Zhang, Y., Maisupova, B., Tao, Y., 2016. The spatiotemporal patterns of vegetation coverage and biomass of the temperate deserts in Central Asia and their relationships with climate controls. Remote Sens. Environ. 175, 271–281. doi:10.1016/j.rse.2016.01.002

Zhang, H.K., Roy, D.P., 2016. Landsat 5 Thematic Mapper reflectance and NDVI 27-year time series inconsistencies due to satellite orbit change. Remote Sens. Environ. 186, 217–233. doi:http://dx.doi.org/10.1016/j.rse.2016.08.022

Zhang, K., Thapa, B., Ross, M., Gann, D., 2016. Remote sensing of seasonal changes and disturbances in mangrove forest: a case study from South Florida. Ecosphere 7, 23. doi:10.1002/ecs2.1366

Zhang, X., Friedl, M.A., Schaaf, C.B., Strahler, A.H., Hodges, J.C.F., Gao, F., Reed, B.C., Huete, A., 2003. Monitoring vegetation phenology using MODIS. Remote Sens. Environ. 84, 471–475. doi:https://doi.org/10.1016/S0034-4257(02)00135-9

Zhang, X., Tan, B., Yu, Y., 2014. Interannual variations and trends in global land surface phenology derived from enhanced vegetation index during 1982–2010. Int. J. Biometeorol. 58, 547–564. doi:10.1007/s00484-014-0802-z

Zhang, X.H., Tian, Q.J., 2013. A mangrove recognition index for remote sensing of mangrove forest from space. Curr. Sci. 105, 1149–1155.

Zhou, Q., Rover, J., Brown, J., Worstell, B., Howard, D., Wu, Z., Gallant, L.A., Rundquist, B., Burke, M., 2019. Monitoring Landscape Dynamics in Central U.S. Grasslands with Harmonized Landsat-8 and Sentinel-2 Time Series Data. Remote Sens. . doi:10.3390/rs11030328

Zhu, Z, Woodcock, C.E., 2014. Continuous change detection and classification of land cover using all available Landsat data. Remote Sens. Environ. 144, 152–171. doi:10.1016/j.rse.2014.01.011

Zhu, Zhe, Woodcock, C.E., 2014. Automated cloud, cloud shadow, and snow detection in multitemporal Landsat data: An algorithm designed specifically for monitoring land cover change. Remote Sens. Environ. 152, 217–234. doi:10.1016/j.rse.2014.06.012

Zhu, Z., Woodcock, C.E., Olofsson, P., 2012. Continuous monitoring of forest disturbance using all available Landsat imagery. Remote Sens. Environ. 122, 75–91. doi:http://dx.doi.org/10.1016/j.rse.2011.10.030

Zuur, A.F., 2012. A beginner's guide to generalized additive models with R. Highland Statistics Ltd, Newburgh.

8 Appendices

Appendix 1: Summary of studies published since the year 2000

Table 12 summary of studies published since the year 2000

Year	Reference	Sensor(s)	Images used	Year(s) of image(s) used
2001	Kovacs et al. (2001)	Landsat TM	3	1986, 1993, 1999
	Loneragan et al. (2001)	Landsat TM	1	1994
2002	Sulong et al. (2002)	Landsat TM	1	1994
	Vasconcelos et al. (2002)	Landsat TM	1	1998
2003	Ruiz-Luna and Berlanga-Robles (2003)	Landsat MSS / TM	4	1973, 1986, 1992, 1997
	Saito et al. (2003)	SPOT-4, ASTER	2	1999, 2000
2004	Krause et al. (2004)	ASTER, Landsat TM / ETM	4	1988, 1991, 1999, 2001
2005	Cornejo et al. (2005)	Landsat MSS / ETM	4	1973, 1986, 1992, 2000
	Manson et al. (2005)	Landsat TM	2	1986, 1997
2006	Béland et al. (2006)	Landsat TM / ETM	3	1986, 1992, 2001
	Emch and Peterson (2006)	Landsat TM / ETM	2	1989, 2000
	Jean-Baptiste and Jensen (2006)	ASTER	1	2005
2007	Baghdadi and Oliveros (2007)	ASTER	1	2004
	Giri et al. (2007)	Landsat MSS /TM / ETM	8	1977, 1989, 2000
	Habshi et al. (2007)	ASTER	3	2002
	Harper et al. (2007) *	Landsat MSS /TM / ETM	8	1972-1979, 1989-1996, 1999-2001
	James et al. (2007)	Landsat TM / ETM	6	1986, 1987, 2002, 2003
	Jupiter et al. (2007)	Landsat ETM	1	2000
2008	Giri and Muhlhausen (2008) **	ASTER, Landsat MSS / TM / ETM	82	1973-1983, 1989-1993, 1997-2000, 2005
	Liu et al. (2008)	Landsat TM	3	1995, 1998, 2002
	Paling et al. (2008)	Landsat TM	3	1999, 2002, 2004
	Phua et al. (2008)	Landsat MSS / TM	3	1973, 1991, 1996
2009	Ferreira et al. (2009)	Landsat TM	2	1995, 2005
	Lee and Yeh (2009)	SPOT-4, Landsat TM	2	1995
2010	Akumu et al. (2010)	ASTER, Landsat TM / ETM	3	1989, 2001, 2003
	Eslami-Andargoli et al. (2010)	Landsat MSS / TM	3	1972, 1990, 2004
2011	Alatorre et al. (2011)	Landsat ETM	4	2004

	Bhattarai and Giri (2011) **	Global Land Survey	128	2000
	Giri et al. (2011) */**	Global Land Survey	1000	2000
	Long and Giri (2011)	Global Land Survey	61	1991-1993, 1999-2005
2012	França et al. (2012)	Landsat TM	1	2010
	Kumar et al. (2012)	Landsat TM / ETM, Resourcesat 1	3	1991, 2000, 2006
	Raha et al. (2012)	Landsat MSS	2	1975, 1989
2013	Chen et al. (2013)	Landsat TM / ETM / OLI	4	1985, 1996, 2002, 2013
	Eslami-Andargoli et al. (2013)	Landsat MSS / TM / ETM	3	1972, 1990, 2004
	Kirui et al. (2013) */**	Landsat MSS / TM	8	1984, 1985, 1990, 1992, 2000, 2002, 2008, 2010
	Li et al. (2013)	Landsat MSS / TM / ETM	70	1973-1978, 1986-1990, 1992-1996, 1998, 2000 - 2012
	Zhang and Tian (2013)	Landsat TM	2	2006
2014	Jia et al. (2014)	Landsat TM / ETM	25	2008 - 2010
2015	Abdul Aziz et al. (2015)	Landsat TM / ETM / OLI	6	1988, 1995, 1999, 2001, 2009, 2013
	Aziz et al. (2015)	Landsat MSS / TM / ETM / OLI	9	1978, 1988, 1989, 1995, 1999, 2001, 2009, 2013, 2014
	Dutta et al. (2015) */**	Landsat OLI	6	
	Giri et al. (2015) *	Global Land Survey, Landsat MSS / TM	10	1973, 1975, 1990, 1997, 2000, 2001, 2006, 2010
	Ibharim et al. (2015)	Landsat TM / ETM	2	1993, 1999
	Jones et al. (2015)	Landsat TM	1	2011
	Kamal et al. (2015)	Landsat TM	2	2009, 2011
	Kanniah et al. (2015) *	Landsat TM / ETM / OLI	7	1989, 2000, 2005, 2007, 2009, 2013, 2014
	Lagomasino et al. (2015) **	Landsat TM	16	1993-2009
	Pastor-Guzman et al. (2015) **	Landsat OLI	6	2013, 2014
2016	Asbridge et al. (2016) **	Landsat TM / ETM / OLI	85	1987-2014
	Hossain et al. (2016)	Landsat ETM / OLI	2	2013, 2014
	Jones et al. (2016)	Landsat TM / ETM / OLI	5	2010, 2011, 2014
	Nardin et al. (2016)	Landsat TM / ETM / OLI	158	1989, 1990, 1993 - 2014
	Son et al. (2016)	Landsat TM / ETM / OLI	5	1989, 1996, 2009, 2003, 2014
	Zhang et al. (2016) **	Landsat TM / ETM / OLI	150	1985 - 2011

* Number of images not explicitly reported. **Years of images not explicitly reported.

Appendix 2: Validation of Observed vs predicted EVI.

In Figure 41 we show the linear regression that compares the observed and the predicted EVI values for all study sites. When using the mean values per date (Figure 41 top panel), it is easy to see that some models show low predictive power (i.e. $R^2 < 0.30$), and others show a moderate predictive power (i.e. $30 \leq R^2 \leq 50$). For example, EVI models have a moderate agreement with observed EVI values in the sites where (Coupland et al., 2005), (Saenger and Moverley, 1985), and (Nicholas C Wilson and Saintilan, 2012) undertook their field campaigns (Figure 41B/D/E). In sharp contrast, when the data are grouped by month (Figure 41 bottom panel), the EVI models show better predictive power across all sites, due to lower influence of daily fluctuations. For example, EVI models for (Saenger and Moverley, 1985), (Coupland et al., 2005) and (Metcalfe et al., 2011a) have the highest R^2 values of all models i.e. 0.93, 0.90 and 0.90 respectively. The residuals of all the regressions (not shown) are randomly distributed, indicating that errors are stochastic and showing no signs of heteroscedasticity or non-linear associations between observed and predicted values. These results suggest that in mangrove ecosystems GAMs may be better predictors of seasonal changes than inter-annual variations.

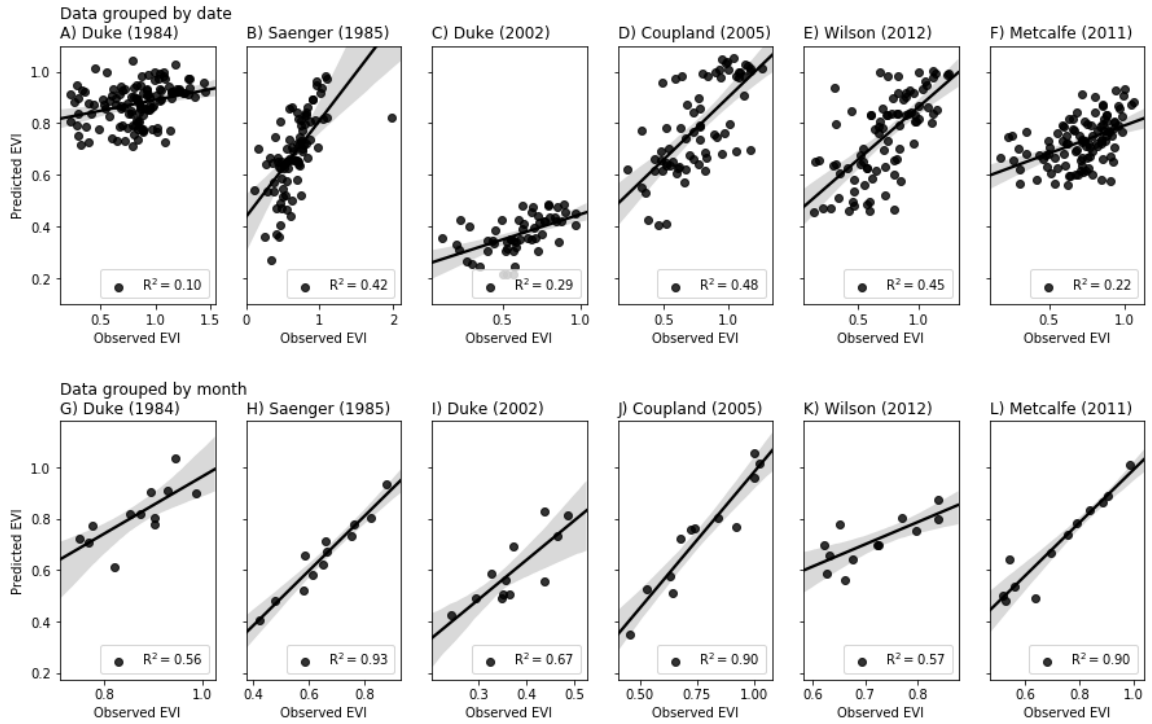

Figure 41: Observed EVI vs EVI model for all sites. Top panel shows the linear regression of the mean observed EVI per date, while the bottom panel shows the linear regression of the monthly means of the model and EVI observations.

Validation: Predicted EVI vs in situ variables

We validated our EVI model against *in situ* data by running a linear regression between the EVI model and every in situ variable from (Duke et al., 1999). When the data are grouped by date (i.e. chronological order), the highest correlations with the EVI model come from the leaf production rate (R^2 = 0.20), total leaf area (R^2 = 0.16) and net leaf production (R^2 = 0.11). When the data are aggregated by month however, the correlation of the variables with EVI increases in most cases (e.g. leaf production rate (R^2 = 0.27), standing stock (R^2 = 0.14)).

Moving forward

We have identified several ways in which the remote sensing and ecology communities can take phenology modelling to the next level. Firstly, we can evaluate accuracy by gathering and/or sharing field data with sufficient temporal resolution as to compare it with satellite imagery. These data could include leaf area index, litter fall, leaf onset, biomass, and other measurements of plant phenology and growth that aid in assessing model accuracy and potential bias.

Secondly, GAMs and high-resolution imagery (i.e. equal or better than 1.5 × 1.5m) can be used to model phenological changes on single plants. By modelling phenology and the factors that affect it, users can take preventive or corrective measurements before the plant (or crop) fails or dies. More importantly, high resolution imagery could potentially be used to create models at the same scale as the data collection plots, inform policy and monitor restoration projects (Lee et al., 2019).

Thirdly, incorporating independent datasets to the GAMs will allow us to examine which environmental variables have the most influence on mangrove phenology at a continental scale. These datasets could include parameters like temperature, rainfall, humidity and tidal range. Besides altering spectral reflectance value values in the near and short-wave infrared bands (Younes Cárdenas et al., 2017), the tidal range at the time of image acquisition may play an important role in mangrove phenology. Just like temperature and rainfall, the tides vary

seasonally across Australia (Bishop-Taylor et al., 2019) and their impact on mangrove phenology is yet to be assessed.

Lastly, we have demonstrated the usefulness of GAMs with a dense time-series of remotely sensed imagery, but the applications of this work could also be used with Moderate-Resolution Imaging Spectroradiometer (MODIS), Sentinel or other satellite sensors. Creating maps of mangroves around the world is important, but we currently have the technology to process large datasets in just hours, so why not model (and forecast) phenology under different climate change scenarios? This means detecting changes in the start of season and peak growing season dates over time and how that may correlate with changing weather and climatic patterns.

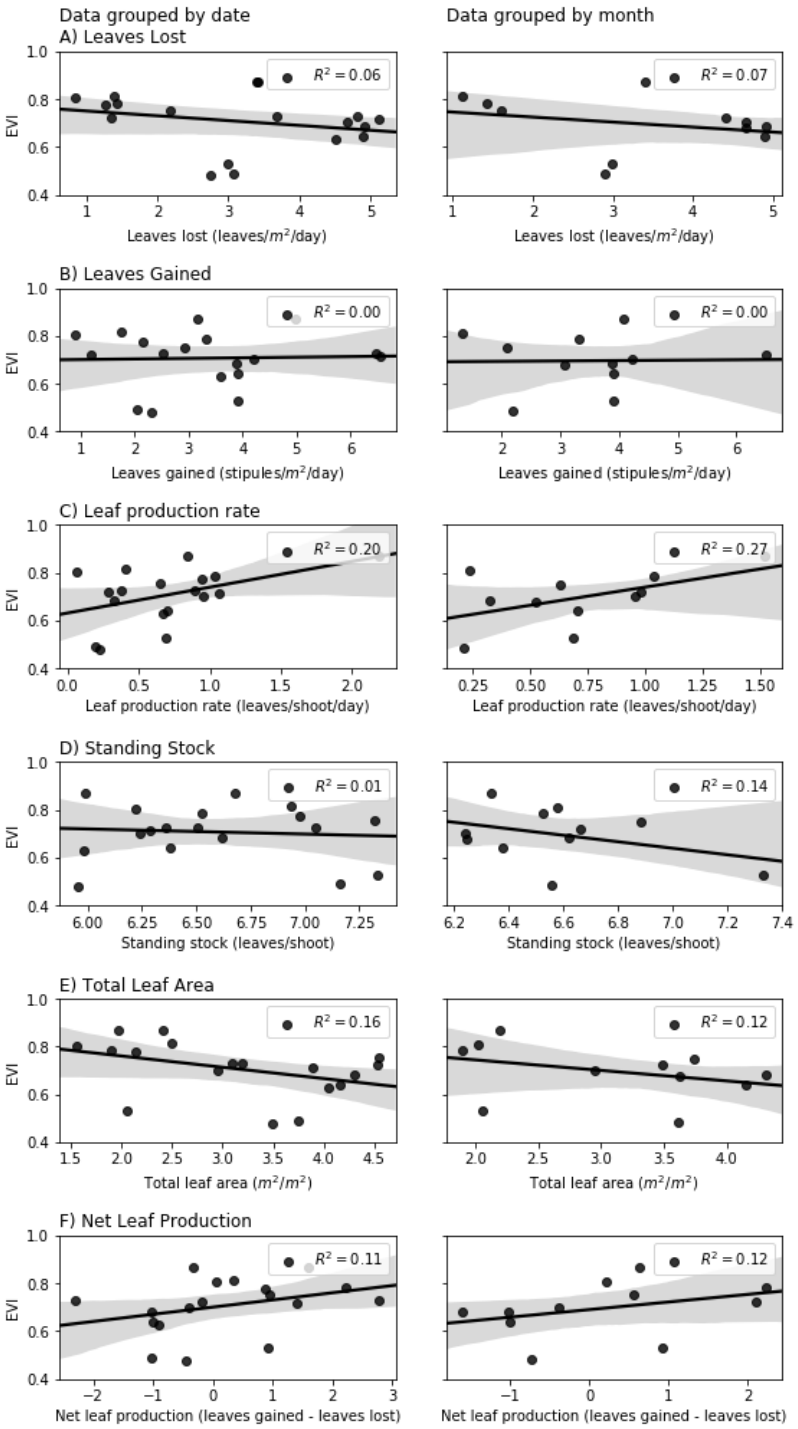

Figure 42: Linear regression between the in situ variables (columns) and the EVI model. The left panel shows the data grouped by date and on the right panel, the data are grouped by month. Black line shows the linear model fit and shaded areas represent the 5-95 confidence interval.

In summary, after comparing the *in situ* data from Duke et al. (1999) with the EVI model, we can say that the models seem to be more related to the leaf production rate, total leaf area and the net leaf production of mangrove forests.